FORWARDED BY THE CHIEF, BUREAU OF SHIPS

64-5

CR-588-93

FINAL REPORT
ON A
MECHANICAL HYDROFOIL CONTROL SYSTEM
PRELIMINARY DESIGN STUDY PROGRAM

Contract No. NObs-86448
Project Serial No. SF 013 09 05, Task 2637

JULY 1963

Submitted to:

BUREAU OF SHIPS, CODE 632
DEPARTMENT OF THE NAVY
WASHINGTON 25, D.C.

630729-C155

RADIO CORPORATION OF AMERICA
DEFENSE ELECTRONIC PRODUCTS
AEROSPACE COMMUNICATIONS AND CONTROL SYSTEMS DIVISION
CAMDEN 2, N.J. BURLINGTON, MASS.

CR-588-93

FINAL REPORT
ON A
MECHANICAL HYDROFOIL CONTROL SYSTEM
PRELIMINARY DESIGN STUDY PROGRAM

Contract No. NObs-86448
Project Serial No. SF 013 09 05, Task 2637

JULY 1963

Submitted to:

BUREAU OF SHIPS, CODE 632
DEPARTMENT OF THE NAVY
WASHINGTON 25, D.C.

Submitted by:

RADIO CORPORATION OF AMERICA
DEFENSE ELECTRONIC PRODUCTS
AEROSPACE COMMUNICATIONS AND CONTROLS DIVISION
BURLINGTON, MASSACHUSETTS

TABLE OF CONTENTS

TABLE OF CONTENTS (Continued)

TABLE OF CONTENTS (Continued)

TABLE OF CONTENTS (Continued)

TABLE OF CONTENTS (Continued)

TABLE OF CONTENTS (Continued)

TABLE OF CONTENTS (Continued)

TABLE OF CONTENTS (Continued)

LIST OF ILLUSTRATIONS

LIST OF ILLUSTRATIONS (Continued)

LIST OF ILLUSTRATIONS (Continued)

LIST OF ILLUSTRATIONS (Continued)

LIST OF ILLUSTRATIONS (Continued)

FOREWORD

This final report is submitted by the Radio Corporation of America to the Chief, Bureau of Ships, Code 632, in accordance with Item 3 of the Description of Work under Contract No. NObs-86448, Project Serial No. SF 013 09 05, Task 2637. Contract technical monitor for the Bureau of Ships was M. D. Martin.

This report was prepared by R. C. Blanchard, J. Dubbury, J. Hatfield, and D. Wellinger.

SECTION 1

SUMMARY

The purpose of the work reported was to investigate methods for improving the open-loop behavior of hydrofoil craft with emphasis on three different foil suspension techniques and to conduct feasibility and preliminary design studies applying these techniques to the Bureau of Ships 15-ton high-speed test craft (FRESH) for stabilization and control, both manually and automatically, in a State 3 Sea. The three suspension techniques, as may be seen from the diagrams of Figure 1-1, are basically mechanical in nature and have the property of providing a non-rigid connection in one degree-of-freedom between the foil and the hull. In the care of the sprung (or heaving) foil (Figure 1-1a), roughly vertical heaving can be used to minimize angle-of-attack variations normally induced by wave orbital motion. The freedom to rotate of the pivoted (or hinged) foil (Figure 1-1b) and the kite foil (Figure 1-1c) gives these configurations the potential for reducing induced angle-of-attack variations.

Preliminary studies of these three basic foil suspension schemes were conducted to determine their relative merits with respect to their ability to counteract the influences of wave particle orbital motion disturbances on the foil and minimize the resulting forces on the hull. No considerations of overall craft stability were involved in these preliminary studies which are described in Section 4. Stability with regard to individual foil response was considered, particularly for the case of the kite foil in supercavitating flow.

The general conclusions of the preliminary studies may be summarized by stating that the indicated potential performance on both the hinged and kite foils, regarding the isolation of the hull from wave-induced forces, is poorer than for the sprung (or heaving) foil configuration. Additionally, Section 4 of this report includes a study of basic stability problems inherent in the use of a supercavitating foil employing a detached flap in which it is shown that satisfactory stability cannot be obtained. This does not preclude the possibility of successful employment of the kite foil configuration as applied to subcavitating foils, since the extreme hydrodynamic non-linearities associated with cavitation that make stability impossible in the former case, are largely missing in the latter case.

To provide a means for applying controlling forces on the hull and foils of the craft in the presence of the spring-mounted foils; three basic mechanical and hydromechanical mechanisms were evolved. The first provided a lateral foil constraint which permitted two adjacent foils, although individually sprung, to be used mutually for aileron type control by constraining both foils to heave together (see Section 11). The second was introduced in order to permit manual longitudinal stability of the craft and is designed to produce immediate heave forces on the hull by generating so-called reaction forces. This is accomplished essentially by varying the lever arm of the foil strut spring (see Section 11). The third technique is a simple hydromechanical spring-centering device and has been introduced to prevent a static bias displacement of the springs for varying loads on the craft or excessive spring deflections at low frequencies.

Preliminary results on basic craft lateral stability and the nature of the change in basic stability with configuration changes such as foil placement (within limits prescribed for the FRESH craft) and the use of foil dihedral and/or sweep are given in Section 5. Taking these

results in conjunction with the criteria describing limits for the controllability by a human operator as developed and presented in Section 7, it was possible to assess the various configurations for controllability. A preliminary craft configuration, assumed before data on the actual FRESH craft was available, indicated a significant effect due to the addition of dihedral. However the influence of both dihedral and sweep was concluded to be quite small when the actual FRESH craft parameters were used. (See Section 3.) Such widely varying configurations as one airplane (conventional) configuration and three canard configurations (one which used four struts instead of three), for the FRESH craft are shown to yield surprisingly similar dynamic properties, with the most easily controllable, manually, being a canard configuration with slightly longer aft struts than forward struts. These investigations of manual controllability were accompanied by studies of automatic lateral control which are reported in Section 5. The effects of wave-induced disturbances were included in the latter two-dimensional and three-dimensional simulations.

Recommendations for displays and controls necessary for manual control of the craft are included in Section 8 and are basically the same as those found to be acceptable for manual control in the later simulations.

Longitudinal analysis of the complete craft equipped with sprung foils (Section 6) demonstrated a stability problem that was more difficult than originally anticipated. Previous studies of a large subcavitating rigid-strut craft showed craft open-loop longitudinal rate of divergence to be much slower than that for the lateral system.

Comparable divergence rates for the FRESH craft were found to be of the same order as those of the lateral system. This resulted from the cumulative effects of three properties:

(a) The surface proximity effect is destabilizing in the case of a supercavitating foil; that is, the lift increases as submergence of the foil decreases which is opposite to the surface proximity effect for subcavitation operation;

(b) The strut drag represents a much greater destabilizing effect than for the subcavitating craft since, for a given increase in strut immersion, there is a larger incremental downward pitching moment on the craft at the higher speed.

(c) The presence of the spring suspension of the foils aggravates the stability problems generated by items (a) and (b). Item (b) appears to be the most significant with items (c) and (a) following in order of importance.

The rapidity of the resulting longitudinal divergence and the evidence from the later three-dimensional (six-degree-of-freedom) simulation (Section 12) that cross-coupling effects are small make it necessary and possible to split the manual control of the craft between two operations - one for the longitudinal and the other for the lateral system.

The two-dimensional lateral simulation of the craft reported in Section 9 confirmed the analysis of Section 5. Automatic lateral control using ailerons initially and rudders on all three struts in later runs with laterally rigid struts shows that, while roll angles are somewhat larger when using rudders, they are less than one degree in a State 3 Sea and normalized side force (approximately lateral acceleration) is substantially smaller in the latter case. Thus it is concluded that a rudder controlled lateral system is preferable to an aileron controlled system where minimization of lateral accelerations is of prime importance. The effectiveness of the automatic rudder-controlled lateral system leads to the consideration of a two-strut (one forward and the other aft) configuration, and

it is believed that study of such a craft is merited. Also, it appears unnecessary to provide longer aft struts than forward struts to insure automatically controlled lateral stability for this craft.

Manual lateral control of the craft using ailerons and rudders (not simultaneously) confirmed earlier analysis that the stability under manual control of a trained operator was adequate for emergency operation in calm water for both control modes. In a State 3 Sea it is concluded that the probability of loss of control is too great to permit the use of either system for manual control of the craft.

The introduction of strut lateral compliance was found to be a destabilizing factor for either automatic or manual lateral control as was anticipated. Longer aft than forward struts (assumed rigid) were found to improve stability in manual control.

Two-dimensional longitudinal simulation of the craft reported in Section 10 resulted in the evolution of an automatic control system utilizing hydromechanical spring self-centering loops around fore and aft foils, measured relative wave height and heave acceleration controlling reaction forces forward and measured pitch attitude controlling aft reaction forces. Conclusions from runs in State 3 Seas using this control system are that, while sprung foils have reduced heave accelerations particularly in the presence of seas with high encounter frequencies (head, bow) the non-rigid foil support structure has aggravated the problem of longitudinal stability both for automatic and manual control. Manual stabilization of the craft was possible in calm water and in the presence of waves if the aft pitch angle control loop was retained. (Later three-dimensional simulation showed that if the springs of the aft foils were "locked out", that is, rigid aft struts were used, manual stabilization was also possible.)

Either one or the other of these configurations, it seems, is essential to provide sufficient pitch damping for control. With the aft gyro loop closed, calm water stability was deemed sufficient to permit emergency manual operation but in State 3 Seas, like the lateral system, manual longitudinal control is not considered sufficient to be used.

The evolved longitudinal and lateral control systems were combined in a three-dimensional simulation (results are reported in Section 12) of runs made in both a calm sea and a State 3 irregular sea under various relative headings. Both cross-coupling and surge mode effects were small during this simulation, provided roll angles were held to less than 10 to 15 degrees and foil broaching was avoided. As noted earlier, longitudinal manual control was possible without the use of an aft-pitch "aided stabilization" loops provided aft strut springs were locked out. It was further established that longitudinal control in calm water is quite practical with a height sensor display alone but that the heave acceleration signal was a necessary constituent of the longitudinal operator's display for control in a State 3 Sea.

Sections 13 and 14 contain the final design control system description and control system components requirements, and a survey of available rate and vertical reference gyros.

It should be noted that the high speed test craft used as a model for manual control in this study possesses perhaps the most difficult inherent dynamics for manual control of any hydrofoil craft in the planning or construction phase at this time. It is most probable that the manual control of a large subcavitating hydrofoil craft with uncontrolled response more amenable to manual stabilization would show a realistic capability at least for emergency mode control.

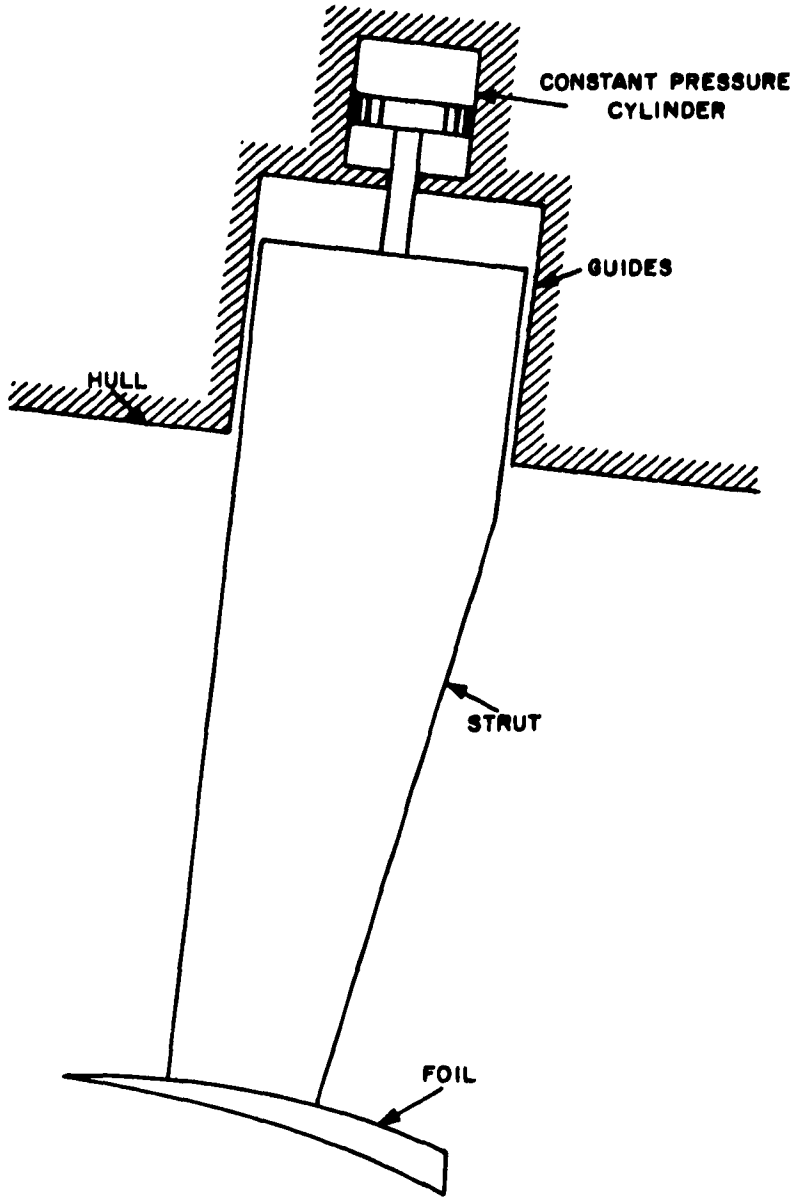

Figure 1-1(a). Sprung Foil Configuration

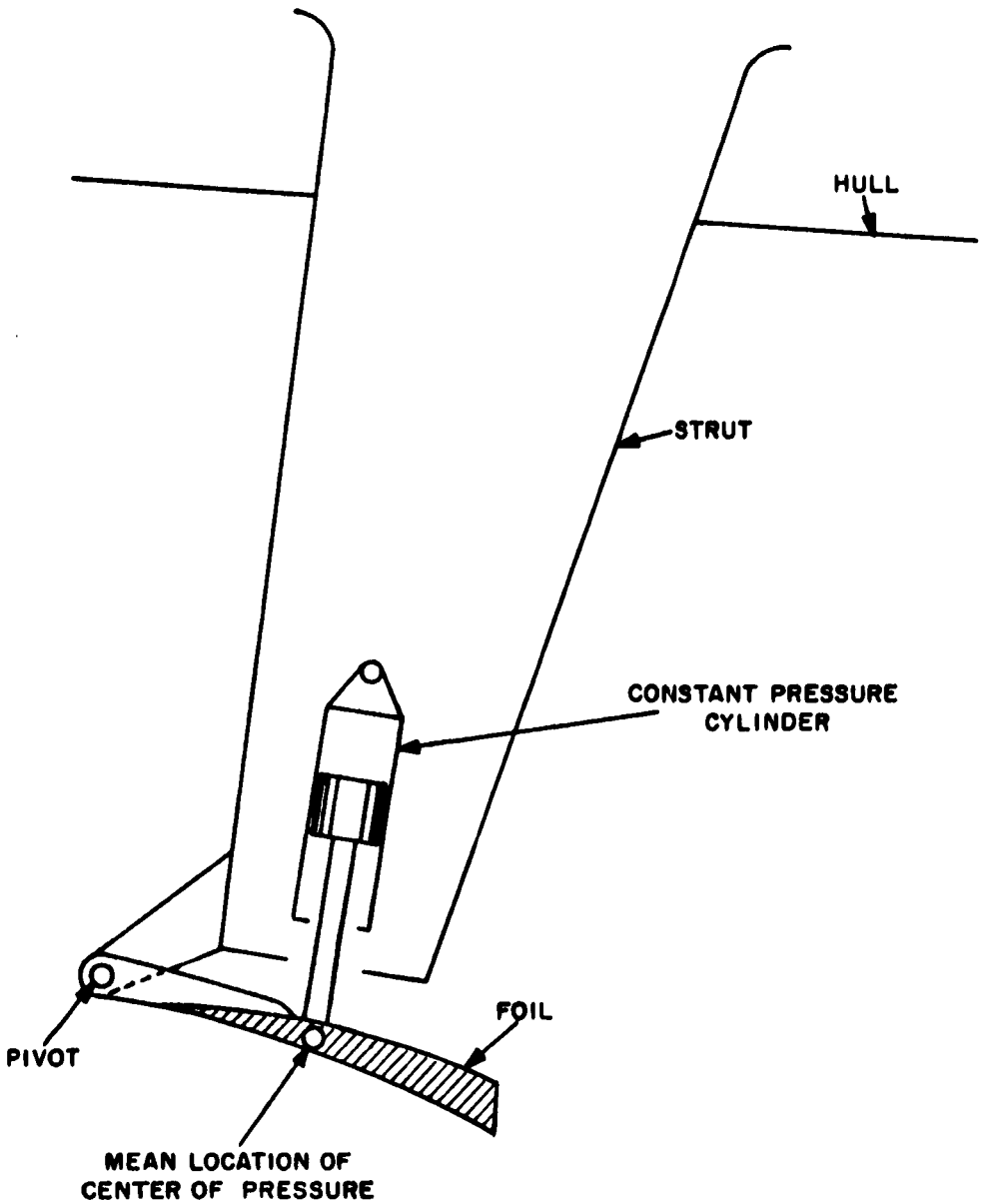

Figure 1-1(b). Hinged Foil Configuration

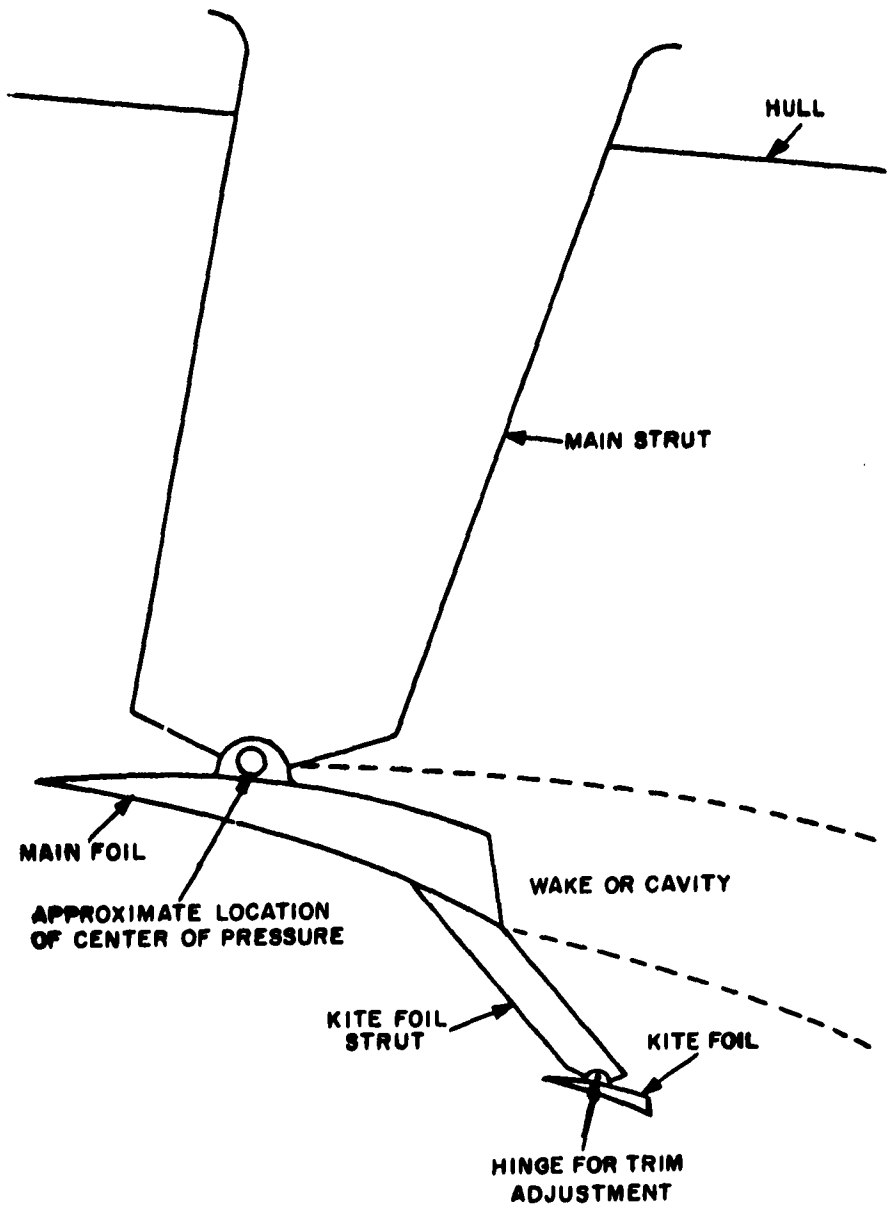

Figure 1-1(c). Kite Controlled Foil Configuration

SECTION 2

GLOSSARY

The following symbols are those most often used in the body of this report. Lesser used symbols are defined as required in the text.

$a_{\overline{G}}$	Acceleration of foil
A	Lever arm of strut drag or aspect ratio
b_s	Span between rear struts
c	Mean chord of foil or strut
C_N	Normal force coefficient on foil
C_{N_C}	Normal force coefficient including effects of virtual inertia
C_{N_I}	Normal force coefficient due to virtual inertia
C_{L_S}	Lift coefficient of strut
C_{D_S}	Drag coefficient of strut
d	Distance of an item above or below the CG measured parallel to the Z axis.
D	Drag
D_A	Aerodynamic drag

$f_1(i)$ incidence effect on foil C_N

$f_2(\zeta)$ submergence effect on foil C_N

$$C_N = f_1(i) f_2(\zeta)$$

F_C Hydrodynamic circulatory force on the foil parallel to and tending positively to compress the spring.

F_I Force on foil due to virtual inertia effects

F_B Balance force producing lateral constraint of aft foils

g Acceleration due to gravity

h_H Heave perturbation of the hull about an equilibrium position.

h_W Height of the wave above mean sea level

$h_{HS}, h_{W_{HS}}$ Height of the height sensor and wave height at the height sensor respectively above mean sea level

h_G Height of the CG above mean sea level in Z direction

h_{GV} Height of the CG above mean sea level measured vertically

i Instantaneous incidence relative to foil lower surface or strut center line.

I_x, I_y, I_z Moments of inertia of craft measured about x, y and z axis respectively.

k Various constants (with suffices) for control systems. Defined in text.

K_F, K_R Fore and aft strut spring stiffnesses

K_{FS}, K_{SS}, K_{PS} Lateral spring stiffness of forward, aft starboard and aft port struts.

K Rolling moment. (positive starboard down)

ℓ Distance of an item fore or aft of the CG, measured parallel to the x axis.

M Pitching moment about y axis (positive nose up)

m_T Total mass of the craft

m_H Mass of the hull

m_F, m_R Mass of the fore and aft unsprung masses (foil and strut)

n Number of struts or foils

N Yawing moment about the z axis (positive when the bow tends to starboard)

p Rolling angular velocity about x axis (positive starboard down)

P Force exerted by spring and reaction on hull (along strut and positive up)

q Pitching angular velocity about y axis (positive nose up)

r	Yawing angular velocity about z axis (positive nose to starboard)
R	Reaction force (positive tending to extend strut)
S	Foil or strut area
s	Laplace operator
T	Jet thrust
u	Velocity component parallel to x axis
u_g	Velocity at craft CG
u_{OM}	Horizontal component of orbital motion (positive in direction of wave propagation)
u_A	Relative velocity of air
v	Side slip velocity parallel to y axis (positive to starboard)
w	Vertical velocity of craft parallel to z axis (positive down)
w_{OM}	Vertical component of wave orbital motion (positive down)
x, y, z	Axes moving with the craft. Positive direction: forward, starboard, and down respectively
y_{FS}, y_{SS}, y_{PS}	Lateral deflections of mid-depth of submergence points of forward, aft starboard, and aft port struts.

ξ	Foil submergence
δ_a	Aileron deflection
δ_b, δ_s	Bow and stern rudder deflections respectively
η	Foil attitude (angle between foil lower surface and x axis, positive in positive lifting sense)
$\psi\theta\phi$	Euler angles defining the craft orientation. ψ yaw about z, θ pitch about y, and ϕ roll about x and taken in that order.
λ	Wave length of regular seas
	Strut hinge to foil length
ξ	Spring deflection (positive for spring extension)
ρ	Water density
τ, T	Various time constants defined in the text
ω	Various critical frequencies defined in the text.

Subscripts

G center of gravity
P port
S starboard or strut
F forward
R rear
H strut hinge point
A aerodynamic

Primed values indicate perturbations in the equations programmed for the two-dimensional simulation.

SECTION 3

CRAFT GEOMETRY AND ASSUMED FOIL-STRUT CHARACTERISTICS

3.1 INTRODUCTION

Details of the FRESH craft geometry were supplied by a communication from the Bureau of Ships. (See Reference 3-1.) These data presented information on permissible location of foil-strut attachment and included the general craft outline with CG location. Moments of inertia were not given and so they were estimated from the craft outline and given weight. They are listed in Figure 3-1. The same figure shows the general outline and pertinent dimensions of the craft that are employed in the work to follow.

Information was also supplied (see Reference 3-2) on the foils proposed for initial sea trials of the FRESH craft. However, for the reasons cited, a different foil section was chosen for this study.

3.2 FOIL AND STRUT SELECTION

3.2.1 NOTATION (FOR THIS SECTION)

The notation is that used in Reference 3-3.

A	is aspect ratio (b^2/S)
ℓ	is vertical distance from lower surface to cavity
δ	is the spray thickness above the foil
C_L	is lift coefficient
C_{L1}	is lift coefficient exclusive of cross flow

E	is ratio of semiperimeter to span
x	is distance aft of leading edge
α	is angle of attack (= A_o in this case)
α_i	is induced angle of attack
τ	is correction factor for variation from elliptical plan form

The foils proposed for the initial sea trials of the high-speed test craft are of cambered parabolic section. This results in a highly non-linear lift curve (see Reference 3-3) combined with unknown, unsteady characteristics in the region of transition between fully wetted and dry upper surface.

Since the primary objectives of the current study are the investigation of sprung foils and manual control, it was decided not to obscure the issue by the inclusion of the non-linear characteristics of the parabolic section foil.

Therefore a conventional supercavitating foil giving an approximately linear lift curve over the speed range of interest (40 to 80 knots) was employed. Thus it is required to use a section which will give a sufficiently small drag to permit takeoff while retaining a dry upper surface at cruise.

Data in Reference 3-3, Figures 17 to 24, give $C_L \approx 0.4$ for $L/D \approx 3.0$ for an aspect ratio 3 foil at a depth of 5 chords (a depth roughly consistent with takeoff conditions). The craft at takeoff suffers further drag increments due to the struts, the hull, and foil skin friction; since on the high-speed test craft the maximum thrust is about half the weight, it appears unlikely that a basic foil L/D ratio much less than 3 can be tolerated. Now, if this foil lift coefficient is to lift the craft at 40 knots, then, at 80 knots, $C_L = 0.1$. Therefore a section is

required giving a dry upper surface at $C_L = 0.1$ and a running depth of about 2 chords. The requirement that the cavity must pass sufficiently far above the lower surface to permit an adequate structural thickness dictates a minimum C_L well above C_{Ld} (see Figures 3-2 and 3-3 prepared from Reference 3-3). The three-term series section with $C_{Ld} = 0.1$, and being only 1 percent thick at the 50-percent chord point (which is clearly structually inadequate), would have a minimum operating $C_L = 0.126$. In addition, the lower surface camber is only about 1.7 percent maximum.

To design a foil capable of safely operating at $C_L = 0.1$ would require a somewhat smaller critical lift coefficient (upper surface just wet), $C_L = 0.08$, say. To achieve this and obtain a reasonable structural thickness requires a very small $C_{Ld} \approx 0.03$. This reduces the maximum lower surface camber to 0.5 percent, which is to all intents and purposes, a flat plate.

Thus a flat plate foil has been assumed for the craft.

Then, from Figure 17d of Reference 3-3, $C_L = 0.08$ at $\alpha = 4^o$ for $A = 3$ and $d/c = 2.0$.

Equation 128 of Reference 3-3 for a flate plate becomes

$$\left(\frac{\ell}{C}\right)_{\text{Total}} = \left(\frac{A}{A+1}\right)\left(\frac{\ell}{C}\right)_{A_o - \alpha_i} = 0.75\left(\frac{\ell}{C}\right)_{A_o - \alpha_i}$$

Now $\alpha_i = \frac{C_{L1}}{\pi A}(1+\tau)$ from Equation 95 of Reference 3-3.

$C_{L1} \approx \frac{1}{E} C_{N,f}(\alpha - \alpha_i)\cos\alpha$ from Equation 94 of Reference 3-3

where $C_{N,f}(\alpha - \alpha_i)\cos\alpha = C_L$ for zero camber.

For the foil planform shown in Figure 3-4,

$$E = 1.27 \quad \therefore \quad C_{L1} = \frac{0.08}{1.27} = 0.063$$

$$\tau = 0.02 \quad \therefore \quad \alpha_i = \frac{0.063\,(1.02)}{\pi \times 3} = 0.00683 \text{ rad}$$

$$= 0.3913^{\circ}$$

$$\therefore \quad A_o - \alpha_i = \alpha - \alpha_i = 3.6087^{\circ}$$

which permits a thickness (scaled from Figure 25d of Reference 3-3) at $d/c = 2.0$ of

$$\left(\frac{\ell}{c}\right)_{\text{Total}} = 5.75\% \text{ at } x/c = 0.5$$
$$= 10.9\% \text{ at } x/c = 1.0$$
$$= 2.71\% \text{ at } x/c = 0.2$$

With the cavity shape thus defined, a thickness-chord ratio of 5 percent was chosen for the foil which would readily fall within the cavity, and the foil planform shape was patterned after the foil planform shape presented in Reference 3-1. (See Figure 3-4.)

The strut section outline shown in Figure 3-4 is precisely that presented in Reference 3-1 as the strut section being considered for preliminary trials of the FRESH craft.

REFERENCES

3-1. Data supplied by the Bureau of Ships, Department of the Navy in a letter dated 13 April 1962, (NObs86448, Ser632B-507).

3-2. Data supplied by the Bureau of Ships, Department of the Navy in a letter dated 6 July 1962 (NObs86448, Ser632B4-966).

3-3. Theoretical and Experimental Investigation of Supercavitating Hydrofoils Operating Near the Free Water Surface, Virgil E. Johnson Jr., NASA TR R93, 1961.

MOMENTS OF INERTIA

$I_{xx} = 4.98 \times 10^4$ SLUG-FT^2

$I_{yy} = 1.97 \times 10^5$ " "

$I_{zz} = 2.43 \times 10^5$ " "

CRAFT WEIGHT = 37,100 LBS.

FIG. 3-1 HIGH SPEED CRAFT GEOMETRY ASSUMED FOR FUTURE ANALYSIS AND SIMULATION

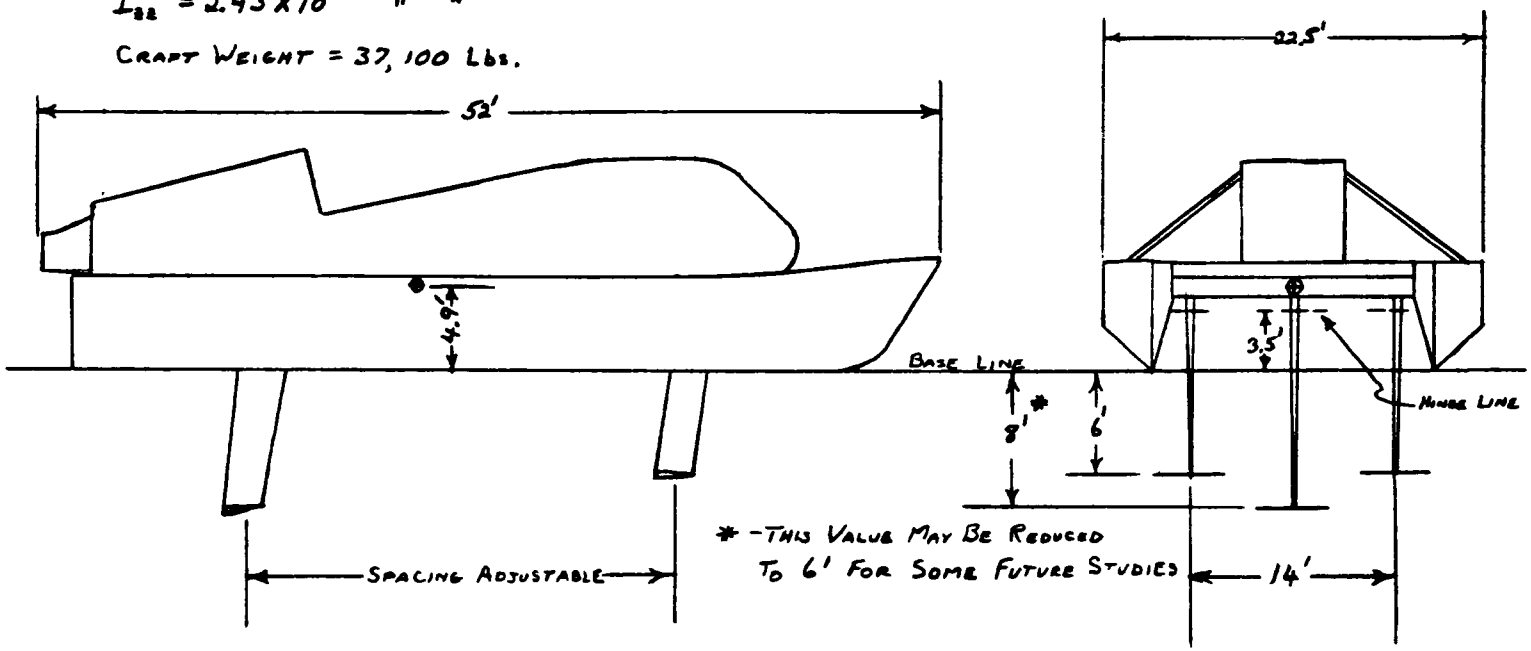

NOTE:

FORE-AFT FOIL SPACING AND ARRANGEMENT ARE VARIABLE

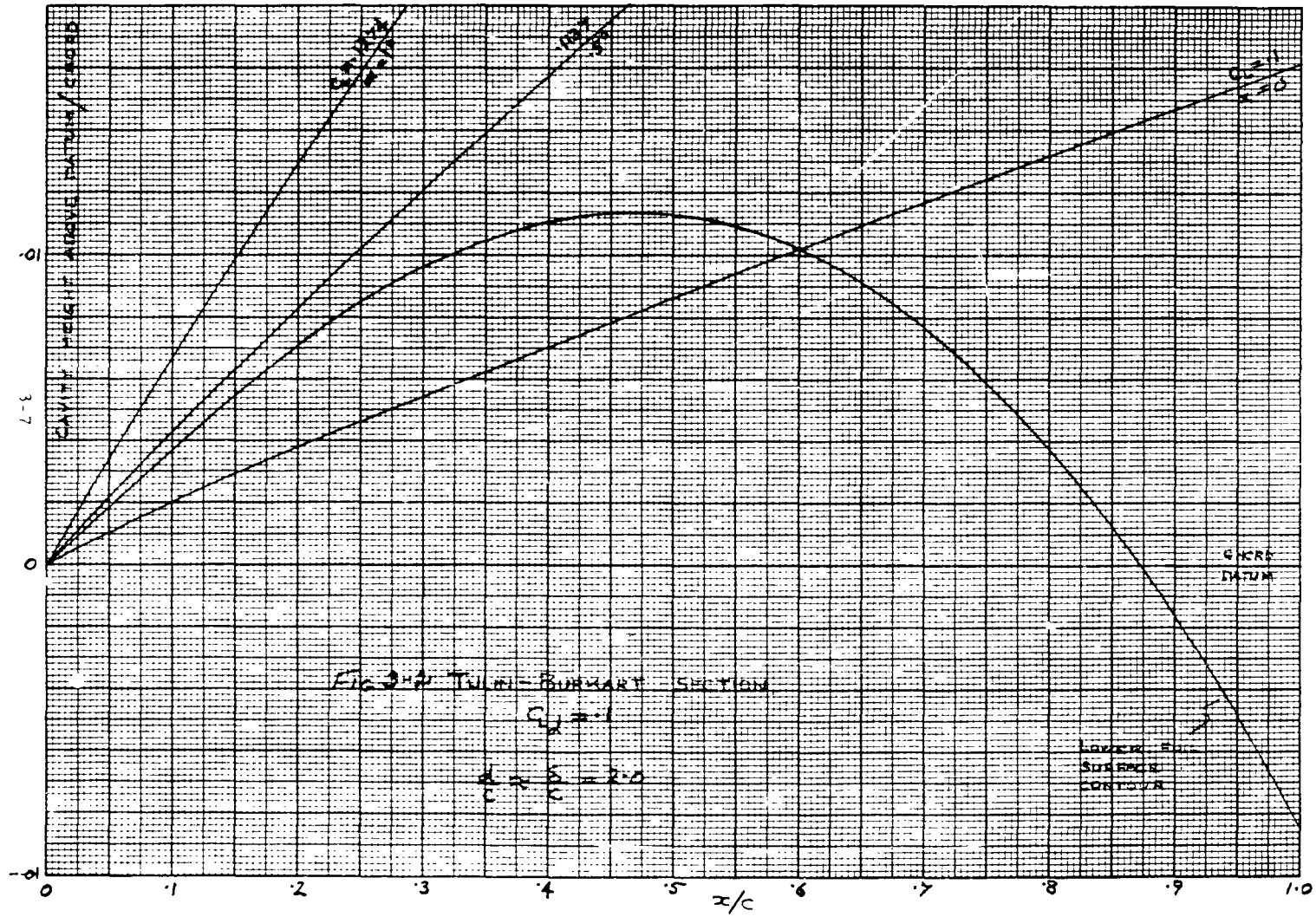

FIG 3-A TULMI-BURHART SECTION

$C_{l_d} = .1$

$\frac{d}{c} = \frac{b}{c} = 2.0$

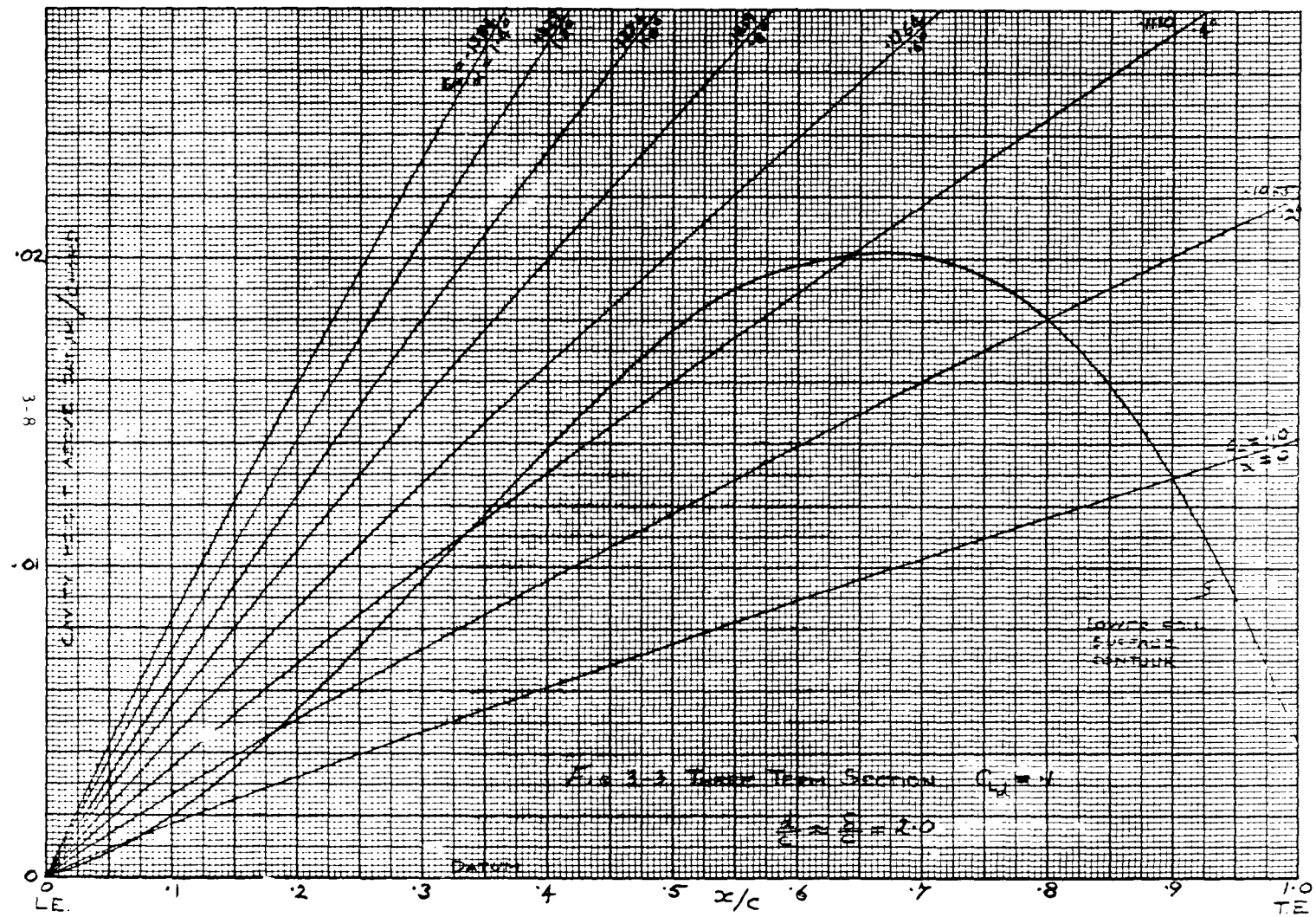

Fig. 3.3 Tunnel Test Section $C_{LX} = 1$

$\frac{x}{c} \approx \frac{\Delta x}{\Delta z} = 2.0$

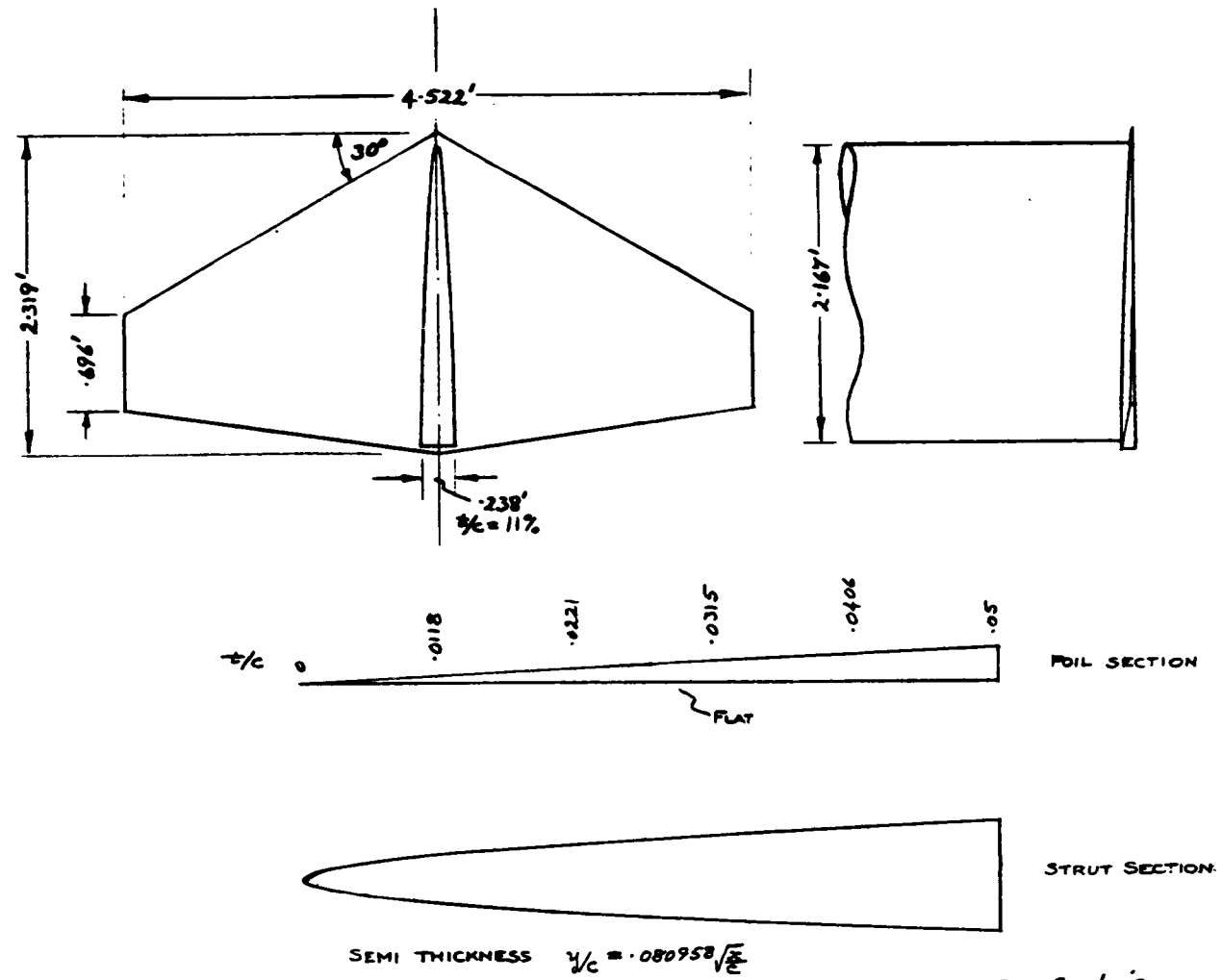

FIG 3-4. STRUT AND FOIL GEOMETRY

SECTION 4

PRELIMINARY DYNAMIC ANALYSIS OF THREE SUSPENSION TECHNIQUES

4.1 INTRODUCTION

The fundamental similarities and differences in performance potential of the Sprung, Hinged, and Kite Foil concepts are investigated and evaluated in this section. Diagrams illustrating the three systems are shown in Figure 4-1. Because of the non-rigid mounting of these three basic foil configurations, the complete equations representing craft longitudinal dynamic behavior are considerably more complicated than the analogous equations for a craft with rigidly mounted foils. In this case, the high speed, (80 knots) and relatively small waves which represent the test craft's environment permit a simplification in the longitudinal equations for the purpose of this comparison.

This simplification is realized with the assumption that hull heave motions are sufficiently small so that the attitude changes transmitted to the foil by pitching of the hull represent a negligible effect. In the case of the kite foil and the hinged foil with zero spring stiffness, such induced foil incidence changes are precisely zero.

The pure heave assumption may be shown to be valid for the sprung foil case by a simple calculation. The root-mean-square orbital velocity (vertical component), $\sqrt{w^2}_{OM}$, for a State 3 Sea is derived in Section 4.6 (see Figure 4-18). If a regular sea corresponding approximately to the peak of the sea spectrum (ω_e = 5 rad/sec) at a craft speed of 80 knots is assumed with the same root-mean-square

orbital velocity, this may be applied, as an input, in Figure 4-4 to the curve of "hull displacement". Thus

$$\sqrt{\overline{h^2}_H} = \left| \frac{h_H}{w_{OM}} \right| \sqrt{\overline{w^2}_{OM}} = 0.0123 \times 1.26 = 0.0155 \text{ ft}$$

Hull pitch attitude change becomes (assuming aft foil stationary)

$$\Delta\theta = \frac{h_H}{\ell} = \frac{0.0155}{30} = 0.000516 \text{ rad}$$

where ℓ is fore-aft foil separation.

This induced incidence change has an equivalent additional orbital motion input component of

$$w_{(OM)\ equiv/u} = 0.000516$$

With u (craft velocity) = 135 ft/sec (80 knots),

$$w_{(OM)\,equiv} = 0.000516 \times 135 = 0.0696 \text{ F/S}$$

This value is more than an order of magnitude below the root-mean-square orbital velocity quoted previously (1.26 F/S from the first equation) and therefore represents a demonstration of the validity of the non-pitch assumption.

The fixed foil case may be similarly checked by using Figure 4-4 to find

$$\sqrt{\overline{h^2}_H} = \left[\frac{1}{s^2} \left| \frac{\ddot{h}_H}{w_{OM}} \right| \right]_{s = 5j} \sqrt{\overline{w^2}_{OM}} = 0.055 \times 1.26 = 0.0806 \text{ ft}$$

$$\Delta\theta = \frac{0.0806}{30} = 0.00269 \text{ rad}$$

$$\text{and } w_{(OM)\,equiv} = 0.00269 \times 135 = 0.363 \text{ F/S}$$

This value, although considerably smaller than the mean square value, is not down by an order of magnitude, and so the approximation of zero pitching must be considered correspondingly poorer.

For the lower end of the encounter frequency spectrum of the State 3 Sea (ω = 1 to 5 rad/sec) the phase difference of the orbital motion inputs on fore and aft foils ϕ = 7.3 to 51.1 degrees respectively, (respective wavelengths of 1380 and 211 feet) assuming a foil separation of 30 feet. Thus, over this range, the motions of the fore and aft foils will tend to be largely in-phase and computation of hull pitch, based on the assumption of a non-heaving aft foil, is conservative.

For frequencies beyond about 3 rad/sec, hull motions are so small as to have negligible influence on the behavior of the hinged foil. (See Figure 4-5 for hinged foil response with and without hull constraint.)

It may thus be concluded that for the encounter frequency range of interest (1.5 to 30 rad/sec for 80 knots in a State 3 head sea) freedom of the hull to pitch would not substantially modify the conclusions drawn from the comparison of the three systems.

4.2. SPRUNG FOIL

4.2.1 EQUATIONS OF MOTION

The hull will receive least fluctuation in lift force (due to the influence of orbital motions on the foil) if the resultant hydrodynamic force on the foil (F) is directed along the axis of the strut spring. It is fortunate

that the vector sum of the lift and drag on the foil changes its direction little in relation to the foil over a wide range of incidence. The schematic arrangement is shown in Figure 4-1a.

The equations of motion of the foil become

$$\left.\begin{aligned} m_h s^2 h_H(s) &= -R(s) \\ m_F s^2 \left\{h_H(s) + \xi\ (s)\right\} &= R(s) - F(s) \end{aligned}\right\} \qquad (4\text{-}1)$$

where m_h is the equivalent mass of the hull

m_F is the mass of the foil plus the unsprung portion of the strut

h_H is the heave of the hull (positive down)

R is the reaction transmitted along the strut

F is the hydrodynamic force on the foil (positive in the normal lifting sense)

ξ is the spring deflection

All variables are taken as small perturbations from the equilibrium steady state.

Now $R(s) = -K\,\xi(s)$ (4-2)

where K is the spring stiffness.

Substituting Equation 4-2 in Equation 4-1 gives

$$\xi(s) = \frac{-F(s)}{K\left(\frac{m_H + m_F}{m_H}\right) + m_F s^2} \qquad (4\text{-}3)$$

The force on the foil must include all necessary unsteady effects, thus

$$F(s) = C_N(\ )\ \frac{\rho}{2}\ S u^2 \qquad (4\text{-}4)$$

where ρ is the water density

u is the relative free stream velocity assumed constant, since at supercavitating speeds, the horizontal component or orbital motion is very small

S is the foil plan area

C_N is as defined in Equation 4-5.

The only hydrodynamic perturbations experienced by the foil are in heave, due to the combined effects of spring deflection, ξ , hull heave h_H, and the vertical component of orbital motion measured positive downward.

The assumed form of the normal force coefficient as derived from Reference 4-1 is

$$C_N(s) = B\ (1 + \beta s)\left\{\xi(s) + h_H(s) - \frac{w_{OM}}{s}\ (s)\right\} \qquad (4\text{-}5)$$

β controls the magnitude of the virtual inertia effects.

$$B = \frac{1}{u}\ \frac{\partial C_N}{\partial i}\quad \text{(steady state)}$$

Thus, using Equations 4-1 (2nd part), 4-2, 4-4, 4-5, and 4-3 gives

$$\frac{\xi(s)}{w_{OM}(s)} = \frac{m_H s\ (1 + \beta\ )}{K\left\{1 + \left(\beta + \frac{m_H}{k_m E}\right)\ + \frac{m_H}{K}\ s^2 + \frac{m_H}{K}\left(\beta + \frac{m_F}{E}\right) s^3\right\}}$$

where $k_M = \frac{m_H}{m_F + m_H}$; $E = \frac{\rho}{2} S u^2 B$

Equation 4-6,in combination with Equation 4-2 and the first of Equation 4-1, gives R(s) and $h_H(s)$. From Equation 4-6 the following special cases can be developed.

(1) Hull prevented from heaving ($m_H = \infty$, $k_M = 1$)

$$\frac{\xi(s)}{w_{OM}(s)} = \frac{E(1 + \beta s)}{K\left\{1 + \frac{E}{K} s + \left(\frac{\beta E + m_F}{K}\right) s^2\right\}} \qquad (4\text{-}7)$$

(2) Rigidly mounted foil ($K = \infty$)

$$\frac{h_H(s)}{w_{OM}(s)} = \frac{1 + \beta s}{s\left\{1 + \left(\beta + \frac{m_H}{k_m E}\right) s\right\}} \qquad (4\text{-}8)$$

(3) Rigidly mounted foil and zero hull heaving. ($K + \infty$ and $m_H = \infty$)

$$\frac{R(s)}{w_{OM}(s)} = -E(1 + \beta s) \qquad (4\text{-}9)$$

(4) Zero stiffness spring ($K = 0$)

$$\frac{\xi(s)}{w_{OM}(s)} = \frac{1 + \beta s}{s\left\{1 + \left(\beta + \frac{m_F}{E}\right) s\right\}} \qquad (4\text{-}10)$$

4.2.2 EXAMPLE

The foil, whose dimensions are presented below, was chosen for preliminary numerical evaluation and purposes of illustration. It serves as a useful basis for comparing the three methods of mounting and it is felt that the conclusions are unaffected by any realistic changes in the foil configuration. A comparison of Figures 4-4 and 4-16 will show that, for two quite different foil sizes, the dynamic behavior for nearly comparable mass spring resonances (K = 2515 lb/ft in Figure 4-4 and K = 1000 lb/ft in Figure 4-16) is very similar indeed.

Foil geometry:

Span = 6 ft, chord = 2 ft, area = 12 ft^2

Aspect ratio = 3.0

m_F = 31.06 slugs, m_H = 1700 slugs, k_M = 0.982

Speed u = 80 knots = 135.2 ft/sec

β = 0.01012 sec, E = 2515.3 slugs/sec

The spring deflection for a range of spring stiffnesses (with hull heave zero) as a function of encounter frequency is plotted in Figure 4-2. The reaction on the hull for the same range of spring stiffnesses (also with hull heave zero) as a function of encounter frequency is plotted in Figure 4-3.

The hull acceleration for a rigid strut (K = ∞) and for K = 2515.3 lb/ft are plotted as functions of encounter frequency in Figure 4-4.

4.2.3 CONCLUSIONS

(1) The spring is most effective in reducing reaction transmitted to the hull at high frequency.

(2) For a finite spring stiffness there is a frequency below which a substantially rigid strut reaction exists. This critical frequency diminishes with spring stiffness.

(3) Substantial spring deflections only occur for combinations of low spring stiffness around the hull-spring resonant frequency. Section 4.6 develops a control loop for maintaining spring deflections small at all frequencies.

(4) There is a small frequency range over which the hull acceleration with the sprung foil arrangement exceeds that produced by the rigid strut. This resonance effect peaks at 1.2 rad/sec in the example given in Figure 4-4. At this peak the foil displacement is zero. It is also possible that the peak is fictitious since no account has been taken of natural hull aerodynamic damping.

(5) The effect of foil mass variation is of small significance.

(6) The spring effectively isolates the hull at frequencies well beyond the probable bandwidth of an accelerometer loop.

4.3 HINGED FOIL

4.3.1 EQUATIONS OF MOTION

The schematic arrangement is shown in Figure 4-1b.

Let the inertia about the hinge be I_F slugs ft^2.

Let the mass of the foil be m_F slugs.

The foil movement is restrained by a torsion spring of stiffness T lb ft/rad at the pivot.

F_H and M_H are the hydrodynamic normal force and moment on the foil referred to the leading edge.

α_F is the perturbation in pitch displacement of the foil in radians.

Thus, the equations of motion are

$$\left.\begin{aligned} R(s) - F_H(s) &= m_F\left\{s^2 h_H(s) + k_G C s^2 \alpha_F(s)\right\} \\ M_R(s) + M_H(s) - k_L C F_H(s) &= k_G C m_F s^2 h_H(s) + I_F s^2 \alpha_F(s) \\ -R(s) &= m_H s^2 h_H \end{aligned}\right\} \quad (4\text{-}11)$$

(The quantities $k_G C$, $k_L C$ are defined in Figure 4-1b.)

Now the pivot spring restoring moment perturbation

$$M_R(s) = -T\,\alpha_F(s) \quad (4\text{-}12)$$

Based on Reference 4-1, the hydrodynamic normal force and moment on the foil will be of the form

$$\left.\begin{aligned} F_H(s) &= \phi_Z(s)\left\{h_H(s) - \frac{w_{OM}(s)}{s} + k_L C\,\alpha_F(s)\right\} + \phi_\alpha(s)\,\alpha_F(s) \\ M_H(s) &= \mu_Z(s)\left\{h_H(s) - \frac{w_{OM}(s)}{s} + k_L C\,\alpha_F(s)\right\} + \mu_\alpha(s)\,\alpha_F(s) \end{aligned}\right\} \quad (4\text{-}13)$$

where ϕ_Z, ϕ_α, μ_Z and μ_α are defined in Equation 4-16, Orbital motion is assumed irrotational so that it does not contribute moments on the foil that would otherwise exist due to the stream's rotational inertia.

Substituting Equations 4-12 and 4-13 in Equation 4-11 and eliminating R(s) gives

$$\left.\begin{aligned} Ah_H(s) + B\alpha_F(s) &= C w_{OM}(s) \\ Dh_H(s) + E\alpha_F(s) &= F w_{OM}(s) \end{aligned}\right\} \quad (4\text{-}14)$$

where $A = \phi_Z(s) + (m_H + m_F)\, s^2$

$B = k_L C \phi_Z(s) + \phi_\alpha(s) + m_F\, k_G C\, s^2$

$C = \phi_Z(s)/s$

$D = k_L C \phi_Z(s) - \mu_Z(s) + k_G C\, m_F\, s^2$

$E = k^2_L C^2 \phi_Z(s) + k_L C \left\{\phi_\alpha(s) - \mu_Z(s)\right\} - \mu_\alpha(s) + T + I_F\, s^2$

$F = \frac{1}{s}\left\{k_L C \phi_Z(s) - \mu_Z(s)\right\}$

Solving Equation 4-14 gives

$$\left.\begin{aligned} \frac{h_H(s)}{w_{OM}(s)} &= \frac{CE - BF}{AE - BD} \\ \frac{\alpha_F(s)}{w_{OM}(s)} &= \frac{AF - CD}{AE - BD} \end{aligned}\right\} \quad (4\text{-}15)$$

From Reference 4-1 the following functions were derived for substitution in A, B, C, D, E, F.

$$\phi_Z(s) = \frac{\pi}{4}\, \rho\, \mu\, S\, s \left\{1 + 0.6766\, \frac{Cs}{\mu}\right\}$$

$$\phi_\alpha(s) = \frac{\pi}{4}\rho\mu^2 S\left\{1 + 1.0886\ \frac{Cs}{\mu}\ 0.3976\ \frac{C^2 s^2}{\mu^2}\right\}$$

$$\mu_Z(s) = \frac{-5}{64}\ \pi\rho\mu S C s\left\{1 + 0.8891\ \frac{Cs}{\mu}\right\} \qquad (4\text{-}16)$$

$$\mu_\alpha(s) = \frac{-5}{64}\ \pi\rho\mu^2 SC\left\{1 + 2.144\ \frac{Cs}{\mu} + 0.4958\ \frac{C^2 s^2}{\mu^2}\right\}$$

4.3.2 EXAMPLE

For numerical evaluation the foil was taken as being geometrically identical to that assumed in the previous "sprung foil" section (Section 4.2).

The mass of the foil m_F = 18.63 slugs (a reduction from the previous case since no strut is attached).

The foil CG location was taken as $k_G = 0.55 + k_L$.

The foil inertia about its own CG ($I_{F(CG)}$) was taken as 6.398 slugs ft^2.

Then the moment of inertia about the pivot is found as

$$I_F = I_{F(CG)} + (k_{G_C})^2 m_F$$

$$= 6.398 + \left[(0.55 + k_L)\ 2\right]^2 \times 18.63$$

which becomes: $I_F = 28.94 + 81.99\ k_L + 74.53\ k^2_L$

The results are plotted in Figure 4-5 and 4-6.

4.3.3 CONCLUSIONS

(1) The hinged foil reduces reactions on the hull at all frequencies.

(2) The reductions in hull acceleration are poor at high frequency compared with the sprung foil.

(3) The hull acceleration attenuation is improved by moving the hinge point well forward of the leading edge (see Figure 4-5, $k_L = 1.0$). If this process is extended sufficiently, the hinged foil approaches the sprung foil in behavior as would be expected (hence the improvement). However, this results in an undesirable mechanical arrangement - a long arm from the foil to the hinge.

(4) Variation of spring stiffness has little effect at high frequency (see Figure 4-5).

(5) The drag penalty associated with the hinge and spring housing is undesirable.

(6) Since the sprung foil carries all of its control mechanization above the water, there is no equivalent drag penalty and provided that spring deflections are kept small, the sprung foil seems much more promising.

4.4 TRAILING FLAP KITE FOIL

The concept of a kite foil involves the use of a statically stable foil pivoted to the strut, having zero static pitching moment about the hinge (see Figure 4-1c). Thus an auxiliary foil or flap is required to control the lift coefficient at which the pitching moment will be zero under steady-state conditions.

Structural stiffness is a prime requirement for any supercavitating foil, so that an auxiliary foil having a span comparable with the main

foil would need multiple support brackets. If these brackets penetrate the flow beyond the cavity, an increase in the fundamentally large drag associated with cavitation is unavoidable. Therefore, as a special case of the kite foil configuration, it has been decided to consider initially an auxiliary foil of the trailing edge flap type having no such hardware in the stream.

In the supercavitating regime only the lower surfaces of both foil and flap will be effective, so that beyond some small negative flap angle the lower surface of the flap will cavitate and become completely ineffective.

Now, the neutral point $\frac{\partial C_M}{\partial C_L} = 0$ of supercavitating foils is close to the theoretical thin foil value of 0.3125 chord aft of the leading edge, so that the hinge must be placed at some point forward of this to give static stability. Cambered foils such as the Tulin-Burkart have centers of pressure ($C_M = 0$) typically located between 0.37 and 0.50 chords aft of the leading edge depending on camber and C_L. Thus (neglecting the probable cavitation of the flap) substantial negative flap deflection would be required to bring the pitching moment to zero. The resulting steady-state configuration would be far from the originally designed section and degraded performance would result.

Consideration therefore is reduced to substantially uncambered foils with trailing edge flaps. It is assumed that the upper surface is at all times dry, as wetting would produce large pitching moment variations.

With the trailing edge flap lower surface completely wet, the foil neutral point is at 0.3125 chord. With the flap completely cavitated, the neutral point will be at $0.3125\ (1 - k_\eta)$. This limits the possible range of hinge positions (see Figure 4-7).

4.4.1 EQUATIONS OF MOTION

All nomenclature is the same as for the hinged foil (of the previous section) except as shown in Figure 4-1c.

Then the equations of motion become

$$\begin{aligned} R(s) - F_H(s) &= m_F\left\{ s^2 h_H(s) + (k_G - k_H)\, C s^2 \alpha_F(s)\right\} \\ M_H(s) + k_H C\, F_H(s) &= (k_G - k_H)\, C m_F S h_H(s) + I_F s^2 \alpha_F(s) \\ -R(s) &= m_H s^2 h_H(s) \end{aligned} \tag{4-17}$$

Based on Reference 4-1 the hydrodynamic normal force and moment on the foil will be of the form

$$\begin{aligned} F_H(s) &= \phi_Z(s)\left\{ h_H(s) - \frac{w_{OM}(s)}{s} - k_H C \alpha_F(s)\right\} + \phi_\alpha(s)\, \alpha_F(s) \\ M_H(s) &= \mu_Z(s)\left\{ k_H(s) - \frac{w_{OM}(s)}{s} - k_H\, C \alpha_F(s)\right\} + \mu_\alpha(s)\, \alpha_F(s) \end{aligned} \tag{4-18}$$

Substituting Equations 4-18 and 4-17 and eliminating R(s) gives

$$\begin{aligned} A h_H(s) + B \alpha_F(s) &= C\, w_{OM}(s) \\ D h_H(s) + E \alpha_F(s) &= F\, w_{OM}(s) \end{aligned} \tag{4-19}$$

Where

$$A = \phi_Z(s) + (m_H + m_F)\, s^2$$

$$B = -k_H C \phi_Z(s) + \phi_\alpha(s) + (k_G - k_H)\, C m_F s^2$$

$$C = \phi_Z(s)/s$$

$$D = (k_G - k_H)\, Cm_F s^2 - \mu_Z(s) - k_H C \phi_Z(s)$$

$$E = -\mu_\alpha(s) + k_H C\,(\mu_Z(s) - \phi_\alpha(s) + k^2{}_H\, C^2\, \phi_Z(s) + I_F s^2$$

$$F = -\left\{\frac{\mu_Z(s) + k_H C\, \phi_Z(s)}{s}\right\}$$

$\phi_Z(s)$, $\phi_\alpha(s)$, $\mu_Z(s)$, $\mu_\alpha(s)$ being defined in Equation 4-16.

4.4.2 EXAMPLE

The foil dimensions are the same as those assumed for the sprung and hinged foils, except that the undersurface must be nearly flat.

The foil CG was taken as 0.55 C.

The mass of the foil was taken as 18.63 slugs (as for the hinged foil).

The foil inertia about its CG was taken as 6.398 slugs ft^2 (as for the hinged foil). Then, a computation similar to that shown in Section 4.2.2 yields

$$I_F = 28.94 - 81.94\, k_H + 74.53\, k^2{}_H.$$

The results in terms of reactions on the struts are shown in Figure 4-8. All the results were calculated for the zero hull heave condition since this somewhat reduces computation and (as previous experience has shown) only affects the behavior significantly at very low frequency.

4.4.3 CONCLUSIONS

(1) Strut reaction attenuation is poor compared with either the sprung or hinged foil system, particularly at the higher frequencies where servo loops are most ineffective. In the range 5 to 200 rad/sec, only about 3-db (30 percent) reduction in strut reaction is achieved.

(2) Efforts to improve the high frequency performance by reducing the mass and inertia of the foil and by adding mass balance proved fruitless.

(3) The underwater location of the hinge is undesirable insofar as overall system drag is concerned.

(4) Wetting of the upper surface at low speed and at very small incidences at high speed could produce a forward movement of neutral point resulting in instability. Even if this could be prevented at high speed the foils would gradually be required to be locked under low speed take-off conditions.

(5) The overall results show little promise when applied to supercavitating conditions. Therefore, the trailing flap kite foils will not be considered further. The following analysis will consider the more general kite foil configuration.

4.5 SEMI-DETACHED (KITE) FOIL

A "kite" foil configuration has been investigated that utilized an attached, trailing edge flap for control. In this section, the concept is extended to the more general case of a semi-detached control foil (see Figure 4-9) to determine whether such a configuration may be capable of inherent stability while maintaining a near constant lift force at supercavitating speeds and allowing for the hydrodynamic non-linearities likely to be present.

4.5.1 STABILITY REQUIREMENTS AND CALCULATIONS

A freely hinged foil is required such that the pitching moment about the hinge is zero while a positive lift is being developed. It is also necessary (though not sufficient) that the foil be statically stable; i. e., a change in foil incidence will produce a pitching moment so as to restore the original incidence, or $\frac{\partial C_M}{\partial \alpha} < 0$, where C_M = pitching moment coefficient and α = angle of incidence. This condition can be achieved by using a tandem foil system with the hinge being positioned forward of the neutral point of the combination. (The neutral point is defined as that point at which $\frac{\partial C_M}{\partial \alpha} = 0$.)

With subcavitating hydrofoils operating between zero lift and near stall (or inception of cavitation), both $\frac{\partial C_M}{\partial \alpha}$ and $\frac{\partial C_L}{\partial \alpha}$ are nearly constant. With a supercavitating foil this is not so. There are three distinct flow regimes. At small incidences the foil will be fully wetted (except at the blunt trailing edge). As incidence is increased further, a small cavitation bubble will start on the upper surface at the sharp leading edge and spread toward the trailing edge. Further incidence increase will produce a fully cavitated foil with the whole upper surface dry. The regime under which the foil is operating at any given moment will depend on incidence, cavitation number, submergence and ventilation.

The effects of transferring from one regime to another result in extreme non-linearities are shown in Figure 4-10. (C_N = normal force coefficient and $C_{M_{LE}}$ = moment coefficient about the leading edge.)

To make an approximate estimate of typical characteristics of a supercavitating kite foil arrangement, the configuration shown in Figure 4-9 was assumed. The aft foil was displaced below the main fore foil to avoid the aft foil becoming submerged in the cavity from the fore foil.

$$C_{N_1} c_1^2 k_H + C_{M_1} c_1^2 - C_{N_2} c_2 c_1 (1 - k_H) + C_{M_2} c_2^2 = 0 \qquad (4\text{-}20)$$

where

C_{N_1}, C_{N_2} = normal force coefficients of fore and aft foils respectively

C_{M_1}, C_{M_2} = moment coefficients of fore and aft foils respectively

c_1, c_2 = chords of fore and aft foils respectively

or if $r \triangleq \frac{c_2}{c_1}$, then Equation (4-20) becomes

$$C_{M_{TOT}} = C_{N_1} k_H + C_{M_1} - C_{N_2} r (1-k_H) + C_{M_2} r^2 = 0 \qquad (4\text{-}21)$$

where C_{N_1} and C_{M_1} are functions of α_1 and C_{N_2} and C_{M_2} functions of α_2.

The only interference effect assumed between the foils is the influence of the fore foil on the incidence of the aft foil.

It was assumed that

$$\alpha_2 = \beta \alpha_1 + \eta \qquad (4\text{-}22)$$

where β is some constant $0 < \beta < 1.0$ and η is defined as in Figure 4-9. Differentiating Equation 4-21 with respect to α_1 gives .

$$\frac{dC_{M_{TOT}}}{d\alpha_1} = k_H \frac{dC_{N_1}}{d\alpha_1} + \frac{dC_{M_1}}{d\alpha_1} - \left\{ r(1-k_H) \frac{dC_{N_2}}{d\alpha_2} - r^2 \frac{dC_{M_2}}{d\alpha_2} \right\} \frac{d\alpha_2}{d\alpha_1} \qquad (4\text{-}23)$$

For positive static stability $\frac{dC_{M_{TOT}}}{d\alpha_1} < 0$ when η is held constant.

Thus, Equation (4-23) becomes:

$$\left[\frac{dC_{M_{TOT}}}{d\alpha_1}\right]_{\eta = \text{constant}} = k_H \frac{dC_{N_1}}{d\alpha_1} + \frac{dC_{M_1}}{d\alpha_1} - \beta r \left\{ (1-k_H) \frac{dC_{N_2}}{d\alpha_2} - r \frac{dC_{M_2}}{d\alpha_2} \right\} < 0 \qquad (4\text{-}24)$$

When η is varied to satisfy Equation 4-21 (i. e., maintain equilibium) its derivative, with respect to α_1, becomes

$$\frac{dC_{M_{TOT}}}{d\alpha_1} = k_H \frac{dC_{N_1}}{d\alpha_1} + \frac{dC_{M_1}}{d\alpha_1} - \left(\beta + \frac{d\eta}{d\alpha_1}\right) \left\{ r(1-k_H) \frac{dC_{N_2}}{d\alpha_2} - r^2 \frac{dC_{M_2}}{d\alpha_2} \right\} = 0 \qquad (4\text{-}25)$$

$$\left[\frac{dC_{M_{TOT}}}{d\alpha_1}\right] = \left[\frac{dC_{M_{TOT}}}{d\alpha_1}\right]_{\eta = \text{constant}} - r\,\frac{d\eta}{d\alpha_1}\left\{(1-k_H)\,\frac{dC_{N_2}}{d\alpha_2} - r\,\frac{dC_{M_2}}{d\alpha_2}\right\} = 0 \qquad (4\text{-}26)$$

or

$$\left[\frac{dC_{M_{TOT}}}{d\alpha_1}\right] = \left[\frac{dC_{M_{TOT}}}{d\alpha_1}\right]_{\eta = \text{constant}} - r\,\frac{d\eta}{dC_{N_{TOT}}}\,\frac{dC_{N_{TOT}}}{d\alpha_1}\left\{(1 - k_H)\,\frac{dC_{N_2}}{d\alpha_2} - r\,\frac{dC_{M_2}}{d\alpha_2}\right\} = 0 \qquad (4\text{-}27)$$

Where the total normal force coefficient is defined by

$$C_{N_{TOT}} \equiv \frac{C_{N_1}\,c_1 + C_{N_2}\,c_2}{c_1 + c_2} = \frac{C_{N_1} + rC_{N_2}}{1 + r} \qquad (4\text{-}28)$$

In Equation 4-27 $\dfrac{dC_{N_{TOT}}}{d\alpha_1}$ is always positive.

The pitching moment about the hinge due to the rear foil is

$$M_\eta = -C_{N_2}\,c_2\,g\,(1 - k_H)\,c_1 + C_{M_2}\,c_2^{\,2}g$$

$$= -g\,c_1^{\,2}\,r\left\{(1 - k_H)\,C_{N_2} - C_{M_2}\,r\right\} \qquad (4\text{-}29)$$

Differentiating Equation 4-29 with respect to α_2 gives

$$\frac{dM_\eta}{d\alpha_2} = -g\, c_1^{\,2}\, r \left\{ (1 - k_H) \frac{dC_{N_2}}{d\alpha_2} - r \frac{dC_{M_2}}{d\alpha_2} \right\} \tag{4-30}$$

$\frac{dM_\eta}{d\alpha_2}$ is always negative for a foil aft of the hinge so that

$\left\{ (1 - k_H) \frac{dC_{N_2}}{d\alpha_2} - r \frac{dC_{M_2}}{d\alpha_2} \right\}$ must always be positive.

Thus, in Equation 4-27, $\frac{dC_{N_{TOT}}}{d\eta}$ must be negative to provide positive stability, i.e., to insure that $\frac{dC_{M_{TOT}}}{d\alpha_1} < 0$.

Using the data plotted in Figure 4-10 for a 10-degree wedge foil (extracted from California Institute of Technology Report 47-6) for both foils in Equations 4-21 and 4-23 (assuming $\beta = 0.4$) resulted in the curves shown in Figures 4-11 and 4-12. The regions of these curves in which $\frac{dC_{N_{TOT}}}{d\eta} > 0$ then clearly imply, from Equation 4-28 that the system is statically unstable. For example, with $k_H = 0.35$ and $r = 0.3$ the ranges $-0.05 < C_{N_{TOT}} < 0.05$ and $0.18 < C_{N_{TOT}} < 0.264$ cannot be achieved with any fixed flap angle (η). (See Figure 4-11.)

4.5.2 CONCLUSIONS

The basic kite foil concept requires that high-frequency disturbances due to wave orbital motions will be substantially attenuated, leaving

the autopilot with the relatively low-frequency duties associated with the maintenance of stability and control. Thus, although it is possible to make kite foils run in the unstable range (see Figure 4-11, $k_H = 0.30$ and 0.35) by the use of a tight loop, this contravenes the basic concept.

It is necessary, therefore, to choose a hinge position giving positive static stability over the whole required incidence range; i.e., a hinge position $k_H < 0.25$ as evident in Figure 4-11.

However, as the hinge position is moved forward, the overall foil normal force coefficient $C_{N_{TOT}}$ diminishes due to the down load on the rear foil. In Figure 4-12 the normal force performance of the kite foils is compared with a single rigid foil of the same total chord. Thus, for a given submerged foil area, the lift available will be substantially below that of a rigid foil when the hinge has been positioned to give marginal stability.

The autopilot would control the craft via the rear foil angle, η, and the extreme variations in $dC_{M_{TOT}}/d\eta$ would represent an added design problem.

The dynamic performance is partly dependent on $\frac{dC_{M_{TOT}}}{d\alpha_1}$ and $\frac{dC_{M_{TOT}}}{d\eta}$, both of which vary greatly with incidence, so that the dynamic response will vary widely with $C_{N_{TOT}}$, i.e., with craft speed.

From a practical viewpoint, the drag associated with the rear foil support brackets and hinge fairing would further reduce the foil lift-drag ratio.

It may thus be concluded that the kite foil is not practical where serious hydrodynamic non-linearities are present. This does not preclude the possibility of successful employment on subcavitating craft.

4.6 DETAILED STUDY OF SPRUNG FOIL PERFORMANCE

In this section the following studies have been made:

(1) Studies similar to those in Section 4.2 but with a foil more typical of the high speed test craft.

(2) Investigations with hydraulic foil attitude control to restrain low frequency spring deflections.

(3) Study of the response to the orbital motion disturbance of a State 3 head sea.

(4) Investigations with spring self-centering and height control.

4.6.1 EQUATIONS OF MOTION

The foil is assumed mounted as in Figure 4-1a except that foil angular displacement (or attitude variation) η and a controllable portion of spring reaction R_C are included.

Thus, as in Section 4.2.1, Equation 4-1,

$$\left.\begin{aligned} m_H s^2 h_H(s) &= -R(s) \\ m_F s^2 \left\{ h_H(s) + \xi(s) \right\} &= R(s) - F(s) \end{aligned}\right\} \qquad (4\text{-}31)$$

Now, however, instead of Equations 4-2 and 4-4

$$R(s) = -K\,\xi(s) + R_C(s) \qquad (4\text{-}32)$$

$$F(s) = \frac{\rho}{2} \mu^2 S \left\{ C_{N_h}(s) + C_{N_\eta}(s) \right\} \tag{4-33}$$

It is assumed in Equation 4-32 that R_C is capable of being included in a control loop. Physically this situation could be closely approximated by a pneumatic spring where the supply of extra air to (or the valving of air from) the high pressure side can provide variation in R_C.

In Equation 4-33 the hydrodynamic normal forces are split into those associated with the heaving of the foil and those associated with the (flap or foil attitude) control.

The heaving contributions to normal force coefficient perturbations are of the form

$$C_{N_h} = Bs \frac{(1 + \beta s)}{(1 + \gamma s)} \left\{ \xi(s) + h_H(s) - \frac{w_{OM}(s)}{s} \right\} \tag{4-34}$$

The term $(1 + \gamma s)$ is included to give a closer approximation to the data of Reference 4-1 than was given by Equation 4-5. However, it has proved to have little practical significance.

The flap or foil attitude quantity η was assumed to vary at sufficiently low frequency for a simple linear relationship to be legitimate.

$$C_{N_\eta}(s) = D\eta(s) \tag{4-35}$$

Combining Equations 4-31, 4-32, 4-33, 4-34, and 4-35 gives

$$\xi(s) = \frac{R_C(s)\left\{1 + \left(\frac{m_H}{k_M E} + \beta\right)s + \frac{\gamma m_H}{k_M E} s^2\right\} - \eta(s)\frac{m_H G s}{E}(1 + \gamma s) + w_{OM}(s)\, m_H s(1 + \beta s)}{K\left\{1 + \left(\frac{m_H}{k_M E} + \beta\right)s + m_H\left(\frac{\gamma}{k_m E} + \frac{1}{K}\right)s^2 + \frac{m_H}{K}\left(\frac{m_F}{E} + \beta\right)s^3\right\}} \tag{4-36}$$

Where

$$E = \frac{\rho}{2} S \mu^2 B \qquad G = \frac{\rho}{2} S \mu^2 D \qquad k_M = \frac{m_H}{m_F + m_H}$$

Then hull displacement can be obtained from Equation 4-31 (1st equation) and Equation 4-32.

$$h_H(s) = \frac{1}{m_H s^2} \left\{ K \xi(s) - R_C(s) \right\} \tag{4-37}$$

The following special cases can be obtained from Equations 4-31, 4-36 and 4-37

(1) Zero hull heave

$$\xi(s) = \frac{R_C(s)(1+\gamma s) - \eta(s) G (1+\gamma s) + w_{OM}(s) E (1+\beta s)}{K\left\{1 + \left(\gamma + \frac{E}{K}\right)s + \left(\frac{m_F + \beta E}{K}\right)s^2\right\}}$$

(2) Rigidly mounted foil ($K = \infty$)

$$h_H(s) = \frac{w_{OM}(s)(1+\beta s) - \eta(s)\frac{G}{E}(1+\gamma s)}{s\left\{1 + \left(\frac{m_T}{E} + \beta\right)s + \frac{m_T \gamma}{E} s^2\right\}}$$

Where $m_T = m_H + m_F$.

(3) Zero stiffness spring (K = 0)

$$\xi(s) = \frac{R_C(s)\left\{1 + \left(\frac{m_H}{k_M E} + \beta\right)s + \frac{\gamma m_H}{k_M E}\, s^2\right\} - \eta(s)\, \frac{m_H G s}{E}\,(1 + \gamma s) + w_{OM}(s)\, m_H s(1 + \beta s)}{m_H s^2\left\{1 + \left(\frac{m_F}{E} + \beta\right)s\right\}}$$

4.6.2 FOIL CONFIGURATION AND HYDRODYNAMICS

The foil was assumed to carry a steady-state load of 13,000 pounds (roughly one-third the estimated weight of the high speed test craft) at a lift coefficient of 0.2 and a speed μ = 80 knots. (C_L = 0.2 was chosen in an effort to ensure operation with a fully cavitated upper foil surface although final foil section and planform, chosen after this was completed, results in a C_2 of approximately 0.1.)

Then foil area S = 3.576 ft^2

If aspect ratio is 3, then span b = 3.275 feet and chord C = 1.092 feet.

Assume mass of foil and associated strut m_F = 5 slugs. From assumed load of 13,000 pounds m_H = 403.73 slugs.

Thus k_M = 0.9878 and m_T = 408.73 slugs.

Difficulty arises in choosing the hydrodynamic quantities B, β, γ since the unsteady force data of Reference 4-1 is only given for two-dimensional supercavitating surfaces. Subcavitating data suggest that the effects of finite aspect ratio diminish as frequency increases. Assuming this to be the case with supercavitating foils and allowing for the fact that induced downwash effects are smaller on supercavitating foils due to their small lift curve slope, and that surface proximity tends to increase lift curve slope, then the slightly pessimistic two-dimensional values were chosen.

Thus $B = \frac{\pi}{2u} = 0.01162$ sec/ft

$\beta = 0.005523$ sec $\quad \gamma = \frac{58.53}{10^6}$ sec

Then $E = \frac{\rho}{2} s u^2 B = 755.6$ slugs/sec

Consistent with a fully rotatable foil $D = 1.1$

Then $G = 71,500$ lb/rad

Substituting these quantities in Equation 4-36 gives

$$\xi(s) = \frac{R_C(s)\left\{1 + 0.5466s + 31.67\times10^{-6}s^2\right\} - \eta(s)\ 38,215s(1 + 58.32\times10^{-6})}{K\left\{1 + 0.5466s + (31.67\times10^{-6} + \frac{403.73}{K}s^2 + \frac{4.902}{K}s^3\right\}}$$

$$+ \frac{w_{OM}(s)\ 403.73S\ (1 + 0.005523s)}{K\left\{1 + 0.5466s + (31.67\times10^{-6} + \frac{403.73}{K}s^2 + \frac{4.902}{K}s^3\right\}} \quad (4\text{-}38)$$

4.6.3 RESPONSE OF FOIL TO ORBITAL MOTION INPUT

The spring deflection response (Equation 4-38 with $R_C(s) = \eta(s) = 0$) to orbital motion encounter frequency for spring stiffness $K = 0$, 200, 1000 and 5000 lb/ft is shown in Figure 4-13. The corresponding hull reactions are given in Figure 4-14.

Resonance effects occur with all three non-zero values of finite spring stiffness, the peaking of spring deflection ξ becoming more pronounced as spring stiffness K is reduced. At the peak resonance point the foil heave is zero. However, the presence of slight damping associated with hull aerodynamics and the spring would probably reduce this resonance effect. The resonance frequency is, in all cases, low and may

be substantially eliminated by a simple loop in which spring deflection controls foil attitude. This is discussed in the next section.

The spring is most effective in reducing reactions on the hull at the higher frequencies where it would be most difficult to provide an effective accelerometer controlled loop. Of the four spring stiffnesses investigated, an approximation to K = 0, such as K = 200 requires an excessively large volume of entrapped high pressure air* (assuming a pneumatic spring); K = 5000 gives little attenuation over an important part of the power spectrum of a State 3 Sea (see Figure 4-18) so that a value of K = 1000 lb/ft was chosen as the most promising value for further consideration.

It is apparent, apart from the low frequency resonance already discussed, that the system is well damped by the hydrodynamic forces.

For K = 1000 the spring deflection is small everywhere; even at the resonant frequency of $\omega = 1.55$ rad/sec the spring deflection is only ± 0.750 ft per ft/sec of orbital motion. At $\omega = 10$ rad/sec the spring deflection has diminished to ± 0.1 ft per ft/sec of orbital motion.

4.6.4 FOIL ATTITUDE CONTROL LOOP PRODUCING A REDUCTION IN LOW FREQUENCY SPRING DEFLECTION

It has been shown that the heaving foil substantially attenuates the reactions transmitted to the hull (compared with the rigid strut) except in the very low frequency range (below $\omega = 2.3$ for K = 1000 lb/ft). This section is concerned with the design of a simple mechanical foil attitude control loop to give a useful attenuation of hull reactions in this low frequency range.

*Assuming the entrapped air is at a pressure of 1000 lb/in^2 above ambient, then piston diameter = 4.007 in. The volume of entrapped air is 8.34, 1.67 and 0.333 ft^3 for K = 200, 1000 and 5000 lb/ft respectively (See Section 11).

The relevant part of Equation 4-36 ($R_C(s) = 0$) is

$$\xi(s) = \frac{w_{OM}(s)\, m_H s (1 + \beta s) - \eta(s) \dfrac{m_H G s}{E} (1 + \gamma s)}{K\left\{1 + \left(\dfrac{m_H}{k_M E} + \beta\right)s + m_H\left(\dfrac{\gamma}{k_M E} + \dfrac{1}{K}\right)s^2 + \dfrac{m_H}{K}\left(\dfrac{m_F}{E} + \beta\right)s^3\right\}} \quad (4\text{-}39)$$

It was assumed that the foil attitude is varied by moving the whole strut about a pivot at its point of attachment to the hull. This avoids the drag associated with the housing of a hinge below the water, the drag penalty resulting from flap deflection, and the loss of control that would result from the flap moving into the cavity.

The strut length from the hinge point to the foil was assumed to be 7 feet and the inertia about the hinge of the strut and foil 180 slugs ft^2.

A hydraulic jack mounted 2 feet below the hinge with a total travel of 0.7 foot gives a foil attitude range of 20 degrees. A 1-inch diameter jack provides a hydromechanical natural frequency of 138.2 rad/sec.

Supercavitating foils produce resultant forces whose direction changes only slightly with incidence. Thus, by mounting the foil such that this resultant force passes close to the hinge at the top of the strut, little steady-state load on the jack would arise.

The hydraulic damping may be controlled independently by the choice of hydraulic valve, so that a damping coefficient of $\xi = 0.4$ was assumed. The resulting transfer function (jack displacement/input displacement command) is

$$H(s) = \frac{1}{1 + 0.005787s + 52.33 \times 10^{-6} s^2} \quad (4\text{-}40)$$

The simplest possible regulating relationship between $\eta(\ )$ and $\xi(\ )$ was chosen

$$\eta(s) = C_\eta \, H(s) \, \xi(s) \tag{4-41}$$

where C_η is a simple gain to be determined.

The resulting frequency responses are plotted in Figures 4-15, 4-16, and 4-17. It is obvious that a substantial improvement has been achieved. For $C_\eta = 0.1$, the peak reaction on the hull has been reduced by about 18 db and 14.5 db relative to the open loop and rigid strut cases respectively.

A comparison of two closed loop cases with a rigid strut ($K = \infty$) are included in Figure 4-16 to demonstrate the importance of the spring in the closed loop case.

For these cases

$$\eta(s) = - \overline{C}_\eta \, R(s) \, H(s) \, C(s) \tag{4-42}$$

where $\overline{C}_\eta$ is the equivalent of C_η for the unsprung case

where $C(s)$ is the compensation

$C(s) = 1$ for $\overline{C}_\eta = 0.5 \times 10^{-5}$

$C(s) = \dfrac{1 + s/16.57}{1 + s/96.57}$ for $C_\eta = \dfrac{1}{3} \times 10^{-4}$

The compensation was employed to improve the poor performance of the uncompensated case. It is probable that the compensation is not optimum; however, the results in the unsprung condition are so far short

of satisfactory that it may reasonably be assumed that the sprung system with closed loop will be superior, especially at higher frequencies.

The effect of closing the loop on spring deflection is substantial. For example for w_{OM} = sin 1.6 t

$\lvert\xi\rvert_{max}$	= 0.750 ft	C_η	= 0
	= 0.0912 ft		= 0.1
	= 0.0490 ft		= 0.2
	= 0.0143 ft		= 0.5

Except for C_η = 0.5, these represent maximum spring deflections, all other frequencies giving smaller spring deflection responses. It can be safely assumed that spring deflections will not significantly increase the probability of foil broaching compared with the normal rigid strut case.

The foil attitude variations associated with the closed loop are also very small. Again for w_{OM} = sin 1.6 t

$\lvert\eta\rvert_{max}$	= 0.523 deg	C_η	= 0.1
	= 0.554 deg		= 0.2
	= 0.580 deg		= 0.5

Except for C_η = 0.5, these are maximum values, all other frequencies giving smaller responses.

4.6.5 RESPONSE TO A STATE 3 HEAD-SEA

Hull reaction attenuation has thus been studied without any consideration of the excitation spectrum over which attenuation is required.

It is desirable that the high speed test craft be capable of traversing a State 3 Sea at 80 knots. Eighty knots far exceeds the propagation velocity of those frequency components constituting the majority of the energy of a State 3 Sea. Thus the power spectra of head or stern seas will not differ greatly as seen from the craft. Beam seas will give low frequency spectra representing no significant test of the improvement in riding comfort provided by the sprung foil system. Therefore this present section has been restricted to a head sea.

The Neumann spectrum of the sea surface (see Reference 4-2) is

$$\left[A(\omega_o)\right]^2 = \frac{51.6}{\omega_o^6} e^{\frac{-2g^2}{u_w^2 \omega_o^2}} \quad ft^2/rad/sec \qquad (4\text{-}43)$$

where ω_o (rad/sec) is the wave encounter frequency as seen by an observer stationary in relation to the sea.

u_w is an equivalent wind speed (16 knots = 27.0 ft/sec per State 3 Sea)

Equation 4-43 can be written in terms of surface perturbation relative to mean surface level as

$$\left[H_o(\omega_o)\right]^2 = \frac{1}{2}\left[A(\omega_o)\right]^2 = \frac{25.8}{\omega_o^6} e^{\frac{-2g^2}{u_w^2 \omega_o^2}} \qquad (4\text{-}44)$$

Now surface orbital motion can be approximated in terms of surface perturbation and frequency as $w_{(OM)} = h\omega_o$

Thus the surface orbital motion becomes

$$\left[W_o(\omega_o)\right]^2 = \frac{25.8}{\omega_o^4} e^{\frac{-2g^2}{u_w^2 \omega_o^2}} \qquad (4\text{-}45)$$

However, the foil is not working at the surface but at some depth below it. The attenuation factor being

$$\frac{w_{(OM)}}{w_{(OM)_o}} = e^{\frac{-\zeta \omega_o^2}{g}} \tag{4-46}$$

Then the power spectrum of the orbital motion below the surface becomes

$$\left[W_{(\omega_o)}\right]^2 = \frac{25.8}{\omega_o^4} e^{-\left(\frac{2g^2}{u^2 w \omega_o^2} + \frac{2\zeta\omega_o^2}{g}\right)} \tag{4-47}$$

It is required to express the power spectrum of orbital motion in terms of encounter frequency ω_e. For a head sea this relationship is

$$\omega_e = \omega_o \left(1 + \frac{u\,\omega_o}{g}\right) \tag{4-48}$$

and conversely

$$\omega_o = \frac{g}{2u}\left(-1 + \sqrt{1 + \frac{4\,\omega_o u}{g}}\right) \tag{4-49}$$

Thus, in terms of encounter frequency, the power spectrum becomes

$$\left[W(\omega_e)\right]^2 = \left[W(\omega_o)\right]^2 \frac{d\,\omega_o}{d\,\omega_e} \qquad -\left(\frac{2g^2}{u^2 w_o^2} + \frac{2\zeta\omega_o^2}{g}\right) \tag{4-50}$$

$$= \frac{25.8\,e}{\omega_o^4\left(1 + \frac{2u\,\omega_o}{g}\right)}$$

where ω_o is obtained from Equation 4-49.

From Equation 4-50 the mean-square orbital motion velocity is

$$\overline{w^2_{OM}} = \int_0^\infty \left[W(\omega_e)\right]^2 \, d\,\omega_e \tag{4-51}$$

At u = 80 knots = 135.168 ft/sec and submergence $\mathcal{S}$ = 2 feet, and for a State 3 Sea u_W = 16 knots = 27.036 ft/sec, Equations4-50 and 4-49 become

$$\left[W(\omega_e)\right]^2 = \frac{25.8 \; e^{-\left(\frac{2.837}{\omega_o^2} + 0.1242\,\omega_o^2\right)}}{\omega_o^4\,(1 + 8.396\,\omega_o)} \quad ft^2/sec^2/rad/sec \tag{4-52}$$

$$\omega_o = 0.1191\left(-1 + \sqrt{1 + 16.791\,\omega_e}\right) \tag{4-53}$$

The corresponding power spectrum of orbital motion is plotted in Figure 4-18.

The hull root mean square acceleration is given by

$$\left.\begin{aligned} \sqrt{\overline{\ddot{h}_M^2}} &= \frac{\sqrt{\overline{R^2}}}{m_H} \quad ft/sec^2 \\ \overline{R^2} &= \int_0^\infty \left[W(\omega_e)\right]^2 \left|\frac{R(j\omega_e)}{w_{OM}(j\omega_e)}\right|^2 \, d\,\omega_e \quad lb^2 \end{aligned}\right\} \tag{4-54}$$

The results are shown in Table 4-1.

Table 4-1

$K = \infty$	$C_\eta = 0$	$\sqrt{\overline{h_H^2}} = 2.336$ ft/sec^2	$\sqrt{\overline{\xi^2}} = 0$
$= 1000$ lb/ft	$= 0$	$= 0.518$ ft/sec^2	$= 0.209$ ft
$= 1000$ lb/ft	$= 0.1$ ft^{-1}	$= 0.234$ ft/sec^2	$= 0.095$ ft

The foil being considered in the foregoing computations has a steady state $C_L = 0.2$. Root mean square hull acceleration will be proportional to the reciprocal of the steady-state lift coefficient (other parameters remaining unchanged). Thus, the data obtained on the high speed test craft implying a steady state $C_L = 0.1$ would approximately double these values of RMS hull acceleration.

The spring deflections for K = 1000 lb/ft, $C_\eta = 0.1$ ft^{-1} are such that the 3σ value, covering 99.7 percent of all deflections for a State 3 Sea at 80 knots, is only $\pm$ 0.284 ft. The most important shortcoming of the sprung foil, the aggravation of foil broaching by foil heave, has been substantially eliminated.

Figure 4-19a shows the power spectra of the reactions on the hull for the rigid strut, the sprung strut, and the sprung strut with foil attitude control loop.

To illustrate the attenuation of the infinitesimal sinusoidal components of the reaction on the hull, the square roots of the power spectra coordinates are plotted on a db basis (see Figure 4-19b).

4.6.6 SYSTEM BEHAVIOR WITH PNEUMATIC CONTROL FOR SPRING SELF CENTERING AND FOIL ATTITUDE INPUTS FOR FOIL DEPTH CONTROL

The system thus far is adequate with respect to the perturbation of orbital motions. However, two other requirements are necessary to fulfill the minimum needs of a control system.

These are:

(a) A self-centering control for the spring

(b) A mean depth control loop.

System (a) is necessary to compensate for changes in craft weight and CG location (variation in fuel and payload).

System (b) is necessary to maintain the correct mean depth of submergence of the forward foils and may be supplied by the autopilot or, in emergency mode, by the operator.

A. Self-Centering System

The spring is assumed to be pneumatic with self-centering accomplished by valving air into or out of the high pressure chamber above the piston. If the piston is prevented from moving, a constant steady-state spring deflection ξ would result. If the flow rate of air in'o (or out of) the high pressure chamber is made proportional to ξ then an approximate integration results.

Thus, let

$$R_C(s) = \frac{-k_R}{S} \xi(s) \qquad (4\text{-}55)$$

where k_R is a suitable constant

Substitution of Equation 4-55 in Equation 4-32 gives the total reaction applied to the hull as

$$R(s) = -\xi(s) \left(K + \frac{k_R}{s}\right) \qquad (4\text{-}56)$$

B. Depth Control Loop

The previous foil attitude control relationship (Equation 4-41) is modified to include the effects of a height error signal.

Thus

$$\eta(s) = \left\{ \xi(s)\, C_\eta + (h_H(s) - h_{Ho}(s))\, C_H(s) \right\} H(s) \qquad (4\text{-}57)$$

Where $h_H(s)$ is the hull height

$h_{Ho}(s)$ is the hull height command

$C_H(s)$ is combined compensation and gain in the height loop

$H(s)$ is the transfer function of the hydraulic jack (as before).

The above control loops may be designed to be essentially low frequency in nature since (a) the spring centering is only required to compensate for very gradual changes (in the absence of banked turns which are not anticipated for the high speed test craft) and (b) the depth control is required only to maintain a correct mean hull height and not to contour waves.

Thus, it may reasonably be assumed that the response of the system to orbital motion will remain substantially uneffected and that stability and response to height command are the primary design criteria.

Substitution of Equations 4-55 and 4-57 in Equation 4-36 and omitting orbital motion input gives

$$\xi(s) = \frac{s \left\{ h_{Ho}(s) - h_H(s) \right\} C_H(s)\, F_\eta(s)}{\frac{1}{H(s)} \left\{ s\, D(s) + k_R F_R(s) \right\} + s\, C_\eta\, F_\eta(s)} \qquad (4\text{-}58)$$

where

$$F_\eta(s) = \frac{m_H G s}{E} (1 + \gamma s)$$

$$F_R(s) = 1 + \left(\frac{m_H}{k_M E} + \beta\right) s + \frac{\gamma m_H}{k_M E} s^2$$

$$D(s) = K\left\{1 + \left(\frac{m_H}{k_M E} + \beta\right) s + m_H\left(\frac{\gamma}{k_M E} + \frac{1}{K}\right) s^2 + \frac{m_H}{K}\left(\frac{m_F}{E} + \beta\right) s^3\right\}$$

Now

$$h_H(s) = \frac{-R(s)}{m_H s^2} = \left(\frac{Ks + k_R}{m_H s^3}\right) \xi(s) \qquad (4\text{-}59)$$

Thus from Equations 4-58 and 4-59

$$h_H(s) = \frac{(Ks + k_R)\left\{h_{Ho}(s) - h_H(s)\right\} C_H(s) F_\eta(s)}{m_H s^2 \left[\frac{1}{H(s)}\left\{s D(s) + k_R F_R(s)\right\} + s C_\eta F_\eta(s)\right]} \qquad (4\text{-}60)$$

Values of k_R = 100 and 200 slugs/sec^3 were tried. These values give time constants of 10 and 5 seconds respectively in Equation 4-56 with K = 1000 lb/ft. The height open loop transfer function showed little change between the two so far as magnitude is concerned but a somewhat greater phase lag with the greater value of k_R. Thus it was decided to fix k_R at 100 slugs/sec^3.

A log (magnitude) vs phase plot of the open height loop transfer function showed compensation to be desirable and the final value chosen for $C_H(\ )$ becomes

$$C_H(s) = \frac{1}{200}\left\{\frac{1 + 3.232s}{1 + 0.8594s}\right\} \qquad (4\text{-}61)$$

To check both the stability and response of the complete system to a height command, the hull height response to a unit step input height command was calculated by the frequency response method of Reference 4-3. The result is shown in Figure 4-20; the response is considered reasonable.

This analysis has assumed that the rear foil follows sufficiently rapid that no substantial hull pitch angle develops. Analysis and simulation reported later include pitch attitude effects.

It may be concluded that within the limitations imposed by this single foil analysis, satisfactory longitudinal control incorporating a sprung foil has been achieved.

REFERENCES

4-1. "A Study of the Hydroelastic Instability of Supercavitating Hydrofoils" by Paul Kaplan and C.J. Henry. Stevens Institute of Technology, Report R-838, March 1961.

4-2. "On Wind Generated Wave Motion at Subsurface Sea Levels" by G. Neumann. Transactions of the American Geophysical Union, Vol. 36, p. 985.

4-3. "Analytical Design of Linear Feedback Controls" by G. C. Newton, L. A. Gould, J. F. Kaiser (published by Wiley) p. 333-335.

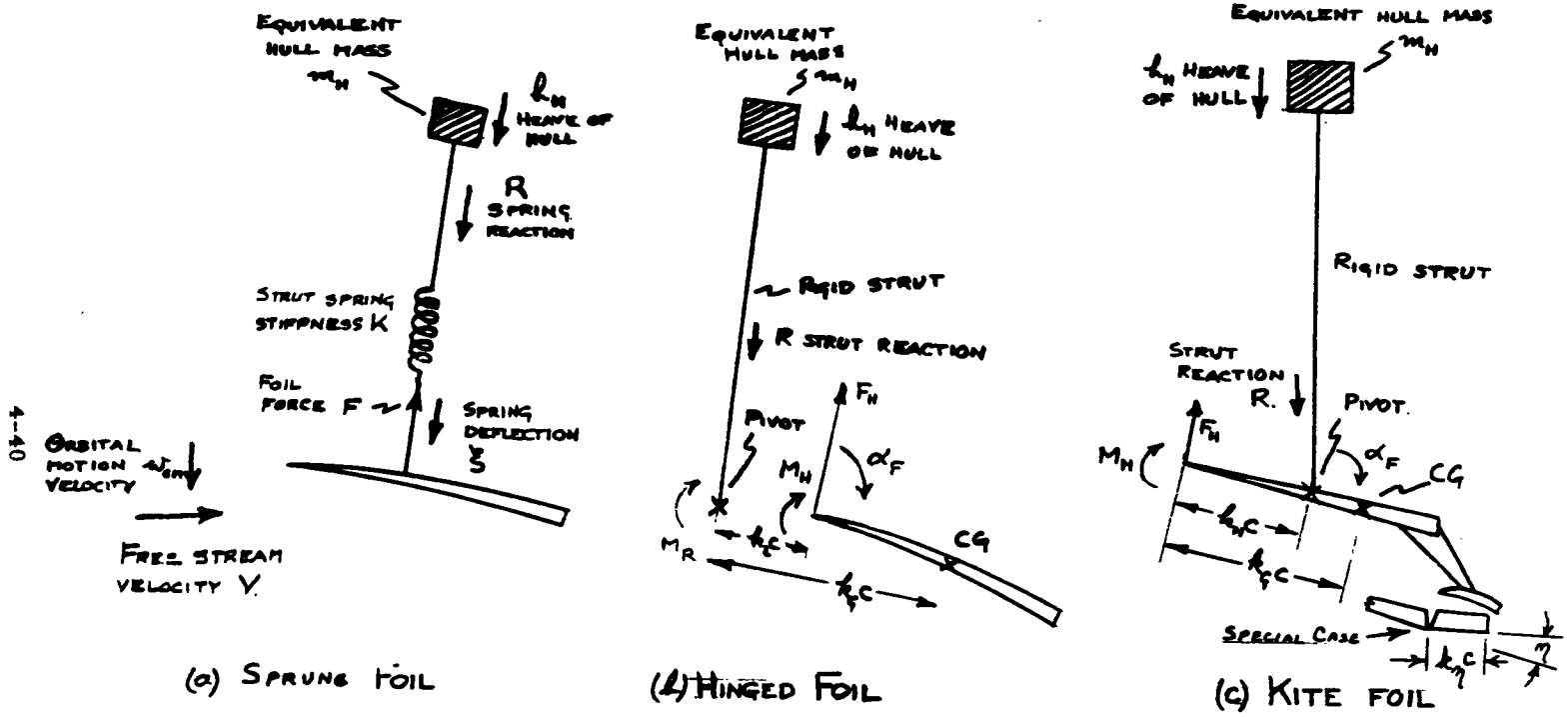
EQUIVALENT HULL MASS m_H
h_H HEAVE OF HULL
R SPRING REACTION
STRUT SPRING STIFFNESS K
FOIL FORCE F
SPRING DEFLECTION ζ
ORBITAL MOTION VELOCITY $\dot{\zeta}_{orb}$
FREE STREAM VELOCITY V
(a) SPRUNG FOIL
EQUIVALENT HULL MASS m_H
h_H HEAVE OF HULL
RIGID STRUT
R STRUT REACTION
PIVOT
F_H
M_H
α_F
M_R
$h_F c$
CG
(b) HINGED FOIL
EQUIVALENT HULL MASS m_H
h_H HEAVE OF HULL
RIGID STRUT
STRUT REACTION R.
PIVOT
F_H
M_H
α_F
CG
$h_H c$
$h_F c$
SPECIAL CASE
$h_\eta c$
η
(c) KITE FOIL

FIG 4-1

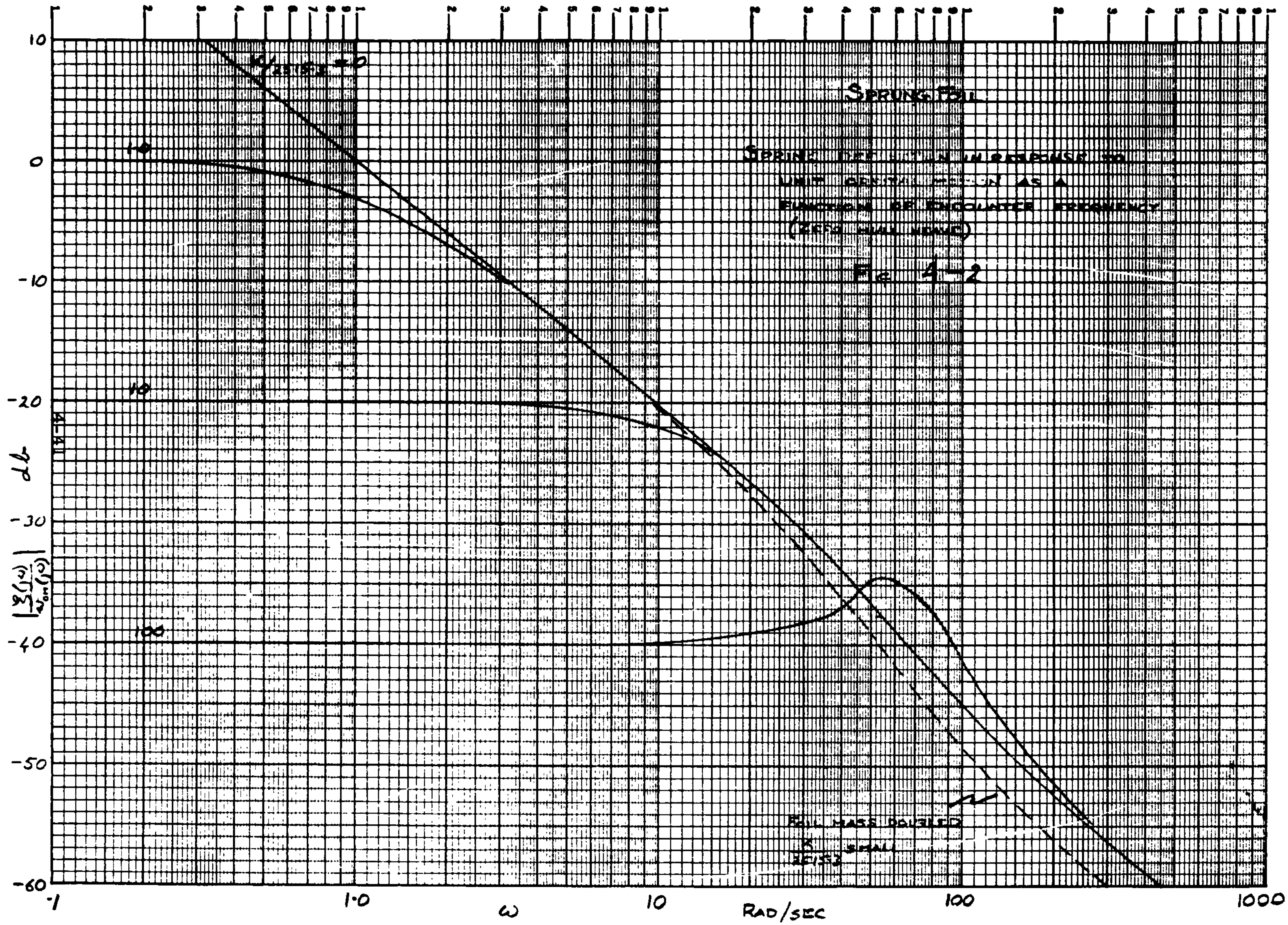
Sprung Foil
Fig 4-2
10
0
-10
-20
-30
-40
-50
-60
db
·1
1·0
10
100
1000
ω
Rad/sec
100
Foil mass doubled

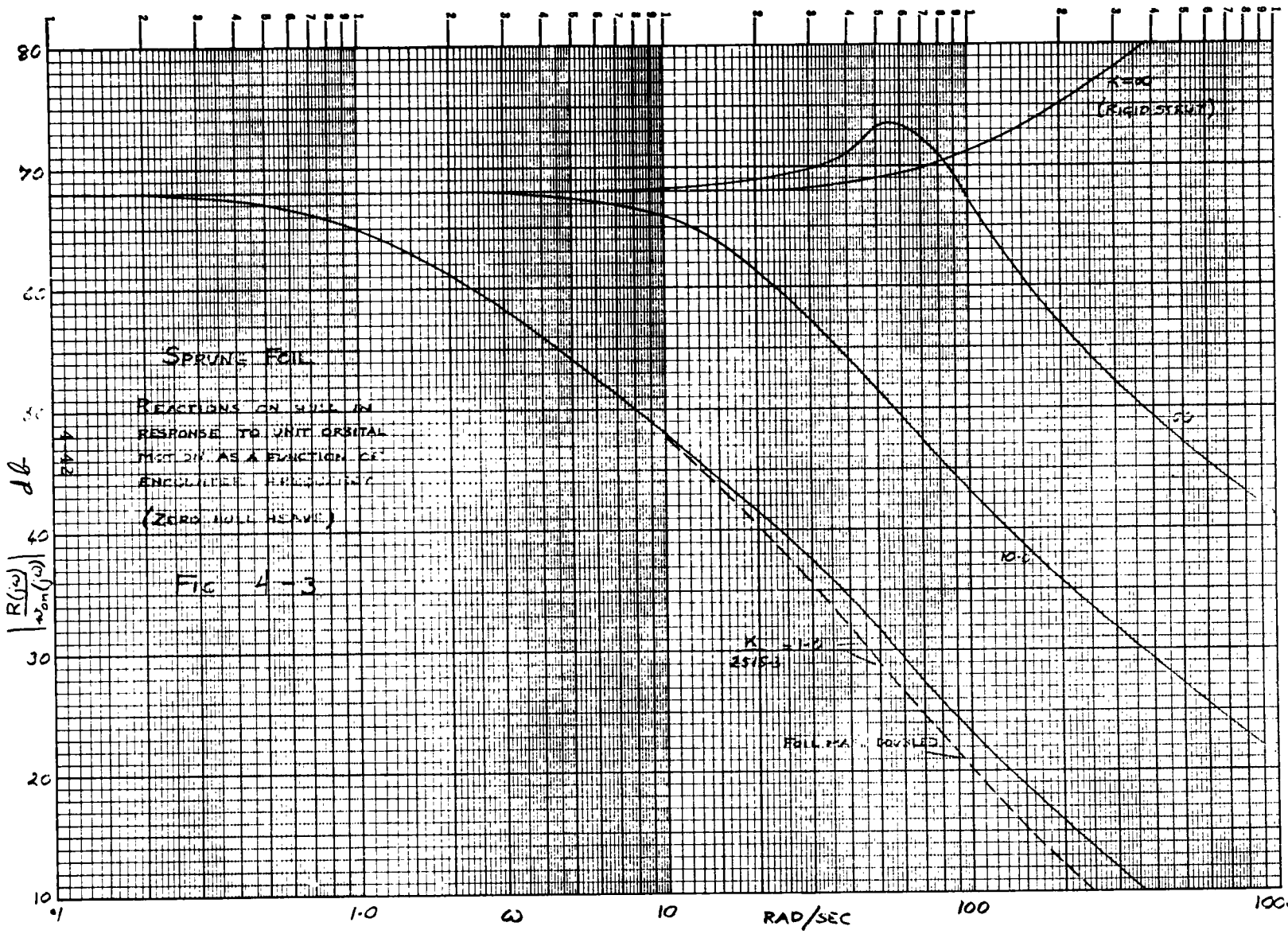
80
70
60
50
40
30
20
10
.1
1.0
ω
10
100
1000
RAD/SEC
dB
$\left|\frac{R(j\omega)}{z_{on}(j\omega)}\right|$
K=∞
(RIGID STRUT)
50
10
K / 25(S+1)
FULL F.A. COUPLED
SPRUNG FOIL
REACTIONS ON HULL IN
RESPONSE TO UNIT ORBITAL
MOTION AS A FUNCTION OF
ENCOUNTER FREQUENCY
(ZERO HULL MASS)
FIG 4-3

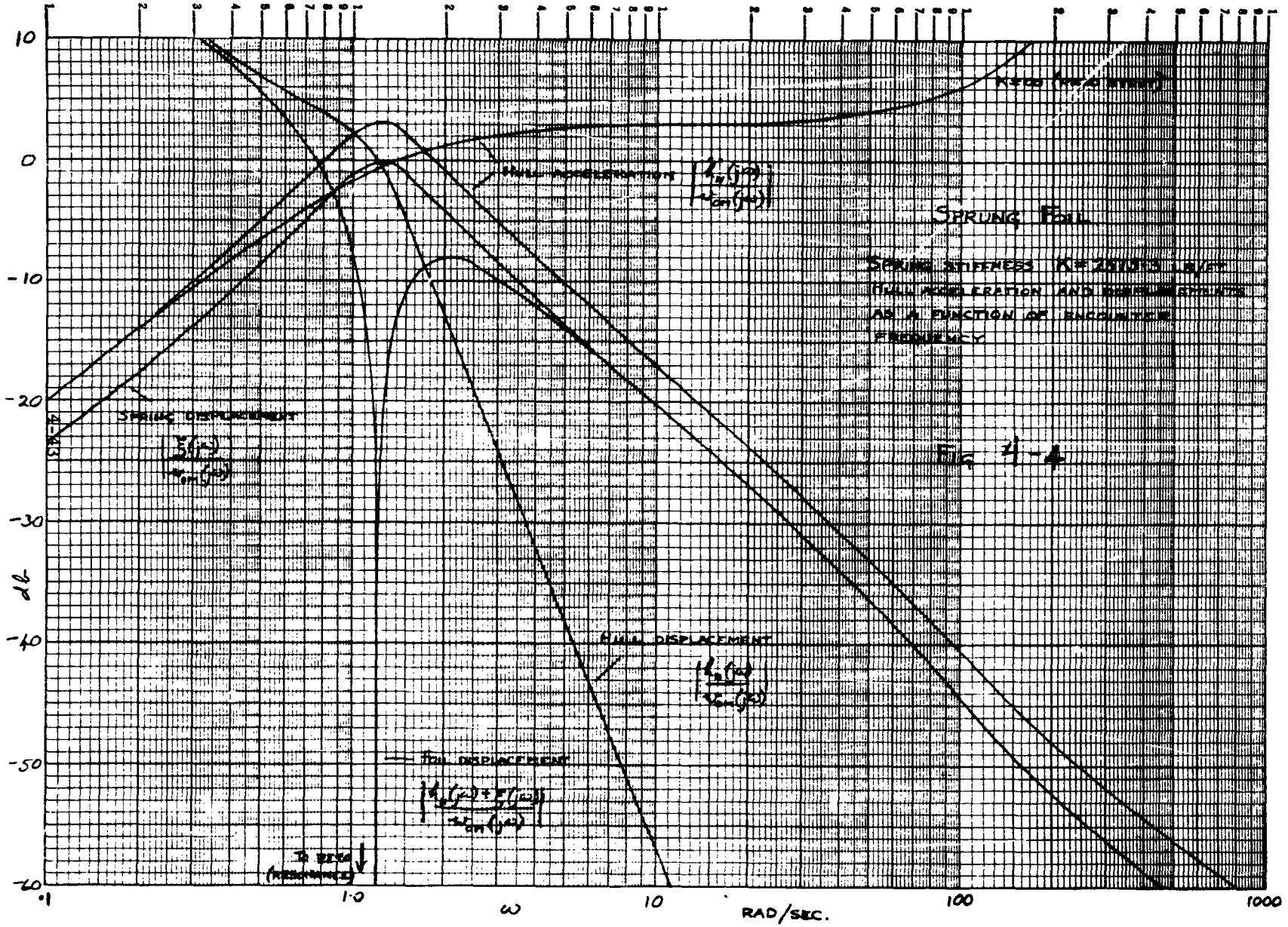
10
0
-10
-20
-30
-40
-50
-60
dB
.1
1.0
10
100
1000
ω
RAD/SEC.
SPRUNG FOIL
SPRING STIFFNESS (K = 2870.3 LB/FT)
HULL ACCELERATION AND DISPLACEMENTS
AS A FUNCTION OF EXCITATION
FREQUENCY
FIG 4-4
HULL ACCELERATION
HULL DISPLACEMENT
SPRING DISPLACEMENT
TOTAL DISPLACEMENT

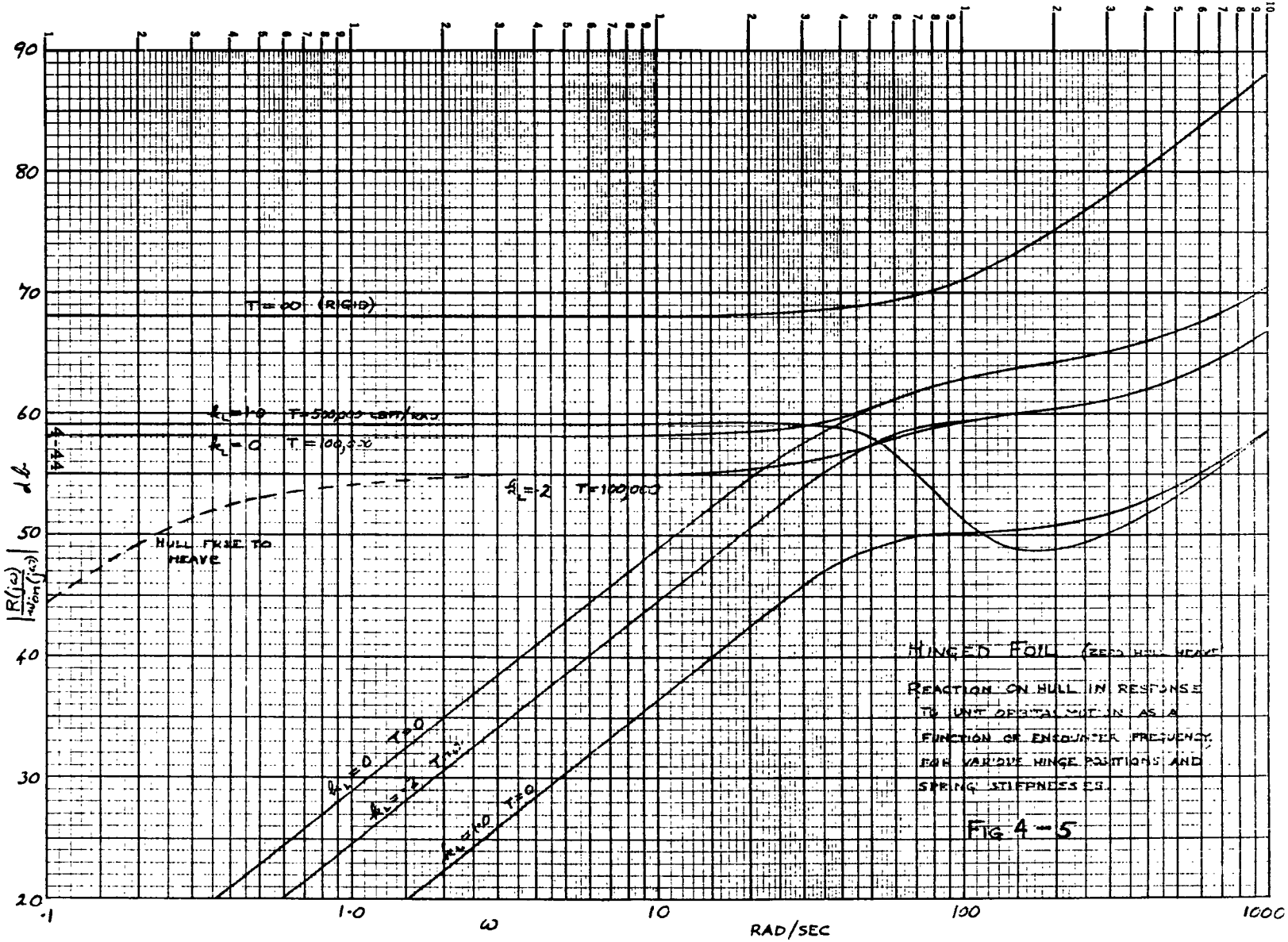

HINGED FOIL (FEED HULL HEAVE)

REACTION ON HULL IN RESPONSE TO UNIT OFFSET INPUT AS A FUNCTION OF ENCOUNTER FREQUENCY FOR VARIOUS HINGE POSITIONS AND SPRING STIFFNESSES.

FIG 4-5

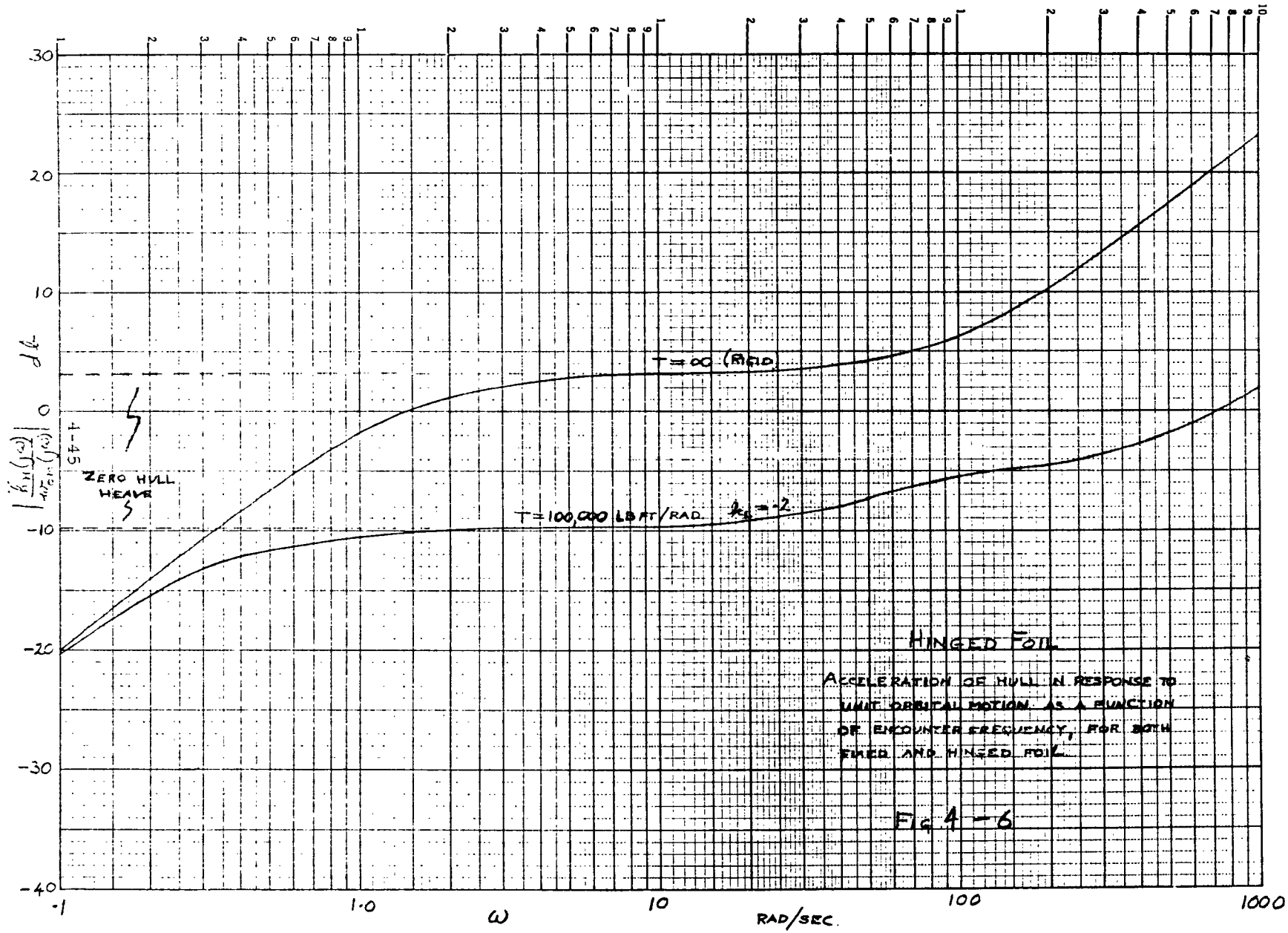

HINGED FOIL

ACCELERATION OF HULL IN RESPONSE TO UNIT ORBITAL MOTION, AS A FUNCTION OF ENCOUNTER FREQUENCY, FOR BOTH FIXED AND HINGED FOIL.

Fig 4-6

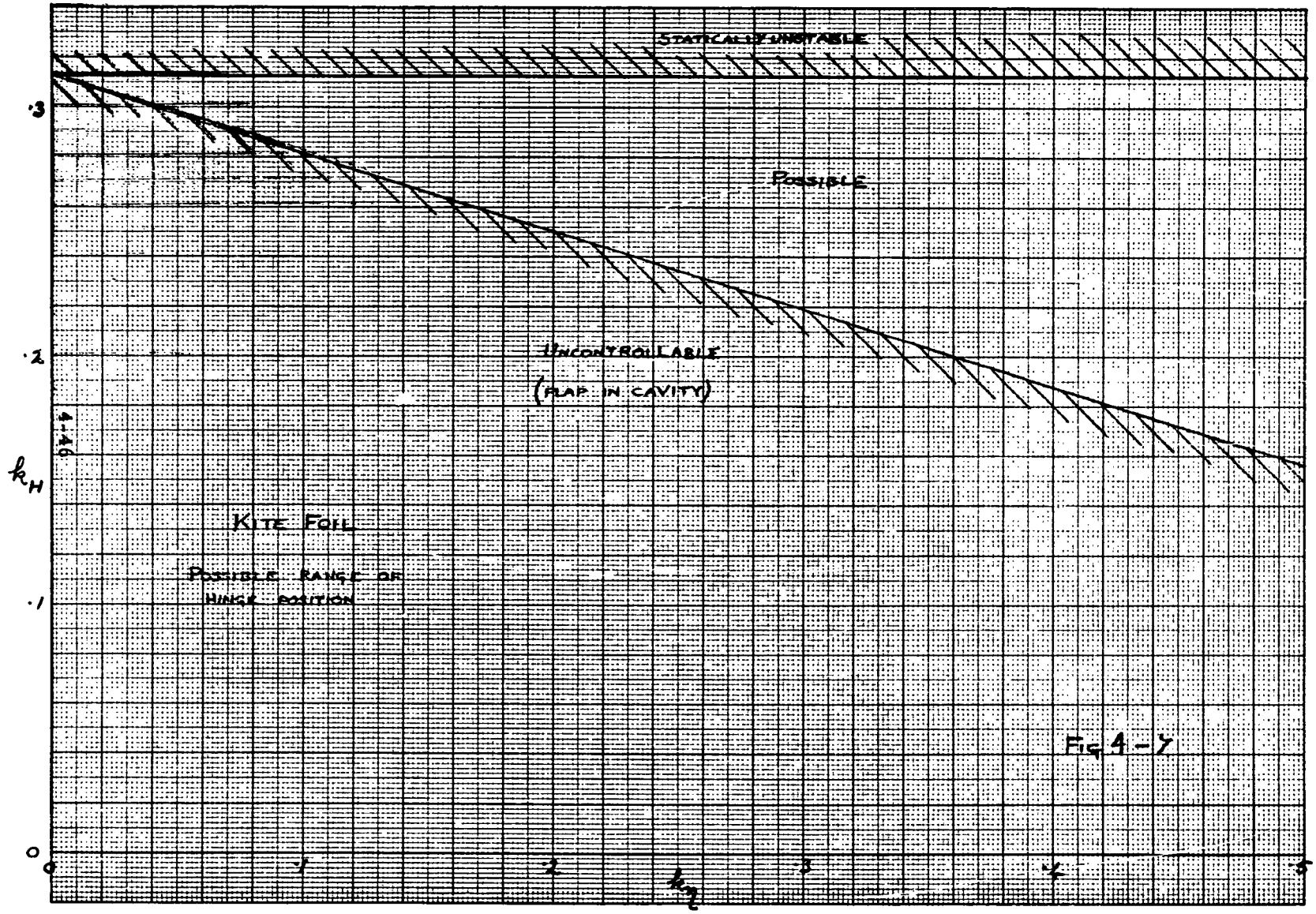
STATICALLY UNSTABLE
POSSIBLE
UNCONTROLLABLE
(FLAP IN CAVITY)
4-46
KITE FOIL
POSSIBLE RANGE OF HINGE POSITION
k_H
.3
.2
.1
0
1
2
3
4
5
k_2

Fig 4-7

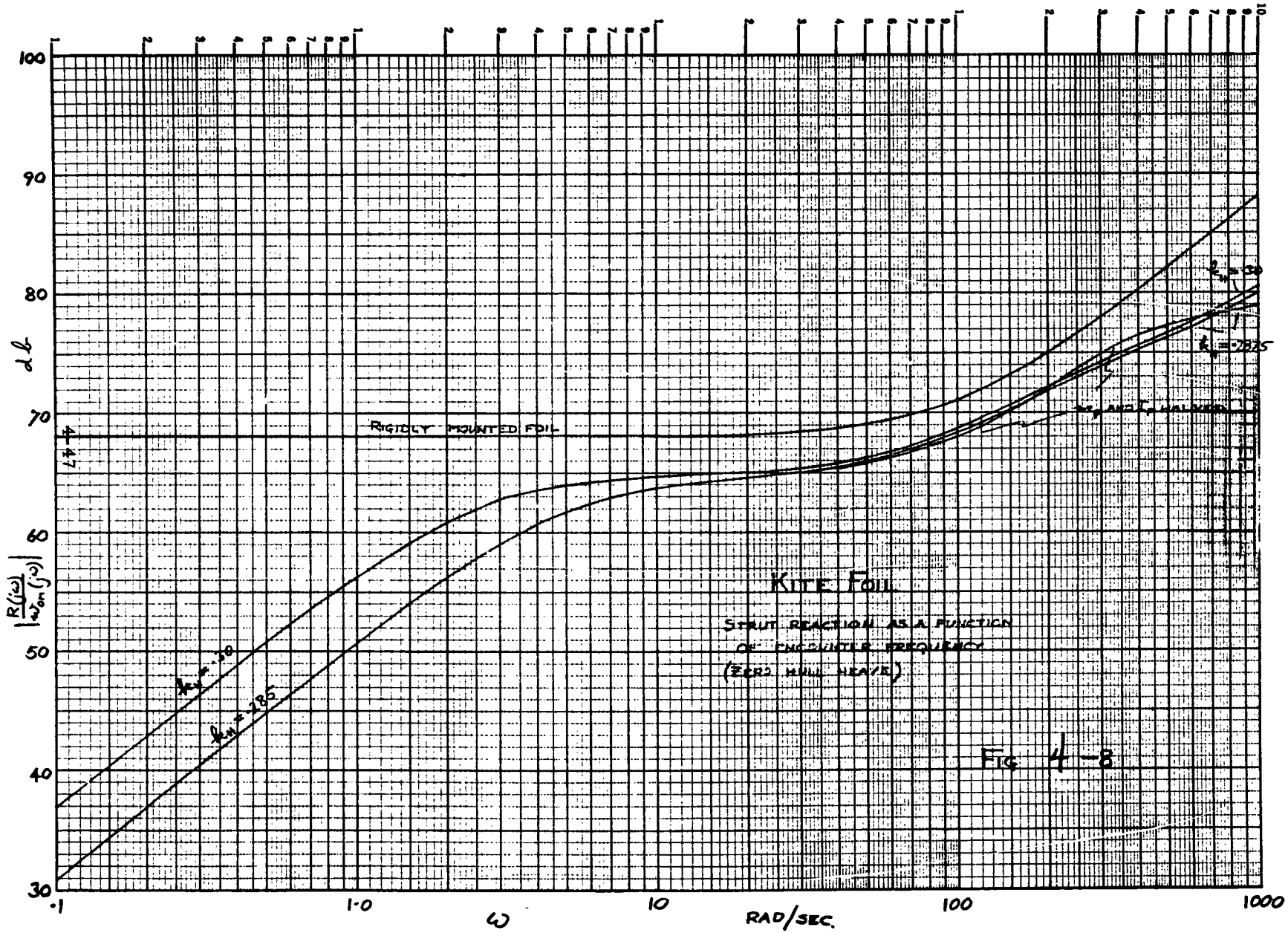
100
90
80
70
60
50
40
30
dB
4.47
RIGIDLY MOUNTED FOIL
$k_w = .30$
$k_w = .285$
$k_w = .20$
$k_w = .2825$
$\frac{R(j\omega)}{w_{on}(j\omega)}$
.1
1.0
10
100
1000
ω
RAD/SEC.
KITE FOIL
STRUT REACTION AS A FUNCTION
OF ENCOUNTER FREQUENCY
(ZERO HULL HEAVE)
FIG 4-8

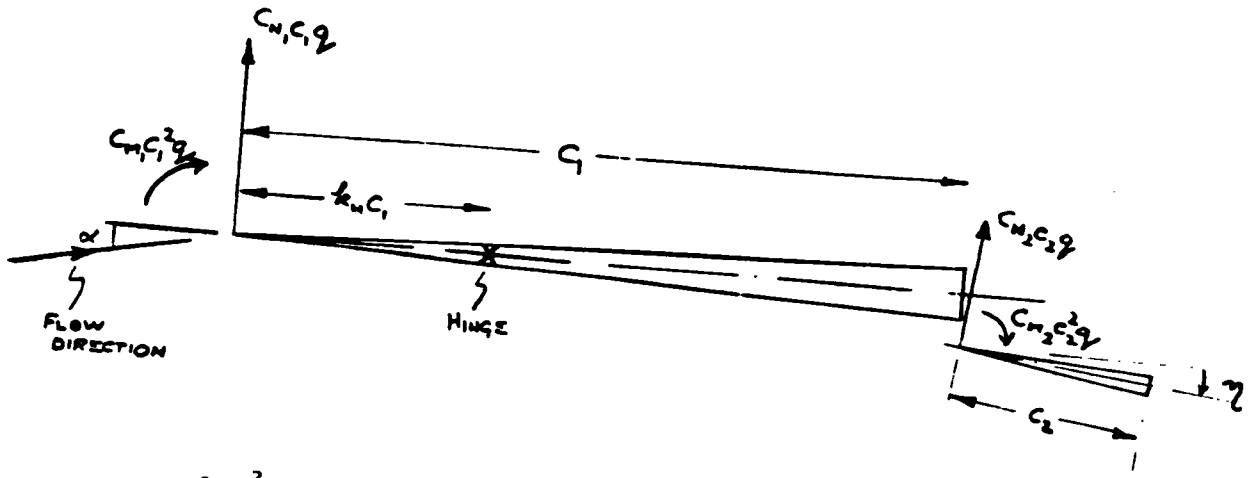

$q = \frac{\rho}{2} u^2$

FORCES AND MOMENTS REFER TO UNIT SPAN

ASSUMED KITE FOIL CONFIGURATION

Figure 4-9.

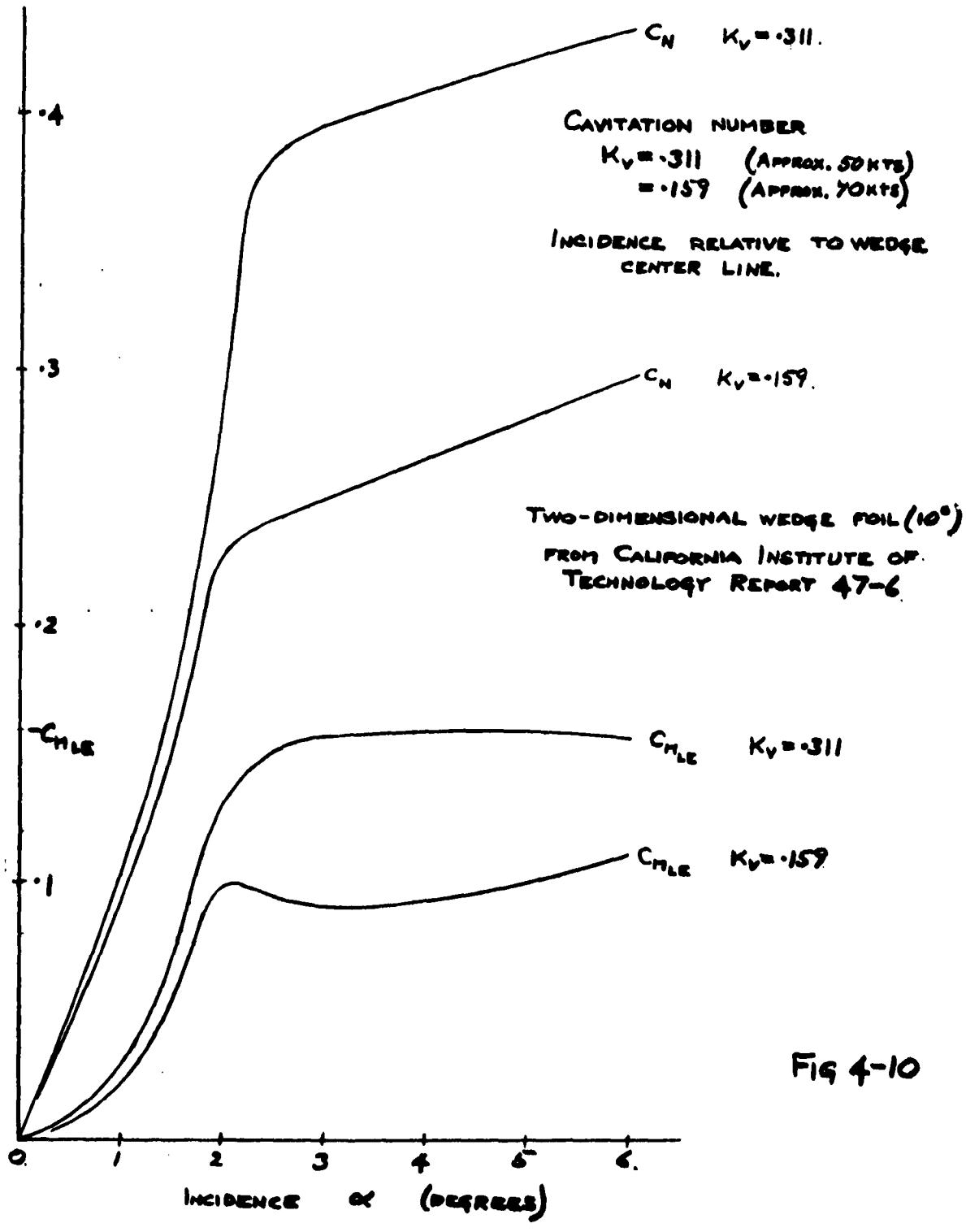
C_N $K_v = .311$.
CAVITATION NUMBER
$K_v = .311$ (APPROX. 50 KTS)
$= .159$ (APPROX. 70 KTS)
INCIDENCE RELATIVE TO WEDGE CENTER LINE.
C_N $K_v = .159$.
TWO-DIMENSIONAL WEDGE FOIL (10°)
FROM CALIFORNIA INSTITUTE OF TECHNOLOGY REPORT 47-6
$C_{M_{LE}}$ $K_v = .311$
$C_{M_{LE}}$ $K_v = .159$
.4
.3
.2
$-C_{M_{LE}}$
.1
0
1
2
3
4
5
6.
INCIDENCE α (DEGREES)

FIG 4-10

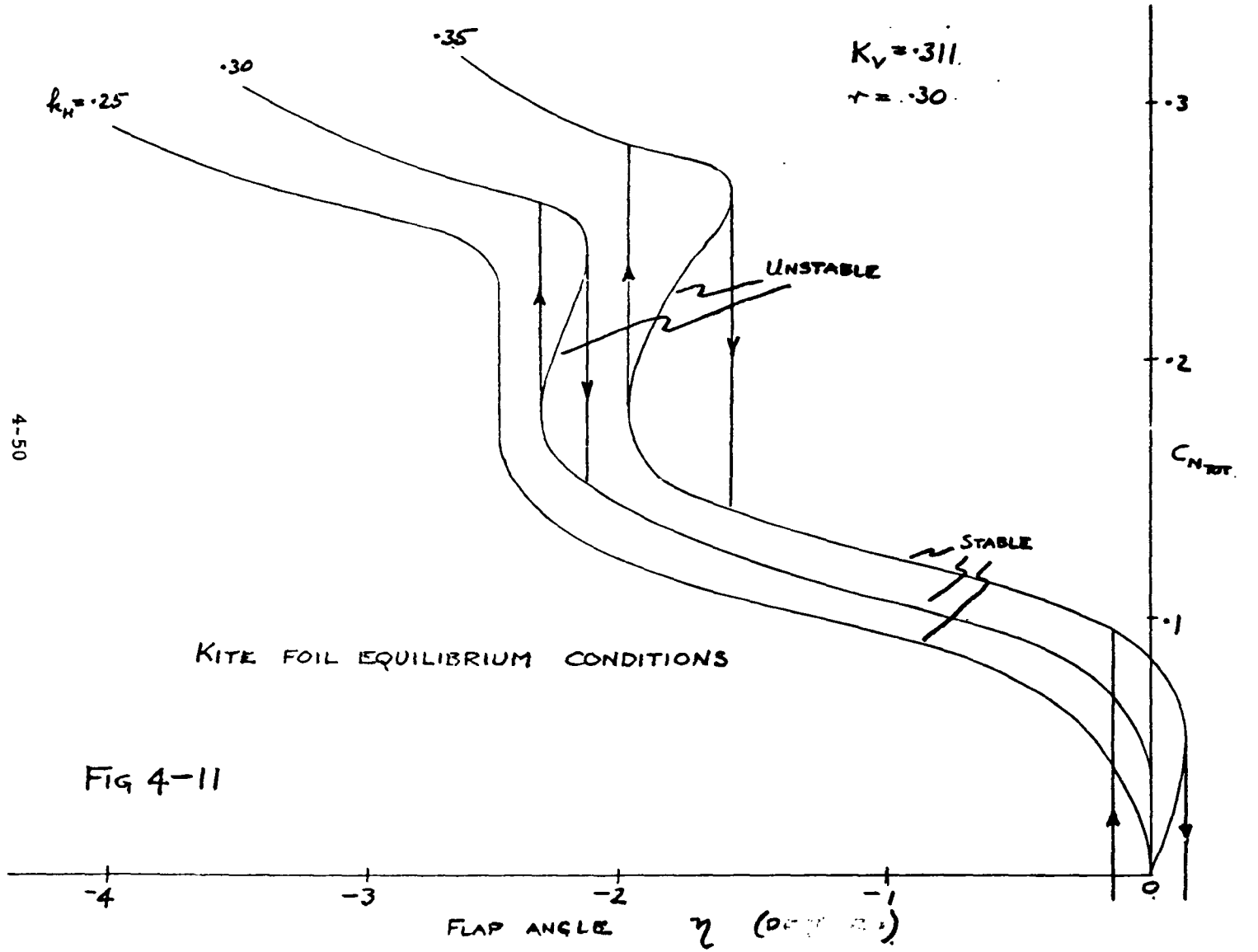

KITE FOIL EQUILIBRIUM CONDITIONS

FIG 4-11

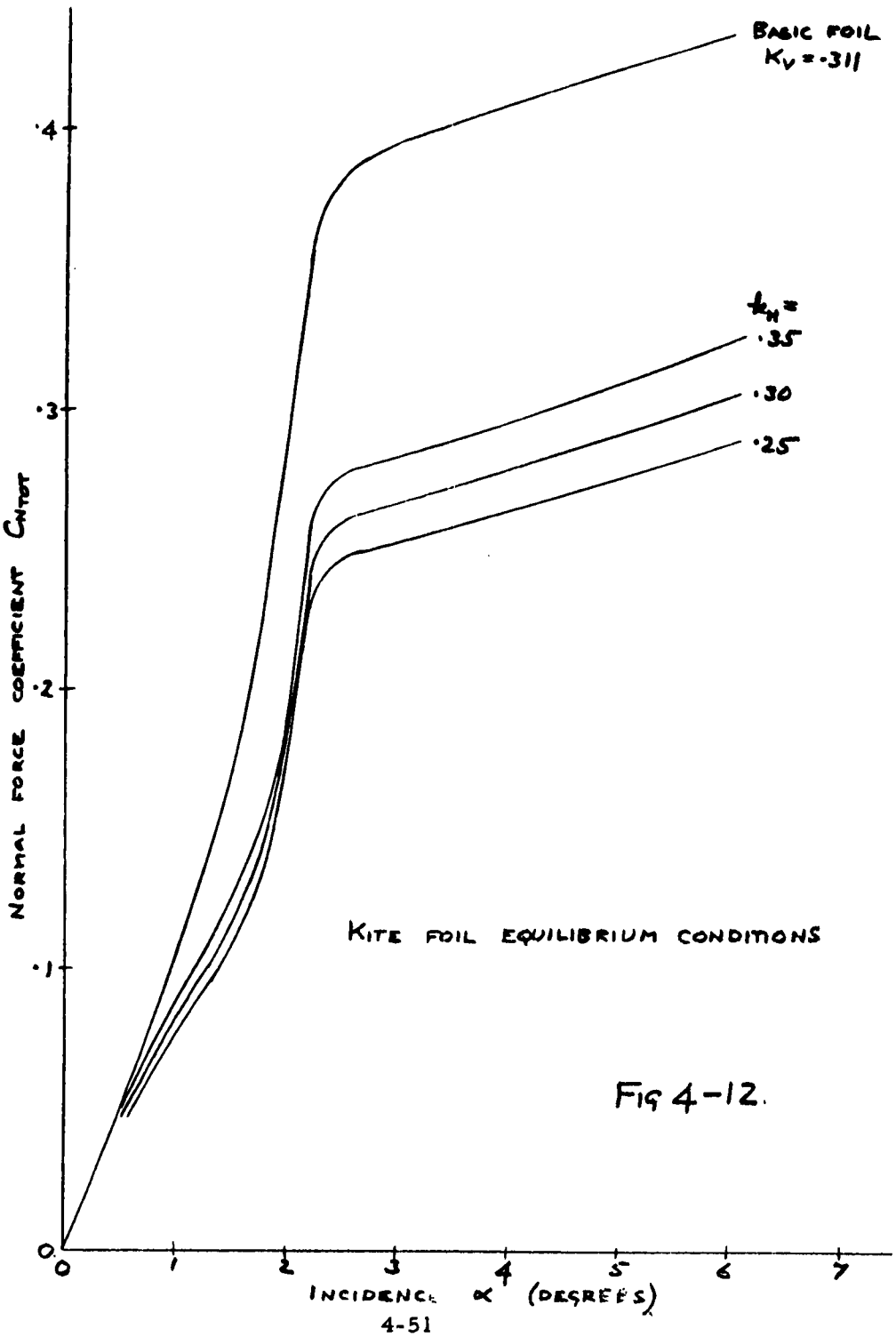

KITE FOIL EQUILIBRIUM CONDITIONS

Fig 4-12.

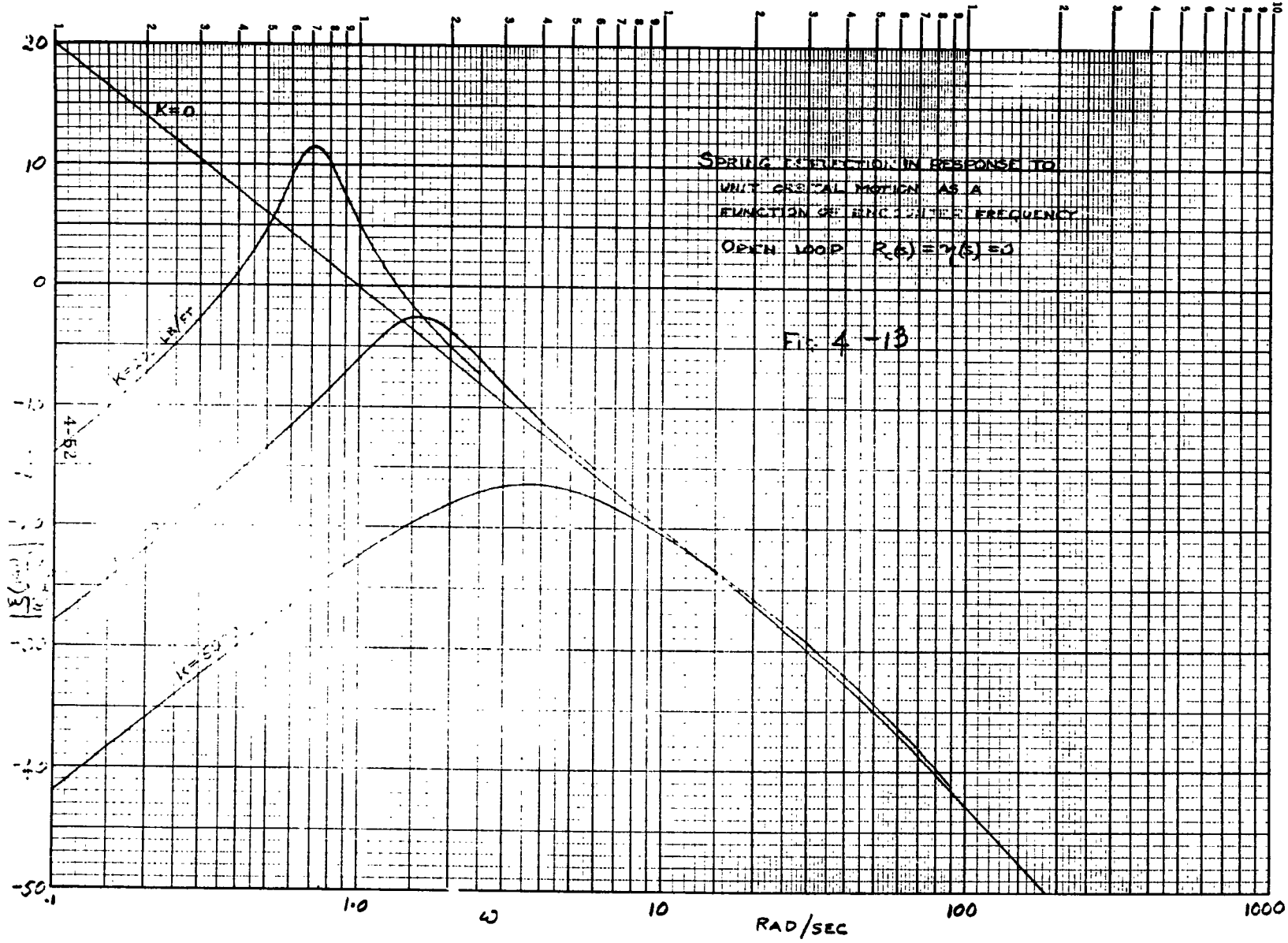
SPRING DEFLECTION IN RESPONSE TO
UNIT GRAVITATIONAL MOTION AS A
FUNCTION OF EXCITATION FREQUENCY
OPEN LOOP $K_c(s) = \gamma(s) = 0$
Fig. 4-13
K=0
K=2 LB/FT
K=5
20
10
0
-10
-20
-50
.1
1.0
10
100
1000
ω
RAD/SEC
4-62

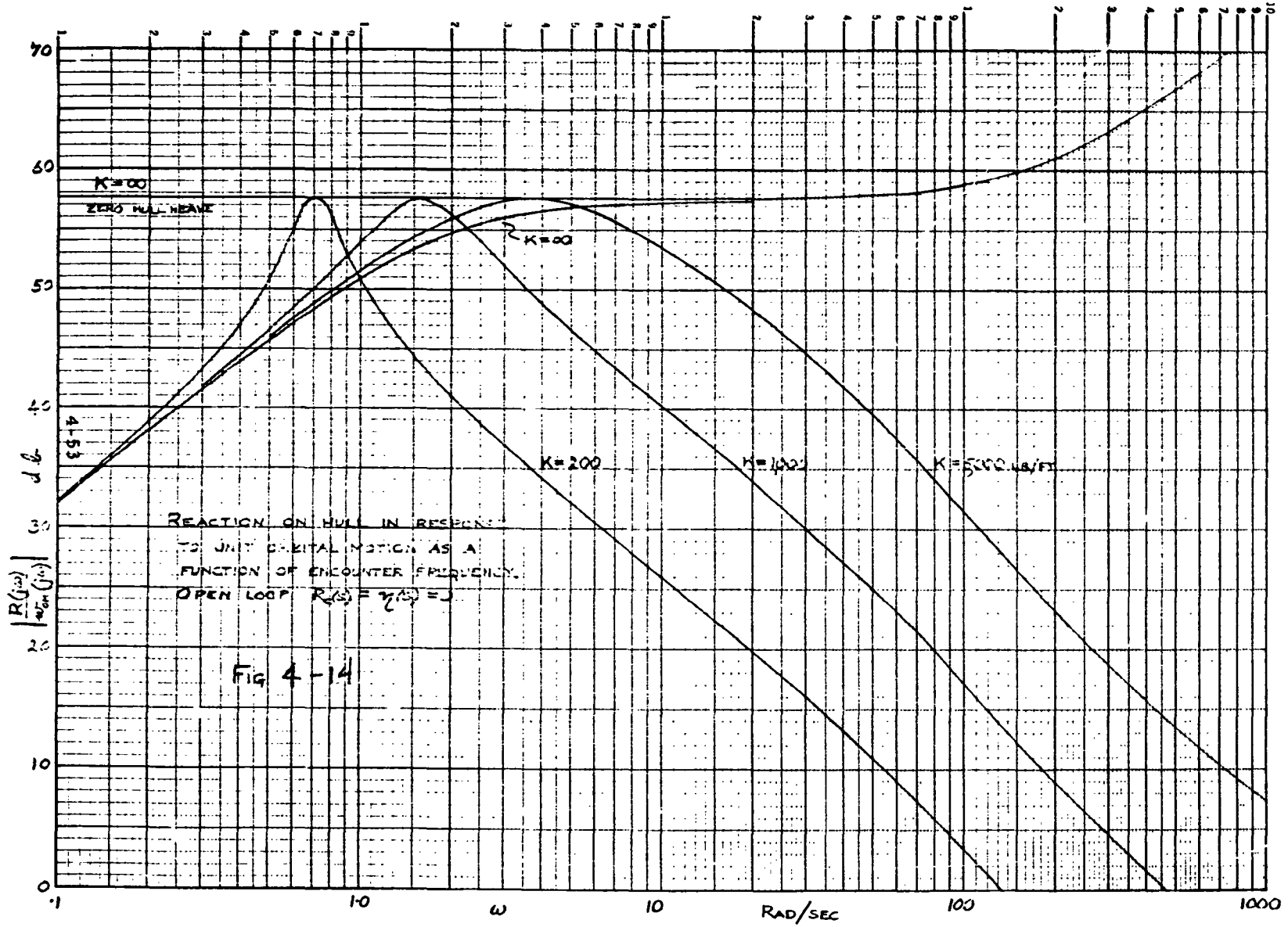
70
60
50
40
30
20
10
0
K=∞
ZERO HULL WEAVE
K=∞
K=200
K=400
K=5000 LB/FT
4-53
d b
$\left|\frac{R(j\omega)}{\eta_{Com}(j\omega)}\right|$
REACTION ON HULL IN RESPONSE
TO UNIT VERTICAL MOTION AS A
FUNCTION OF ENCOUNTER FREQUENCY.
OPEN LOOP $R(s) = \eta(s) = 1$
.1
1.0
ω
10
RAD/SEC
100
1000

Fig 4-14

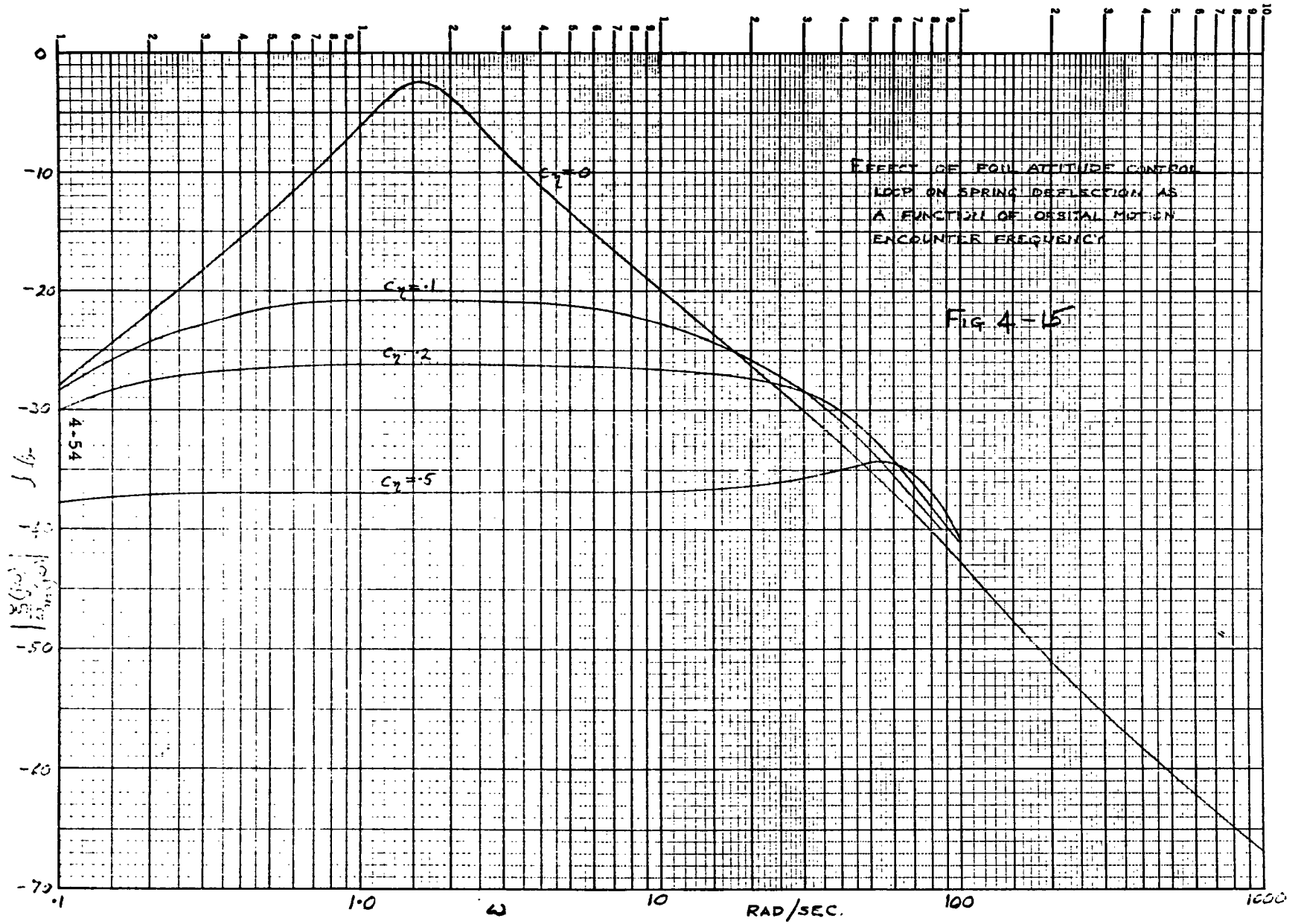
0
-10
-20
-30
-40
-50
-70
.1
1.0
10
100
1000
ω
RAD/SEC.
$C_\gamma = 0$
$C_\gamma = .1$
$C_\gamma = .2$
$C_\gamma = .5$
EFFECT OF ROLL ATTITUDE CONTROL LOOP ON SPRING DEFLECTION AS A FUNCTION OF ORBITAL MOTION ENCOUNTER FREQUENCY
FIG 4-15
4-54

FIG 4-55
RAD/SEC
ω
1000
100
10
1.0
.1
70
60
50
40
30
20
10
0
dB
K=∞ UNCONTROLLED
K=60 C_T=.5
K=60 C_T=.3
K=60 C_T=.2
K=1000 C_T=.4
K=1000 C_T=.2
K=1000 C_T=.5
4-55

Fig 4-14
ROLL ATTITUDE AMPLITUDE RATIO FOR VARIOUS VALUES OF C_{l_p} AS A FUNCTION OF ORBITAL PORTION ENCOUNTER FREQUENCY
$C_{l_p}=-5$
$C_{l_p}=-2$
$C_{l_p}=-1$
4-56
RAD/SEC
ω
$\left|\frac{\eta(j\omega)}{\eta_{on}(j\omega)}\right|$ dB

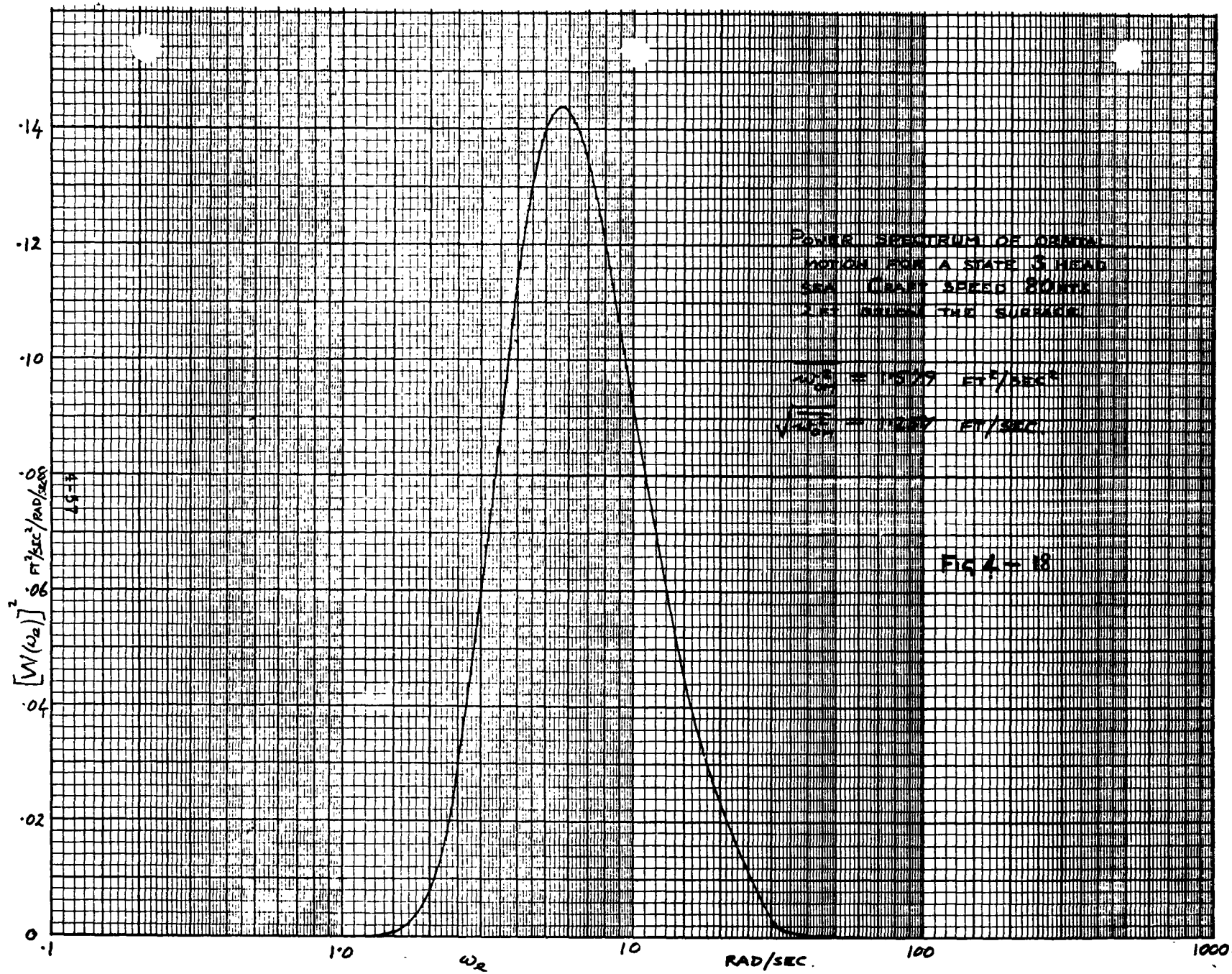
·14
·12
·10
·08
·06
·04
·02
0
$[W(\omega_a)]^2$ FT²/SEC²/RAD/SEC
$\zeta = .7$
·1
1·0
10
100
1000
ω_a
RAD/SEC
POWER SPECTRUM OF ORBITAL MOTION FOR A STATE 3 HEAD SEA CRAFT SPEED 80 KTS 2 FT ABOVE THE SURFACE
$\sigma_{\dot{z}}^2 = 15.29$ FT²/SEC⁴
$\sqrt{\sigma_{\dot{z}}^2} = 3.907$ FT/SEC

Fig 4 - 18

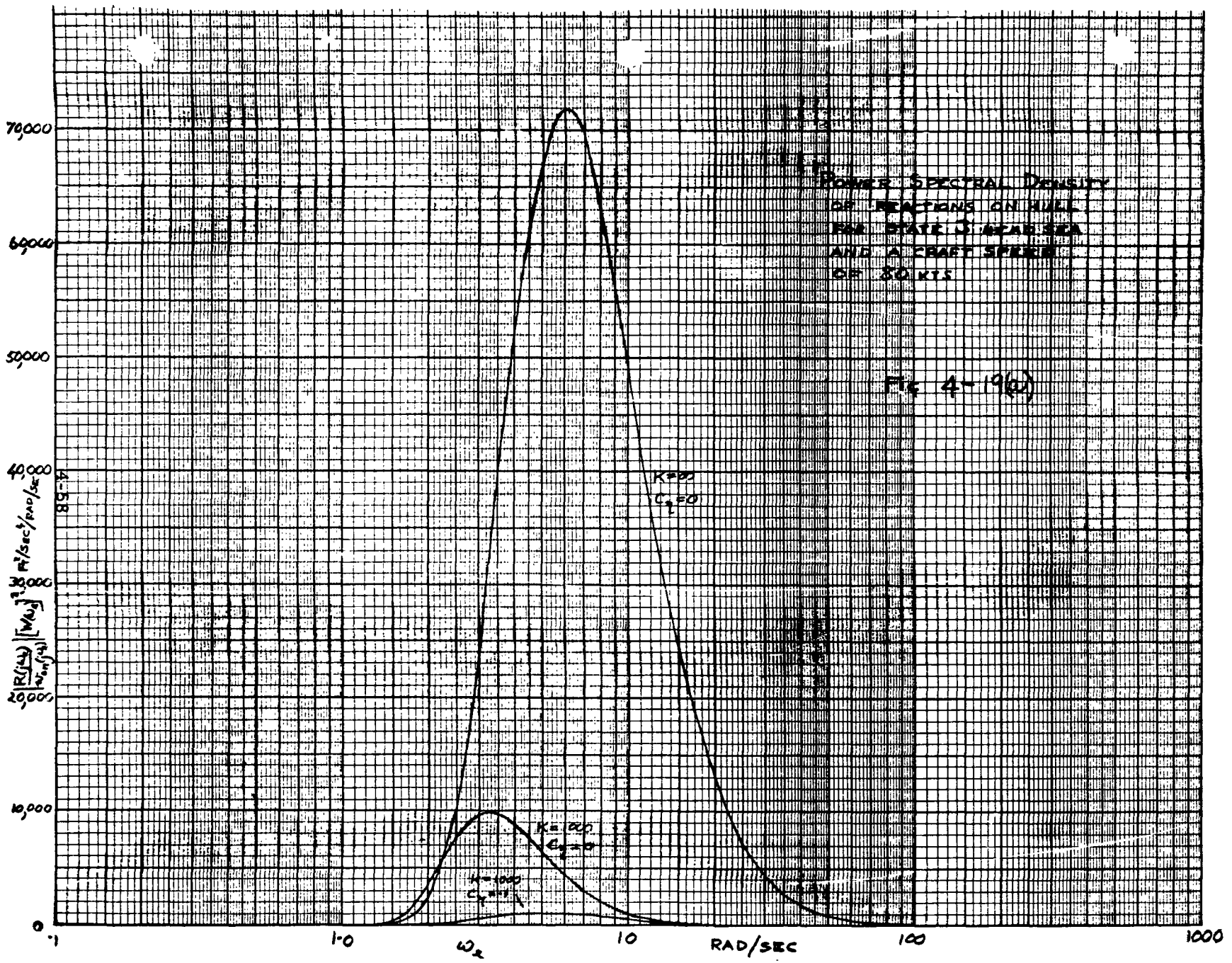
70,000
60,000
50,000
40,000
30,000
20,000
10,000
0
.1
1.0
10
100
1000
RAD/SEC
ω_e
$\frac{R(\omega_e)}{|H(j\omega_e)|^2}$ $|H(j\omega_e)|^2$ FT²/SEC⁴/RAD/SEC
K=∞
C_L=0
K=100
C_L=0
K=1000
C_L=1
POWER SPECTRAL DENSITY OF REACTIONS ON HULL FOR STATE 3 HEAD SEA AND A CRAFT SPEED OF 80 KTS
Fig 4-19(d)
4-58

RELATIVE MAGNITUDES OF THE INFINITESIMAL SINUSOIDAL COMPONENTS
RELATIVE MAGNITUDES OF REACTIONS ON HULL
FOR STATE 3 SEA AND CRAFT SPEED OF 80 KTS
K=1000 C7=0.1
K=100 C7=0.1
K=10 C7=0.1
RAD/SEC
1000
100
10
1.0
.1
ω

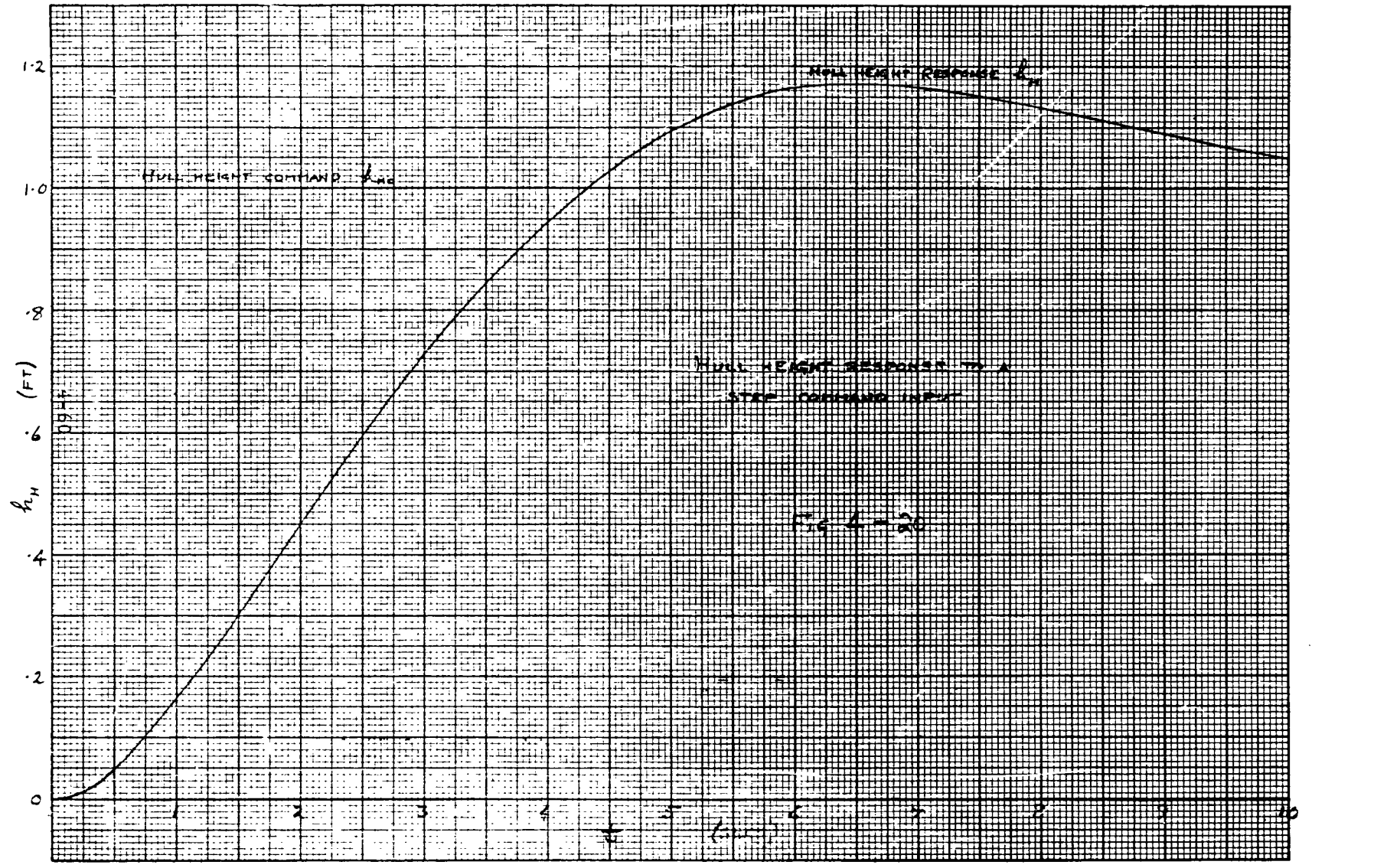

HULL HEIGHT RESPONSE TO A STEP COMMAND INPUT

FIG 4 - 20

SECTION 5

LATERAL DYNAMICS AND CONTROL SYSTEM DESIGN FOR THE CRAFT WITH SPRUNG FOILS

5.1 INTRODUCTION

The equations used to compute stability derivatives are included in this section. The lateral dynamics of the craft were investigated with various foil-strut arrangements. Also investigated were the effects of dihedral and sweepback. The possibilities of making manual control of the craft easier by using various combinations of rudder and aileron control have been explored.

5.2 EQUATIONS USED FOR STABILITY DERIVATIVES

The stability derivatives were computed by finding the changes in lift forces acting on the struts and foils caused by perturbations in side slip, roll rate, and yaw rate. The changes in drag forces are small compared to those in the lift forces and were neglected, as were the virtual inertia effects caused by entrained water. Strut forces were calculated by assuming that the whole of each foil was operating under the same conditions as its mid-span point. The forces acting on foils that were not split were computed by finding the conditions under which the starboard and port panels of the foil were operating, and then assuming that the whole of each panel was operating under the same conditions as its mid-span point.

The incremental lift forces acting on a foil having dihedral and sweep were computed by finding the components of velocity of the mid-span point of each foil in a plane perpendicular to the quarter chord span

line, and in directions along and perpendicular to the projection of the reference direction of motion onto this plane. It was assumed that a pair of foils having dihedral and sweep would be separated by a distance so that the flow disturbance caused by one foil would not affect the other foil.

Sweep angle, Λ, and dihedral angle Γ, were defined in the following way.

Assume x, y, z form a right-handed orthogonal system of axes fixed in the craft with x aligned along the reference direction of motion and the x-z plane lying in the vertical plane of symmetry. Assume that the axes are rotated through a positive angle Λ about the z axis, and denote the new axes positions by x', y', z'. Next assume that the x', y', z', axes are rotated through a negative angle ($-\Gamma$) about the x'axes, and let the new axes positions be x'', y'', and z''. y'' will now be parallel to the quarter chord span line of a starboard foil having sweep Λ and dihedral Γ. These axes rotations are shown diagramatically in Figure 5-1. For a port foil the rotations are through a negative angle ($-\Lambda$) about the z axis and a positive angle Γ about the x' axis.

With these assumptions made, the stability derivatives are given by the following equations. *

$$(Y_v)_{F,R} = -\frac{1}{2}\rho u_o \left[2Sa_1c_2\left(c_2\frac{\partial C_L}{\partial i} + 2a_2C_L\right)\right]_{F,R} \qquad (5\text{-}1)$$

$$(K_v)_{F,R} = -\frac{1}{2}\rho u_o \left[Sb_s a_1 c_3\left(c_2\frac{\partial C_L}{\partial i} + 2a_2 C_L\right)\right]_{F,R} - (Y_v)_{F,R}\, d_{F,R} \qquad (5\text{-}2)$$

*Note that Y_v is shorthand for $\partial Y/\partial v$. This is similar for the other derivatives.

$$(Y_p)_{F,R} = -(Y_v)_{F,R}\, d_{F,R} - \frac{1}{2}\rho u_o \left[Sb_s a_1 c_2 \left(c_3 \frac{\partial C_L}{\partial i} + 2a_3 C_L\right)\right]_{F,R} \quad (5\text{-}3)$$

$$(K_p)_{F,R} = -(Y_p)_{F,R}\, d_{F,R} - \frac{1}{2}\rho u_o \left[S \frac{(b_s)^2}{2} a_1 c_3 \left(c_3 \frac{\partial C_L}{\partial i} + 2a_3 C_L\right)\right]_{F,R} \quad (5\text{-}4)$$

$$(Y_r)_F = +(Y_v)_F \ell_F + \frac{1}{2}\rho u_o \left[2Sb_s (a_1)^2 c_2 C_L\right]_F \quad (5\text{-}5)$$

$$(Y_r)_R = -(Y_v)_R \ell_R + \frac{1}{2}\rho u_o \left[2Sb_s (a_1)^2 c_2 C_L\right]_R \quad (5\text{-}6)$$

$$(K_r)_{F,R} = -(Y_r)_{F,R}\, d_{F,R} + \frac{1}{2}\rho u_o \left[S(b_s)^2 (a_1)^2 c_3 C_L\right]_{F,R} \quad (5\text{-}7)$$

$$a_1 = +\cos\Lambda\cos\beta + \sin\Lambda\sin\Gamma\sin\beta \quad (5\text{-}8)$$

$$a_2 = +\sin\Lambda\cos\beta - \cos\Lambda\sin\Gamma\sin\beta \quad (5\text{-}9)$$

$$a_3 = -\cos\Gamma\sin\beta \quad (5\text{-}10)$$

$$c_2 = +\sin\Lambda\sin\beta + \cos\Lambda\sin\Gamma\cos\beta \quad (5\text{-}11)$$

$$c_3 = +\cos\Gamma\cos\beta \quad (5\text{-}12)$$

$$\beta = \tan^{-1}\{\tan\Lambda\sin\Gamma\} \quad (5\text{-}13)$$

(Note that β is a positive rotation about the y'' axis (see Figure 5-1) required to make the x'' axis align with the projection of the x axis on the x'' - z'' plane.)

$$(Y_v)_{\bar{F}_1\bar{R}} = -\frac{1}{2}\rho\, u_o\left[kS\ \frac{\partial C_L}{\partial i}\right]_{\bar{F}_1\bar{R}} \tag{5-14}$$

$$Y_v = (Y_v)_F + (Y_v)_R + (Y_v)_{\bar{F}} + (Y_v)_{\bar{R}} \tag{5-15}$$

$$K_v = (K_v)_F + (K_v)_R - (Y_v)_{\bar{F}}\, d_{\bar{F}} - (Y_v)_{\bar{R}}\, d_{\bar{R}} \tag{5-16}$$

$$N_v = (Y_v)_F \ell_F - (Y_v)_R \ell_R + (Y_v)_{\bar{F}} \ell_{\bar{F}} - (Y_v)_{\bar{R}} \ell_{\bar{R}} \tag{5-17}$$

$$Y_p = (Y_p)_F + (Y_p)_R - (Y_v)_{\bar{F}}\, d_{\bar{F}} - (Y_v)_{\bar{R}}\, d_{\bar{R}} \tag{5-18}$$

$$K_p = (K_p)_F + (K_p)_R + (Y_v)_{\bar{F}}\, (d_{\bar{F}})^2 + (Y_v)_{\bar{R}} (d_{\bar{R}})^2 \tag{5-19}$$

$$N_p = (Y_p)_F \ell_F - (Y_p)_R \ell_R - (Y_v)_{\bar{F}} \ell_{\bar{F}}\, d_{\bar{F}} + (Y_v)_{\bar{R}} \ell_{\bar{R}}\, d_{\bar{R}} \tag{5-20}$$

$$Y_r = (Y_r)_F + (Y_r)_R + (Y_v)_{\bar{F}} \ell_{\bar{F}} - (Y_v)_{\bar{R}} \ell_{\bar{R}} \tag{5-21}$$

$$K_r = (K_r)_F + (K_r)_R - (Y_v)_{\bar{F}}\, d_{\bar{F}} \ell_{\bar{F}} + (Y_v)_{\bar{R}}\, d_{\bar{R}} \ell_{\bar{R}} \tag{5-22}$$

$$N_r = (Y_r)_F \ell_F - (Y_r)_R \ell_R + (Y_v)_{\bar{F}}\, (\ell_{\bar{F}})^2 + (Y_v)_{\bar{R}}\, (\ell_{\bar{R}})^2 \tag{5-23}$$

5.3 EFFECTS OF LATERALLY CONSTRAINING THE AFT FOILS, SWEEPBACK AND DIHEDRAL

The following analyses were made before any details of the FRESH craft were available, and it was necessary to make many assumptions about the characteristics of the craft. The assumptions that were made are given in Appendix B. The assumed craft is called the preliminary craft.

5.3.1 UNCONTROLLED LATERAL STABILITY OF THE PRELIMINARY CRAFT CONFIGURATION

For the basic canard configuration assumed, the lateral characteristic equations of the craft at a speed of 80 knots were found with the following foil configurations:

(1) Independently sprung foils. It was assumed that the rear foils were independently sprung and were incapable of applying rolling moments.

(2) Laterally constrained foils, with no dihedral or sweepback. It was assumed that the rear foils, even though sprung, were constrained to move together, so that for the purpose of this analysis, they behaved as fixed foils.

(3) Laterally constrained foils, with $18^{\circ}48'$ dihedral and no sweepback. It was calculated that $18^{\circ}48'$ of dihedral provided the maximum reduction in K_v (rolling moment due to sideslip).

(4) Laterally constrained foils, with $18^{\circ}48'$ of dihedral and 30° of sweepback.

The characteristic equations were all found with submergences of 2 and 3 feet of the front and rear foils respectively. The linearized lateral mode equations of motion are given in Appendix A. The effects of the front foil were very small and were neglected.

Stability derivatives used for these four cases are listed in Table 5-1.

Table 5-1. Stability Derivatives Used for the Uncontrolled Lateral Stability Investigation at Normal Submergence

		Independently Sprung Foils	Laterally Constrained Foils		
			$\Gamma = 0$, $\Lambda = 0$	$\Gamma = 18^{\circ}48'$, $\Lambda = 0$	$\Gamma = 18^{\circ}48'$, $\Lambda = 30^{\circ}$
Y_v	lb sec ft^{-1}	-1.216×10^3	-1.216×10^3	-1.419×10^3	-1.518×10^3
Y_r	lb sec rad^{-1}	$+1.20 \times 10^3$	$+1.20 \times 10^3$	$+3.553 \times 10^3$	$+4.212$
Y_ϕ	lb rad^{-1}	$+3.71 \times 10^4$	$+3.71 \times 10^4$	$+3.71 \times 10^4$	$+3.71 \times 10^4$
Y_p	lb sec rad^{-1}	$+8.978 \times 10^3$	$+8.978 \times 10^3$	$+6.636 \times 10^3$	$+7.516 \times 10^3$
N_v	lb sec	$+1.20 \times 10^3$	$+1.20 \times 10^3$	$+2.672 \times 10^3$	$+3.39 \times 10^3$
N_r	lb ft sec rad^{-1}	-1.437×10^5	-1.437×10^5	-1.608×10^5	-1.670×10^5
N_p	lb ft sec rad^{-1}	-1.19×10^4	-1.19×10^4	$+5.08 \times 10^3$	-1.30×10^3
K_v	lb sec	$+8.978 \times 10^3$	$+8.978 \times 10^3$	$+6.636 \times 10^3$	$+6.308 \times 10^3$
K_r	lb ft sec rad^{-1}	-1.19×10^4	$+6.4 \times 10^3$	-1.497×10^4	-2.437×10^4
K_p	lb ft sec rad^{-1}	-6.62×10^4	-1.627×10^5	-1.309×10^5	-1.275×10^5

The factored forms of the characteristics equations, omitting the overall multiplying constants, are given below.

Case (1) $\left(\frac{s}{0.9997} - 1\right)\left(\frac{s}{0.4342} + 1\right)\left[\left(\frac{s}{1.858}\right)^2 + 1.516\left(\frac{s}{1.858}\right)^2 + 1\right]$

(2) $\left(\frac{s}{0.7179} - 1\right)\left(\frac{s}{0.5251} + 1\right)\left[\left(\frac{s}{2.011}\right)^2 + 1.719\left(\frac{s}{2.011}\right)^2 + 1\right]$

(3) $\left(\frac{s}{0.4376} - 1\right)\left(\frac{s}{0.8681} + 1\right)\left[\left(\frac{s}{1.782}\right)^2 + 1.535\left(\frac{s}{1.782}\right) + 1\right]$

(4) $\left(\frac{s}{0.3877} - 1\right)\left(\frac{s}{0.8481} + 1\right)\left[\left(\frac{s}{1.862}\right)^2 + 1.491\left(\frac{s}{1.862}\right) + 1\right]$

Note that each of these expressions has a right-half plane pole, so that all the configurations are unstable. However, the right-half plane poles of the four cases get progressively closer to the origin.

The times to double amplitude of the divergent roots of the four cases are 0.694 second, 0.967 second, 1.59 seconds and 1.79 seconds respectively.

The four expressions demonstrate the effectiveness of laterally constrained foils, foil dihedral, and foil sweepback in reducing the uncontrolled divergence rate of the preliminary craft.

5.3.2 TRANSFER FUNCTIONS FOR MANUAL LATERAL CONTROL

An investigation was carried out to determine the ease with which a man could control the preliminary craft with the foil configurations that were listed in the previous section. In most cases, only the normal foil submersion cases were considered. Note that the high-speed test craft will

never encounter situations in which the differential submergences of the fore and aft foils will be continuously different, to any large extent, for any considerable period of time. In a State 3 Sea, whatever the heading angle and the craft flying speed (assumed to be a minimum of 40 knots), the differential foil submergence will be continuously changing at a fairly high frequency. Thus, although the craft will tend to be more unstable when the submersion of the fore foil is much larger than that of either aft foil, this will be only a transitory condition. For these reasons, an analysis at normal foil submersions is expected to give a reasonable idea of the controllability of the craft.

A. Independently Sprung Foils

Since the foils are independently sprung, no aileron control is possible in this case. It was assumed that there was a bow rudder which consisted of a fully rotating front strut. If the rudder had been assumed to be a front strut trailing edge flap, the transfer functions found would have been the same except for a different value of gain. The transfer functions relating roll angle and yaw rate to bow rudder deflection are given below:

$$\frac{\phi(s)}{\delta_b(s)} = \frac{-22.61\left[\left(\frac{s}{3.352}\right)^2 + 0.1627\left(\frac{s}{3.352}\right) + 1\right]}{\left(\frac{s}{0.9997} - 1\right)\left(\frac{s}{0.4342} + 1\right)\left[\left(\frac{s}{1.858}\right)^2 + 1.516\left(\frac{s}{1.858}\right) + 1\right]}$$

$$\frac{r(s)}{\delta_b(s)} = \frac{+5.40\left(\frac{s}{1.049} - 1\right)\left[\left(\frac{s}{1.746}\right)^2 + 1.666\left(\frac{s}{1.746}\right) + 1\right]}{\left(\frac{s}{0.9997} - 1\right)\left(\frac{s}{0.4342} + 1\right)\left[\left(\frac{s}{1.858}\right)^2 + 1.516\left(\frac{s}{1.858}\right) + 1\right]}$$

The rudder stability derivatives used are:

$$Y_{\delta_b} = + 4.10 \times 10^4 \text{ lb rad}^{-1}$$
$$N_{\delta_b} = + 7.29 \times 10^5 \text{ lb ft rad}^{-1}$$
$$K_{\delta_b} = - 2.87 \times 10^5 \text{ lb ft rad}^{-1}$$

The first of the transfer functions is discussed in Section 7. The second transfer function has a right-half plane zero as well as a right-half plane pole, and it is apparent that a man could not stabilize the craft by sensing yaw rate and controlling by means of a bow rudder.

Even if a man could stabilize the craft by sensing roll angle and controlling the bow rudder, this system does not permit the use of flat turns. The craft configuration assumed has widely spaced rear foils, and flat turns will thus be necessary. In other words, to be able to make flat turns, some aileron control is necessary.

B. Laterally Constrained Foils

Laterally constraining the foils not only reduces the uncontrolled divergence rate of the craft, but enables aileron control to be used. The roll angle - aileron deflection transfer function is given below.

$$\frac{\phi(s)}{\delta_a(s)} = \frac{13.8\left[\left(\frac{s}{1.042}\right)^2 + 1.494\left(\frac{s}{1.042}\right) + 1\right]}{\left(\frac{s}{0.7179} - 1\right)\left(\frac{s}{0.5251} + 1\right)\left[\left(\frac{s}{2.011}\right)^2 + 1.719\left(\frac{s}{2.011}\right) + 1\right]}$$

The ability of a man to control this case is discussed in Section 7. It was assumed that aileron control consisted of rotation of each complete rear foil. The aileron stability derivatives used to compute the transfer function were

$$Y_{\delta_a} = 0$$

$$N_{\delta_a} = 0$$

$$K_{\delta_a} = +1.84 \times 10^6 \text{ lb ft rad}^{-1}$$

C. Laterally Constrained Foils, $\Gamma = 18^{\circ}48'$, $\Lambda = 0$

With this foil configuration, the transfer functions, relating roll angle to various combinations of ailerons and rudders, were found. It was assumed that the bow and stern rudders were coupled together in such a manner that a deflection of the rudder combination resulted in a side force, a rolling moment but no yawing moment. The deflection of the combination of rudders is here defined as δ_1 where $\delta_1 = \delta_b + 0.816\ \delta_s$. The combination of aileron deflection and δ_1 deflection is defined as δ_3 where $\delta_3 = c_1 \delta_a - c_2 \delta_1$ where c_1 and c_2 are constants.

The transfer functions computed are given below.

(i) $c_1 = 1,\ c_2 = 0$ $\quad \frac{\phi(s)}{\delta_3(s)} = \left[35.26\right]\left[\left(\frac{s}{2.030}\right)^2 + 1.144\left(\frac{s}{2.030}\right) + 1\right] / \Delta(s)$

(ii) $c_1 = 1,\ c_2 = 1/2$ $\quad \frac{\phi(s)}{\delta_3(s)} = 42.00\left[\left(\frac{s}{1.792}\right)^2 + 1.042\left(\frac{s}{1.792}\right) + 1\right] / \Delta(s)$

(iii) $c_1 = 1,\ c_2 = 1$ $\quad \frac{\phi(s)}{\delta_3(s)} = 48.75\left[\left(\frac{s}{1.664}\right)^2 + 0.9894\left(\frac{s}{1.664}\right) + 1\right] / \Delta(s)$

(iv) $c_1 = 1,\ c_2 = 2$ $\quad \frac{\phi(s)}{\delta_3(s)} = 62.24\left[\left(\frac{s}{1.528}\right)^2 + 0.9354\left(\frac{s}{1.528}\right) + 1\right] / \Delta(s)$

(v) $c_1 = 0,\ c_2 = 1 \quad \frac{\phi(s)}{\delta_3(s)} = 13.49\left[\left(\frac{s}{1.220}\right)^2 + 0.8247\left(\frac{s}{1.220}\right)+1\right]/\Delta(s)$

where $\Delta(s) = \left(\frac{s}{0.4376} - 1\right)\left(\frac{s}{0.8681} + 1\right)\left[\left(\frac{s}{1.782}\right)^2 + 1.535\left(\frac{s}{1.782}\right)+ 1\right]$

The rudder and aileron stability derivatives used are as follows:

$$
\begin{aligned}
Y_{\delta_b} &= +4.10 \times 10^4 \text{ lb rad}^{-1} \\
N_{\delta_b} &= +7.29 \times 10^5 \text{ lb ft rad}^{-1} \\
K_{\delta_b} &= -2.87 \times 10^5 \text{ lb ft rad}^{-1} \\
Y_{\delta_s} &= +1.23 \times 10^5 \text{ lb rad}^{-1} \\
N_{\delta_s} &= -8.92 \times 10^5 \text{ lb ft rad}^{-1} \\
K_{\delta_s} &= -9.23 \times 10^5 \text{ lb ft rad}^{-1} \\
Y_{\delta_1} &= +1.42 \times 10^5 \text{ lb rad}^{-1} \\
N_{\delta_1} &= 0 \\
K_{\delta_1} &= -1.04 \times 10^6 \text{ lb ft rad}^{-1} \\
Y_{\delta_a} &= +8.49 \times 10^4 \text{ lb rad}^{-1} \\
N_{\delta_a} &= -6.16 \times 10^5 \text{ lb ft rad}^{-1} \\
K_{\delta_a} &= +9.84 \times 10^5 \text{ lb ft rad}^{-1}
\end{aligned}
$$

As implied by criteria in Section 7, the lower the natural frequency of the numerator term, the easier it is for a man to control the craft laterally. Thus, it would appear that the more rudder combination (δ_1) and less aileron (δ_a) that is used, the easier it will be for a man to stabilize the craft. However, difficulties occur in flat turns when rudders are used to provide correcting rolling moments. As previously stated, flat turns cannot be made when rudders alone are used

to apply rolling moments. When ailerons and rudders are used to apply rolling moments, in order for a flat turn to be made, the craft will have to side-slip much more for a given turning rate than when ailerons alone are used. The rudders will be tending to apply strut forces that will be in the opposite direction to that required for the turn to be made. The net side force will be that required for the turn, and the centrifugal rolling moment will be completely opposed by the ailerons.

For these reasons, the only one of the cases that has been investigated further in Section 7 is the one in which ailerons alone are used for stability (rudder commands are always required for producing yaw rates in turns).

The system where ailerons alone are used has also been investigated at normal fore foil and zero aft foil submergences, and also at zero fore foil and normal aft foil submergences. The stability derivatives used for these two cases are shown below.

		Front Foil Sub. = 2 ft Rear Foil Sub. = 0 ft	Front Foil Sub. = 0 ft Rear Foil Sub. = 3 ft
Y_v	lb sec ft^{-1}	-5.07×10^2	-1.115×10^3
Y_r	lb sec rad^{-1}	-3.047×10^3	$+8.953 \times 10^3$
Y_ϕ	lb rad^{-1}	$+3.71 \times 10^4$	$+3.71 \times 10^4$
Y_p	lb sec rad^{-1}	-2.14×10^2	$+4.508 \times 10^3$
N_v	lb sec	-3.928×10^3	$+8.072 \times 10^3$
N_r	lb ft sec rad^{-1}	-1.130×10^5	-6.486×10^4
N_p	lb ft sec rad^{-1}	$+5.478 \times 10^4$	-3.272×10^4
K_v	lb sec	-2.14×10^2	$+4.508 \times 10^3$
K_r	lb ft sec rad^{-1}	$+3.473 \times 10^4$	-5.277×10^4
K_p	lb ft sec rad^{-1}	-7.955×10^4	-1.160×10^5
Y_{δ_a}	lb rad^{-1}	$+8.49 \times 10^4$	$+8.49 \times 10^4$
N_{δ_a}	lb ft rad^{-1}	-6.16×10^5	-6.16×10^5
K_{δ_a}	lb ft rad^{-1}	$+9.84 \times 10^5$	$+9.84 \times 10^5$

The roll angle to aileron deflection transfer functions for these submergences are given below.

Front Foil Submersions = 2 feet,
Rear Foil Submersions = 0 foot.

$$\frac{\phi(s)}{\delta_a(s)} = \frac{100.9\left(\frac{s}{1.037}-1\right)\left(\frac{s}{1.778}+1\right)}{\left(\frac{s}{0.9286}-1\right)\left(\frac{s}{0.1211}-1\right)\left(\frac{s}{0.9313}+1\right)\left(\frac{s}{1.787}+1\right)}$$

Front Foil Submersions = 0 foot,
Rear Foil Submersions = 3 feet.

$$\frac{\phi(s)}{\delta_a(s)} = \frac{335.9\left[\left(\frac{s}{2.260}\right)^2 + 0.7292\left(\frac{s}{2.260}\right)+1\right]}{\left(\frac{s}{0.07973}+1\right)\left(\frac{s}{0.5077}+1\right)\left[\left(\frac{s}{1.969}\right)^2 + 0.9264\left(\frac{s}{1.969}\right)+1\right]}$$

Note the second transfer function has no right-half plane poles, i. e., the craft is open loop stable under these conditions. There is a pole extremely close to the origin in the left-half plane, however, so that recovery from any disturbance will be extremely slow.

The transfer function relating roll angle to bow rudder deflection was also computed for the case of laterally constrained aft foils with dihedral but no sweep with fore and aft foil submergence of 2 and 3 feet respectively. The function was found to be as follows:

$$\frac{\phi(s)}{\delta_b(s)} = \frac{-23.3\left[\left(\frac{s}{3.056}\right)^2 + 0.3597\left(\frac{s}{3.056}\right)+1\right]}{\left(\frac{s}{0.4376}-1\right)\left(\frac{s}{0.8681}+1\right)\left[\left(\frac{s}{1.782}\right)^2 + 1.535\left(\frac{s}{1.782}\right)+1\right]}$$

This transfer function is discussed in Section 7.

D. Laterally Constrained Foils $\Gamma = 18^{\circ}48'$, $\Lambda = 30^{\circ}$

The transfer function relating roll angle to bow rudder deflection was calculated for this case.

$$\frac{\phi(s)}{\delta_b(s)} = \frac{-25.04\left[\left(\frac{s}{3.080}\right)^2 + 0.4326\left(\frac{s}{3.080}\right) + 1\right]}{\left(\frac{s}{0.3878} - 1\right)\left(\frac{s}{0.8481} + 1\right)\left[\left(\frac{s}{1.862}\right)^2 + 1.491\left(\frac{s}{1.862}\right) + 1\right]}$$

This case is included in Section 7.

5.4 EFFECTS OF VARIOUS FOIL ARRANGEMENTS AND STRUT LENGTHS

After the work reported in Section 5.3 was accomplished, further details of the high-speed test craft were provided by the Bureau of Ships, which resulted in a number of modifications in the craft assumed for the simulation. (See Figure 3-1.)

The moments of inertia about the x and z axes were re-estimated to have the following values.

$$I_x = 4.98 \times 10^4 \text{ slug ft}^2$$
$$I_z = 2.43 \times 10^5 \text{ slug ft}^2$$

The strut lengths, chords, and possible locations on the hull shown in the drawings supplied by the Bureau of Ships were used. It was noted that there will be a negative pitching moment of approximately 2.5×10^5 lb ft at 80 knots as a result of the unusual thrust line location. *

*It was later determined that the negative pitching moment at 80 knots with reference foil submergences was somewhat less than estimated here.

A constant parabolic section is used for the struts, and it was assumed that the struts will be operating over the linear portion of the C_L vs i range, i. e., it was assumed that both surfaces of each strut will be non-cavitated. The lift curve slope at an equivalent aspect ratio of unity was taken to be the same as that given in Reference 5-1. This reference gives hydrodynamic data for a constant parabolic section having a thickness to chord ratio of 0.15. (The data supplied by the Bureau of Ships stated that the struts have a constant parabolic section with a thickness to chord ratio (t/c) of 0.11. However, it was believed that this section will have lift characteristics not very different from those of a section with t/c = 0.15.) The following formula was used to find $\partial C_L/\partial i$ as a function of aspect ratio, A:

$$\frac{1}{\partial C_L/\partial i} = \frac{1}{(\partial C_L/\partial i)_{\substack{\text{Infinite} \\ \text{Aspect Ratio}}}} + \frac{1}{\pi A} .$$

In order to find an equivalent aspect ratio, each strut was treated as being half of a wing, having a span equal to twice the depth of submersion of the strut, moving in an infinite fluid. In other words, each foil was treated as being a perfect reflector, and the effect of the air-water surface was neglected. Figure 5-2 shows a plot of $(\partial C_L/\partial i)$ S versus strut submergence where S is the product of mean chord and span.

The foil section chosen (see Section 3) was one which has a fully cavitated upper surface. The values of C_L and $\partial C_L/\partial i$ for the foils have been taken as 0.1 and 1.0 respectively, for reasons given in Appendix B.

5.4.1 ANALYSIS OF VARIOUS FOIL AND STRUT ARRANGEMENTS

The large bow down pitching moment resulting from engine thrust and strut-foil drag at 80 knots necessitates the foils being positioned further

forward than is usual when this large pitching moment is not present. The further forward the struts are, the more negative is N_v (yawing moment due to sideslip). In general, a moderately positive N_v is desirable, (see Appendix B) so, to minimize the effects of the large negative pitching moment, in all the configurations considered here each forward foil has been assumed to provide a lift force equal to 40 percent of the craft' s weight. (Information supplied by the Bureau of Ships showed that 40 percent of the craft's weight is the largest permissible single foil loading.)

The transfer functions relating roll angle to aileron deflection for the following cases were found.

(a) Airplane configuration

40-40-20 loading

ℓ_F = 11.76 ft, ℓ_R = 13.33 ft (max possible)

ζ_F = 2.5 ft, ζ_R = 4.5 ft

(b) Canard configuration

40-30-30 loading

ℓ_F = 26 ft (max possible), ℓ_R = 6.10 ft

ζ_F = 2.5 ft, ζ_R = 4.5 ft

(c) Canard configuration

40-30-30 loading

ℓ_F = 26 ft (max possible), ℓ_R = 6.10 ft

ζ_F = 2.5 ft, ζ_R = 2.5 ft

(d) Canard configuration

40-30-30 loading

ℓ_F = 26 ft (max possible), ℓ_R = 6.10 ft

ζ_F = 2.5 ft, ζ_R = 4.5 ft

A fourth strut carrying no foil and situated 13.33 ft aft of the CG and 4.5 ft submerged depth, is included.

No dihedral or sweep was used in any of the above cases. A minimum foil submergence of 2.5 feet was used to avoid broaching in a State 3 Sea.

Assuming that each front strut was submerged 2.5 feet and that each rear strut was submerged 4.5 feet, with a 3-strut arrangement, and with each front foil having a lift equal to 40 percent of the weight of the craft, the aircraft configuration in Case (a) was the configuration that resulted in the largest value of N_v. The canard configuration given in Case (b) has the struts located so as to maximize N_v for this configuration and, as is shown in Table 5-2, N_v was positive but very small in this case.

Rear struts were taken to be 2 feet longer than front struts in Cases (a) and (b), as the data provided on the high-speed test craft indicated a 2-foot difference in length between the two types of struts used with this craft.

To obtain some idea as to the controllability, both manual and automatic, of craft having large positive as well as large negative values of N_v, Cases (c) and (d) were analyzed. Case (c) was similar to (b) except that the submergences of both rear and front struts were taken as 2.5 feet. The resulting value of N_v was large and negative, but was not so

negative as to make control of the craft by ailerons alone impossible. (If N_v is sufficiently negative, the transfer function relating roll angle to aileron deflection has a right-half plane zero as well as a right-half plane pole.) Case (d) is similar to (b) except that a fourth strut was included, situated 13.33 feet aft of the CG. This fourth strut was assumed to have a submerged depth of 4.5 feet. This case had a large positive value of N_v.

The stability derivatives used in these four cases are given in Table 5-2. The computed transfer functions are listed below.

Case (a)

$$\frac{\phi(s)}{\delta_a(s)} = \frac{6.348\left[\left(\frac{s}{6.862}\right)^2 + 1.887\left(\frac{s}{6.862}\right) + 1\right]}{\left(\frac{s}{1.082} - 1\right)\left(\frac{s}{1.699} + 1\right)\left(\frac{s}{6.120} + 1\right)\left(\frac{s}{27.56} + 1\right)}$$

Case (b)

$$\frac{\phi(s)}{\delta_a(s)} = \frac{4.041\left(\frac{s}{7.461} + 1\right)\left(\frac{s}{9.052} + 1\right)}{\left(\frac{s}{1.219} - 1\right)\left(\frac{s}{1.629} + 1\right)\left(\frac{s}{7.398} + 1\right)\left(\frac{s}{35.67} + 1\right)}$$

Case (c)

$$\frac{\phi(s)}{\delta_a(s)} = \frac{2.112\left(\frac{s}{1.461} + 1\right)\left(\frac{s}{10.08} + 1\right)}{\left(\frac{s}{1.248} - 1\right)\left(\frac{s}{1.802} + 1\right)\left(\frac{s}{4.810} + 1\right)\left(\frac{s}{20.20} + 1\right)}$$

Case (d)

$$\frac{\phi(s)}{\delta_a(s)} = \frac{5.084\left[\left(\frac{s}{12.56}\right)^2 + 1.881\left(\frac{s}{12.56} + 1\right)\right]}{\left(\frac{s}{1.134} - 1\right)\left(\frac{s}{1.716} + 1\right)\left(\frac{s}{9.90} + 1\right)\left(\frac{s}{50.48} + 1\right)}$$

Table 5-2. Stability Derivatives

	Case (a)	Case (b)	Case (c)	Case (d)
Y_v, lb sec ft^{-1}	-8.51×10^3	-1.09×10^4	-6.08×10^3	-1.54×10^4
Y_r, lb sec rad^{-1}	$+1.17 \times 10^4$	$+1.72 \times 10^3$	-2.79×10^4	$+6.11 \times 10^4$
Y_ϕ, lb rad^{-1}	$+3.71 \times 10^4$	$+3.71 \times 10^4$	$+3.71 \times 10^4$	$+3.71 \times 10^4$
Y_p, lb sec rad^{-1}	$+8.75 \times 10^4$	$+1.16 \times 10^5$	$+5.92 \times 10^4$	$+1.63 \times 10^5$
N_v, lb sec	$+1.17 \times 10^4$	$+1.72 \times 10^3$	-2.79×10^4	$+6.11 \times 10^4$
N_r, lb ft sec rad^{-1}	-1.35×10^6	-1.70×10^6	-1.52×10^6	-2.49×10^6
N_p, lb ft sec rad^{-1}	-1.76×10^5	-7.12×10^4	$+2.72 \times 10^5$	-7.10×10^5
K_v, lb sec	$+8.75 \times 10^4$	$+1.16 \times 10^5$	$+5.92 \times 10^4$	$+1.63 \times 10^5$
K_r, lb ft sec rad^{-1}	-1.54×10^5	-5.50×10^4	$+2.89 \times 10^5$	-6.94×10^5
K_p, lb ft sec rad^{-1}	-1.01×10^6	-1.30×10^6	-6.58×10^5	-1.86×10^6
$K_{\delta a}$, lb ft rad^{-1}	$+2.08 \times 10^6$	$+1.56 \times 10^6$	$+1.56 \times 10^6$	$+1.56 \times 10^6$

The open loop gain-phase plots for these four cases are shown in Figures 5-3 through 5-6. It was assumed that the transfer function relating aileron deflection to aileron servo input command was

$$\frac{1}{\left(\frac{s}{130}\right)^2 + 0.8\left(\frac{s}{130}\right) + 1}$$

This transfer function was based on a preliminary estimate of foil and strut inertias and jack sizes. (It was proposed to control the incidence of each outboard foil by rotating the foil and strut about a pivot point attached to the hull. Thus, there were, strictly speaking, no differential flap deflections, but roll control was achieved by controlling the incidence of each outboard foil.)

Figures 5-3 through 5-6 indicated that there would be no difficulty in automatically controlling roll-angle in any of the four cases investigated. The effects of using a lead-lag compensating network of the form $\frac{0.04s + 1}{0.004s + 1}$ have been shown on the gain-phase plots. This compensation appeared to be reasonably good for all four cases. The closed-loop responses of the four cases will be fairly similar.

A discussion on the manual controllability of the cases is given in Section 7.

The effects of including dihedral would have been small for the following reason. The principal effect of dihedral is to reduce K_v (rolling moment due to sideslip). As shown in Section 5.3, Table 5-1, reductions in K_v on the order of 2.3×10^3 lb sec could be obtained by using dihedral. However, as can be seen from Table 5-2, with the present assumed craft, the values of K_v associated with the preliminary craft reported in Section 5.3 were much smaller than those given in Table 5-2 as a result of the smaller strut chords, smaller lift curve slopes and shorter struts that were assumed for the previous craft configuration; thus, the conclusion that dihedral was significant for the preliminary craft, whereas it would not be for the present craft.

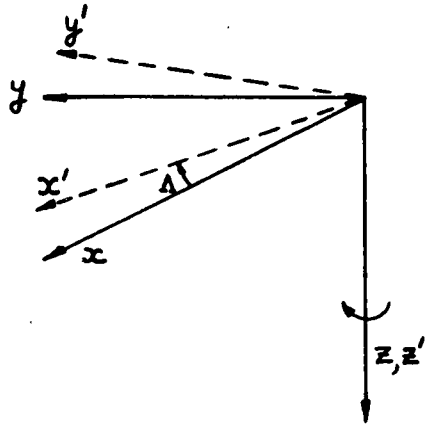

x in reference direction of motion.

x, z in vertical plane of symmetry.

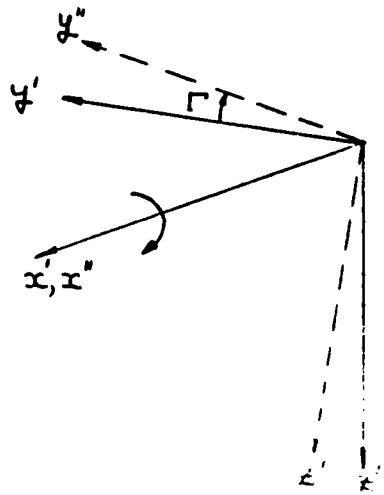

y" parallel to quarter chord span line of starboard foil.

FIG. 5-1 DIAGRAM DEFINING SWEEPBACK AND DIHEDRAL ANGLES.

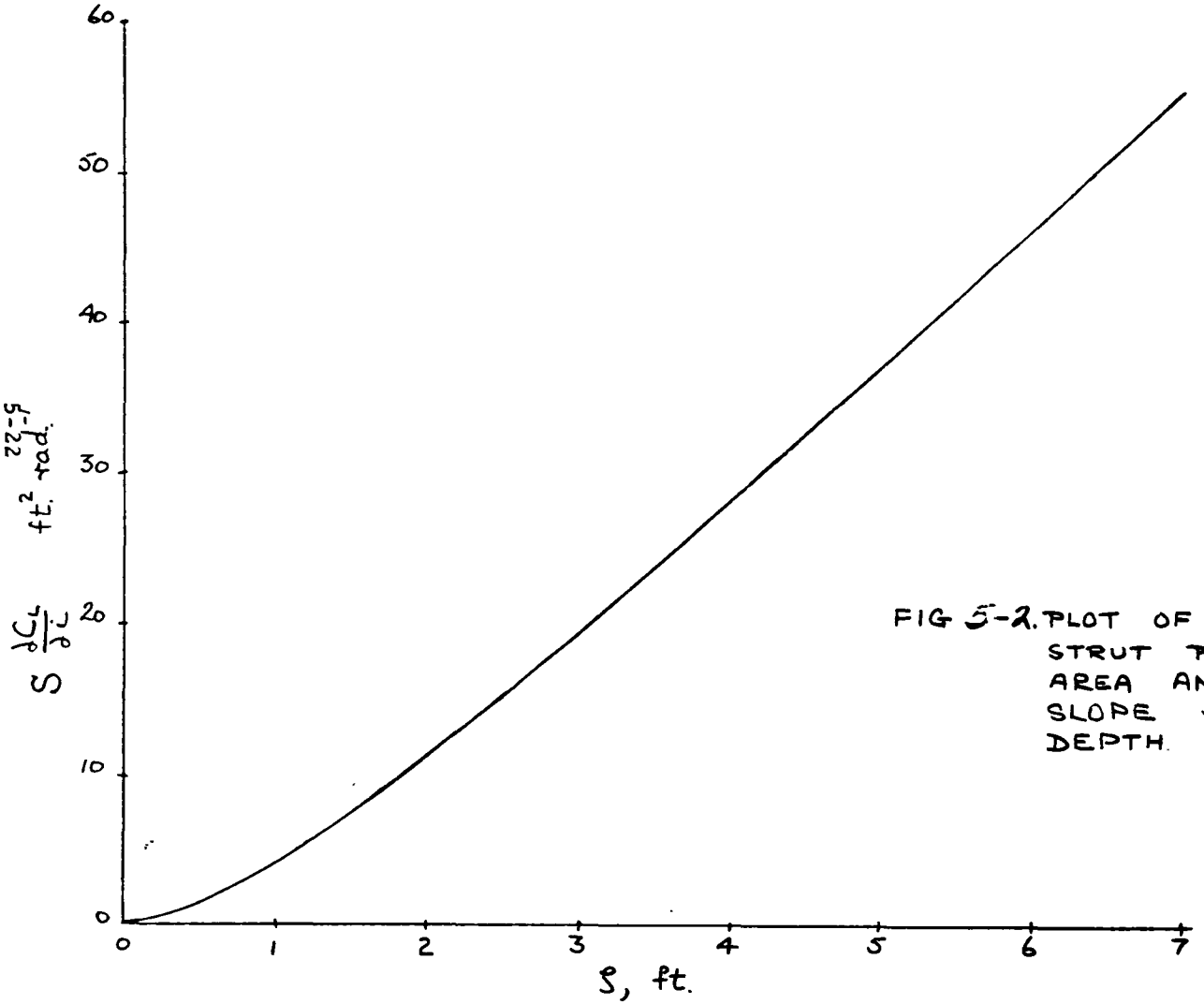

FIG 5-2. PLOT OF PRODUCT OF STRUT PROJECTED WETTED AREA AND LIFT CURVE SLOPE VS. SUBMERGED DEPTH.

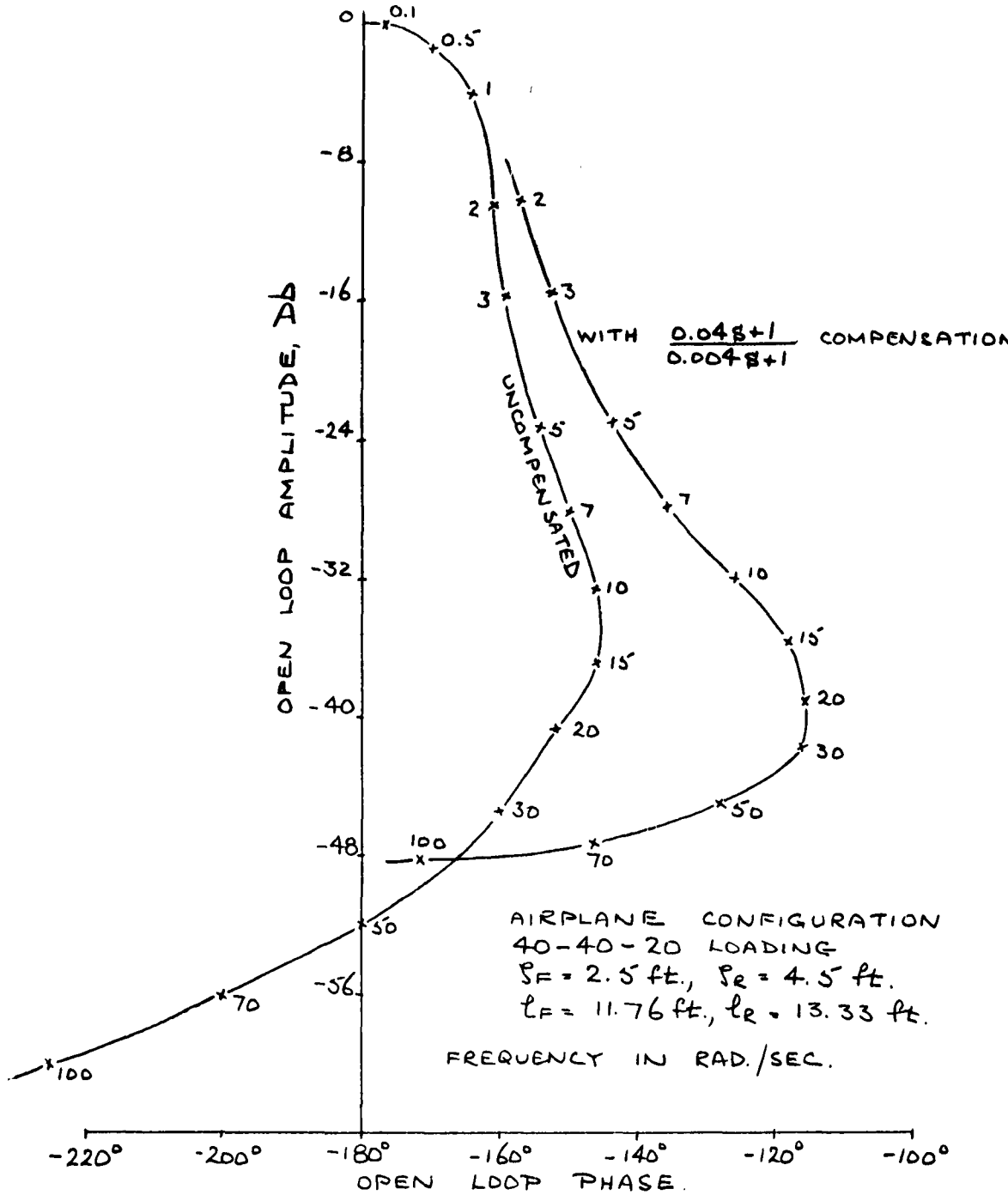

FIG. 5-3. CASE A. OPEN LOOP GAIN-PHASE PLOT

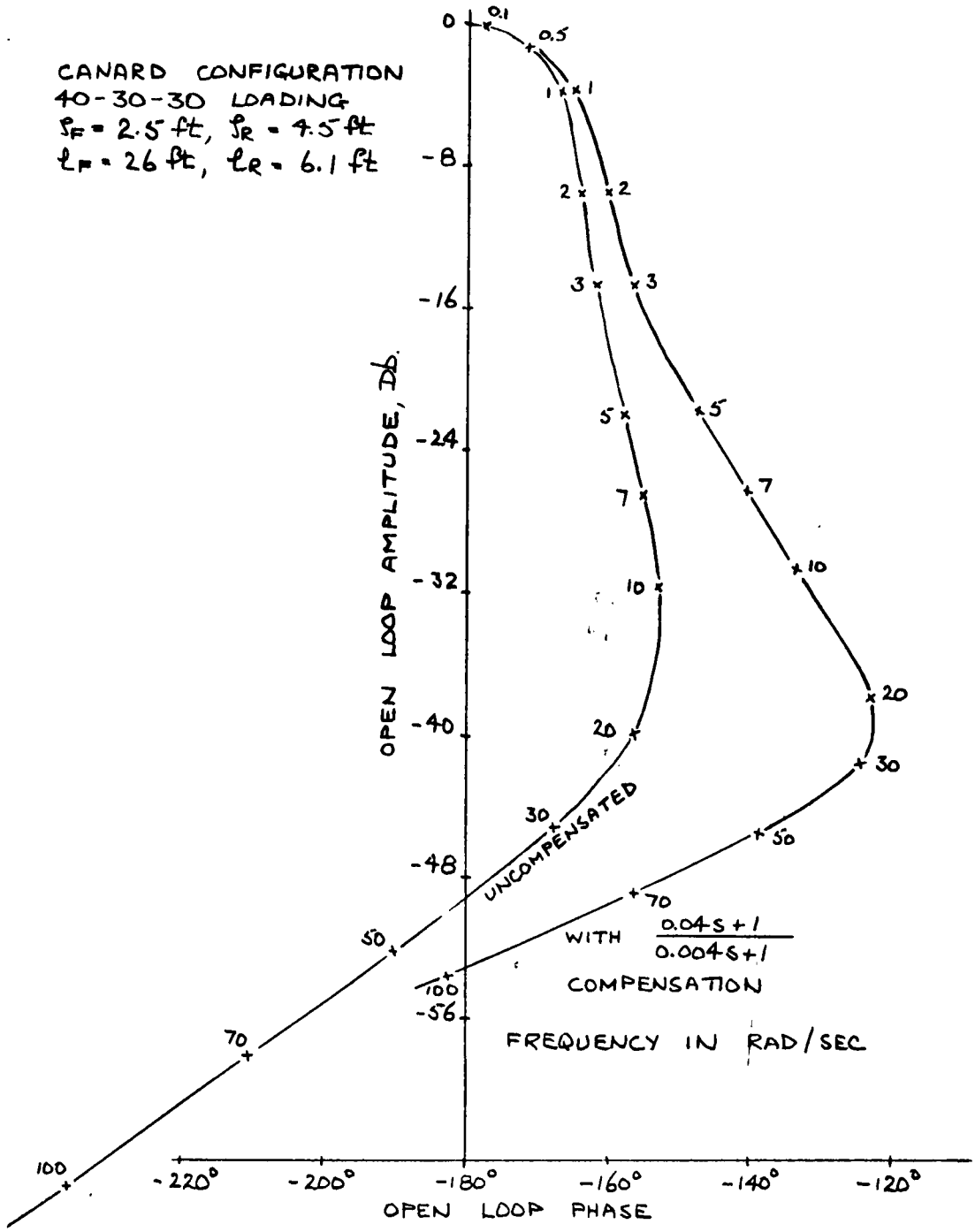

FIG 5-4. CASE B OPEN LOOP GAIN-PHASE PLOT.

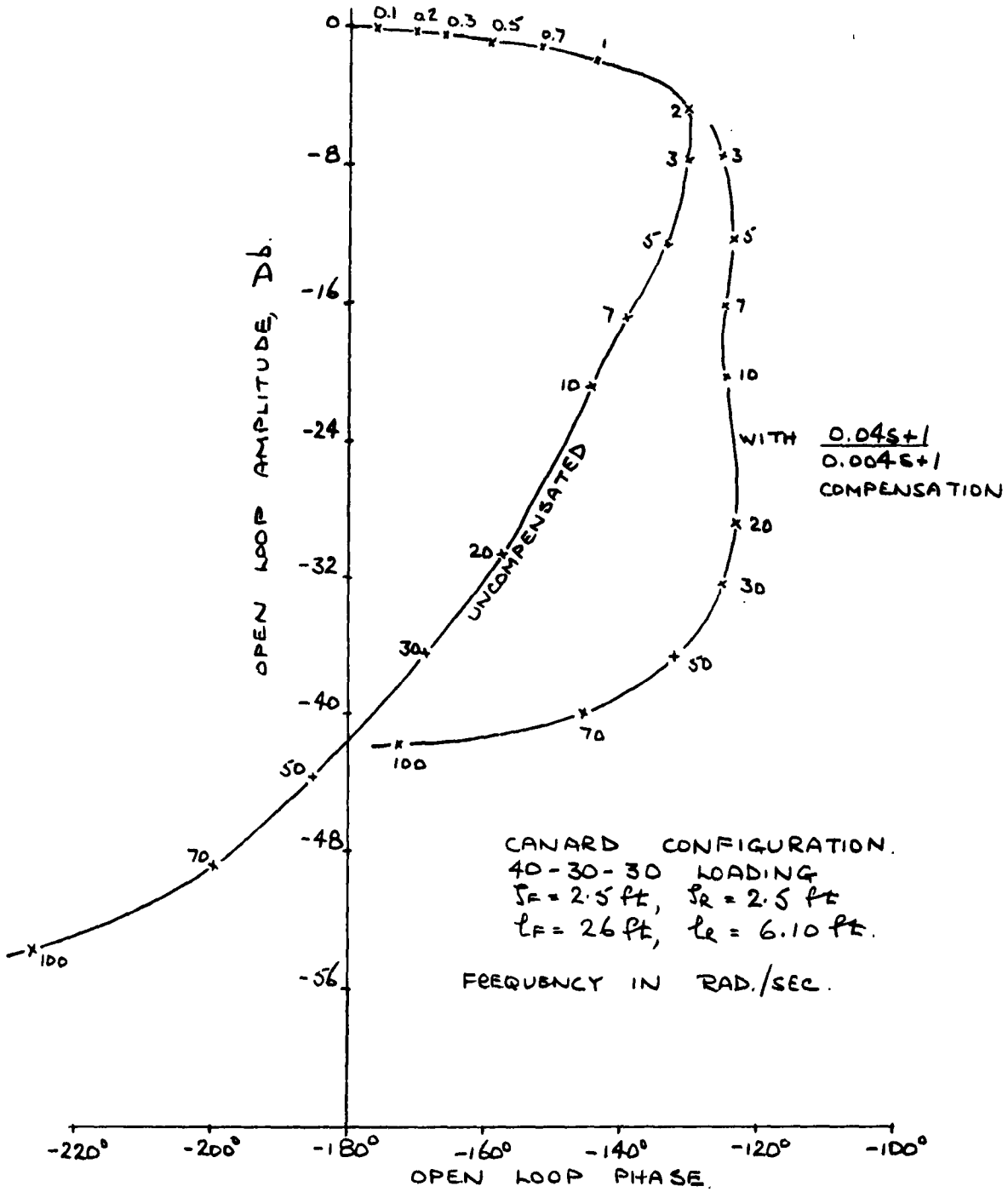

FIG 5-5. CASE C. OPEN LOOP GAIN PHASE PLOT

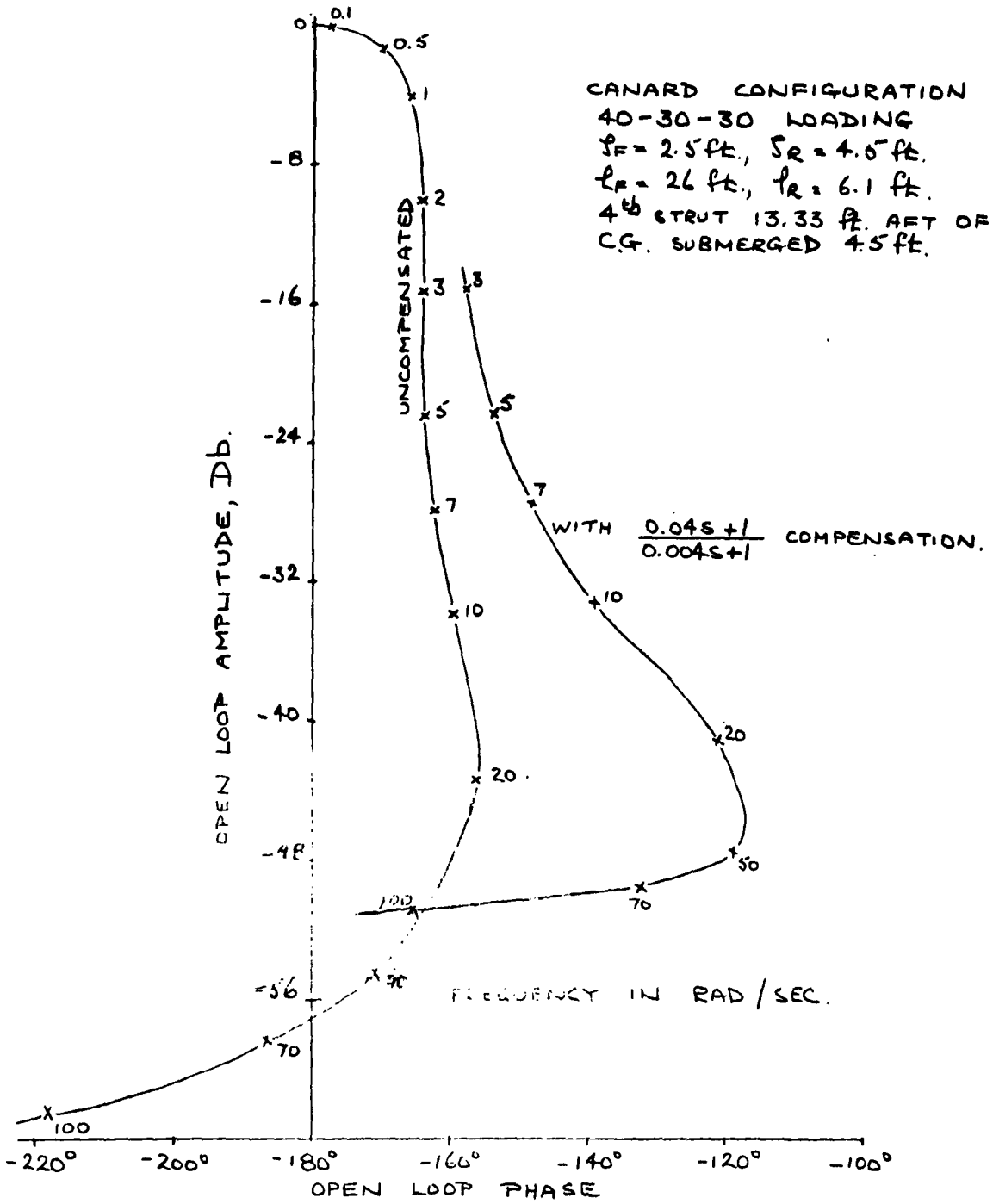

FIG. 5-6. CASE D OPEN LOOP GAIN-PHASE PLOT

SECTION 6

LONGITUDINAL DYNAMICS AND CONTROL SYSTEM DESIGN FOR THE CRAFT WITH SPRUNG FOILS

6.1 EQUATIONS FOR THE LONGITUDINAL ANALYSIS OF THE COMPLETE CRAFT EQUIPPED WITH SPRUNG FOILS

To verify and extend the work on the sprung foil longitudinal behavior of the high-speed test craft described in Section 4, an analysis of the overall craft dynamic characteristics has been undertaken.

Because unacceptable heave accelerations would result from any intentional contouring at high speeds in large waves, the normal operating regime of this craft is assumed to be restricted to platforming operation. Consequently, gravity forces are not expected to contribute to significant changes in forward speed. In addition, although surge acceleration may be as high as 0.1g in a State 3 Sea as a result of varying strut immersion (and therefore drag), such accelerations produce surge velocity perturbations of less than a couple of feet per second at typical wave encounter frequencies. Accordingly the surge mode is not included in the following analysis.

A body-centered coordinate system is assumed at the craft C.G. with x, y, and z axes forward, right, and down, respectively.

In general, the nomenclature used is that presented in the glossary (Section 2) with additions or exceptions as noted. (Many symbol definitions are repeated here for clarity.)

6.1.1 FORCES AND MOMENTS ON THE HULL

$$m_H(\dot{w}_G - u\theta) = m_H g \cos\theta - n_F R_F \cos\eta_F - n_R R_R \cos\eta_R \qquad (6\text{-}1)$$

where n_F, n_R = number of fore and aft struts respectively.

Let $\theta = \theta_o + \theta'$, $R_F = R_{F_o} + R'_F$ $R_R = R_{R_o} + R'_R$ $\eta_F = \eta_{F_o} + \eta'_F$, $\eta_R = \eta_{R_o} + \eta'_R$ all dashed quantities being perturbations.

Also $\dot{w}_G - u\dot{\theta} = -\frac{\ddot{h}'_G}{\cos\theta_o}$, where w_G = velocity of C. G. along the z axis, thus Equation 6-1 becomes

$$-\frac{m_H \ddot{h}'_G}{\cos\theta_o} = m_H g \cos\theta_o - m_H g \left(\sin\theta_o\right)\theta' - n_F R_{F_o} \cos\eta_{F_o}$$
$$- n_F R'_F \cos\eta_{F_o} + n_F \eta'_F R_{F_o} \sin\eta_{F_o} - n_R R_{R_o} \cos\eta_{R_o}$$
$$- n_R R'_R \cos\eta_{R_o} + n_R \eta'_R R_{R_o} \sin\eta_{R_o} \qquad (6\text{-}2)$$

Steady state requires that

$$m_H g \cos\theta_o - n_F R_{F_o} \cos\eta_{F_o} - n_R R_{R_o} \cos\eta_{R_o} = 0$$

Thus Equation 6-2 becomes

$$\frac{m_H \ddot{h}'_G}{\cos\theta_o} = m_H g \left(\sin\theta_o\right)\theta' + n_F R'_F \cos\eta_{F_o} - n_F R_{F_o} \left(\sin\eta_{F_o}\right)\eta'_F$$
$$-n_R R_{R_o} \left(\sin\eta_{R_o}\right)\eta'_R + n_R R'_R \cos\eta_{R_o} \qquad (6\text{-}3)$$

Thus,

$$\ddot{h}'_G = A_1\theta' + A_2\eta'_F + A_3\eta'_R + A_4 R'_F + A_5 R'_R \qquad (6\text{-}4)$$

Where

$$A_1 = g \sin \theta_o \cos \theta_o$$

$$A_2 = - \frac{n_F R_{F_o}}{m_H} \sin \eta_{F_o} \cos \theta_o$$

$$A_3 = - \frac{n_R R_{R_o}}{m_H} \sin \eta_{R_o} \cos \theta_o$$

$$A_4 = \frac{n_F}{m_H} \cos \eta_{F_o} \cos \theta_o$$

$$A_5 = \frac{n_R}{m_H} \cos \eta_{R_o} \cos \theta_o$$

The thrust T is assumed parallel to the x axis

$$I_y \ddot{\theta} = \eta_F R_F (\ell_{HF} \cos \eta_F - d_{HF} \sin \eta_F)$$

$$+N_R R_R (-\ell_{HR} \cos \eta_R - d_{HR} \sin \eta_R) + n_F M_{SF} + n_R M_{SR} - T d_T \qquad (6\text{-}5)$$

Subscripts HF and HR refer to dimensions to the fore and aft strut hinge points respectively. M_{SF} and M_{SR} are pitching moment contributions of fore and aft strut drags respectively.

Let $T = T_o + T'$ = total thrust

$$M_{SF} = - D_{SF} \left\{ d_{HF} + \overbrace{\quad}^{\frown}_{F} \cos \eta_F - \frac{\zeta_F}{2} \right\} \qquad (6\text{-}6)$$

$\overbrace{\quad}^{\frown}_{F}$ is the length, along the strut, from the hinge point to the fore foil and the strut drag is assumed parellel to the craft "x" axis at all times.

In terms of craft geometry (and assuming products of perturbation quantities zero)

$$\zeta_F = \zeta_{F_o} + h_{wF} - h'_g + \alpha_1 \, \theta' + \alpha_2 \, \eta'_F + \alpha_3 \, \xi'_F \tag{6-7}$$

where

$$\alpha_1 = - \left\{ \ell_{HF} \cos \theta_o + d_{HF} \sin \theta_o + \asymp_{F_o} \sin (\eta_{F_o} + \theta_o) \right\}$$

$$\alpha_2 = - \asymp_{F_o} \sin (\eta_{F_o} + \theta_o)$$

$$\alpha_3 = \cos (\eta_{F_o} + \theta_o)$$

ξ' is the perturbation spring deflection

$$\begin{aligned} \asymp_F \cos \eta_F &= \left(\asymp_{F_o} + \xi'_F \right) (\cos \eta_{F_o} - \eta'_F \sin \eta_{F_o}) \\ &= \asymp_{F_o} \cos \eta_{F_o} - \eta'_F \asymp_{F_o} \sin \eta_{F_o} + \xi'_F \cos \eta_{F_o} \end{aligned} \tag{6-8}$$

$$D_{SF} = C_{DSF} \frac{\rho}{2} C_{SF} \, \zeta_F \, u^2 \triangleq \beta_1 \, \zeta_F \tag{6-9}$$

Substituting Equations 6-7, 6-8 and 6-9 into 6-6 gives

$$M_{SF} = \gamma_0 + \gamma_1 \, h'_G + \gamma_2 \, \theta' + \gamma_3 \, \eta'_F + \gamma_4 \, \xi'_F + \gamma_5 \, H_{wF} \tag{6-10}$$

where

$$\gamma_0 = \beta_1 \, \zeta_{F_o} \left\{ d_{HF} + \asymp_{F_o} \cos \eta_{F_o} - \frac{\zeta_{F_o}}{2} \right\}$$

$$\gamma_1 = \beta_1 \left\{ d_{HF} + \asymp_{F_o} \cos \eta_{F_o} - \zeta_{F_o} \right\}$$

$$\gamma_2 = -\gamma_1 \, \alpha_1$$

$$\gamma_3 = \beta_1 \overline{\overline{\wedge}}_{F_o} \zeta_{F_o} \sin \eta_{F_o} - \alpha_2 \gamma_1$$

$$\gamma_4 = - \left\{ \alpha_3 \gamma_1 + \beta_1 \zeta_{F_o} \cos \eta_{F_o} \right\}$$

$$\gamma_5 = - \gamma_1$$

$$\beta_1 = C_{DSF} \frac{\rho}{2} C_{SF} u^2$$

Similarly

$$M_{SR} = \phi_0 + \phi_1 h'_G + \phi_2 \theta' + \phi_3 \eta'_R + \phi_4 \xi'_R + \phi_5 h_{wR} \qquad (6\text{-}11)$$

where

$$\phi_0 = - \beta_2 \zeta_{R_o} \left\{ d_{HR} + \overline{\overline{\wedge}}_{R_o} \cos \eta_{R_o} - \frac{\zeta_{R_o}}{2} \right\}$$

$$\phi_1 = \beta_2 \left\{ d_{HR} + \overline{\overline{\wedge}}_{R_o} \cos \eta_{R_o} - \zeta_{R_o} \right\}$$

$$\phi_2 = - \phi_1 \delta_1$$

$$\phi_3 = \beta_2 \overline{\overline{\wedge}}_{R_o} \zeta_{R_o} \sin \eta_{R_o} - \delta_2 \phi_1$$

$$\phi_4 = - \left\{ \delta_3 \phi_1 + \beta_2 \zeta_{R_o} \cos \eta_{R_o} \right\}$$

$$\phi_5 = - \phi_1$$

$$\beta_2 = C_{DSR} \frac{\rho}{2} C_{SR} u^2$$

$$\delta_1 = \left\{ \ell_{HR} \cos \theta_o - d_{HR} \sin \theta_o - \overline{\overline{\wedge}}_{R_o} \sin (\eta_{R_o} + \theta_o) \right\}$$

$$\delta_2 = - \overline{\overline{R}}_{R_o} \sin (\eta_{R_o} + \theta_o)$$

$$\delta_3 = \cos (\eta_{R_o} + \theta_o)$$

$$n_F R_F (\ell_{HF} \cos \eta_F - d_{HF} \sin \eta_F)$$

$$= \psi_0 + \psi_1 R'_F + \psi_2 \eta'_F \qquad (6\text{-}12)$$

Where

$$\psi_0 = n_F R_{F_o} (\ell_{HG} \cos \eta_{F_o} - d_{HF} \sin \eta_{F_o})$$

$$\psi_1 = n_F (\ell_{HF} \cos \eta_{F_o} - d_{HF} \sin \eta_{F_o}) = \frac{\psi_o}{R_{F_o}}$$

$$\psi_2 = - n_F R_{F_o} (\ell_{HF} \sin \eta_{F_o} + d_{HF} \cos \eta_{F_o})$$

$$n_R R_R (-\ell_{HR} \cos \eta_R - d_{HR} \sin \eta_R)$$

$$= \nu_0 + \nu_1 R'_R + \nu_2 \eta'_R \qquad (6\text{-}13)$$

Where

$$\nu_0 = -n_R R_{R_o} (\ell_{HR} \cos \eta_{R_o} + d_{HR} \sin \eta_{R_o})$$

$$\nu_1 = \frac{\nu_o}{R_{R_o}}$$

$$\nu_2 = n_R R_{R_o} (\ell_{HR} \sin \eta_{R_o} - d_{HR} \cos \eta_{R_o})$$

Substituting Equations 6-10, 6-11, 6-12 and 6-13 into Equation 6-5 gives

$$I_y\ddot{\theta} = \psi_0 + \psi_1 R'_F + \psi_2 \eta'_F + \nu_0 + \nu_1 R'_R + \nu_2 \eta'_R$$

$$+ n_F (\gamma_0 + \gamma_1 h'_G + \gamma_2 \theta' + \gamma_3 \eta'_F + \gamma_4 \xi'_F + \gamma_5 h_{wF})$$

$$+ n_R (\phi_0 + \phi_1 h'_G + \phi_2 \theta' + \phi_3 \eta'_R + \phi_4 \xi'_R + \phi_5 h_{wR})$$

$$- d_T (T_o + T')$$

or

$$\ddot{\theta} = \mu_0 + \mu_1 R'_F + \mu_2 R'_R + \mu_3 \eta'_F + \mu_4 \eta'_R + \mu_5 h'_g + \mu_6 \theta'$$

$$+ \mu_7 \xi'_F + \mu_8 \xi'_R + \mu_9 h'_{wF} + \mu_{10} h_{wR} + \mu_{11} T' \qquad (6\text{-}14)$$

Where

$$\mu_0 = \frac{\psi_o + \nu_o + n_F \gamma_o + n_R \phi_o - d_T T_o}{I_y} = 0 \text{ (normally)}$$

$$\mu_1 = \psi_1 / I_y \qquad \mu_2 = \frac{\nu_1}{I_y}$$

$$\mu_3 = \frac{\psi_2 + n_F \gamma_3}{I_y} \qquad \mu_4 = \frac{\nu_2 + n_R \phi_3}{I_y}$$

$$\mu_5 = \frac{n_F \gamma_1 + n_R \phi_1}{I_y} \qquad \mu_6 = \frac{n_F \gamma_2 + n_R \phi_2}{I_y}$$

$$\mu_7 = \frac{n_F \gamma_4}{I_y} \qquad \mu_8 = \frac{n_R \phi_4}{I_y}$$

$$\mu_9 = \frac{n_F \gamma_5}{I_y} \qquad \mu_{10} = \frac{n_R \phi_5}{I_y}$$

$$\mu_{11} = -d_T / I_y$$

6.1.2 DYNAMIC EQUATIONS ASSOCIATED WITH THE FOILS

A. Fore Foil

Referring displacement of fore foil to inertial axes, centered at the C.G. and having its $\bar{x}$ axis parallel to mean sea surface, positive $\bar{z}$ axis downward

$$\bar{x}_F = \ell_{HF} \cos\theta + d_{HF} \sin\theta + \Big\}_F \sin(\theta + \eta_F) \tag{6-15}$$

$$\bar{z}_F = -\ell_{HF} \sin\theta + d_{HF} \cos\theta + \Big|_F \cos(\theta + \eta_F) - h'_G \tag{6-16}$$

Differentiating Equations 6-15 and 6-16 twice and neglecting products of variables gives

$$\ddot{\bar{x}}_F = -\ell_{HF} \ddot{\theta}' \sin\theta_o + d_{HF} \ddot{\theta}' \cos\theta_o + \ddot{\xi}'_F \sin(\theta_o + \eta_{F_o}) + \Big\}_{F_o} (\ddot{\theta}' + \ddot{\eta}'_F) \cos(\theta_o + \eta_{F_o}) \tag{6-17}$$

$$\ddot{\bar{z}}_F = -\ell_{HF} \ddot{\theta}' \cos\theta_o - d_{HF} \ddot{\theta}' \sin\theta_o + \ddot{\xi}'_F \cos(\theta_o + \eta_{F_o}) - \Big\}_{F_o} (\ddot{\theta}' + \ddot{\eta}'_F) \sin(\theta + \eta_{F_o}) - \ddot{h}'_G \tag{6-18}$$

The acceleration of the fore foil along the strut is,

$$\begin{aligned} a_F &= \ddot{\bar{x}}_F \sin(\theta_o + \eta_{F_o}) + \ddot{\bar{z}}_F \cos(\theta_o + \eta_{F_o}) \\ &= \ddot{\xi}'_F - \ddot{\theta}' (\ell_{HF} \cos\eta_{F_o} - d_{HF} \sin\eta_{F_o}) - \ddot{h}'_G \cos(\theta_o + \eta_{F_o}) \end{aligned} \tag{6-19}$$

Thus the equation of motion of the foil becomes

$$m_F\left\{\ddot{\xi}'_F - \ddot{\theta}'\left(\ell_{HF}\cos\eta_{F_o} - d_{HF}\sin\eta_{F_o}\right) - \ddot{h}_G\cos\left(\theta_o + \eta_{F_o}\right)\right\} = R_F - F_F + m_F g\cos\left(\eta_F + \theta\right) \tag{6-20}$$

where F_F, F_R are the hydrodynamic forces on the fore and aft foils respectively.

Now $$R_F - F_F + m_F\, g\cos\left(\eta_F + \theta\right)$$

$$= R_{F_o} + R'_F - F_{F_o} - F'_F + m_F\, g\cos\left(\eta_{F_o} + \theta_o\right)$$

$$- m_F\, g\left(\theta' + \eta'_F\right)\sin\left(\eta_{F_o} + \theta_o\right) \tag{6-21}$$

For steady-state equilibrium

$$R_{F_o} - F_{F_o} + m_F\, g\cos\left(\eta_{F_o} + \theta_o\right) = 0 \tag{6-22}$$

Thus, substituting Equations 6-21 and 6-22 in Equation 6-20 gives

$$m_F\left\{\ddot{\xi}_F - \ddot{\theta}'\left(\ell_{HF}\cos\eta_{F_o} - d_{HF}\sin\eta_{F_o}\right) - \ddot{h}'_G\cos\left(\theta_o + \eta_{F_o}\right)\right\}$$

$$= R'_F - F'_F - m_F g\left(\theta' + \eta'_F\right)\sin\left(\eta_{F_o} + \theta_o\right) \tag{6-23}$$

B. Aft Foil

By analogy with Equation 6-23, the rear foil gives

$$m_R\left\{\ddot{\xi}_R + \ddot{\theta}'\left(\ell_{HR}\cos\eta_{R_o} + d_{HR}\sin\eta_{R_o}\right) - \ddot{h}'_G\cos\left(\theta_o + \eta_{R_o}\right)\right\}$$

$$= R'_R - F'_R - m_R g\left(\theta' + \eta'_R\right)\sin\left(\eta_{R_o} + \theta_o\right) \tag{6-24}$$

C. Spring Reactions

It will be assumed that the spring reaction is divided into the simple reaction of a linear spring and a force subject to control (self-centering action).

Thus, $$R'_F = R'_{CF} - \xi'_F K_F \tag{6-25}$$

and $$R'_R = R'_{CR} - \xi'_R K_R \tag{6-26}$$

K_F and K_R are fore and aft foil spring stiffnesses respectively.

R'_{CF} and R'_{CR} are fore and aft control quantities achieved by cylinder pressurization.

D. Hydrodynamic Forces on the Foils

1. Fore Foil

$$F'_F = \left\{ \frac{C'_{L_{CF}}}{\cos(\theta_o + \eta_{F_o})} + C'_{N_{I_F}} \right\} \frac{\rho}{2} S_F u^2 \tag{6-27}$$

Where $C'_{L_{CF}}$ is the circulatory lift coefficient increment and $C'_{N_{IF}}$ is the normal force coefficient exerted on the foil by virtual inertia.

Now

$$C'_{N_{IF}} = \frac{\pi}{4} \frac{a_1 c_F}{u^2} \left\{ a_F - \dot{w}_{om_F} \right\}$$

where $a_1 = 1.353$ (approximation derived from data in Ref. 6-1)

$$= 1.063 \frac{C_F}{u^2} \left\{ a_F - \dot{w}_{om_F} \right\} \tag{6-28}$$

a_F being defined in Equation 6-19

$$C'_{L_{CF}} = i'_F \frac{\partial C_{LF}}{\partial i_F} + \zeta'_F \frac{\partial C_{LF}}{\partial \zeta_F} \tag{6-29}$$

$$i'_F = (\dot{z}_F - w_{om_F})/u + \eta'_F + \theta' \tag{6-30}$$

$$= \frac{1}{u}\left[\dot{\xi}'_F \cos(\theta_o + \eta_{F_o}) - \dot{\theta}'(\ell_{HF} \cos\theta_o + d_{HF} \sin\theta_o) - \dot{h}'_G \right.$$

$$\left. - \overline{\overline{F_o}} (\dot{\theta}' + \dot{\eta}'_F) \sin(\theta_o + \eta_{F_o}) - w_{om_F} \right] + \eta'_F + \theta'$$

$\zeta'_F = h_{wF} - h'_G + \alpha_1 \theta' + \alpha_2 \eta'_F + \alpha_3 \xi'_F$ from Equation 6-7.

2. Rear Foil (by similarity with fore foil)

$$F'_R = \left\{ \frac{C'_{L_{CR}}}{\cos(\theta_o + \eta_{R_o})} + C'_{N_{IR}} \right\} \frac{\rho}{2} S_R u^2 \tag{6-31}$$

$$C'_{N_{IR}} = 1.062798 \frac{c_R}{u^2} \left\{ a_R - \dot{w}_{om_R} \right\} \tag{6-32}$$

where $a_R = \ddot{\xi}'_R + \ddot{\theta}'(\ell_{HR} \cos\eta_{R_o} - d_{HR} \sin\eta_{R_o})$

$$- \ddot{h}'_G \cos(\theta_o + \eta_{R_o}) \tag{6-33}$$

$$C'_{L_{CR}} = i'_R \frac{\partial C_{LR}}{\partial i_R} + \zeta'_R \frac{\partial C_{LR}}{\partial \zeta_R} \tag{6-34}$$

$$i'_R = \frac{1}{u}\left[\dot{\xi}'_R \cos(\theta_o + \eta_{R_o}) + \dot{\theta}'(\ell_{HR}\cos\theta_o - d_{HR}\sin\theta_o) - \dot{h}'_G - \overbrace{\quad}^{\quad} R_o(\dot{\theta}' + \dot{\eta}'_R)\sin(\theta_o + \eta_{R_o}) - w_{om_R}\right] + \eta'_R + \theta' \quad (6\text{-}35)$$

$$\zeta'_R = h_{wR} - h'_G + \delta_1\theta' + \delta_2\eta'_R + \delta_3\xi'_R \quad (6\text{-}36)$$

6.1.3 LOW FREQUENCY BEHAVIOR

If the masses and virtual inertias of the foils are considered negligible (an assumption that yields good results at and below about 8 rad/sec for the high-speed test craft as demonstrated by the example in Section 6.3), then Equations 6-23 and 6-24 become

$$R'_F = F'_F \quad (6\text{-}37)$$

$$R'_R = F'_R \quad (6\text{-}38)$$

The force on the fore foil becomes

$$F'_F = \frac{\rho}{2} S_F u^2 \frac{1}{\cos(\theta_o + \eta_{F_o})}\left\{i'_F \frac{\partial C_{LF}}{\partial i_F} + \zeta'_F \frac{\partial C_{LF}}{\partial \zeta_F}\right\} \quad (6\text{-}39)$$

where,

$$i'_F = \frac{1}{u}\left[\dot{\xi}'_F \cos(\theta_o + \eta_{F_o}) - \dot{\theta}'(\ell_{HF}\cos\theta_o + d_{HF}\sin\theta_o) - \dot{h}'_G - \overbrace{\quad}^{\quad} F_o(\dot{\theta}' + \dot{\eta}'_F)\sin(\theta_o + \eta_{F_o}) - w_{om_F}\right] + \eta'_F + \theta' \quad (6\text{-}40)$$

$$\zeta'_F = h_{wF} - h'_G + \alpha_1\theta' + \alpha_2\eta'_F + \alpha_3\xi'_F \qquad (6\text{-}41)$$

The force on the rear foil becomes

$$F'_R = \frac{\rho}{2} s_R u^2 \frac{1}{\cos(\theta_o + \eta_{R_o})} \left\{ i'_R \frac{\partial C_{LR}}{\partial i_R} + \zeta'_R \frac{\partial C_{LR}}{\partial \zeta_R} \right\} \qquad (6\text{-}42)$$

$$i'_R = \frac{1}{u} \left[\dot{\xi}'_R \cos(\theta_o + \eta_{R_o}) + \dot{\theta}' (\ell_{HR} \cos\theta_o - d_{HR} \sin\theta_o) - \dot{h}'_G \right.$$

$$\left. - \overline{\overline{R_o}} (\dot{\theta}' + \dot{\eta}'_R) \sin(\theta_o + \eta_{R_o}) - w_{om_R} \right] + \eta'_R + \theta' \qquad (6\text{-}43)$$

$$\zeta'_R = h_{wR} - h'_G + \delta_1\theta' + \delta_2\eta'_R + \delta_3\xi'_R \qquad (6\text{-}44)$$

6.2 LONGITUDINAL PARAMETERS OF THE SPRUNG FOIL HIGH-SPEED TEST CRAFT

6.2.1 CRAFT PARAMETERS USED IN THE COMPUTATIONS OF SECTION 6.4

m_H = 1112 slugs

m_F = 12.6 slugs

m_R = 14.8 slugs

θ_o = 0

n_f = 1

n_R = 2

η_{F_o} = 4.36 deg; η_{R_o} = 5.24 deg

I_y = 1.97×10^5 slug-ft^2

S_F = S_R = 6.82 ft^2

u = 135 ft/sec (80 knots)

$\overline{\overline{\quad}}_{F_o}$ = 9.5 ft

$\overline{\overline{\quad}}_{R_o}$ = 11.5 ft

K_F = K_R = 1000 lb/ft

ζ_{F_o} = 2.5 ft; ζ_{R_o} = 4.5 ft

ρ = 2 slugs

d_T = 3.4 ft

d_{HF} = 1.4 ft

d_{HR} = 1.4 ft

ℓ_{HF} = 25.28 ft

ℓ_{HR} = 7.15 ft

R_{F_o} = 11,287 lb

R_{R_o} = 13,019 lb

$\partial C_{L_F}/\partial i_F = 1.134$; $\partial C_{L_R}/\partial i_R = 1.078$

$\partial C_{L_F}/\partial \zeta_F = \partial C_{L_R}/\partial \zeta_R = -0.0022$

$w_{om_F} = w_{om_R} = 0$

$R'_{CF} = R'_{CR} = 0$ (pressure control forces)

$C_{DSF} = C_{DSR} = 0.012$

6.3 SIMPLIFYING APPROXIMATIONS FOR THE LONGITUDINAL ANALYSIS

Early in the analysis it was recognized that hydrodynamic damping forces on the foils (angle of incidence induced by heave velocity) were much larger at low frequencies than inertial forces associated with the foil structure (including virtual inertia effects). Over the appropriate frequency regime then, these inertial forces may be neglected

with a consequent reduction in the order of the characteristic equation describing the system.

The following example indicates the range of frequencies over which this approximation is useful.

Consider the hull to be held stationary: then the characteristic equation describing foil behavior at the forward foil is

$$\xi'_F \left[\left(m_F + m_{wF} \right) s^2 + \frac{\partial F'_F}{\partial \dot{\xi}'_F} s + K_F \right] = 0 \qquad (6\text{-}45)$$

with $m_F = 12.6$ slugs

$m_{wF} = 10.8$ slugs

$K_F = 1000$ lb/ft

$$\frac{\partial F'_F}{\partial \dot{\xi}'_F} = \rho/2 \, S_F \, u \, \frac{\partial C_{LF}}{\partial \dot{\imath}_F} = 1040 \text{ lb-sec/ft}$$

Therefore, $\xi'_F (23.4 s^2 + 1040 s + 1000) = 0 \qquad (6\text{-}46)$

the roots being found at

$s = -43.3 \text{ sec}^{-1}$

or $s = -0.983 \text{ sec}^{-1}$

It will be seen from Equation 6-46 that, if the s^2 term is dropped as negligible, the remaining root is

$$s = -\frac{1000}{1040} = -0.962 \text{ sec}^{-1}$$

which is a very good approximation to the smaller root of the above quadratic. The larger root contributes phase shift of only 10 degrees at about 8 rad/sec, a frequency somewhat above that of peak energy density (6 rad/sec) for a State 3 head sea at a speed of 80 knots. Accordingly, the elimination of the foil inertia effects permits a useful simplification which was utilized in the following calculations leading to the roots of the characteristic equation for several configurations.

6.4 POLES OF THE CHARACTERISTIC EQUATION

Using the data and method of Sections 6.2 and 6.3, and including Equations 6-4, 6-14 and 6-37 through 6-44, the characteristic equation for three configurations has been computed. The roots of these equations are shown below and have been plotted in Figure 6-1.

Basic Sprung Foil Configuration

Characteristic Equation = $(s+0.501)(s-2.01)(s+1.40+2.96j)(s+0.075 \pm 1.15j)$

Sprung Foil Configuration Minus Surface Proximity and Strut Drag Effects

Characteristic Equation = $s^2(s-0.084\pm0.445j)(s+1.07\pm2.54j)$

Rigid Strut Configuration

Characteristic Equation = $(s-1.54)(s+6.62)(s+0.765\pm1.20j)$

It will be observed that the assumption of rigidly attached foils reduces the number of roots from six to four. Also the divergent root (right-half-plane pole on the axis) disappears when the basic configuration is computed minus the surface proximity and strut drag

effects. Although the surface proximity effect is destabilizing (unlike the analogous effect at subcavitating speeds) it is nevertheless rather weak in its effect on the divergent pole in comparison to the strut-induced pitching moment effect.

The strut-drag effect is not unique to this craft or its relatively high operating speeds. This same effect has been included in previous analog computer simulations of a large, subcavitating craft which was, with the aid of the stabilizing surface proximity effect, nevertheless marginally stable. However, with the much higher speed of the present craft and with its fairly large struts relative to the size of the craft, the strut-drag effect is so much increased that a divergent root of significant proportion results.

It is also interesting to note that the divergent root is present whether the foils are sprung or rigidly attached to the hull although its position is somewhat altered.

Considerations of control techniques for the longitudinal system follow in the next section.

6.5 CONTROL OF THE LONGITUDINAL SYSTEM

Some computations of the characteristic equation for the longitudinal dynamic behavior of the sprung foil craft were presented in Section 6.4. Computations of the entire transfer functions relating some important variables are listed below. The computations were made using the data of Section 6.2, unless otherwise noted.

6.5.1 USE OF FORWARD FOIL INCIDENCE FOR CONTROL

Craft C.G. heave and pitch attitude are related to forward foil incidence control as follows:

$$\frac{h_G}{\eta_F} = \frac{\left[-1.461\ s^4+123.5s^3+89.54s^2+132.0s+5283\right] \times 10^6}{(s+0.501)(s-2.01)(s+1.396\pm 2.96j)(s+0.075\pm 1.15j)} \qquad (6\text{-}47)$$

$$\frac{\theta}{\eta_F} = \frac{\left[-0.290s^4+21.08s^3+14.97s^2+47.36s-5.515\right] \times 10^6}{(s+0.501)(s-2.01)(s+1.396\pm 2.96j)(s+0.075\pm 1.15j)} \qquad (6\text{-}48)$$

From these expressions, the transfer function relating the heave at any point along the craft longitudinal centerline to the forward incidence control may be computed simply as

$$\frac{h_x}{\eta_F} = \left[\frac{h_G}{\eta_F}\right] + \ell_x \left[\frac{\theta}{\eta_F}\right] \qquad (6\text{-}49)$$

where ℓ_x is the distance forward of the C.G.

The characteristic equation of the craft contains a right-half-plane real pole at s=2.01 (see Equations 6-47 and 6-48). To ensure the greatest chance for stabilizing the system, it is desirable to arrange the system transfer function so that it will not contain any right-half-plane zero, i.e., that the numerator of the function does not include roots with real positive parts. It is obvious from the numerators of both equations that at least one pole with a real part does exist, since at least one sign change occurs in the coefficients. Thus, it is impractical to consider control of the craft (either manual or automatic) represented by Equations 6-47 and 6-48 by sensing pitch attitude (θ) or measuring the heave at the C.G. (h_G).

The more general case represented by Equation 6-49 may be considered. Since this equation yields the transfer function connecting forward foil incidence with heave motion measured at a point ℓ_x

(forward of the C.G. is (+)) along the "x" axis, it was thought that some real value of ℓ_x could yield a function having no zeros with positive real parts. Substitution of Equations 6-47 and 6-48 into Equation 6-49 and a subsequent investigation of the characteristics of the resulting numerator polynomial showed that there is no real value of ℓ_x that yields all coefficients with a common sign and therefore the function will have zeros with positive real parts. Accordingly, it must be concluded that a heave measurement, no matter where within or without the hull outline it may be taken, may not be expected to permit stabilization of the longitudinal system in either manual or automatic mode using forward incidence control.

6.5.2 USE OF FORWARD AND AFT FOIL INCIDENCE CONTROL

Calculation of the functional relationships connecting aft foil incidence change with heave at the C.G. and pitch attitude was also computed using the data of Section 6.2. The results are shown below.

$$\frac{h_G}{\eta_R} = \frac{[-4.139s^4+246s^3+167.6s^2+1051s-5708]\times 10^6}{(s+0.501)(s-2.01)(s+1.396\pm 2.96j)(s+0.075\pm 1.15j)} \qquad (6\text{-}50)$$

$$\frac{\theta}{\eta_R} = \frac{[-0.02093s^4-1.738s^3-0.9245s^2-25.24s+20.92]\times 10^6}{(s+0.501)(s-2.01)(s+1.396\pm 2.96j)(s+0.075\pm 1.15j)} \qquad (6\text{-}51)$$

It is clear that neither expression possesses zeros which all contain negative real parts. Thus control of the craft using aft incidence control and either heave at the C.G. or pitch attitude measurement is not likely to provide a stable system.

Combining Equations 6-50 and 6-51 as

$$\frac{h_x}{\eta_R} = \frac{h_G}{\eta_R} + \ell_x \frac{\theta}{\eta_R} \qquad (6\text{-}52)$$

and using ℓ_x = 27 feet (location of height sensor forward of the C.G.) yields

$$\frac{h_{HS}}{\eta_R} = \frac{\left[-4.704s^4+199s^3+142.7s^2+369s-5143\right] \times 10^6}{(s+0.501)(s-2.01)(s+1.396\pm2.96j)(s+0.075\pm1.15j)} \qquad (6\text{-}53)$$

and a similar calculation gives

$$\frac{h_{HS}}{\eta_F} = \frac{(-9.30s^4+692.6s^3+493.7s^2+1411s+5134) \times 10^6}{(s+0.501)(s-2.01)(s+1.396\pm2.96j)(s+0.075\pm1.15j)} \qquad (6\text{-}54)$$

It is thus possible to combine the action of fore and aft incidence control in a simple ratio so that the operator's control stick motion will produce proportional but different incidence changes fore and aft. Thus, the overall transfer function relating operator's stick motion to heave at the height sensor becomes

$$\frac{h_{HS}}{\text{Stick Motion}} = k_{\eta_F}\left[\frac{h_{HS}}{\eta_F}\right] + k_{\eta_R}\left[\frac{h_{HS}}{\eta_R}\right]$$

$$= k_{\eta_F}\left[\left(\frac{h_{HS}}{\eta_F}\right) + \frac{k_{\eta_R}}{k_{\eta_F}}\left(\frac{h_{HS}}{\eta_R}\right)\right] \qquad (6\text{-}55)$$

The expression within the brackets may now be analyzed for suitability of control for various values of the ratio $\frac{k_{\eta_R}}{k_{\eta_F}}$.

The numerator of this expression may then be written as

$$10^6 \left[(-9.30-4.704 \frac{k_{\eta_R}}{k_{\eta_F}}) s^4 + (692.6+199 \frac{k_{\eta_R}}{k_{\eta_F}}) s^3 \right.$$

$$\left. + (493.7+142.7 \frac{k_{\eta_R}}{k_{\eta_F}}) s^2 \; 6 \; (1411+369 \frac{k_{\eta_R}}{k_{\eta_F}}) s + (5134-5143 \frac{k_{\eta_R}}{k_{\eta_F}}) \right]$$

(6-56)

A common sign for all coefficients (+) may be assured, provided

$$-3.461 < \frac{k_{\eta_R}}{k_{\eta_F}} < -2.247$$

The other condition required to be met to guarantee no poles of the above expression with real positive parts may be written as

$$a_1(a_3a_2-a_4a_1) - a_3^2 a_0 \begin{cases} > 0 \text{ (for coefficients with (+) signs)} \\ < 0 \text{ (for coefficients with (-) signs)} \end{cases} \quad (6\text{-}57)$$

where a_i is the coefficient of s^i in Equation 6-56, i = 1, 2, 3, 4. Substitution of the coefficients of Equation 6-56 into the left-hand side of Equation 6-57 using values of the ratio k_{η_R}/k_{η_F} between -3.461 and and -2.247 results in a negative value for the expression and thus failure to satisfy the inequality of Equation 6-57. Accordingly, it must be concluded that no single combination of fore and aft incidence control is likely to permit stabilization of the craft represented by the Equations 6-53 and 6-54.

6.5.3 USE OF FORWARD AND AFT REACTION CONTROL

The quantities R'_{CF} and R'_{CR} may be found in the equations presented in Section 6.1. They represent perturbation forces which may be applied, if desired, essentially in parallel with those produced by the pneumatic springs. Because no spring deflection is required before forces will be felt on the hull with this control, it was believed that a better opportunity for stability might be thus afforded.

The pertinent equations are (note that the quantity h_{HS} is still defined at ℓ_x = 27 feet):

$$\frac{h_{HS}}{R'_{CF}} = \frac{(4459s^4+1406s^3+8359s^2+32,560s-11,340)}{(s+0.501)(s-2.01)(s+1.396\pm2.96j)(s+0.075\pm1.15j)} \qquad (6\text{-}58)$$

and

$$\frac{h_{HS}}{R'_{CR}} = \frac{(-202s^4-1810s^3-2795s^2-63,230s-5070)}{(s+0.501)(s-2.01)(s+1.396\pm2.96j)(s+0.075\pm1.15j)} \qquad (6\text{-}59)$$

Once again a combination of fore and aft reaction control may be represented as

$$\frac{h_{HS}}{\text{Stick Input}} = \frac{h_{HS}}{R'_{CF}} + k_{RC}\,\frac{h_{HS}}{R'_{CR}} \qquad (6\text{-}60)$$

The numerator of Equation 6-60 becomes

$$\left[(4459-202\,k_{RC})\,s^4 + (1406-1810\,k_{RC})\,s^3 + (8359-2795\,k_{RC})\,s^2 + (32,560-63,230\,k_{RC})\,s - 11,340-5070\,k_{RC}\right] \qquad (6\text{-}61)$$

now, for $k_{RC} < -2.24$; all coefficients above are (+)

$k_{RC} > 22.1$; all coefficients above are (-)

it remains to show the boundaries of the second criterion (Equation 6-57) and to determine whether there is any region of overlap with the first criterion.

Substituting the coefficients of s that appear in Equation (6-61) and simplifying the resulting expression yields

$$a_1(a_3a_2 - a_4a_1) - a_3^2 = 0.504 \times 10^{12}\left[k_{RC}^3 - 34.24\,k_{RC}^2 + 34.02\,k_{RC} - 8.57\right]$$

The factored form of this expression is

$$a_1(a_3a_2 - a_4a_1) - a_3^2a_0 = 0.504 \times 10^{12}(k_{RC} - 0.490)(k_{RC} - 0.526)(k_{RC} - 33.2) \qquad (6\text{-}62)$$

Investigation of these roots shows

$a_1(a_3a_2 - a_4a_1) - a_3^2a_0 = (+)$ for $0.490 < k_{RC} < 0.526$ and $k_{RC} > 33.2$

$= (-)$ for $0.526 < k_{RC} < 33.2$ and $k_{RC} < 0.490$

It will be observed that a region satisfying both criteria exists within the boundaries of

$$22.1 < k_{RC} < 33.2$$

Taking $k_{RC} = 27$;

$$\text{numerator of } \frac{h_{HS}}{\text{Stick Input}} = -995s^4 - 47,460s^3 - 67,106s^2 - 1,675,000s - 125,600$$

or

$$\text{numerator of } \frac{h_{HS}}{\text{Stick Input}} = -995(s + 47.0)(s + 0.071)(s + 0.300 \pm 5.94j)$$

Although this set of zeros is entirely confined to those with negative real parts, this does not guarantee stability but merely enhances the possibility of achieving it.

6.6 FURTHER ANALYSIS IN SUPPORT OF THE LONGITUDINAL SIMULATION PROGRAM

The analyses of the previous subsection were carried out for a single craft configuration involving what may be called the reference conditions and represented by the characteristic equation of Equation 6-47. Although the mathematical model used for these calculations included all the useful simplifications that it was deemed justifiable to make, the resulting expressions still contained a fourth order numerator and a sixth order denominator. Because the analytical investigation of more promising additional configurations was overly time-consuming, the simulation facility was utilized to investigate the possibly greater controllability of other configurations as well as to verify the difficulty of control for that case already studied.

Early results from the longitudinal simulation showed that the configuration represented by the parameters of Section 6.2, is, indeed, difficult if not impossible for a human operator to stabilize. Nor is the case derived in the preceding subsection of this report sufficiently docile to permit suitable longitudinal control of the craft.

A craft configuration was found, however, which showed promise of being amenable to control by a human operator. This involved the use of a forward foil, incidence-controlled, all mechanical, spring centering loop as described in Section 4. Back-up analysis was carried out for this case to serve as a check solution for the simulator setup and also to indicate the direction of optimizing controllability on the simulator.

6.6.1 BASIC EQUATIONS FOR THE UNCONTROLLED CRAFT

The basic equations of the craft are presented in Section 6.1. Using the relationship representing the sub-loop of forward foil mechanical incidence control ($\eta'_F = k_{IF}\,\xi'_F$ where $k_{IF} = 0.1$ rad/ft) and an aft spring stiffness of $K_R = 1500$ feet with the remaining parameters as presented in Section 6.2 yields the following craft dynamic equations:

$$s^2 h'_G + (0)\,\theta + 0.9731\xi'_F + 2.686\,\xi'_R = 0.000896\,R'_{CF} + 0.00179\,R'_{CR} - 2.138\,\eta'_R - 0.7713\,\eta_{F_C} \qquad (6\text{-}63)$$

$$-0.06016\,h'_G + (s^2 - 0.2778)\,\theta + 0.1705\,\xi'_F - 0.04897\,\xi'_R = 0.0001274\,R'_{CF} - 0.0000736\,R'_{CR} - 0.03319\,\eta'_R - 0.1712\,\eta_{F_C} \qquad (6\text{-}64)$$

$$(1043\,s - 274.9)\,h'_G - (148,200 - 27,130s)\,\theta - (965s + 14,850)\,\xi'_F + (0)\,\xi'_R = -R'_{C_F} + (141,200 - 753.5s)\,\eta_{F_C} \qquad (6\text{-}65)$$

$$(992.5s - 275.2)\,h'_G - (6055s + 132,500)\,\theta + (0)\,\xi'_F - (933.4s + 1226)\,\xi'_R = (134,450 - 1042s)\,\eta'_R - R'_{C_R} \qquad (6\text{-}66)$$

where

η_{F_C} = additional control input to forward foil incidence.

Simultaneous solution of these equations leads to the following characteristic polynomial:

$$\text{characteristic polynomial} = 953,750\,(s^6 + 16.63\,s^5 + 27.66\,s^4 + 28.10s^3 + 70.12s^2 - 64.98s - 338.8)$$

which, when factored, yields

$$953,750\,(s - 1.42)(s + 14.87)\,(s - 0.274 \pm j2.033)\,(s + 1.86 \pm j0.663)$$

6.6.2 ROOT LOCUS SOLUTION USING ADDITIONAL FORWARD INCIDENCE CONTROL

The equations of the previous section have been utilized to determine the numerator (the zeros) of the function h'_{ξ_F}/η_{F_C} as follows:

$$h'_{\xi_F}/\eta_{F_C} \approx h'_G/\eta_{F_C} + \ell_{HS}\,\theta/\eta_{F_C} - \xi'_F/\eta_{F_C} \qquad (6\text{-}67)$$

where

h'_{ξ_F} = heave of the forward foil

The quantity h'_{ξ_F} was chosen as a possible feedback quantity because its use eliminates the lag otherwise introduced by the spring when heave of the hull is used as primary feedback with forward incidence control. (The latter combination of feedback and control quantities has already been discussed in Section 6.5.)

Simultaneous solution for the zeros of Equations (6-63) through (6-66) and substitution into Equation (6-67) yields

$$\text{zeros of } h'_{\xi_F}/\eta_{F_C} = 138.7 \times 10^6 (s + 1.79s)(s + 0.287 \pm 2.29j)$$

$$(s - 0.581 \pm 1.89j)$$

An additional large real root has been dropped as negligible in the above expression. Thus, the complete expression becomes

$$\frac{h'_{\xi_F}}{\eta_{F_C}} = 145.4 \frac{(s + 1.795)(s + 0.287 \pm 2.29j)(s - 0.581 \pm 1.89j)}{(s - 1.421)(s + 14.87)(s - 0.274 \pm 2.033j)(s + 1.86 \pm 0.663j)}$$

A root locus plot of this expression is shown in Figure 6-2. Additionally, some points are indicated on this same figure that have been plotted from measured simulator data for two specific gains (7.27 on the root locus plot corresponding to

$$\eta_{F_C}/h'_{\xi_F} = 0.05 \text{ rad/ft},$$

and 3.64 corresponding to

$$\eta_{F_C}/h'_{\xi_F} = 0.25 \text{ rad/ft.})$$

These points correspond closely with those which may be expected from the analytically derived locus. It is seen from this plot that the number of right-half-plane poles in the closed loop bear the following relationship to the gain of the system:

$p' = 3$ for $K' < 9.1$

$p' = 2$ for $9.1 < K' < 23.4$

$p' = 4$ for $23.4 < K' < 30.0$

$p' = 2$ for $K' > 30.0$

where

p' = number of closed loop right-half-plane poles

K' = gain along locus derived from analysis

No value of gain associated with the simple feedback loop represented by

$$\eta_{F_C} = k_{\eta_F} h'_{\xi_F}$$

yields stability. Furthermore, a study of possible simple compensation within this loop indicates none lead to a stable system with a reasonable stability margin.

6.6.3 ROOT LOCUS SOLUTION USING A SIMPLE FORWARD REACTION CONTROL LOOP

The basic equations (Equations (6-63) through (6-66)) have been utilized to compute the function

$$h'_{HS}/R'_{C_F}$$

to investigate the use of forward reaction control.

Simultaneous solution of these equations yields the following expression:

$$\frac{h'_{HS}}{R'_{CF}} = \frac{0.004336\,(s + 2.92)\,(s + 14.2)\,(s + 0.474 \pm 2.24j)}{(s - 1.421)(s + 14.87)(s - 0.274 \pm 2.033j)(s + 1.86 \pm 0.663j)}$$

The root locus plot of this function may be seen in Figure 6-3. (The left-half-plane real pole and zero have been assumed to cancel in the plots.) A measured point near the locus at a gain of 2.69 has been

used to verify the analog simulation for this configuration. It is clear from this locus that, although the simple divergence may be eliminated at a gain of 1.87, no value of gain can banish all the closed-loop poles from the right-half-plane. Furthermore, as in the previous case, no series compensation was found that would assure an acceptable stability margin for this case.

Notwithstanding the rather discouraging prospects of control represented by the preceding analytical work, it was possible to evolve a control system configuration on the simulator that utilized fore and aft reaction controls with inputs supplied by height at the forward foil in acceleration signal and pitch attitude to produce a well-behaved, stable configuration. Details of the setup are covered in Section 10.

6.7 OPERATION OF THE SUPERCAVITATING FOILS AT AND BELOW TAKE-OFF SPEED

Take off under design sea state conditions is a major problem on high-speed hydrofoil craft. The high foil loadings and poor low-speed characteristics make high hull-borne speeds mandatory in the absence of an auxiliary low-speed foil system.

Assuming that no auxiliary means of producing low-speed lift are available, the problem is reduced to that of minimizing the speed of take off and thus minimizing the punishment the hull (and crew) will be subjected to by wave impact. This procedure requires operation of a supercavitating foil at speeds well below design speed.

The hull draught of the FRESH craft is 2.3 feet with zero foil lift. Thus, while partial lift by the foils below take-off speed might be employed, because the rate of change of draught with foil lift is a minimum (due to hull shape) for small foil lifts, not much relief in terms of wave-hull impact may be expected until foil lift can amount to a large fraction of craft weight. Furthermore, since foil lift varies with the square of forward speed, substantial foil lift will not be produced until craft speed approaches take-off speed.

Thus it is clear that foil lift may be expected to relieve wave impact forces appreciably only at speeds close to take off and hull structure must be designed appropriately.

Control loop signals must be prevented from driving the foil incidence to large angles during this period since the drag would increase to the point where take off would be impossible for the FRESH craft with the assumed foils.

The speed at which, in calm water with the CG at 8.4 feet above the surface (nominal strut submergence of 2.5 feet forward and 4.5 feet aft), drag equals the maximum thrust (18,000 pounds) is 41.5 knots. With foil incidence at an angle of over 20 degrees at this speed, the drag contributed by the foils accounts for practically the entire amount. Although the foils are capable of producing the required lift at slightly lower speeds, the drag exceeds the thrust available.

The calm water speed with the hull base line just touching the surface is 45 knots, the increased strut drag being primarily responsible for reducing the thrust available to overcome foil drag.

However, by taking advantage of forward momentum to ensure a minimum hull-borne time for take off, it is possible to accelerate in displacement to some 43 knots with little or no foil incidence, then demand a sudden increase of incidence so that by the time the craft has lifted clear (during which time the drag has exceeded 18,000 pounds) the speed will drop to about 42 knots.

Since the thrust available from a jet engine depends significantly on temperature, take off should be possible at slightly lower speed under cold conditions.

These speeds are quoted for the maximum craft weight of 37,184 pounds; at lower weights, reduce take-off speeds should be possible.

Landing should be a less hazardous procedure since there is no thrust limitation and the full lift capabilities of the foils can be employed. However, it must be borne in mind that maximum lift occurs at an angle of incidence of 40 degrees or so which may prove to be mechanically inconvenient. The craft will naturally tend to settle stern first, since the aft foils are substantially more heavily loaded under the zero thrust conditions.

Reference

6-1. P. Kaplan and C. J. Henry, "A Study of Hydro-elastic Instability of Supercavitating Hydrofoils," Davidson Laboratory Report No. R-838, Stevens Institute of Technology, March 1961.

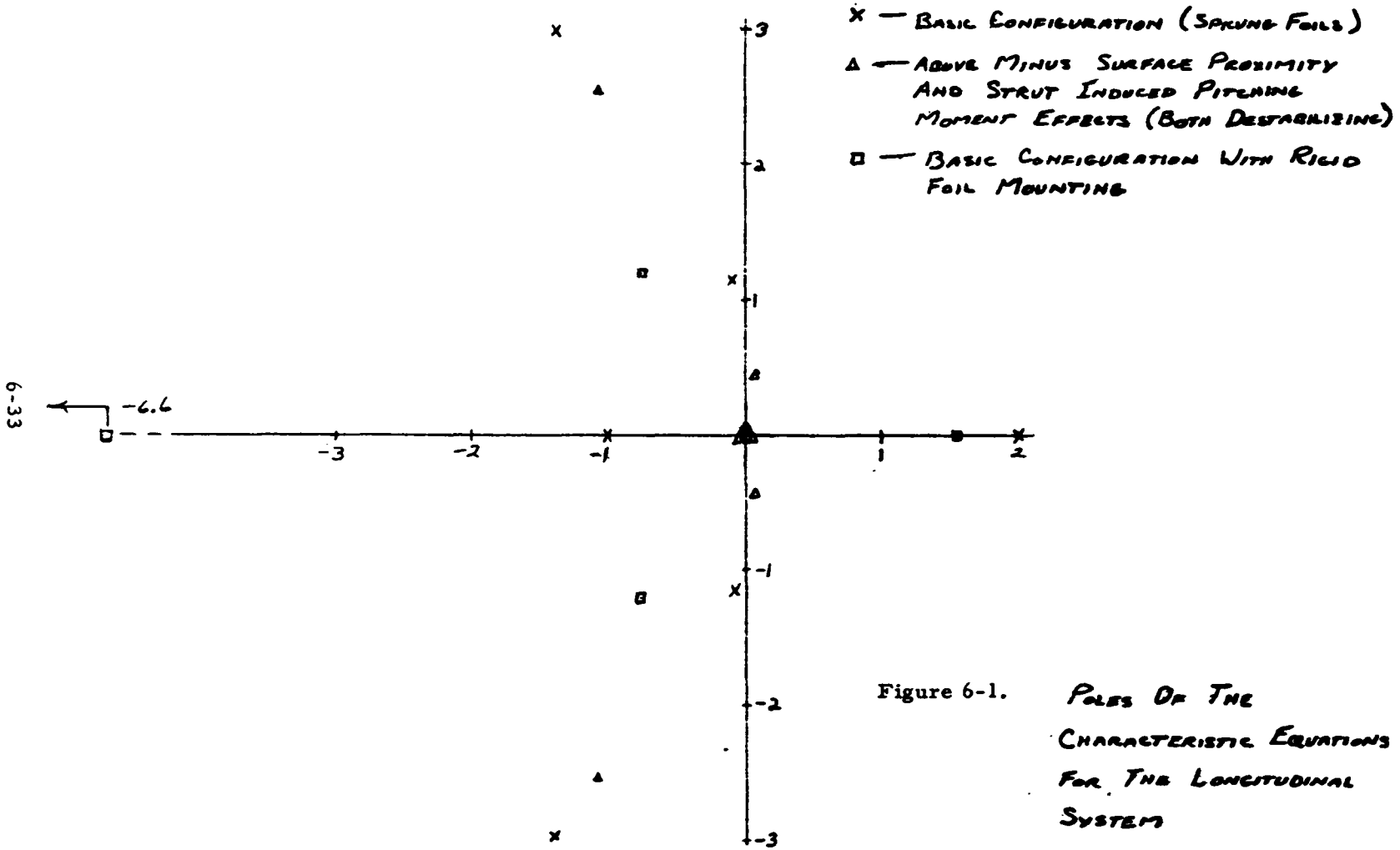

Figure 6-1. Poles Of The Characteristic Equations For The Longitudinal System

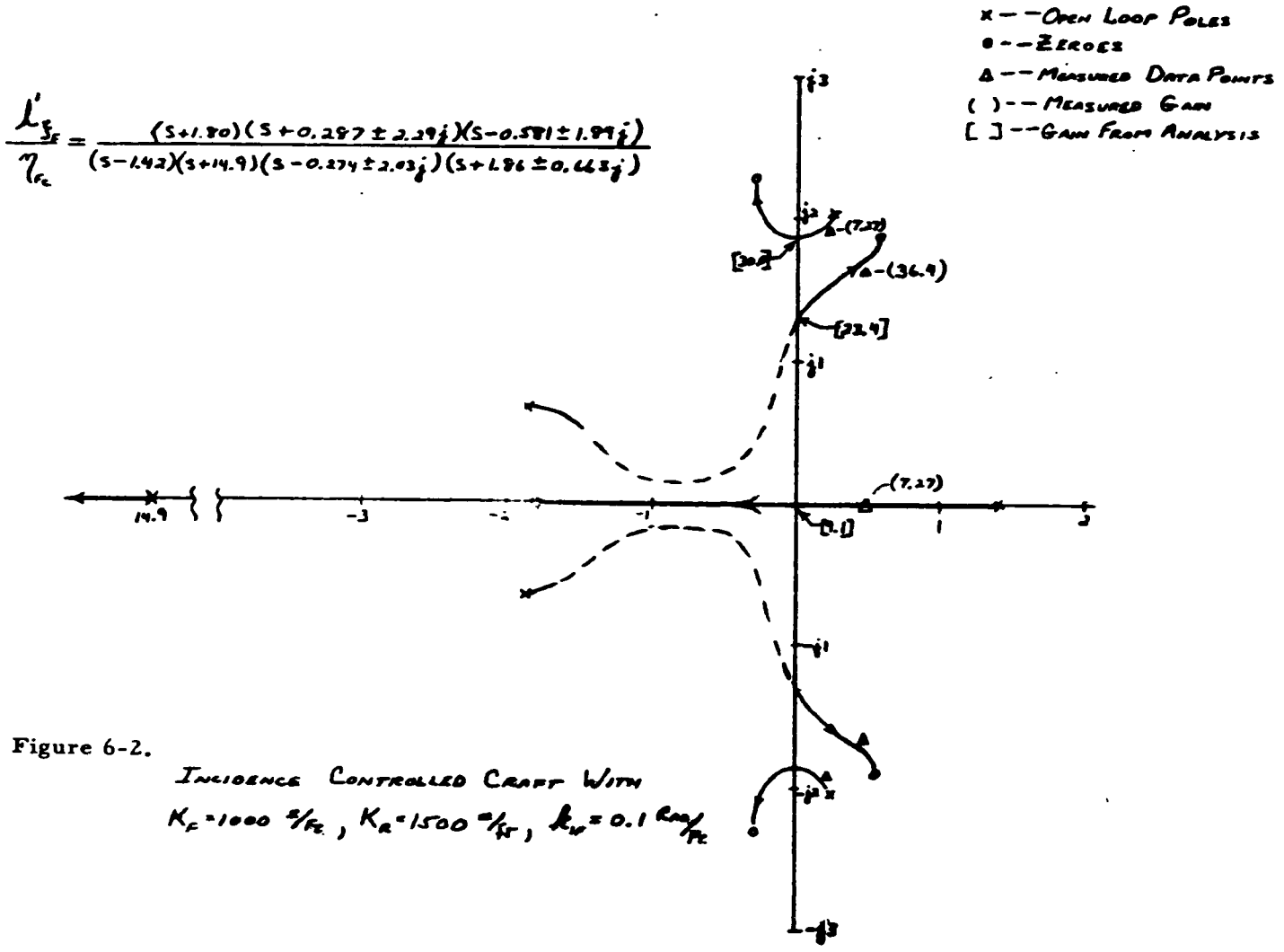

Figure 6-2.

Incidence Controlled Craft With

$K_c = 1000\ ^{g}/_{c}$, $K_a = 1500\ ^{rad}/_{sr}$, $k_w = 0.1\ ^{rad}/_{fps}$

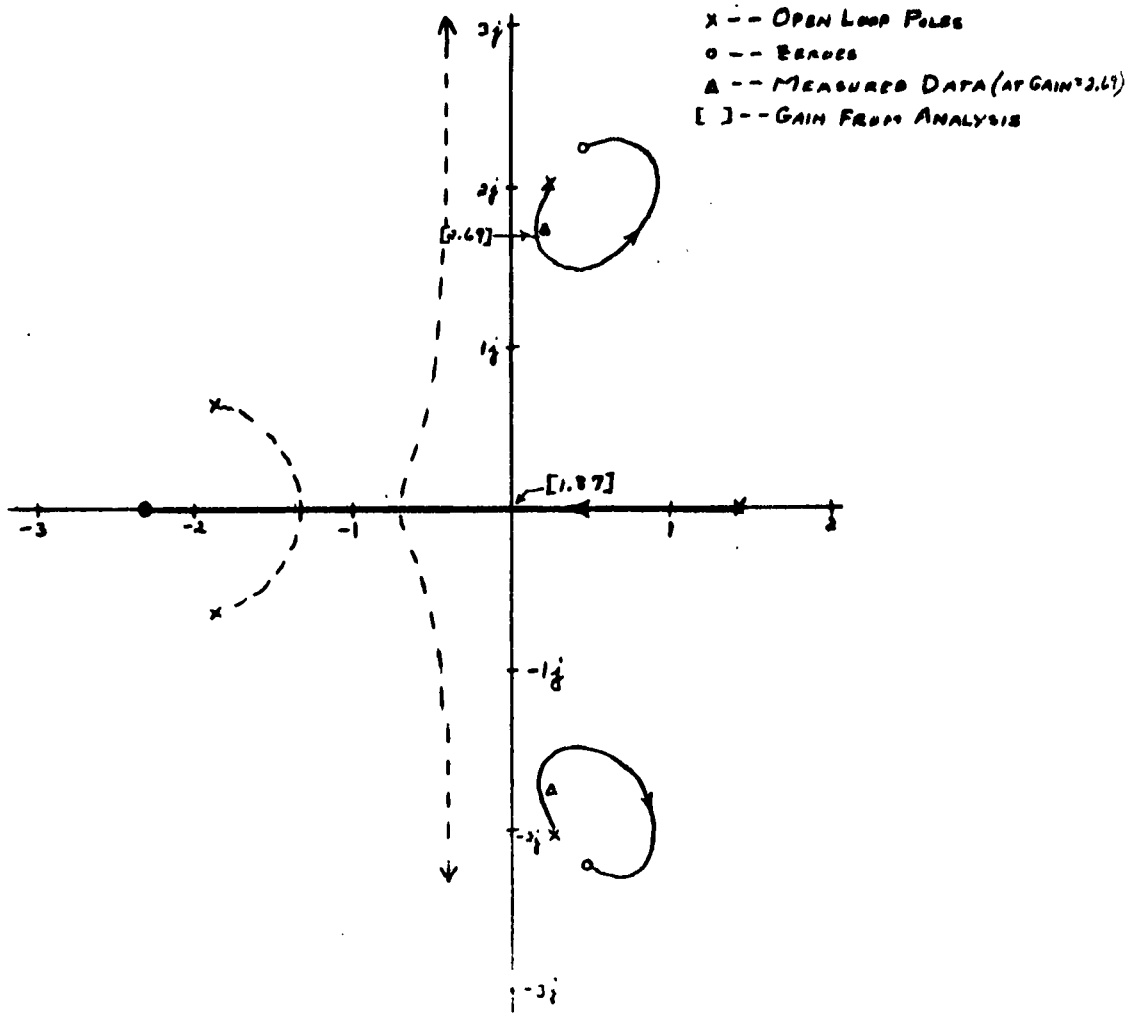

$$\frac{\mathcal{L}_{HS}}{R'_{CF}} = \frac{(s+2.92)(s+0.474 \pm 2.24j)}{(s-1.421)(s-0.274 \pm 2.033j)(s+1.86 \pm 0.663j)}$$

Figure 6-3. Reaction Controlled Craft With $K_P = 1000$ ft-lb/rad, $K_R = 1500$ ft-lb/rad, $K_{IP} = 0.1$ rad/ft-lb

SECTION 7

CONSIDERATIONS IN THE MANUAL CONTROL OF HYDROFOIL CRAFT

7.1 HUMAN OPERATOR CHARACTERISTICS AND SYSTEM REQUIREMENTS

7.1.1 INTRODUCTION

Reliability of the control system is of no small concern in the operation of fully-submerged foil hydrofoil craft. The possibility of equipment failure within the control system leads logically to considerations of two specific aspects of this problem. First is the action that may have to be taken, either manually or by some automatic monitor, immediately upon determination of the occurrence of a failure to prevent catastrophic impact of the craft with the water until speed is reduced to a safe level for landing. (The high-speed test craft is to be designed to sustain full impact at cruise speed and at any reasonable entry attitide.) Second is the ability to revert to an "emergency" operational mode which will permit foilborne operation to be resumed and the mission to be completed, even though some loss of craft performance and/or effectiveness occurs.

The latter circumstance will be considered in detail in the following work. In this case, human control of the craft in both longitudinal and lateral modes will be studied as an effective replacement for the electronic autopilot in the event of autopilot malfunction.

Following the establishment of human control criteria, the dynamic characteristics of the high-speed test craft will be introduced and the

relative controllability of different craft configurations will be considered.

7.1.2 MINIMUM EQUIPMENT REQUIRED FOR MANUAL CONTROL

Although many aircraft have been controlled using trailing edge flaps actuated solely by the operator's muscle power, the hydrofoil loadings (on the order of 20 to 40 times those of small aircraft) effectively eliminate the use of muscle power alone for hydrofoil control surface actuation. It must be assumed that some power amplification device is present and operative at all times between the operator's control stick motions and the lift control element(s). Failure in such a device must be assumed to jeopardize, if not entirely prevent, the ability to resume foilborne operation, even in an emergency manual mode.

In addition to control surface power boosters, if emergency manual control is desired at night, control function sensors must be assumed to be available and operational in order to supply the necessary pilot displays.

7.1.3 PROPERTIES OF THE HUMAN CONTROL ELEMENT

Control of the longitudinal and lateral modes of a hydrofoil craft fall into the category of a "compensating tracking task", i.e., the visual display is the system forcing function minus the modified control response (modified by the dynamics of the system being controlled). Considerable attention has been given in the literature to the general problem of tracking various input time functions. Data of Reference 7-1 were taken using mostly statistical inputs with the simple test setup as diagrammed below

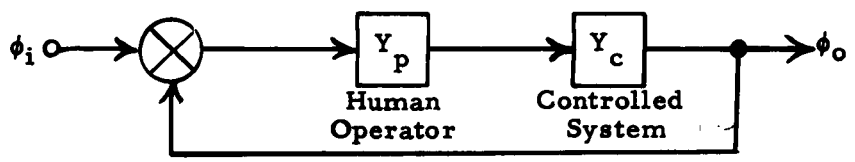

By measurements on the output quantity it is possible to deduce the value of Y_p for various input functions and values of the controlled quantity of the form $Y_c = 1, \frac{1}{(s+1)}, \frac{1}{(s/2+1)}, K/s, \frac{s+1}{s}, \frac{0.5\,s+1}{5\,s+1}$ ...etc.

In every case where a statistical input was used for the various forms of Y_c, a pure delay having a Laplace form of $e^{-\tau s}$ appeared as a constituent of the "best fit" Y_p function. Only in the limited series of tests using pure sine wave inputs was this delay term missing.

In regard to other terms, it was found that the operator could be described by an expression of the form

$$Y_p = \frac{K_p\, e^{-\tau s}\,(T_L\, s + 1)}{(T_I\, s + 1)\,(T_N\, s + 1)} \qquad (7\text{-}1)$$

where the value of τ varied from 0.15 to 0.30 second. The remaining parameters turn out to be widely variable depending on the form of Y_c and the input, but have the general trend

$$\frac{1}{T_I} < \frac{1}{T_L} \ll \frac{1}{T_N}$$

The high frequency lag represented by T_N was frequently missing completely from the representation. For cases where $Y_c = K_c$, the human operater adjusted his gain (K_p) to compensate for a change in K_c over a wide range. Introduction of a lag in Y_c resulted in the introduction of the lead term ($\frac{1}{T_L}$) at a frequency tending to cancel the effects of the introduced lag.

These studies are only indicative of the considerations involved in the control of a hydrofoil craft since, in the lateral system of a typical

fully-submerged foil craft, a right-half plane pole is always present. None of the tests covered such a dynamic configuration. In Reference 7-2, a study of considerable detail has been carried out involving the human control of a system having the general form

$$Y_c(s) = \frac{A(s^2 + 2\zeta_\phi \omega_\phi s + \omega_\phi^2)}{\underbrace{(s + 1/T_s)}_{\text{Spiral}} \underbrace{(s + 1/T_R)}_{\substack{\text{Roll} \\ \text{Subsidence}}} \underbrace{(s^2 + 2\zeta_d \omega_d s + \omega_d^2)}_{\text{Dutch Roll}}} \qquad (7\text{-}2)$$

This function is typical of the lateral dynamics of aircraft and is therefore pertinent in the present discussion.

In the early part of Reference 7-2, the general form of the operator's characteristics (Y_p) is presented and is identical to Equation (7-1).

The following rules describe the manner in which the significant parameters of this transfer function are varied by the human:

(1) The human adapts the form of his equalizing characteristic to achieve stable good low-frequency closed-loop response. A low-frequency lag (T_I) is generated when it would improve low-frequency characteristics without jeopardizing high-frequency stability to the extent that it may not be controlled with the addition of a single first order lead (T_L).

(2) After the equalizing function form has been adopted, actual values (of T_I, T_L) are selected to be those that would result in an open loop phase margin between 60 and 110 degrees.

There is an obvious similarity between these rules governing the human's characteristics and the selection of compensation made by the serve designer to achieve satisfactory system performance.

The studies of Reference 7-2 were split into subsections in which certain simplifications of Equation 7-2 were considered initially. Thus, attention is first directed at human control of a system having a transfer function of the form

$$Y_c(s) = \frac{\pm K_\phi}{(\pm T_s\, s + 1)(T_R\, s + 1)} \qquad (7\text{-}3)$$

If the denominator contains a right-half plane pole $(-T_s\, s + 1)$, then the above expression approximates the form of the transfer function for the lateral system of a hydrofoil craft.

Conclusions resulting from control consideration of Equation 7-3 (still assuming a human characteristic as in Equation 7-1), and spiral divergence follow.

(1) For the case of $T_s/T_R > 30$ and $T_s > 10$ to 20 sec, stabilization of the right-half plane pole is essentially no more difficult than if the unstable pole represented by T_s were replaced by a pure integration. In this case operator "opinion" (regarding controllability) is "good". This case is <u>not</u> representative of the lateral system problem for a hydrofoil craft.

(2) For $T_s < 10$ sec (T_s is typically 1 to 3 seconds for a hydrofoil craft), no serious problems of stabilization are presented since the operator can introduce a lead term to enhance control. However, the pilot will have to exert substantially <u>more attention</u> than in the previous case to maintain control.

7.1.4 LIMITS OF CONTROLLABILITY FOR UNSTABLE POLES

Considering only the limits of stability and disregarding operator opinion for the moment, a lower bound on the value of T_s may be

established for the stabilization of a right-half plane pole on the real axis.

Assuming that the operator can introduce a lead term such that $T_L = T_R$, the open loop function becomes

$$Y(s) = \frac{-K e^{-\tau s}}{(1 - T_s s)}$$

The boundary value of T for possible stabilization of this function may be obtained by noting that the phase must be reduced from a lag of 180 degrees, at least briefly, as a function of frequency. The limiting condition may be deduced by noting that the value of the function

$$\frac{d(\angle Y(s))}{d\omega} < 0 \quad \text{For all } "\omega"$$

Since

$$Y(s) = \frac{-K_\phi e^{-\tau s}}{1 - T_s s} = \frac{-K_\phi e^{-\tau \omega j}}{\sqrt{1 + T_s^2 \omega^2}\ e^{j \tan^{-1}(-T_s \omega)}} \quad \text{For } s = j\omega$$

$$\angle Y(s) = -\tau\omega - \tan^{-1}(-T_s \omega)$$

then

$$\frac{d(\angle Y(s))}{d\omega} = -\tau + \frac{T_s}{1 + T_s^2 \omega^2} = \frac{T_s - \tau - \tau T_s^2 \omega^2}{1 + T_s^2 \omega^2}$$

and

$$\frac{d(\angle Y(s))}{d\omega} < 0 \quad \text{For all } \omega \text{ if } T_s \leq \tau.$$

Using a value for τ of 0.25 second (this includes an approximation for $\frac{1}{T_L s + 1}$), the limiting value of T_s becomes 0.25 second.

Reference 7-3 describes some actual tests of the limiting value of T_s that was controllable by a human pilot. For these tests the system being controlled had a transfer function of the form

$$Y_c(s) = \frac{K_c}{(T_R s + 1)(-T_s s + 1)} \tag{7-4}$$

where

$$T_R = T_s \geq 0.43 \text{ second for stability}$$

(The system transfer function may be deduced from descriptions of the tests.)

It may be assumed that the operator introduced a simple lead term roughly cancelling the T_R term and was able then to stabilize the right-half plane pole represented by T_s if it was equal to or greater than 0.43 second. This is somewhat poorer performance than predicted above (where T_s for stability was computed to be a minimum of 0.25 second) but it is considered fair agreement since certain unavoidable higher order dynamics were associated with the experiment. No input disturbance was used in these tests since random motions of the pilot's control and system noise were sufficient. These test conditions are similar to those of the high-speed hydrofoil craft environment since important wave disturbances only begin at a frequency ($\sim$ 3 rad/sec) which is at the upper limit of human control capability. The important frequency regime within which human-craft stabilization is achieved ($\omega < 3$ rad/sec), is, therefore, devoid of significant external input.

It is interesting to note that Reference 7-3 also describes an experiment to establish the limiting value of unstable poles for a case in which the system was "destabilized by a moment introduced proportional to $\dot{\psi}$", where $\dot{\psi}$ is yaw rate. Although it is not clearly stated by the author, this statement may be interpreted, along with other information presented, to imply a system function of the form

$$Y_c(s) = \frac{K_c}{(A s^2 - B s + 1)}$$

where A, B are positive valued and which, for critical damping, [the author's "zero frequency" (damped natural) condition] may be written

$$Y_c(s) = \frac{K_c}{(-T_s s + 1)^2} \qquad (7\text{-}5)$$

Note the existence of a double right-half plane pole which must clearly be more difficult to stabilize than the previous case. Accordingly a value of $T_s \geq 0.96$ second was found to be necessary to allow stabilization by a human operator. Note also that assuming the human operator provides a double lead-lag network,

$$\left(\frac{\alpha \tau s + 1}{\tau s + 1}\right)^2$$

at a low frequency, the double right-half-plane pole of Equation 7-5 can be shown to be stabilized over a quite small range of gains by conventional feedback synthesis techniques. The chart of Figure 7-1 includes a sketch of the Nyquist diagram that applies to this case as well as a log-magnitude versus phase plot of the open loop function with and without the assumed human-supplied double lead network. It will be observed that the permissible open loop gain variations for stability are narrow indeed, involving only a 25 percent margin between minimum and maximum allowable gain. It is easy to understand from this example why this case represents the approximate limit of human control capability.

(As indicated on page 10 of Reference 7-2, there is evidence supporting the assumption that the human operator can generate a double lead term under certain circumstances, but the implication is clear that this occurs toward the limit of human capability.)

7.1.5 ADAPTABILITY OF THE HUMAN OPERATOR'S GAIN CONTROL (K_p)

The average absolute gain provided by the human operator in the performance of a tracking task depends greatly on the method of control available to him. For example, tests are described in Section IV of Reference 7-2 in which an operator performs a tracking task using two different means of control; the first involving a two-handed push-pull aircraft type wheel control and the second employing a one-hand-operated left and right stick control. The gain in rad/sec/lb stick force of the controlled element required to elicit an "acceptable opinion" by the operator differed by more than a factor of 10 between the first and second test (see Figure 7-2), indicating that the mechanism of operator control (in this case, the ease with which forces may be applied by the operator in different directions) has an important bearing on the desired gain in the rest of the loop. However, the range of gains of the controlled element over which the operator could adjust his response and still maintain an acceptable opinion was surprisingly large, (see Figure 7-2) being on the order of 5 to 1 for the stick type control and 8 to 1 for the push-pull wheel control.

It is apparent from these tests that the overall gain in the non-human parts of the loop must be adjusted roughly depending on the type of control available to the operator to permit his control gain to assume a value leading to an acceptable opinion. With this condition satisfied, the operator is able to compensate over a surprisingly large range for gain changes elsewhere in the loop and continue to regard his control effectiveness as satisfactory. Accordingly, it is assumed in

following sections that the gain of the non-human components in the loop can be adjusted to permit acceptable human control, other conditions for such control having been met, and that operator capability will be assumed for compensating large variations in gain elsewhere in the loop.

7.1.6 REQUIREMENTS FOR HUMAN CONTROL OF A HYDROFOIL CRAFT

From examples and references presented previously, it is now possible to outline the requirements regarding the open loop dynamic response of a hydrofoil craft if human control is desired. These requirements are divided into two categories: first, for those properties necessary to allow an operator such control that he would rate the task relatively easy for periods of several minutes (it is felt that this operator "opinion" results in a system of merit as an emergency manual control mode for hydrofoil craft); second, the dynamic response which is possible for the operator to stabilize only by giving his entire attention and skill. This situation will rapidly fatigue the operator until a control reversal results and system stability is lost.

The general rules for the first category require

(1) Using a human operator transfer function of the form

$$Y_p(s) = \frac{K_p e^{-0.25s}(T_L s + 1)}{(T_I s + 1)}$$

in conjunction with the controlled transfer function should allow a phase margin of between 60 and 110 degrees to be developed. The value of the time constants T_I and T_L are at the disposal of the designer and may be chosen to optimize

the open loop function for stability with the knowledge that the human operator will assume such values.

(2) Gain variations in the controlled portion of the loop are less than roughly 2 to 1 from design value during operation under human control.

Some general comments should be made regarding the properties of the closed loop response of a human controlled system. First, with a pure delay of 0.25 second in the loop, and the assumption of a pole near (on either side of) the origin, the closed loop response will be characterized by a bandwidth limited to a very few rad/sec. The requirement for at least 60 degrees of phase margin may not be met otherwise. Such a situation results in the fact(Reference 7-1) that, at a frequency of about 3 rad/sec, the operator begins to abandon attempts to perform the tracking function.

Secondly, if not already provided in the non-human loop dynamics, a low-frequency lag (T_I) will be introduced by the operator to enhance the low-frequency performance of the system.

Under the second category, involving the limits of stabilization of right-half-plane poles a symmetrical (about the origin) pair of real axis poles are limited to values of $T_s \geq 0.43$ second, and a pole of second order in the positive real axis($\frac{1}{(T_s s - 1)^2}$) is limited to values of approximately $T_s \geq 1$ second.

7.2 HUMAN OPERATOR CONTROL OF THE LATERAL SYSTEM FOR A PRELIMINARY CRAFT CONFIGURATION

7.2.1 LATERAL CONTROL PROBLEM

Specific lateral dynamics for a preliminary craft configuration as presented in Section 5 were used for this series of analyses of lateral

performance. Although this craft configuration is not that used for further analysis and simulation, it is included because of the results of the effects of dihedral and sweepback. Initially, some calculations were made for the laterally "sprung" or heaving foils; i.e., for a three-strut craft in which all foils are free to heave independently with no reaction forces on the hull (spring rate ~0). With such a configuration it is clear that substantial rolling moments cannot be supplied using an aileron type control (including differential incidence control of the two adjacent foils). Control rolling moments may, however, be applied by the rudder. Therefore, the following initial configuration utilized rudder control of the craft with roll angle as the primary feedback quantity.

7.2.2 LATERALLY UNCONSTRAINED (SPRUNG) FOILS

A canard configuration was assumed with a rudder on the single forward strut for the introduction of rolling moments. The open loop craft response (see Section 5.3.2)for nominal fore-aft strut submergences and a speed of 80 knots may be represented by

$$\frac{\phi(s)}{\delta_b(s)} = \frac{-K_c \left[(s/3.35)^2 + \frac{0.163}{3.35}\, s + 1\right]}{(s/0.999 - 1)\,(s/0.434 + 1)\left[(s/1.86)^2 + \frac{1.52}{1.86}\, s + 1\right]}$$

The human controller's transfer function assumes the form

$$Y_p(s) = \frac{K_c\, e^{-0.25s}(T_L\, s + 1)}{(T_I\, s + 1)}$$

In this case, T_L has been chosen to cancel the factor $(s/0.434 + 1)$ and T_I has been assumed to be zero. The resulting open loop characteristic in the form of a Nyquist sketch and gain-phase plot is evident

in Figure 7-3. Since the open loop function possesses a right-half plane pole, a single positive (counter-clockwise) encirclement of the "-1" point is necessary to insure stability. This encirclement exists, as may be seen in Figure 7-3, only with a very small phase margin, and clearly does not satisfy the requirements for an acceptable manual control system. (The Nyquist plot sketches appearing in Figure 7-3 and those which follow are not to scale.)

7.2.3 LATERALLY CONSTRAINED FOILS

As a result of the unsatisfactory configuration for human control manifest, a laterally constrained foil configuration was assumed in the following analyses for several different control configurations. (Section 11 suggests one method for accomplishing lateral constraint which essentially prevents differential heave of the two adjacent foils while permitting in-phase heave. Such an arrangement permits the use of differential foil deflection or aileron-like lateral control without jeopardizing the reduction in longitudinal heave acceleration that results from the action of sprung foils.)

7.2.4 BOW-RUDDER CONTROLLED FOILS WITH DIHEDRAL

The open loop craft transfer function for this laterally constrained configuration, as presented in Section 5.3.2,takes the form

$$\frac{\phi(s)}{\delta_b(s)} = \frac{-K_c\left[(s/3.06)^2 + \frac{0.358}{3.06}s + 1\right]}{(s/0.438 - 1)(s/0.868 + 1)\left[(s/1.78)^2 + \frac{1.54}{1.78}s + 1\right]}$$

The open loop response plotted in Figure 7-4 includes the operator's transfer function of the form:

$$Y_p(s) = K_p e^{-0.25s}(s/0.868 + 1)$$

There is substantial improvement in this configuration regarding the ability to stabilize the craft laterally with the improvement being largely a result of the added dihedral and not the constraining of the foils. The control rolling moments are still generated by rudder action and the craft is not yet so easily controllable that it could be termed "acceptable."

(In Section 5.4 it is concluded that, as a result of the much larger strut influence for the FRESH craft over that produced by the assumed strut characteristics of this preliminary craft, dihedral has a much smaller influence on craft dynamic behavior in the former craft than is found here.)

The addition of sweepback angle to the above configuration was found to be of very small significance as seen by the form of the transfer function derived in Section 5.3.2 and shown below

$$\frac{\phi(s)}{\delta_b(s)} = \frac{K_c\left[\left(\frac{s}{3.08}\right)^2 + \left(\frac{0.432}{3.08}\right)s + 1\right]}{\left(\frac{s}{0.388} - 1\right)\left(\frac{s}{0.848} + 1\right)\left[\left(\frac{s}{1.86}\right)^2 + \left(\frac{1.49}{1.86}\right)s + 1\right]}$$

This configuration was not considered sufficiently different to warrant the construction of a frequency plot.

Besides the difficulties demonstrated in manual control of this configuration, two important factors lead to the consideration of additional configurations. These factors are:

(1) The requirement for coordinating all turns at this high speed when using rudder control alone leads to relatively large roll angles with consequent danger of foil broaching. Thus the flat turns preferred cannot be made using rudders alone.

(2) Conditions of fore-aft differential foil submergence with the forward foil shallow result in virtually complete loss of control effectiveness.

Accordingly, lateral control of the craft using differential incidence (aileron) control has been considered in the next section.

7.2.5 CONSTRAINED STRAIGHT FOILS - AILERON (DIFFERENTIAL INCIDENCE)CONTROL

The craft dynamic characteristics for this case (again from Section 5.3.2)take the form

$$\frac{\phi(s)}{\delta_a(s)} = \frac{K_c\left[\left(\frac{s}{1.04}\right)^2 + \frac{1.49}{1.04}\,s + 1\right]}{\left(\frac{s}{0.718} - 1\right)\left(\frac{s}{0.525} + 1\right)\left[\left(\frac{s}{2.01}\right)^2 + \frac{1.72}{2.01}\,s + 1\right]}$$

with

$$Y_p(s) = K_p e^{-0.25s}\left(\frac{s}{1.5} + 1\right)$$

The operator's lead term has been chosen at a frequency other than that of the negative real pole of $\phi(s)/\delta_a(s)$, since it proved advantageous in this case.

The plot of Figure 7-5 shows that this case qualifies as a system controlled sufficiently easy by the operator to indicate acceptable emergency performance. The use of aileron control does, of course, permit flat turns at high speeds. It is therefore considered preferable also for the three-strut configuration over the previous cases involving forward rudder control.

An additional configuration, identical to that just described but with the addition of dihedral, was investigated and the transfer function for this case is (from Section 5.3.2)

$$\frac{\phi(s)}{\delta_a(s)} = \frac{K_c\left[\left(\frac{s}{2.03}\right)^2 + \frac{1.14}{2.03}s + 1\right]}{\left(\frac{s}{0.438} - 1\right)\left(\frac{s}{0.868} + 1\right)\left[\left(\frac{s}{1.78}\right)^2 + \frac{1.53}{1.78}s + 1\right]}$$

This expression is identical in the denominator (as it must be) to that previously described with rudder control. The numerator zero location is more propitious than in the previous case but will not affect the conclusions of the previous section (i.e., this configuration is unacceptable for emergency manual control). The associated frequency plots will be roughly similar to those of Figure 7-4.

7.2.6 PROPERTIES OF THE CONTROLLED LATERAL SYSTEMS AT OTHER THAN MEAN STRUT IMMERSION FOR THE AILERON CONTROLLED CASE

Because of the requirement to operate the test craft in a State 3 Sea and the flexibility of pitch trim attitude control available to the operator, some craft transfer functions have been computed for the two extremes of differential strut immersion presented in Section 5.3.2. (The migration of poles and zeros of the open-loop craft-operator combination corresponding to these cases may be seen in Figure 7-6.) The presence of a pole and zero at s = -8 and +8 respectively is a result of an approximation made to the operator's pure delay characteristic response. Namely

$$e^{-0.25s} \approx \frac{(s/8 - 1)}{(s/8 + 1)}$$

In all cases in which manual controlled performance has been considered previously, differential strut immersion resulting in a very shallow-running aft strut produces a lateral mode that cannot be stabilized by a human operator whether or not the same configurations

at nominal strut immersion were stable. This is, at first glance, a disquieting conclusion. It must be recognized, however, that wave encounter in a Sea State 3 at foilborne speeds, regardless of relative heading, will result in only very short periods during which a troublesome differential immersion condition exists.

This effect could be precipitated, however, by substantial negative pitch trim adjustment, with disastrous results. Thus, it must not be possible for the operator to command such attitudes and his commands must be restricted to a range of $\theta_c \geq 0$. Even then the transient response of the craft to changes in commanded trim must be such as to minimize overshoots which could result in loss of control.

Controlled stability tends generally to be improved as differential strut immersion is altered from shallow aft to shallow forward.

7.3 HUMAN OPERATOR CONTROL USING AILERONS FOR THE FRESH CRAFT WITH SPRUNG FOILS

The fundamental considerations in the control of unstable systems have been presented in Section 7.1. A variety of assumed lateral configurations were also considered relative to the ease of manual lateral control for a preliminary craft configuration (Section 7.2) and it was concluded that aileron-type control was, for several reasons, preferable to control using rudder(s) and could provide a manually-controlled system sufficiently stable for emergency operation.

In this section, the four configurations presented have been considered for ease and effectiveness of manual control using the criteria previously presented in Section 7.1. Aileron-type control was assumed in all cases. The results of this analysis of manual control effectiveness are shown in Figure 7-7 and have, in every case, less gain margin than the best (straight foils with no dihedral or sweep) that was presented previously. (See Section 7.2 and Figure 7-5.) The configuration having the greatest gain margin of the four presented in Figure 7-7 is that of a simple, straight foil canard configuration with 40 percent loaded forward strut and no dihedral or sweep. (The fact that the phase margin for this case falls 3 degrees below the desired 60 percent is not considered significant.)

Notwithstanding the variations in gain margin indicated in Figure 7-7, these different configurations have yielded surprisingly similar results with respect to manual lateral control. The fact that they are, in all cases, poorer from this standpoint, than the aileron-controlled configuration of Section 7.2 is attributable to several important differences between the previously assumed and the present configuration. The most important of these appears to be the greatly increased value of K_v (rolling moment due to sideslip) which is the result of larger strut chords, a much greater value of $(\partial C_L/\partial i)$ struts and longer struts.

Simulation studies are discussed in Section 9 using the revised lateral configuration considered in this section. The runs were made in real-time to permit a human operator, rather than the analog of a human operator, to be used in the evaluation of the manual controllability of the high-speed test craft. It was possible to verify the relative effectiveness of manual control as implied by the plot of Figure 7-7. This simulation included runs at 80 and 50 knots (representing typical cruise and takeoff speeds respectively) and in regular waves representative of a State 3 Sea.

7.4 MANUAL LONGITUDINAL CONTROL

The constrained pitching approximation used in the preliminary longitudinal dynamic studies of Section 4 was found to eliminate this analysis as a useful one for defining the limits of longitudinal manual control. The complete analysis of Section 6 shows, conclusively, that the sprung foil configuration, is not amenable to simple, single-loop automatic control and therefore is not amenable to manual control without aided stabilization. This result is verified in the simulation programs reported in Sections 10 and 12.

REFERENCES

7-1. The Human Operator as a Servo System Element, D. T. McRuer and E. S. Krendel; Journal of the Franklin Institute, May - June 1959.

7-2. The Determination of Lateral Handling Quality Requirements from Airframe-Human Pilot System Studies, I. L. Ashkenas, D. T. McRuer; WADC Tech Report 59-135, June 1959.

7-3. A Study of the Characteristics of Human-Pilot Control Response to Simulated Aircraft Lateral Motions, D. C. Cheatham; NACA Report 1197, 1954.

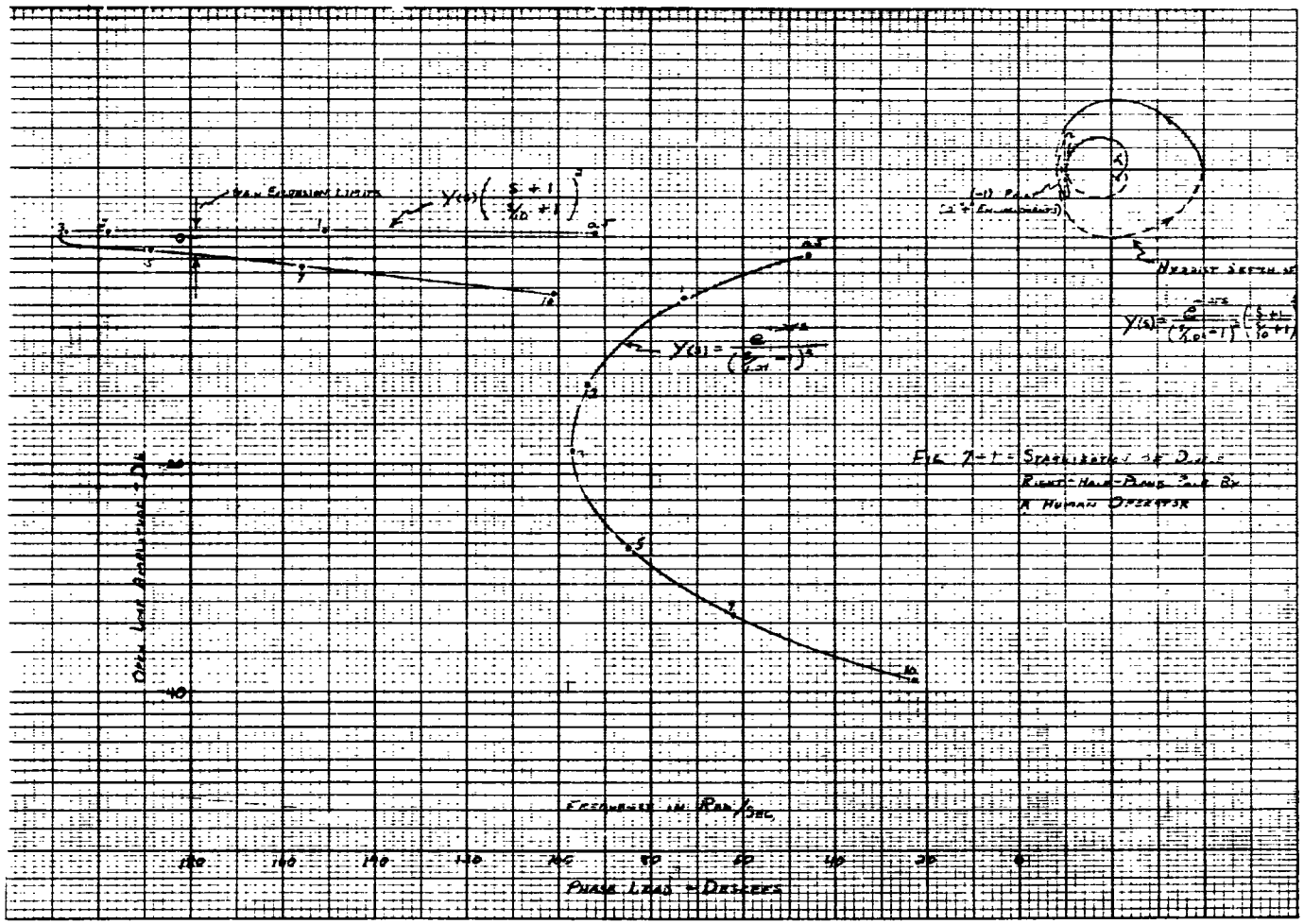

Figure 7-1. Stabilization of Double Right-Half-Plane Pole by a Human Operator

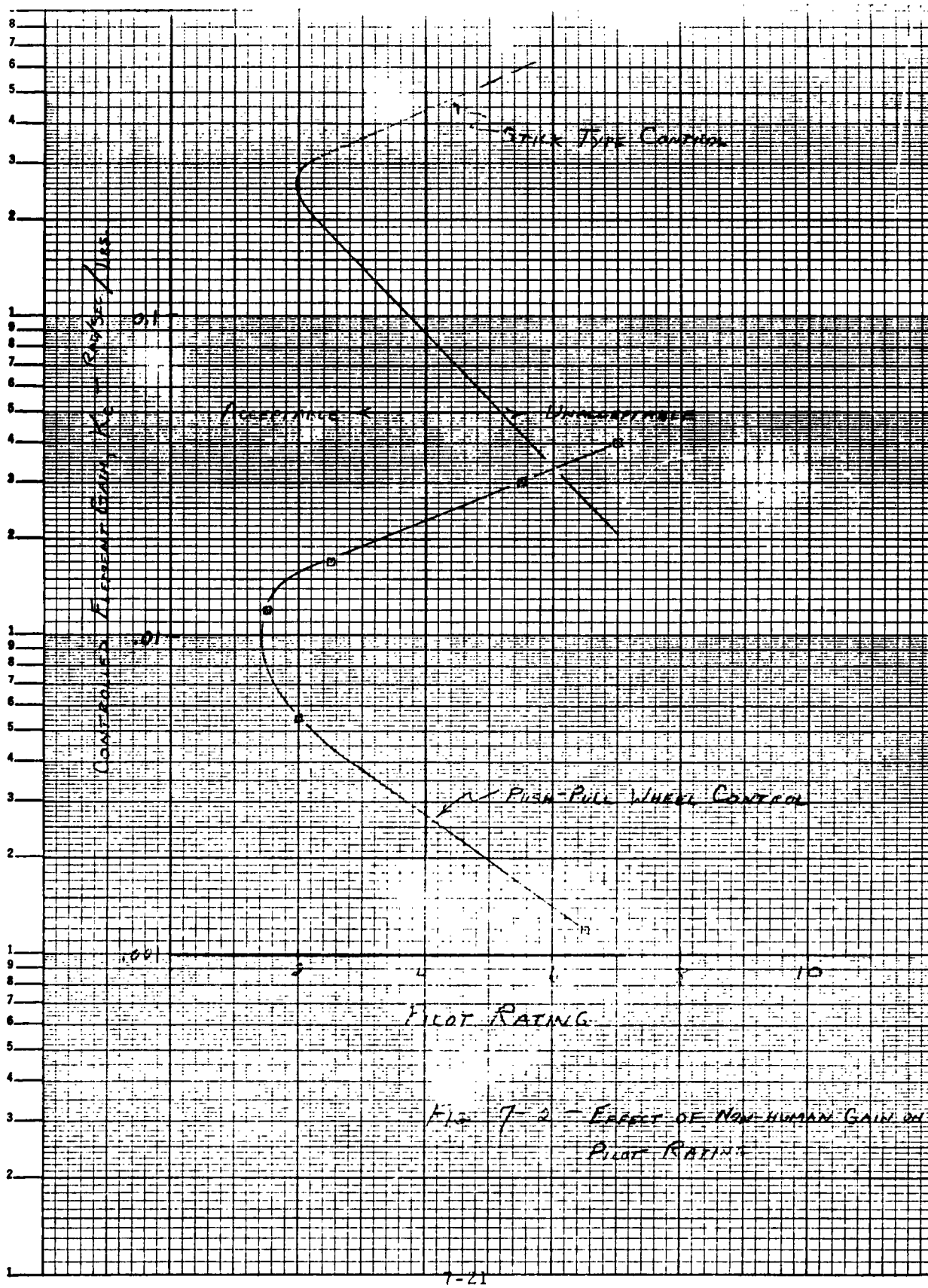

Fig. 7-2 — Effect of Non-Human Gain on Pilot Rating

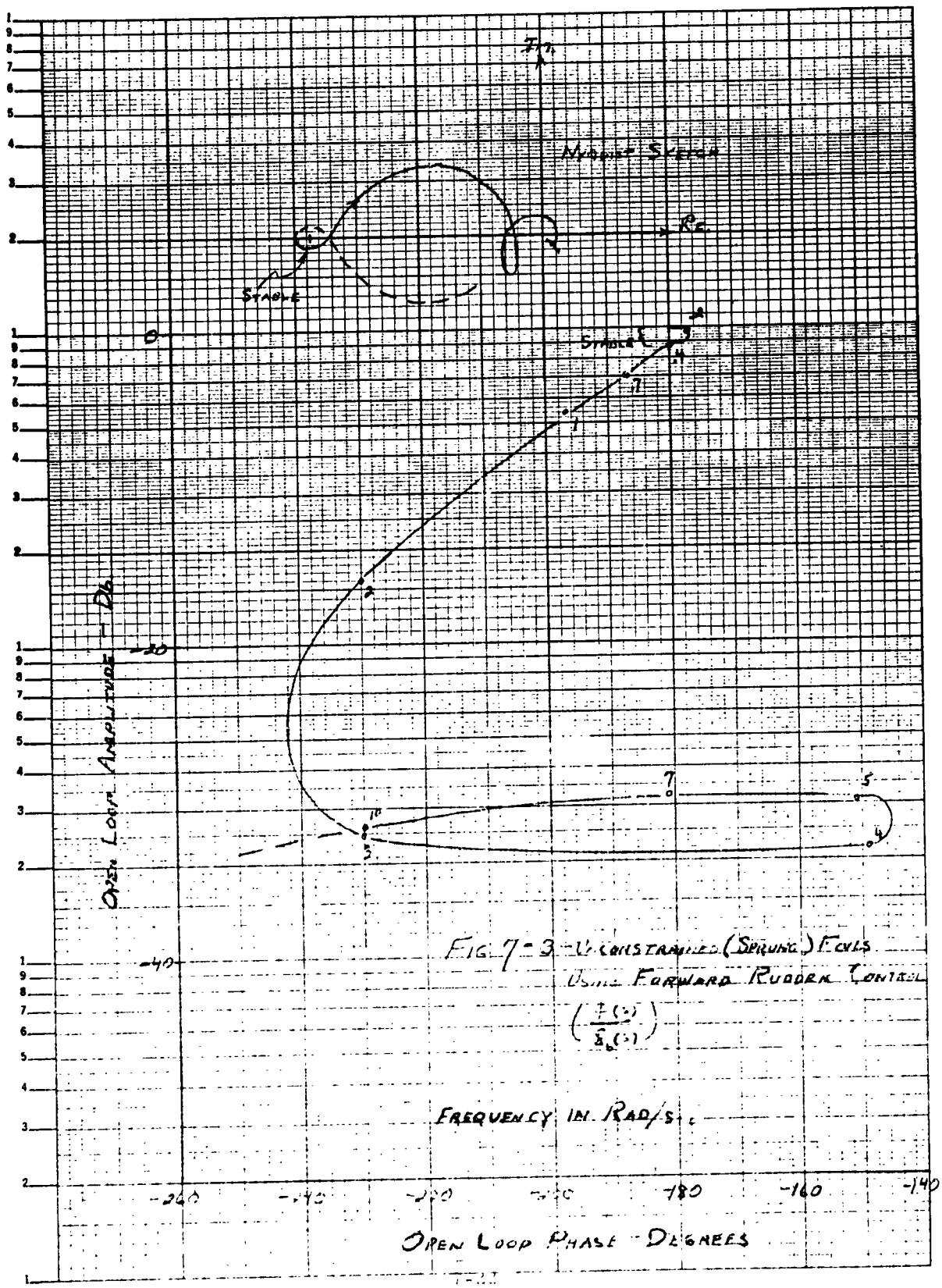

FIG 7-3 U CONSTRAINED (SPRUNG) EQNS
USING FORWARD RUDDER CONTROL
$\left(\frac{\dot{r}(s)}{\delta_r(s)}\right)$

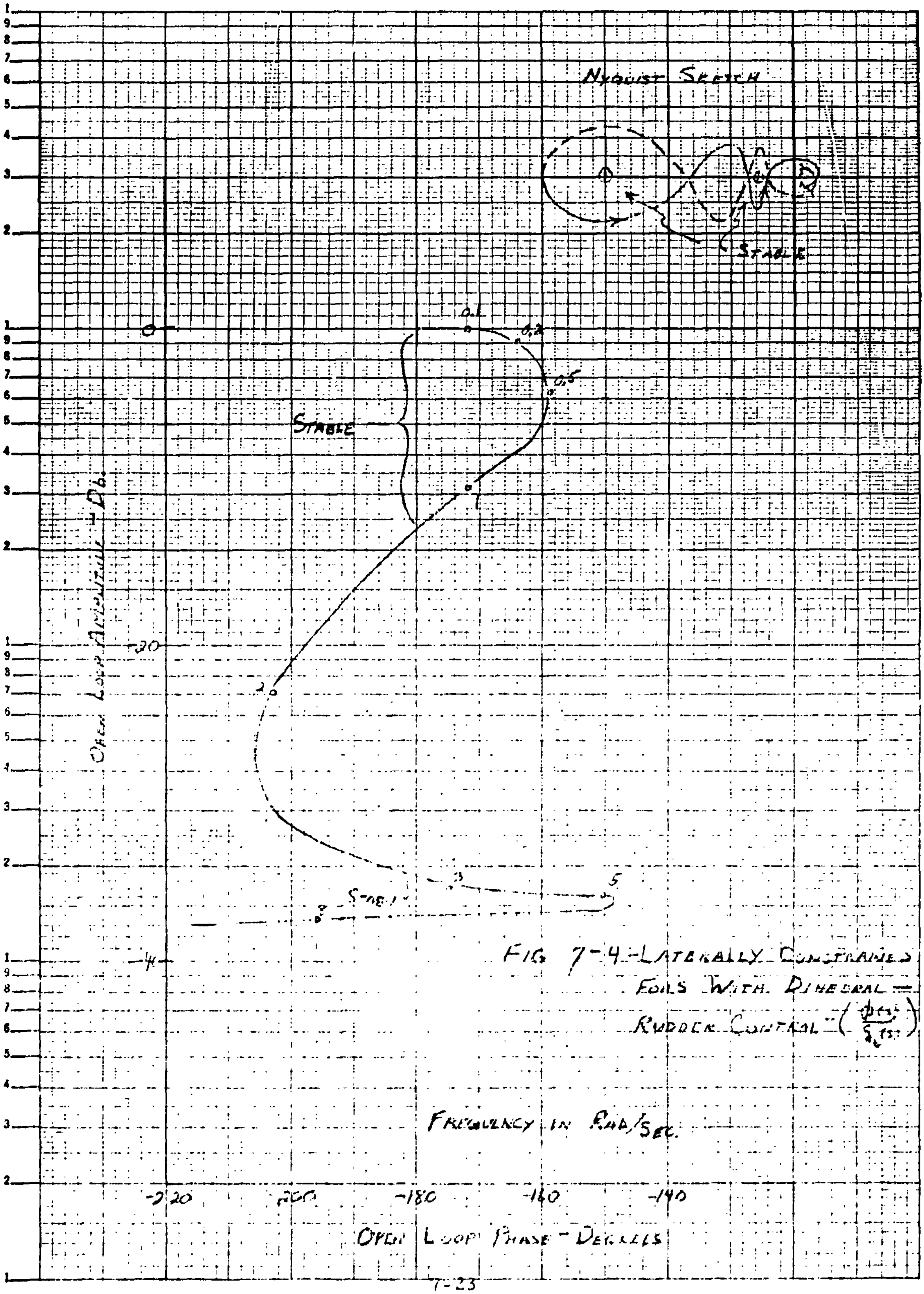

FIG 7-4 - LATERALLY CONSTRAINED FOILS WITH DIHEDRAL — RUDDER CONTROL

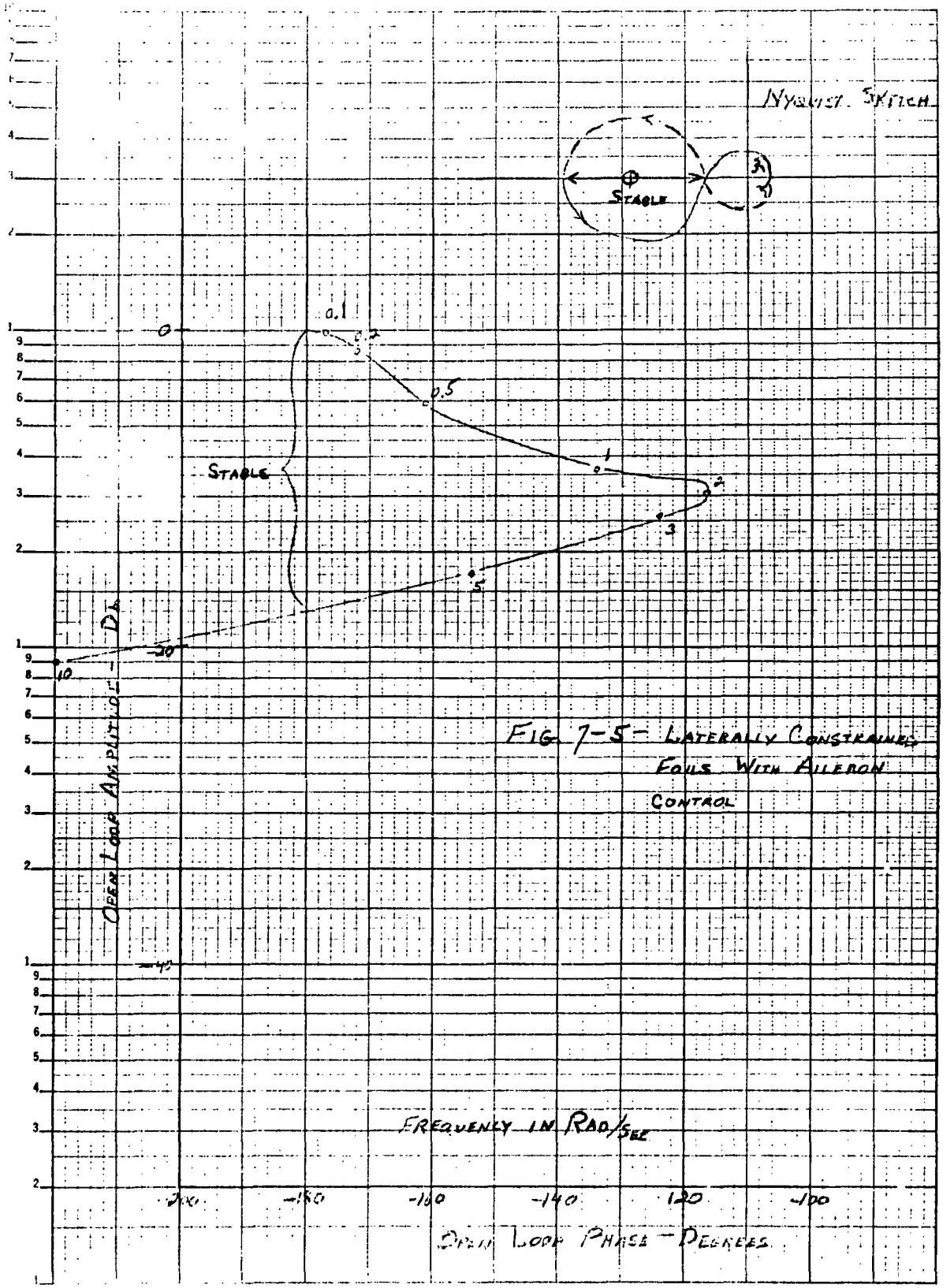

FIG. 7-5 - LATERALLY CONSTRAINED FOILS WITH AILERON CONTROL

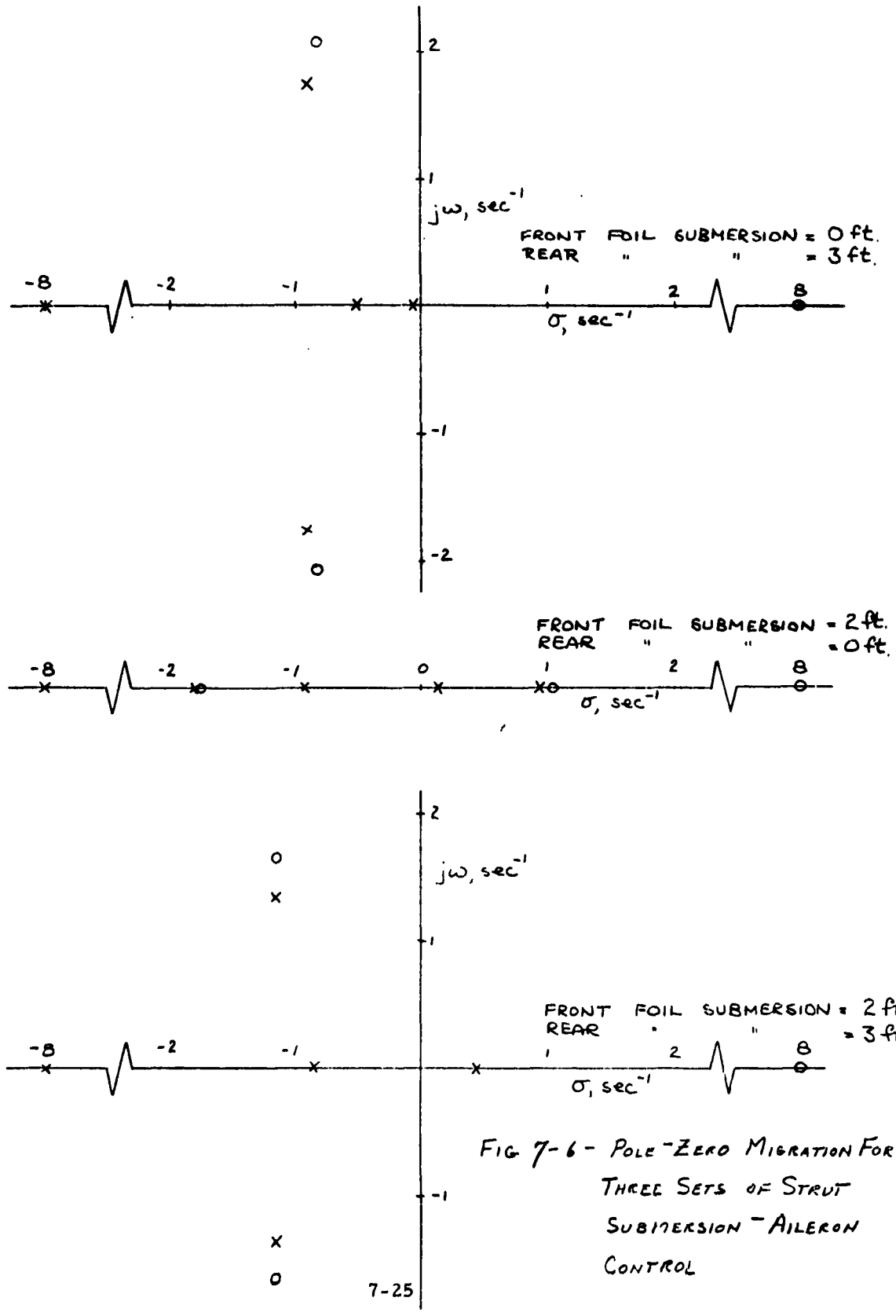

FIG 7-6 - POLE-ZERO MIGRATION FOR THREE SETS OF STRUT SUBMERSION - AILERON CONTROL

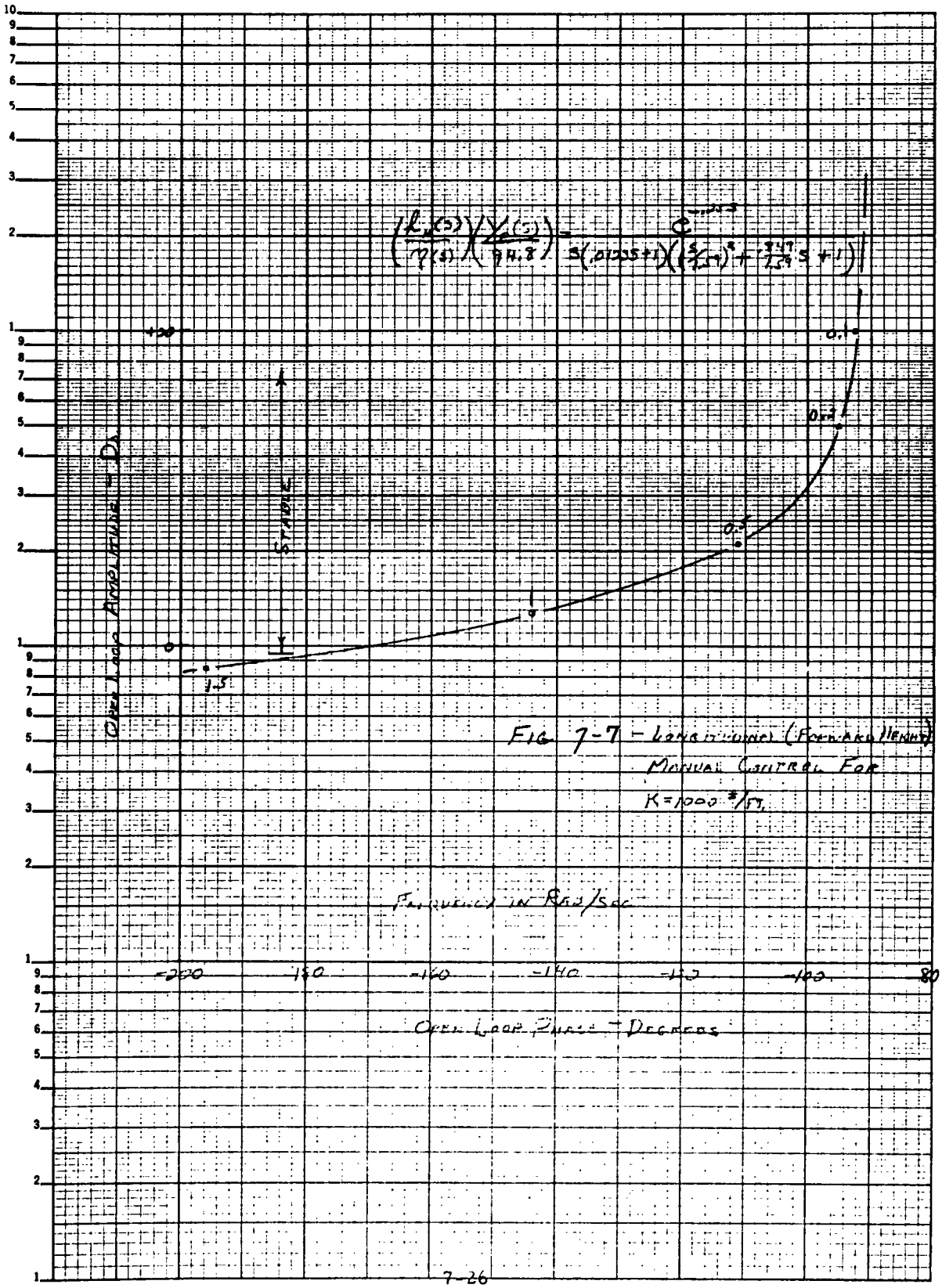

Fig 7-7 - Longitudinal (Forward Henry) Manual Control For K=1000 #/ft.

SECTION 8

RECOMMENDATIONS FOR DISPLAYS AND CONTROLS USED IN MANUAL CONTROL OF THE CRAFT

8.1 GENERAL

The lateral controllability of the high-speed test craft in the manual mode has been shown (see Section 7) to be within the capability of a human operator but it requires greater and more sustained attention than, say, the control of modern aircraft. For this reason, and the fact that the longitudinal and lateral modes of this craft possess no strong cross-coupling influences, it is suggested that one operator be assigned solely to the lateral control of the craft and that a second operator be assigned to the longitudinal control task.

Both operators should be seated facing forward and should be provided with forward-looking displays. Controls should consist of either an aircraft-type wheel or a balanced stick type fingertip control located at the forward end of the right armrest. The latter is preferred, particularly for the lateral control job, and is the method chosen for the lateral system simulation studies. It has the advantage of minimizing the inadvertent feedback that occurs when acceleration of the craft causes arm motions which, in turn, produce control stick deflections.

8.2 LATERAL CONTROL AND DISPLAY DETAILS

The control should be a single-degree-of-freedom stick having its freedom athwartship for control of the lateral system. Spring restraint about the center position should be used to provide "feel",

and there is provision in the mockup used in the simulation studies for varying the stiffness of the spring restraint. A torsion rod is a convenient means for providing the necessary restraint and it has been utilized in the simulation controller. Spring stiffness may be adjusted on this controller from a minimum of about 1 in. - lb to a maximum of 8 in. - lb at full deflection. To minimize inadvertent feedback through the controller as a result of accelerations of the craft, it is clear that the higher spring rates are preferable. Displacement should be limited to ±1.5 inches from the center position. A sketch of the hand control used on the lateral simulation program is shown in Figure 8-1.

An "outside-in" roll angle display is recommended. This type of display is characterized by a horizon line that is fixed with respect to the instrument panel, and a boat symbol that rotates with respect to the fixed horizon line. While this type of display differs from the conventional aircraft artificial horizon, it has been shown (Reference 8-1) that the display-control relationship is more natural and that improved performance results.

The critical operating range of roll angles is relatively narrow for hydrofoil craft; there is no requirement to show roll angles of more than, say, 60 degrees. This fact permits the use of gain in the roll display. That is, the roll orientation shown on the display may be some multiple of the true roll angle, thus making small roll angles more apparent to the observer. Since such a display does not bear a one-to-one correspondence to true roll angle, a calibrated scale should be included to indicate true roll angle.

It has proved desirable to include some prediction or rate information in the roll display and provision has been made in the lateral simulation program for this refinement.

It is clear that if craft operation is desired under conditions where the horizon is not obvious (in fog or during the night in overcast conditions), a lateral display of the type mentioned is essential.

Furthermore, if it is found that a lateral display with augmented angles or one using roll rate inputs is desirable, these benefits may only be realized with the use of a display. In general it appears that the visual observation of the horizon for lateral control is a mode of control suitable for only very limited conditions.

8.3 LONGITUDINAL CONTROL AND DISPLAY DETAILS

As indicated in Section 8.1, either an aircraft wheel or balanced stick type control are considered acceptable for longitudinal control. The longitudinal simulation will employ the stick type control similar to, but oriented differently from, that used in the lateral control problem. (Figure 8-2 shows such a controller in the final form it could assume for use aboard the craft.) In this case the stick will be positioned roughly parallel to the armrest and an upward deflection of the end will produce a pitching motion consistent with stick motion, i.e., nose down. (It will be seen that this motion is consistent with the recommended display.)

The suggested height display combines an electromechanical index with a cathode-ray tube display. The display is a vertical "thermometer" type of presentation with a scale giving a quantitative readout in feet. (See Figure 8-3.) At the top is an area representing a wetted hull condition and, at the bottom, an area indicating forward foil broaching. A horizontal sweep on the CRT is driven vertically directly by the height sensor and indicates the instantaneous height above the water. A long persistence phosphor is used so that the envelope of the excursions of the altitude line remains visible and affords a

direct measure of approximate encountered wave heights. The horizontal mechanical index is positioned by smoothed height information, and indicates average height above the water. It also serves as a backup in case of CRT failure.

Analysis and simulation covered in other sections of this report (Sections 6, 10, 12) demonstrate that single height inputs to the display are not sufficient to permit stable manual control of the craft in most cases and an acceleration signal input was found to be necessary as an additional input to the display along with the height sensor input. Thus, the regions shown in Figure 8-3 to indicate relative wave height would be correct only at very low wave encounter frequencies (< 0.5 rad/sec).

Nevertheless, although the basic height display of Figure 8-3 is not suitable for control of the high-speed test craft, it is still considered a suitable design for any other craft which is sufficiently docile (unlike the FRESH craft) for practical manual control in other than calm seas.

REFERENCE

8-1. Melton and Briggs, Annual Review of Psychology, Annual Reviews, Inc., Palo Alto, California, 1960, p. 76.

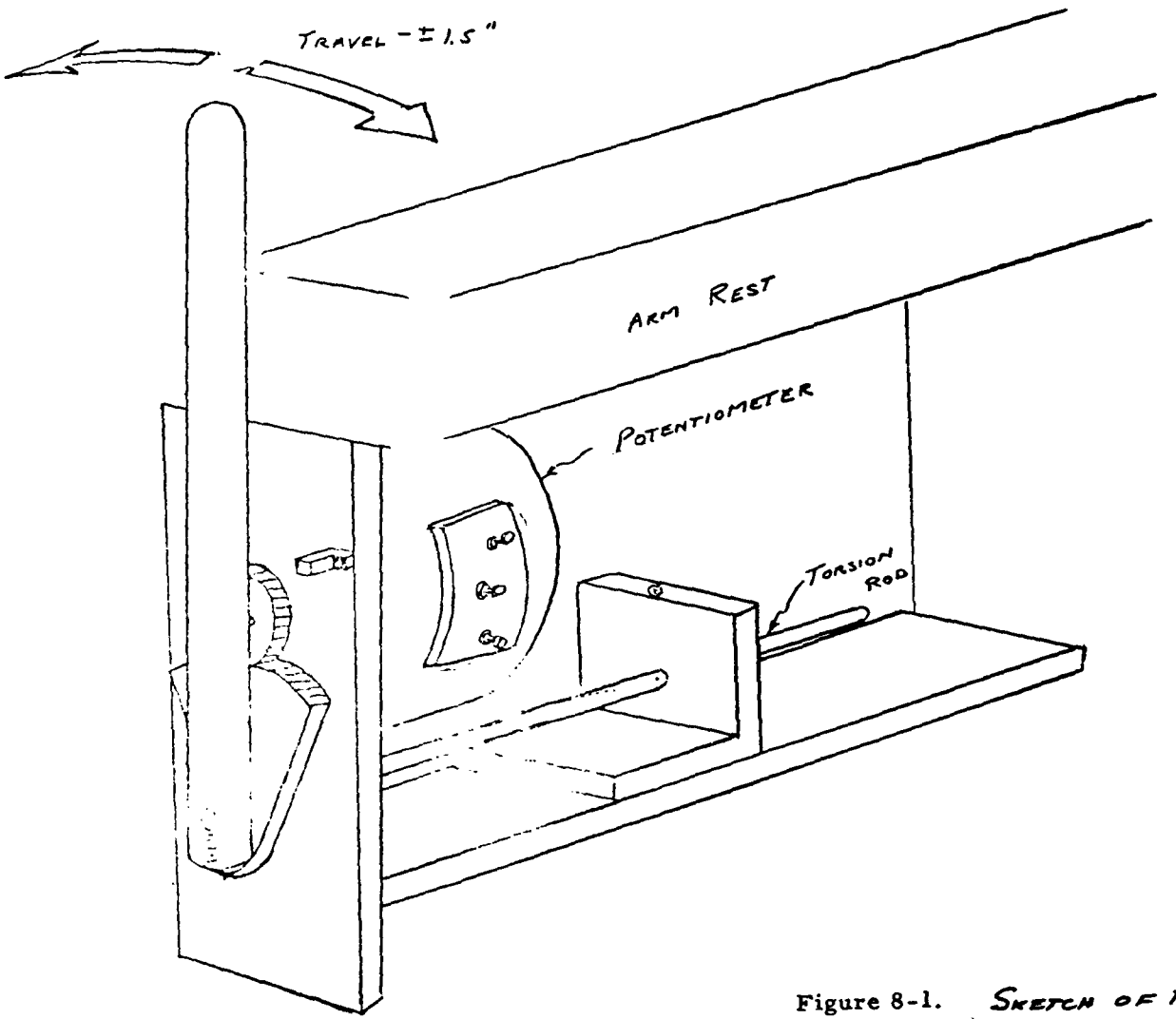

Figure 8-1. SKETCH OF THE HAND CONTROL USED IN THE LATERAL SIMULATION

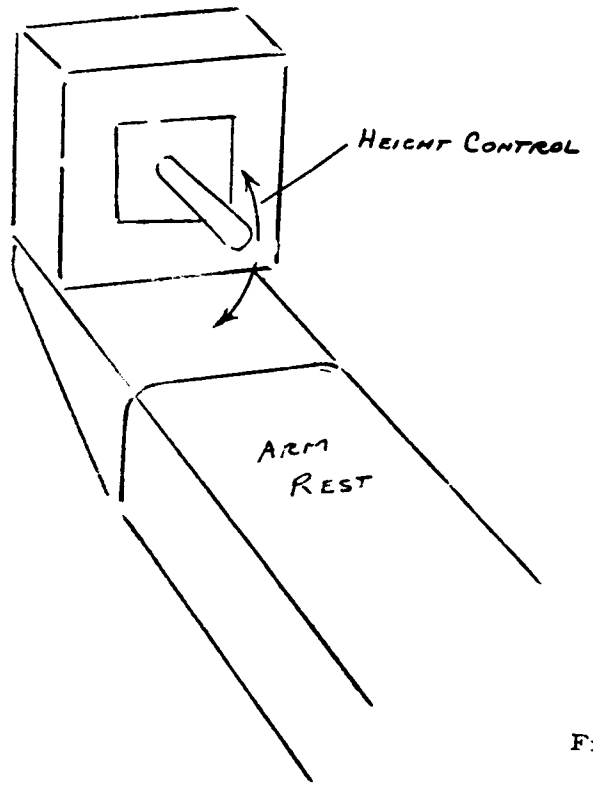

Figure 8-2. SKETCH OF LONGITUDINAL SYSTEM MANUAL CONTROLLER

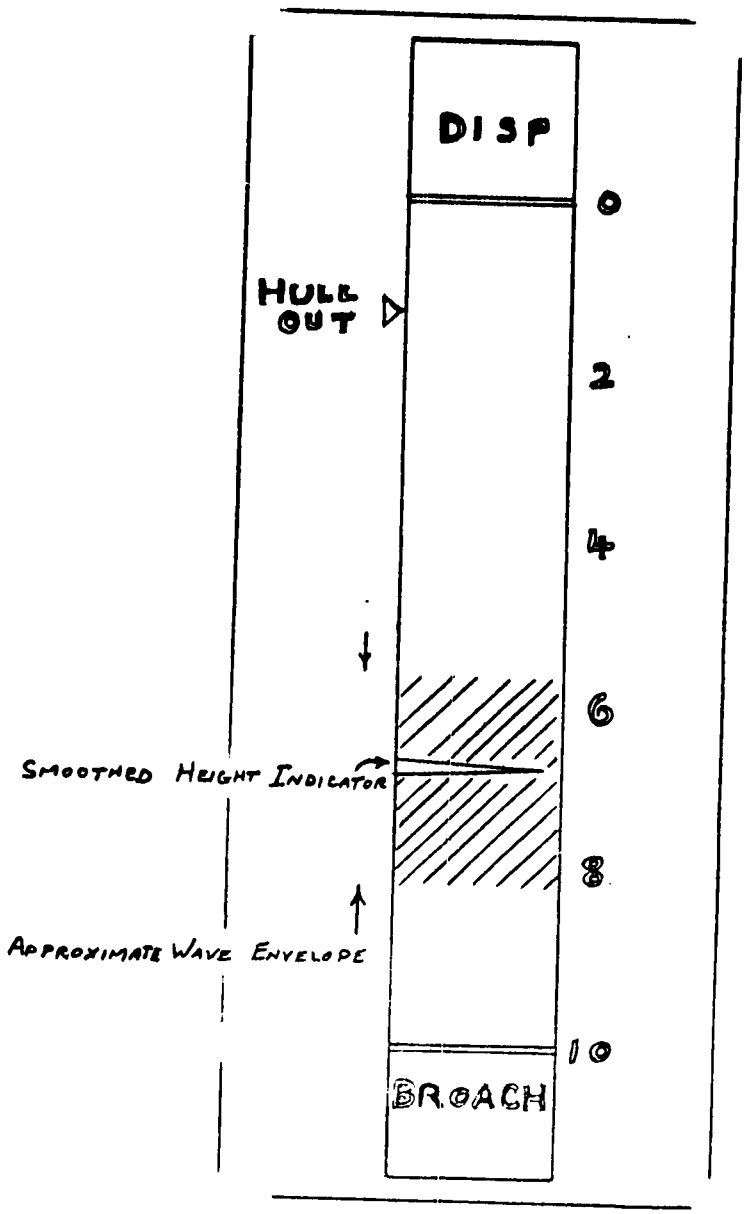

Figure 8-3. RECOMMENDED HEIGHT DISPLAY

SECTION 9

LATERAL SIMULATION OF THE SPRUNG FOIL CRAFT

9.1 GENERAL CONFIGURATION

Throughout the lateral two-dimensional simulation, a canard configuration was considered. Previous analytical work (see Section 5.4) indicated that the lateral performance of the craft with an airplane configuration would be very similar to that with a canard configuration. Foil loadings of 40-30-30 were assumed at a speed of 80 knots. These loadings were chosen when it was anticipated that the maximum drag, and hence, maximum bow-down pitching moment, would occur at 80 knots. Later work has shown that, with the foils selected, maximum drag will occur at takeoff. Assuming that the loadings at takeoff will be 40-30-30, (information supplied by the Bureau of Ships indicates that 40 percent of the craft's weight is the largest permissible single foil loading), the loadings at 80 knots will be more nearly equal than assumed. However, the effects of this changed loading on the lateral performance of the craft will be negligible.

ℓ_F and ℓ_R were taken to be 26.0 feet and 6.1 feet, the same values used for Cases (b) and (c) in Section 5.4.

In Section 5.3, it was shown that the effect of sweepback on the preliminary craft was small. These effects would have been even smaller, due to the different strut characteristics that have been used. The preliminary craft had smaller strut chords and shorter length struts with smaller values for $\partial C_L/\partial i$ than did the craft that was simulated. Thus the preliminary craft had foils that were relatively more prominent in

the lateral dynamics than were the foils in the craft simulated. For this reason, no sweepback was used in any of the runs.

As stated in Section 5.4.1, the effects of including dihedral could also be expected to be small, and no dihedral was used for any of the automatic control system runs. Due to the marginal nature of the manual controllability of the craft, some manually-controlled runs were made with dihedral.

In all control systems considered, it was assumed that the transfer function relating control surface deflections to servo input commands was $\frac{1}{0.02s + 1}$. In Section 5.4, a different transfer function was used for the aileron servo. However, the simulation showed that the required aileron deflections were substantially larger than previously anticipated. For this reason, a transfer function was used which introduced appreciably more phase lag at lower frequencies than did the transfer function used previously. A report of the lateral simulation with automatic control is given in Section 9.2. The manual control runs are reported on in Section 9.3.

9.2 AUTOMATIC CONTROL

9.2.1 GENERAL

Two methods of stabilizing the craft automatically were investigated. The first method was the control of roll angle by means of the ailerons (differential foil control) alone, and the second method involved the use of rudders alone. An approximate simulation of laterally flexible struts was made in some runs. A weak simulated helmsman control loop was synthesized for both control systems to keep the craft heading approximately correct.

9.2.2 AILERON CONTROL OF ROLL ANGLE

A. Inflexible Struts

Two configurations were considered. The first was one in which the rear struts were 2 feet longer than the front strut, and the second was one in which all three struts were assumed to be the same length as the front strut. These cases are referred to as the unequal and equal strut cases. It was thought that the unequal struts case might be more stable than the other due to the larger rear strut submergences, but that if the equal strut case proved to be adequately stable it would be the preferable configuration, as strut drag would be less.

1. Unequal Struts Case

a. Verification of Analysis at 80 Knots

Figure 9-1 shows the gain-phase plot for the transfer function relating roll angle to aileron servo input commands for the reference submergences of $\zeta_F = 2.5$ feet, $\zeta_R = 4.5$ feet at 80 knots. (The transfer function relating roll angle to aileron deflection is given in Section 5.4.) Also shown in the figure is the plot with lead-lag compensation $\frac{0.05s + 1}{0.005s + 1}$ included to improve the closed loop response. With the loop closed as shown in Figure 9-2, the transient response of the system to an initial disturbance in roll angle was found for a range of open loop gains, both with and without the lead-lag compensation.

Without compensation it was found that, with additional loop gain of 20 db (making a total of 32 db since the inherent gain is 12 db), there was a reasonably damped oscillation at approximately 10.5 rad/sec. With additional open loop gain of 32 db (making a total of 44 db) there was a very poorly damped

oscillation at approximately 25 rad/sec. When the additional open loop gain was -12 db (0 db total) there was a very slow convergence. These results are very similar to those expected from the analysis.

With the compensation included and with additional open loop gain of -12 db, 29.6 db and 40 db (making total open loop gains of 0 db, 41.6 db and 52 db, respectively) a slow convergence, a very fast recovery with very little overshoot, and a poorly damped oscillation at approximately 80 rad/sec, were the responses obtained respectively. Again, these results are very similar to those expected from the analysis. (Additional gain of 29.6 db results in a closed loop resonant peak of 3 db.)

b. Design of Simulated Helmsman Loop at 80 Knots

A loop was designed whereby a simulated helmsman controlled heading angle by means of the bow rudder, as shown in Figure 9-3. Because it was expected that the helmsman-heading angle loop would be a weak one in comparison to the roll angle-aileron loop, the following assumptions were made:

(1) The helmsman-heading angle loop could be analyzed assuming the roll angle to be zero.

(2) The roll angle-aileron loop could be analyzed assuming the helmsman-heading angle loop did not exist.

Making these assumptions, the transfer function relating heading angle to bow rudder deflection at 80 knots with $\zeta_F = 2.5$ feet and $\zeta_R = 4.5$ feet was found to be

$$\frac{\psi(s)}{\delta_b(s)} = \frac{4.140\left(\frac{s}{9.571}+1\right)}{s\left(\frac{s}{7.461}+1\right)\left(\frac{s}{9.052}+1\right)}$$

It was assumed, that the helmsman could be approximately represented by $\frac{1}{0.6s+1}$. Although it was realized that this representation was an oversimplification, it was thought to be adequate for the purpose. The time constant of 0.6 second was believed reasonable for a simple lag representation. The gain-phase plot of the function relating heading angle to input to the simulated helmsman is shown in Figure 9-4. (This function has a zero frequency gain of 12.4 db.) The transient responses of the closed loop system to initial disturbances in heading angle were found for additional open loop gains of -6 db and +6.9 db (a total open loop gain of 6.4 db and 19.3 db). (The additional loop gain of the roll angle-aileron compensated loop was kept at 29.6 db.) With the lower value of gain, the response was a well damped oscillation at 1.7 rad/sec. With the higher gain, a limit cycle at a frequency of 3.6 rad/sec resulted. These results are approximately those predictable from the analysis.

With the additional loop gain of the yaw controlling loop set at -6 db, the response of the roll controlling loop to an initial disturbance in roll angle, with the additional gain in this loop of 29.6 db, was found. The response was almost exactly the same as that with no yaw controlling loop.

It was therefore concluded that the assumptions made in the analyses of the two loops were legitimate.

The yaw loop additional gain was kept at -6 db for all subsequent runs.

c. Control System at 50 Knots

Previous experience has indicated that a control system designed for 80 knots should behave well at 50 knots. This was confirmed by checking the response of the system designed for 80 knots to initial disturbance in roll angle and heading angle at 50 knots with ζ_F = 2.5 feet and ζ_R = 4.5 feet. (The additional open loop gains in the roll and heading angle were set at 29.6 db and -6 db respectively.) The responses to both types of disturbances were found to be satisfactory.

d. Performance in a Regular Sea

The performance of the craft with the automatic roll control system in a regular sea was investigated. The sea chosen was one in which the wave height was 4.5 feet and the wave length was 200 feet. The wave height of 4.5 feet was chosen as this is the average of the one-third highest waves in a State 3 Sea. A 200-foot wave length was used, since the encounter frequency corresponding to this wave length is the frequency at which the Neumann Spectrum of a State 3 Sea peaks.

The performance of the craft in quartering, beam and bow seas (ψ_w = 45, 90 and 135 degrees respectively) was investigated at speeds of 80 and 50 knots. The additional open loop gain of the roll angle and heading angle loops were set at 29.6 db and -6 db respectively.

Nominal submergence below mean sea level of the front and rear foils of 2.5 and 4.5 feet respectively was used.

Some results of the investigation are shown in Table 9-1.

Table 9-1. Performance of Unequal Inflexible Struts Case in Regular Sea

Type of Sea	ψ_w (deg)	Speed (knots)	Max Roll Angle (rad)	Max Norm Side Force (ft/sec^2)	Max Aileron Deflection (rad)	Max Aileron Rate (rad/sec)
Quartering	45	80	0.004	13	0.095	0.179
Beam	90	80	0.001	3	0.025	0.028
Bow	135	80	0.003	11	0.075	0.357
Quartering	45	50	0.003	5	0.100	0.091
Beam	90	50	0.002	2.5	0.050	0.042
Bow	135	50	0.005	7	0.150	0.500

e. Performance in a Turn at 80 Knots

With normal submergence of ζ_F = 2.5 feet and ζ_R = 4.5 feet in a calm sea, the bow rudder was deflected until the heading angle steady-state rate was 0.2 rad/sec. (Actually, it was assumed that rudder action was obtained by rotating the complete bow strut.) This heading angle rate corresponds to making a turn of diameter 1350 feet. Various quantities that were recorded are listed below.

Bow rudder deflection	+ 0.047 rad
Aileron deflection	+ 0.207 rad
Roll Angle	- 0.023 rad
Normalized Side Force	+ 27 ft/sec^2
Sideslip Velocity	- 1.6 ft/sec
Sideslip Angle	- 0.0119 rad

In a flat turn (roll angle equal to zero) the diameter of the turn is equal to $2\,u_o/|\dot{\psi}|$, and the normalized side force is $u_o\dot{\psi}$. Also, the heading angle rate is proportional to the bow rudder deflection, as is sideslip velocity. Hence, the quantities listed can be computed for other bow rudder steady-state deflections.

2. Equal Struts Case

a. Verification of Analysis

The gain-phase plot for the transfer function, relating roll angle to aileron servo input commands, for foil submergences $\zeta_F = \zeta_R$ = 2.5 feet at 80 knots, is shown in Figure 9-5. (This transfer function is given in Section 5.4.) Also shown in the figure is the plot when lead-lag compensation $\frac{0.05s+1}{0.005s+1}$ is

added. Without any additional gain being added, the zero frequency gain is 6.6 db. With the compensated loop closed, as in Figure 9-2, the transient response of the system to initial disturbances in roll angle was found for additional loop gains of 40 db and -6 db, giving total loop gains of 46.6 db and 0.6 db respectively. The response when the first gain was used was a poorly damped oscillation at approximately 75 rad/sec. When the second gain was used, a slow convergence resulted.

These results are those expected from an inspection of the gain-phase plot (Figure 9-5). For all the regular sea runs the additional loop gain was set at 26 db, the value which limits the closed loop resonant peak to 3 db.

b. Simulated Helmsman Loop at 80 Knots

The helmsman was again represented by the simple lag $\frac{1}{0.6s+1}$. No analytical work was done for this loop, but the responses to initial disturbances in heading angle were found for various values of additional loop gain at the normal foil submergences of 2.5 feet. An additional gain of -16.5 db proved satisfactory, and this gain was used for all runs.

It was confirmed that the heading angle loop was not affecting the roll angle loop, to any appreciable extent, by repeating transient responses to initial errors in roll angle, both with and without the heading angle loop, and noting that the responses were very similar.

c. Control System at 50 Knots

Transient response at 50 knots, with foil submergences of 2.5 feet, showed that the control system designed for 80 knots was satisfactory at 50 knots.

d. Performance in a Regular Sea

The performance of the craft was investigated in the same seas that were simulated for the unequal strut case. Some of the results of the investigation are shown in Table 9-2.

2. Comparison of Performance of Unequal and Equal Strut Cases in a Regular Sea

Tables 9-1 and 9-2 show that for both cases the maximum roll angles were very small. The other quantities that are listed - maximum normalized side forces, maximum aileron deflections, and maximum aileron rates - while varying for particular seas, are generally much the same for the two cases. Due to the smaller strut-submerged areas, the disturbing forces and couples acting on the equal strut craft were smaller than those acting on the craft with larger rear struts. However, it appears that the dynamic responses of the two cases were such that, despite the different disturbances, the responses were, generally speaking, much the same.

For automatic control the configuration with the equal struts is preferred to that with the longer rear struts, as the strut drag will be less. However, manual control has been shown to be easier with the longer rear struts configuration. (See Figure 7-7.)

B. Flexible Struts

1. General

To obtain some idea of the problem the flexibility of the strut might pose in stabilizing the craft laterally, an approximate simulation of flexible struts was made for the craft which had rear struts 2 feet longer than the front. The following assumptions were made:

Table 9-2. Performance of Equal Strut Case in a Regular Sea

Type of Sea	ψ_w (deg)	Speed (knots)	Max Roll Angle (rad)	Max Norm Side Force (ft/sec^2)	Max Aileron Deflection (rad)	Max Aileron Rate (rad/sec)
Quartering	45	80	0.003	11	0.075	0.278
Beam	90	80	0.003	8	0.060	0.139
Bow	135	80	0.003	8	0.055	0.333
Quartering	45	50	0.007	8	0.125	0.250
Beam	90	50	0.004	4	0.070	0.125
Bow	135	50	0.005	5	0.100	0.500

a. The struts deflected laterally in such a manner that no twisting of the struts occurred. Actually, because of the unsymmetrical section and unsymmetrical loading, some twisting of the struts will occur, and this phenomenon may affect the results appreciably.

b. The inertia effects of the mass of the struts and the entrained water were small enough to be neglected at the frequencies of interest. The ratio of the inertia forces to the damping forces for a strut submergence of 4 feet at 80 knots is approximately $0.007\,\omega$, where ω is the frequency in rad/sec. This ratio is practically independent of strut submergence and is inversely proportional to speed.

c. The forces acting on the submerged portion of a strut were found by assuming that the whole of the submerged portion was operating under the same conditions as the mid-depth of submersion point.

d. The lateral stiffness at the mid-depth of submersion point of a strut was taken to be constant, irrespective of the depth of submersion. This constant was taken to be the lateral stiffness at the lower end of an 11.5-foot long strut supported by pin joints 3 feet apart at its upper end and having the section shown in Figure 3-4. The skin thicknesses assumed and the method used to calculate the strut lateral compliance are given in Appendix G. This stiffness was calculated to be 9188 lb/ft. Later information received from the Bureau of Ships (reference NObs 86448 Serial 632B4-966) indicated that the strut skin thicknesses were approximately twice those assumed. Also, the mid-depth of submersion point of a strut is some distance from the strut tip. For these reasons, the stiffness

used was too small (probably by a factor of 2 or more). However, it is thought that the results are useful in indicating the way in which flexible struts can affect the performance of this craft.

2. Determination of Approximate Gain-Phase Diagram

No analytical work was done to find the transfer function relating roll angle to aileron deflection. To select reasonable compensation, the loop was closed with various compensation networks included, and the transient response of the closed loop system was found for a range of values of additional loop gain. The results enabled that part of the uncompensated open loop gain-phase plot close to the 180-degree phase lag line to be sketched. The plot is shown in Figure 9-6. A comparison of this figure with Figure 9-1, the gain-phase plot for its inflexible struts, shows the effects of the flexible struts. Also shown in the figure is the plot with a lead-lag network $\frac{0.5s+1}{0.05s+1}$ included. This compensation appeared to be reasonable and was used for all subsequent runs with additional loop gain of 0 db. Figure 9-7 shows the transient response of the system, including the compensation and loop gain selected, to an initial disturbance in roll.

3. Simulated Helmsman Loop at 80 Knots

The same simple lag network used for the inflexible strut cases was used to simulate the helmsman. By trial, a value of -16.5 db was deemed satisfactory for the additional loop gain. To confirm that the heading angle controlling loop was not affecting the roll angle loop to any appreciable extent, transient responses to initial roll disturbance were found with and without the heading angle loop being included. The responses were very similar.

4. Performance in a Regular Sea

The performance of the craft was investigated in the same seas that were simulated for the craft with inflexible struts. Table 9-3 gives some of the results of the investigation.

C. Comparison of Performances with Flexible and Inflexible Struts

A comparison of the results in Tables 9-1 and 9-3 (the unequal inflexible struts case and the flexible struts case are directly comparable as the strut lengths are the same), shows that the flexible struts case had much larger maximum roll angles. This is a result of the poorer closed loop response of this case, which more than compensates for the attenuation of the higher frequency disturbing forces by the flexible struts. Apart from the performances of the two cases in quartering seas at 80 knots, the other quantities listed are not very different. The normalized side force (which is the lateral acceleration caused by all the lateral forces, apart from the gravity force, acting on the craft) was very large in the quartering sea 80-knot flexible struts case. The reason for this is not obvious, and it may have been possible to reduce the normalized side force in the case by changes in the control system parameters.

Although no transient responses were investigated to confirm that the flexible struts case control system was satisfactory at 50 knots, the results in Table 9-3 do show that this was so. The closed loop response of the flexible strut case could have been improved by more sophisticated compensation. An inspection of the gain phase diagram in Figure 9-6 shows that a lead-lag lag-lead network would have been better than the lead-lag network that was used.

Table 9-3. Performance of Flexible Struts Case in a Regular Sea

Type of Sea	ψ_w (deg)	Speed (knots)	Max Roll Angle (rad)	Max Norm Side Force (ft/sec^2)	Max Aileron Deflection (rad)	Max Aileron Rate (rad/sec)
Quartering	45	80	0.118	22	0.18	0.358
Beam	90	80	0.029	5	0.038	0.05
Bow	135	80	0.026	7	0.055	0.178
Quartering	45	50	0.111	7	0.125	0.119
Beam	90	50	0.088	4	0.100	0.125
Bow	135	50	0.050	3	0.063	0.217

9.2.3 RUDDER CONTROL OF ROLL ANGLE

A. Configuration

A roll control system using rudders on all three struts was designed for the craft which had inflexible struts, the rear struts being 2 feet longer than the forward strut. In the simple system used, it was initially assumed that the bow and stern rudders would be coupled together so that a deflection of the rudders at nominal submergences (ζ_F = 2.5 feet, ζ_R = 4.5 feet) would produce a rolling moment but no yawing moment.

B. Verification of Analysis

Let $\delta_1 = 0.966\ \delta_s + \delta_b$

where: δ_b = bow rudder deflection

δ_s = stern rudder(s) deflection

Then at nominal submergences at 80 knots

$$Y_{\delta_1} = +1.438 \times 10^6 \text{ lbs/rad}$$

$$N_{\delta_1} = 0$$

$$K_{\delta_1} = -1.52 \times 10^7 \text{ lb ft/rad.}$$

The transfer function relating roll angle to a deflection δ of the rudders is

$$\frac{\phi(s)}{\delta_1(s)} = \frac{0.616\left(\frac{s}{0.155}+1\right)\left(\frac{s}{6.855}+1\right)}{\left(\frac{s}{1.219}-1\right)\left(\frac{s}{1.629}+1\right)\left(\frac{s}{11.54}+1\right)\left(\frac{s}{31.53}+1\right)}$$

It was assumed that the rudder servo mechanism could be represented by the simple lag $\frac{1}{\frac{s}{50}+1}$. Figure 9-8 shows the gain phase diagram of the transfer function relating roll angle to rudder servo input commands. Also shown is the plot when lag-lead compensation $\frac{0.5s+1}{5s+1}$ is used. This compensation improves appreciably the closed loop response.

The responses of the loop, including the compensation, to initial disturbances in roll angle, were found for various loop gains. The inherent loop gain was -4.2 db. With additional gain of 0 db, the system diverged. With additional gain of 4.2 db (total of 0 db), there was a very slow convergent response. When the additional gain was 26.2 db (total of 22 db), which is the value indicated by the analysis for a closed loop resonant peak of 3 db, the response included a very weak damped oscillation at approximately 21 rad/sec. With additional gain of 37.5 db (total of 33.3 db) the response included a very poorly damped 39 rad/sec oscillation.

These results are very close to those predictable by an inspection of the gain-phase diagram in Figure 9-8. For all subsequent runs, the additional loop gain was kept at 26.2 db.

C. Designed Helmsman's Loop

Using rudders alone to stabilize the craft, it was necessary to use the ailerons to provide the rolling moment required to make a flat turn. Figure 9-9 shows the scheme used for the helmsman's loop(with $\delta_l = 0.85\ \delta_s + \delta_b$ for reasons explained below.) The bow rudder provided the necessary yawing moment and the ailerons were used to provide the rolling moment. There was a fixed ratio of 4.49 at 80 knots between ailerons and that part of bow rudder deflections resulting from

helmsman's inputs. This ratio was determined by selecting a fixed helmsman-caused bow rudder deflection and then adjusting the aileron deflection until, in a steady turn, the deflections of the stern rudders were zero. In this condition, the aileron and bow rudder deflections, as well as sideslip velocity, in a steady turn were practically identical to those in a similar turn when the ailerons were used to control the roll angle. Thus, the performance in a 0.2 rad/sec heading angle turn at 80 knots would be practically the same as indicated in Section 9.2.2A Paragraph (1e).

While investigating the response of the helmsman's loop to initial disturbances in heading angle with various values of the gain K_ψ (see Figure 9-9), it was found that the response included a very slowly decaying term which was particularly noticeable in sideslip velocity. By making $\delta_1 = 0.85\ \delta_s + \delta_b$ instead of $\delta_1 = 0.966\ \delta_s + \delta_b$ (see Paragraph (B)), this slowly decaying term was not present, and a satisfactory response was obtained with a value of 0.1 for K_ψ. (This change in δ_1 caused a deflection of the rudders at nominal foil submergences to produce a small yawing moment.) As before, the helmsman was simulated by means of the simple lag $\frac{1}{0.6s + 1}$.

To investigate the effects on the roll loop performance caused by the change in δ_1, the transient response to an initial disturbance in roll angle was recorded. It was quite similar to that found with the original δ_1. Therefore, δ_1 was made equal to $0.85\ \delta_s + \delta_b$ for all subsequent runs.

D. Performance in a Regular Sea

The performance of the craft at 80 knots was investigated in the same regular sea as was simulated in the previous runs. Some of the results of the investigation are summarized in Table 9-4.

Table 9-4. Performance in Regular Sea at 80 Knots of Craft Stabilized by Rudders

Type of Sea	ψ_w (deg)	Max Roll Angle (rad)	Max Norm Side Force (ft/sec^2)	Max Bow Rudder Deflection (rad)	Max Bow Rudder Rate (rad/sec)	Max Aileron Deflection (rad)
Quartering	45	0.015	1.8	0.067	0.069	0.008
Beam	90	0.005	0.5	0.028	0.018	0.001
Bow	135	0.013	2.0	0.043	0.104	0.003

9.2.4 COMPARISON OF PERFORMANCE WITH AILERON AND RUDDER CONTROL OF ROLL ANGLE

The results in Tables 9-1 and 9-4 are for two identical craft, both with inflexible struts, the rear struts being 2 feet longer than the front. These tables show the regular sea performance of the aileron-stabilized and rudder-stabilized craft.

Although the maximum roll angles obtained with the aileron-stabilized craft were smaller than those recorded with the rudder stabilized craft, the maximum roll angles in both cases were very small (<1 deg.). However, the maximum normalized side forces resulting from rudder stabilization were much smaller than those obtained from aileron stabilization. The major disturbing forces acting on the craft were orbital-motion-induced forces acting on the struts. The ailerons were capable of neutralizing only the rolling moments resulting from the disturbing forces, hence the large resulting normalized side forces. Except in a beam sea, the disturbing forces acting on the fore and aft struts were not in phase. Despite the fact that with the simple rudder system used, the bow and stern rudders were constrained to deflect in phase, it is apparent from the results that the rudder-produced strut forces cancelled reasonably well the orbital-motion produced strut forces, resulting in small net forces and moments.

9.2.5 DISCUSSION OF RATE AND DEFLECTION LIMITS

The maximum control surface deflections and rates listed in Tables 9-1 through 9-4 were the values reached in the regular sea simulated. During the three-dimensional simulation it was necessary to provide limits that were appreciably larger than these maximum values to ensure satisfactory operation in an irregular sea.

It was assumed in the two-dimensional simulation that the ailerons consisted of deflecting the entire outboard foils, and that the rudders consisted of deflecting the entire struts. If, instead of the whole struts being used as rudders, trailing edge flaps are used, the rudder deflections should be scaled by the necessary constant.

9.3 MANUAL CONTROL

9.3.1 INTRODUCTION

Manual control of the lateral modes of the simulated FRESH craft is discussed in this section.

Some general comments should be made on the use of a representative transfer function for the human operator. The transfer functions presented in Section 7 are based upon certain assumptions. The most important of these assumptions is that the transfer functions are essentially linear (aside from the pure delay term). Thus, such common non-linearities as threshold and dead space have been ignored as well as the possible effects of encountered acceleration on human performance.

The "ease" of handling of the craft by the operator is not strictly a measure of the physical energy expended by the operator, but rather one of responsivity. Pilot "opinion" as well as a count of the number of control stick reversals per unit time (or change in the sign of the slope of stick deflection) have been used in the following studies as an indication of this quantity. The latter measurement did not correlate well with pilot opinion and it was discarded in later runs.

It should be recognized, also, that while controlling the craft may involve the expenditure of operator energy, this is not necessarily synonymous with fatigue. Indeed, operation of the craft may be difficult or become degraded if the operator is not sufficiently taxed so as to direct his full attention to the control task. A manifestation of this effect may be seen in two cases involving different aileron deflection limits for a beam sea. Because craft stabilization is more difficult with the closer limits, greater care is taken by the operator to prevent large

excursions in roll angle from which recovery may be impossible, with the result being smaller excursions, in general, than for the case using wider deflection limits.

In all of the following runs, a human operator (or a simulated operator) attempted to roll stabilize the craft while a simulated helmsman kept the heading angle approximately correct. The simulated helmsman's loops used were those designed for the automatic roll control systems (see Section 9.2.2-1 b.).

The sea simulated was the same as that used in the automatic control runs. Quartering, beam and bow sea runs were made at speeds of 50 and 80 knots. Roll stabilization by means of the ailerons alone was attempted with laterally inflexible and flexible struts. The strut configuration used was the one in which the rear struts were 2 feet longer than the front strut, since this configuration was shown to be the easiest to control manually (see Figure 7-7). The normal submergences of the front and rear foils were taken as being 2.5 and 4.5 feet respectively. Roll stabilization by means of the bow and stern rudders alone, with inflexible struts, was also attempted.

9.3.2 DESCRIPTION OF CONTROL SETUP

The hand controller used was very similar to the one illustrated and described in Section 8. The majority of the runs were made with a torsion rod that provided a spring stiffness of approximately 7 in. lb/rad. (The length of the control stick, measured to the pivot point, was approximately 6 inches.) The stiffness of 7 in. lb/rad was found to be satisfactory by most operators. By trial and error, a value of 4 for the ratio of aileron servo input command to control stick deflection was found to be satisfactory at 80 knots. At 50 knots the value of the ratio was changed to 10.2 to maintain the same relationship between stick

deflection and aileron effectiveness. With the system that used rudders alone to roll stabilize the craft, a value of 2 for the ratio of bow rudder servo input commands to control stick deflection was found to be satisfactory. (No runs were made with this system at 50 knots.)

9.3.3 METHOD OF CARRYING OUT RUNS

Identical sets of runs were controlled in turn by each of three, or occasionally only two, operators. Before each run, the operator was given practice time to become acquainted with the dynamic characteristics of the craft. Most runs were of 3 minutes duration. After each run, the operator was asked to comment on the controllability of the craft.

9.3.4 AILERON CONTROL OF ROLL ANGLE

A. Configurations Considered

As previously stated, it was assumed throughout the series of runs that the rear struts were 2 feet longer than the front strut. Three values of the lateral stiffness of the struts were considered. (For a discussion of the type of lateral stiffness simulated, see Section 9.2.2 B.) The struts were considered to: (1) be inflexible, (2) have twice the stiffness considered in the automatic control runs, (3) have the same stiffness as used in the automatic control runs.

No sweepback of the rear foils was used. In a few of the flexible strut runs, dihedral was introduced to determine whether it made the manual control problem easier. The dihedral angle used (16.5 degrees) was that which minimized the derivative K_v rolling moment due to sideslip. All three operators found that the dihedral used made no noticeable difference in controlling the craft.

Aileron deflection and rate limits were set at ± 0.5 rad and ± 1 rad/sec respectively for most of the runs. Where the limits were different, special mention will be made in the text.

B. Display

An oscilloscope was used to provide an "outside-in" type of display. Originally the display consisted of a line whose inclination to a horizontal reference was simply the roll angle of the craft. However, after experimenting with adding various proportions of roll rate to the signal, it was agreed that the craft was easier to control with this addition. Some runs were made both with, and without the roll rate addition. It was possible to maintain roll excursions within smaller limits when there was some gain in the display, i.e., when the displayed angle was $K_1 \left[1 + K_2 S\right] \phi(s)$, where $K_1 > 1$. (K_2 is the proportion of rate signal included.) Runs were made with and without this display gain.

C. Inflexible Struts Case

1. Controllability in Calm Water

It was fairly easy to control the craft in calm water at a speed of 80 knots provided the task received the operator's undivided attention, and that the operator had recently been through a learning process to acquaint himself with the characteristics of the craft. Listed below are some of the quantities that were recorded in typical runs.

	Max roll angle (rad)	Max aileron deflection (rad)	Max normalized side force ft/sec^2	Control Stick* reversals per minute
Operator A	0.1	0.06	4.5	85
Operator B	0.125	0.05	6	51

*The number of control stick reversals per minute is the number of times per minute that the operator caused the direction of travel of stick to change.

These runs were made with no roll rate addition to the display and with no display gain.

2. Controllability in a Regular Sea

By trial and error it was found that the craft was easiest to control when the displayed quantity was $(1 + 0.75S)\,\phi\,(s)$. The controllability of the craft in a regular sea having a wave height of 4.5 feet and a wave length of 200 feet was investigated with this addition of roll rate to the display. Some runs were repeated with just roll angle displayed. No display gain was used for any of the 80-knot runs. Table 9-5 lists some of the quantities recorded during the 3-minute runs made at a speed of 80 knots.

With no roll rate addition to the display, Operators B and C both felt that the task of stabilizing the craft was a difficult one that required a lot of concentration. Operator A seemed to find it somewhat easier. All three operators agreed that the addition of the roll rate quantity to the display made stabilizing the craft appreciably easier. With this addition, Operators B and C thought the task of stabilizing the craft was semicomfortable. Operator A felt that the task was easy. During the runs the operators had to give the stabilizing problem full attention, keeping the display in sight at all times. It was found that losing sight of the display for periods as short as 1/2 second could result in large disturbances or even instability.

Table 9-5 shows that the maximum roll angles and normalized side forces were very large. Also, the maximum aileron deflections obtained in some runs were unrealistically large. The aileron rate limits of ± 1 rad/sec were reached in all runs.

There seems to be no correlation between degree of difficulty and the number of control stick reversals per minute, so this latter quantity will not be listed in subsequent tables.

Table 9-5. Summary of Results of Manual Control in Regular Sea at 80 Knots, Aileron Control, Inflexible Struts

Operator	Type of Sea	ψ_w	Roll Rate Included in Display	Max Roll Angle rad	Max Norm Side Force ft/sec^2	Max Aileron Deflection rad	Control Stick Reversals per min
A	Quartering	45°	Yes	0.27	12	0.09	59
B	Quartering	45°	Yes	0.35	13	0.11	54
C	Quartering	45°	Yes	>0.5	27	0.28	54
A	Quartering	45°	No	>0.5	38	0.43	75
B	Quartering	45°	No	>0.5	36	0.33	60
C	Quartering	45°	No	>0.5	26	0.18	48
A	Beam	90°	Yes	0.17	14	0.10	63
B	Beam	90°	Yes	0.28	13	0.10	62
C	Beam	90°	Yes	>0.5	21	0.21	62
A	Beam	90°	No	0.45	22	0.18	44
B	Beam	90°	No	>0.5	28	0.20	55
C	Beam	90°	No	>0.5	50	0.44	51
A	Bow	135°	Yes	0.47	26	0.14	60
B	Bow	135°	Yes	>0.5	26	0.19	90
C	Bow	135°	Yes	>0.5	25	0.18	90

Table 9-6 shows some of the results of manually controlling the craft at 50 knots with aileron deflection limits set at ± 0.5 rad. None of the operators could stabilize the craft in the quartering and bow seas with the aileron rate limits set at ± 1 rad/sec with no roll rate included in display. Increasing the rate limits to ± 2 rad/sec made manual stabilization in these cases possible. With one exception, all cases were controllable with rate limits of ± 1 rad/sec when roll rate was included in the display. This illustrates the importance of including this quantity in the display. All runs shown in the table were made with no display gain.

With the aileron rate limits set at ± 1 rad/sec, a very conscious effort had to be made to keep the disturbances small in order to maintain stability. With one exception, this was possible to accomplish when roll rate was included in the display. Without roll rate addition, and using a ± 1 rad/sec limit, it was impossible to control the craft in quartering and bow seas. As a result of the limit problem, it was decidedly more difficult to control the craft at 50 knots than at 80 knots.

The table shows that the maximum roll angles, normalized side forces, and aileron angles were very large. The aileron deflection limits of ± 0.5 rad were reached in some of the runs. As the so-called ailerons were, in fact, the complete outboard foils deflecting differentially, it was thought that aileron deflections of ± 0.5 rad were excessive, and some runs were repeated with smaller deflection limits. During these runs, the results of which appear in Table 9-7, the display included roll rate. Also, it was helpful to use some display gain. The aileron deflection rate limits were kept at ± 1 rad/sec.

Operator B could not control the craft in a beam sea with deflection limits of ± 0.2 rad without display gain, but was capable of controlling this case with a display gain of 5. The bow sea case, which was the

Table 9-6. Summary of Results of Manual Control in Regular Sea at 50 Knots, Aileron Control, Inflexible Struts, Aileron Deflection limits ±0.5 rad.

Operator	Type of Sea	ψ_w	Roll Rate Included in Display	Aileron Rate Limits rad/sec	Max Roll Angle rad	Max Norm Side Force ft/sec^2	Max Aileron Deflection rad
A	Quartering	45°	Yes	1	0.28	15	0.30
B	Quartering	45°	Yes	1	>0.50	22	0.50
C	Quartering	45°	Yes	1	0.25	10	0.23
A	Quartering	45°	No	2	0.29	16	0.36
B	Quartering	45°	No	2	0.43	23	0.48
C	Quartering	45°	No	2	>0.50	36	0.50
A	Beam	90°	Yes	1	0.36	16	0.30
B	Beam	90°	Yes	1	>0.5	28	0.50
C	Beam	90°	Yes	1	0.25	15	0.34
A	Beam	90°	No	1	0.30	17	0.41
B	Beam	90°	No	1	0.40	20	0.40
C	Beam	90°	No	1	0.39	14	0.33
A	Bow	135°	Yes	1	0.33	12	0.24
B	Bow	135°	Yes	1	0.50	17	0.38
C	Bow	135°	Yes	1	Unable to maintain stability		
A	Bow	135°	No	2	>0.50	30	0.50
B	Bow	135°	No	2	>0.50	25	0.50
C	Bow	135°	No	2	>0.50	26	0.50

Table 9-7. Summary of Results of Manual Control in Regular Sea at 50 Knots, Aileron Control, Inflexible Struts. Aileron Deflection Limits Investigation.

Operator	Type of Sea	ψ_w	Display Gain	Aileron Deflection Limits rad	Max Roll Angle rad	Max Norm Side Force ft/sec^2
A	Beam	90^o	1	0.1	UNSTABLE	
B	Beam	90^o	1	0.1	UNSTABLE	
C	Beam	90^o	1	0.1	UNSTABLE	
A	Beam	90^o	1	0.2	0.15	7
B	Beam	90^o	1	0.2	UNSTABLE	
C	Beam	90^o	1	0.2	0.23	10
A *	Beam	90^o	5	0.2	0.15	9
B	Beam	90^o	5	0.2	0.16	9
C	Beam	90^o	5	0.2	0.15	8
A	Bow	135^o	2.5	0.3	0.32	12
B	Bow	135^o	2.5	0.3	0.39	16
C	Bow	135^o	2.5	0.3	UNSTABLE	
A	Bow	135^o	2.5	0.2	0.35	11
B	Bow	135^o	2.5	0.2	UNSTABLE	
C	Bow	135^o	2.5	0.2	UNSTABLE	

*This was a 10 minute run.

most difficult one to control, could not be controlled by Operator C with deflection limits of ±0.3 rad. It is then concluded that, despite the fact that Operator A could control the craft in a bow sea with deflection limits of ±0.2 rad, deflection limits of at least ± 0.3 rad will have to be provided. The display gain was helpful in aiding the operator to keep roll angles small, an essential requirement when small deflection limits were being used.

An interesting fact emerging from this series of runs is that reducing the aileron deflection limits made stabilizing the craft more difficult, but if stability could be maintained, the resulting disturbances were reduced. This is demonstrated by comparing the beam sea runs using unit display gain in Table 9-7 with the beam sea runs in Table 9-6. The comparison shows that reducing the aileron deflection limits from ±0.5 to ±0.2 rad resulted in smaller disturbances in the runs controlled by Operators A and C. However, Operator B could not control the craft with ±0.2 rad aileron deflection limits.

It is thought this phenomenon can be explained by the following:

(a) Reducing the aileron deflection limits reduces the disturbances that the operator can apply

(b) The increased difficulty in stabilizing the craft requires greater concentration.

3. Simulated Manual Control

Some runs were made with a simulated operator in the loop, to compare the performance of the analytical model with that of actual operators.

Figure 7-7 shows the open loop gain phase plot with the simulated operator in the loop at 80 knots. (Curve B is the relevant one.) The model

used in this figure was a transfer function $e^{-0.25s}\left(\frac{s}{0.95}+1\right)$ relating the operator's output to input. The transportation lag was synthesized by using the second order Pade function

$$\frac{\left(\frac{0.25s}{\sqrt{12}}\right)^2 - \frac{\sqrt{12}}{2}\left(\frac{0.25s}{\sqrt{12}}\right) + 1}{\left(\frac{0.25s}{\sqrt{12}}\right)^2 + \frac{\sqrt{12}}{2}\left(\frac{0.25s}{\sqrt{12}}\right) + 1}$$

This function represents the transportation lag very accurately within the bandwidth of the loop (approximately 8 rad/sec). The lead term was represented by

$$\frac{\frac{s}{0.95} + 1}{\frac{s}{38} + 1}$$

which again represents the lead term fairly accurately within the relevant frequency range. As shown in Section 9.2.2, the inherent loop gain at 80 knots was 12 db. Figure 7-7 indicates that 6 db should be a reasonable total loop gain, so additional loop gain of -6 db was introduced. Figure 9-10 shows the transient response of the loop to an initial roll angle error. Damping was not good, but response was what an inspection of the gain-phase plot would lead one to expect.

Performance of the system in bow and quartering seas was investigated at a speed of 80 knots. The aileron deflection and rate limits were set at 0.5 rad and 1 rad/sec respectively. Some results are given in Table 9-8.

Table 9-8. Performance of System with Simulated Operator in Regular Seas at 80 Knots

Type of Sea	ψ_w	Max rad Angle rad	Max Norm. Side Force ft/sec^2	Max Aileron Deflection rad
Quartering	45^o	0.10	14	0.17
Bow	135^o	0.01	9	0.04

A comparison of results in Tables 9-8 and 9-5 shows that the roll angles in both quartering and bow seas were appreciably less when the simulated operator was controlling the craft. Also, the aileron deflections in the bow sea case were much smaller than when an actual operator was at the controls.

It is thus concluded that, even though the model used for an operator is helpful for predicting stability regions, it cannot be used to predict the responses to all regular inputs. It was particularly poor in predicting the responses to the high-frequency disturbances encountered in a bow sea.

D. Flexible Struts - Case 1

1. Introduction

In this series of runs, the struts were assumed to have twice the lateral stiffness of the struts considered in the automatic control runs. (See Section 9.2.2.B.) That is, the struts were assumed to have a lateral stiffness of 18,376 lb/ft.

2. Controllability in a Regular Sea

The controllability of the craft in a beam sea was investigated at speeds of 80 and 50 knots. Various amounts of roll rate addition to

the display were tried. It did not make much difference whether the displayed quantity was $(1 + 0.5s)\,\phi\,(s)$ or $(1 + s)\,\phi\,(s)$. The results shown in Table 9-9 are for the former displayed quantity. No display gain was used in any of the runs. The aileron deflection and rate limits were set at 0.5 rad and 1 rad/sec respectively.

Table 9-9 shows that again the maximum roll angles, normalized side forces, and aileron deflections were very large. Operator A described the task of maintaining stability as being fairly easy. Operators B and C thought the task was difficult. Operator A thought that the degree of difficulty was about the same as for inflexible struts, although his performance was not as good as when controlling the inflexible strut craft. The other two operators found it somewhat more difficult.

It is noted that only beam seas were investigated. Experience gained with the craft with rigid struts indicated that control in quartering and bow seas would probably be more difficult than in beam seas.

E. Flexible Struts - Case 2

1. Introduction

Each strut was assumed to have a lateral stiffness of 9188 lb/ft, the same value used in the automatic control investigations.

2. Controllability in a Regular Sea

Manual control of the craft in a beam sea at speeds of 80 and 50 knots was attempted. Again, various amounts of roll rate addition were tried. Display gain was not used, and the aileron deflection and rate limits were set at ±0.5 rad and ±1 rad/sec respectively.

Table 9-9. Summary of Results of Manual Control in a Beam Sea, Aileron Control, 18,376 lb/ft Stiffness Struts

Operator	Speed Knots	Max Rad Angle rad	Max Norm Side Force ft/sec^2	Max Aileron Deflection rad
A	80	0.38	19	0.15
B	80	>0.50	44	0.26
C	80	>0.50	25	0.19
A	50	>0.50	29	0.45
B	50	0.42	19	0.35
C	50	0.29	16	0.37

None of the operators could control the craft at a speed of 80 knots. At a speed of 50 knots, some runs of 3-minutes duration were made, but it was found to be an extremely difficult task to maintain stability. All operators agreed that manual control of this case was impractical.

F. Comparison of Controllability with Inflexible and Flexible Struts

The maximum roll angles, normalized side forces, and aileron deflections in a beam sea were somewhat larger for the 18,376 lb/ft stiffness strut craft than for the craft with inflexible struts. Two of the three operators thought that the former craft was slightly more difficult to control, while the other operator found no difference in the difficulty of control between the two cases. However, there was no doubt that reducing the stiffness of the struts to 9188 lb/ft greatly increased the difficulty of control, and, in fact, with this stiffness the craft was uncontrollable at 80 knots and barely controllable at 50 knots.

9.3.5 RUDDER CONTROL OF ROLL ANGLE

A. Configuration Considered

It was assumed that rudder control would be obtained by deflecting each of the three struts. (Again note that if the rudders are, in fact, trailing edge flaps, the rudder deflections will be those recorded in this section multiplied by some constant, the constant depending on the ratio of the total chord to flap chord.) The port and starboard stern rudders were taken to be directly linked, and the relation between the bow and stern rudder deflections was taken to be $\delta_l = \delta_b + 0.85\,\delta_s$. (This is the same relationship as used in the automatic control investigation, Section 9.2.3, Figure 9-9.) The struts were assumed to be inflexible, with the rear struts 2 feet longer than the front strut. The helmsman's loop designed for the automatic control system was used. (See Section 9.2.3) Rudder deflection and rate limits were set at 0.167 rad and 1 rad/sec respectively.

B. Display

An oscilloscope was used to provide an "outside-in" type of display of roll angle. Including a proportion of roll rate in the display did not appear to make the task of controlling the craft any easier, so all runs were made with just roll angle displayed. (Figure 9-11 shows the open loop gain phase plot of a loop using rudders to control roll angle that also includes a transportation lag of 0.25 second. It is clear that lag-lead rather than lead-lag compensation would be required to stabilize the loop. Thus, it was expected that introducing lead into the display would not make stabilizing the craft any easier.)

No display gain was used in any of the runs in this series.

C. Controllability in Calm Water

It was not difficult to control the craft in calm water at a speed of 80 knots, although both operators who controlled these runs agreed that the task was a little more difficult than when the ailerons were used to stabilize the craft. Some of the results recorded in typical runs follow.

	Max Roll Angle (rad)	Max Rudder Deflection (rad)	Max Norm Side Forces ft/sec^2
Operator A	0.10	0.018	<2
Operator B	0.10	0.021	<2

The normalized side forces, although they could not be read very accurately from the recordings, due to noise that was present, were very small in both runs.

D. Controllability in Regular Seas

The controllability of the craft in the 4.5-foot wave height, 200-foot wave length regular sea was investigated. A craft speed of 80 knots only was considered. Some of the results are listed in Table 9-10.

9.3.6 COMPARISON OF AILERON STABILIZATION AND RUDDER STABILIZATION IN REGULAR SEAS

A comparison of the results in Table 9-10 with the relevant ones in Table 9-5 - the results with aileron stabilization - shows that the roll angles in the quartering and beam seas were approximately the same for both types of stabilization, but that in the bow sea the roll angles were appreciably less when the rudders were used.

Noise present in the normalized side force recordings made it difficult to measure accurately the maximum values obtained. However, it is probable that the values listed in Table 9-10 are accurate to within ±3 ft/sec^2. Rudder stabilization resulted in appreciably smaller normalized side forces than did the aileron stabilized runs in the beam and bow sea runs, but the values were approximately the same for the quartering sea cases.

All operators thought that the task of stabilizing the craft with rudders was more difficult and took more concentration than was required for aileron stabilization. The main reason for the difficulty in controlling with rudders was that with the rudder limits used, ± 1/6 rad, great care was required to keep roll angles small to ensure that rudder control was sufficient for recovery. Limits of ± 1/6 rad might appear to be too small. However, it was assumed in the simulation that the flow on both sides of the struts would not be cavitated. The flow on one side of a strut will be cavitated well before the strut is rotated through 1/6 rad, resulting in a lift curve slope reduced approximately by a factor of 2 from the non-cavitating value, and hence reduced rudder

Table 9-10. Summary of Results of Manual Control in Regular Sea at 80 Knots, Rudder Stabilized Craft

Operator	Type of Sea	ψ_w	Max Roll Angle rad	Max Norm Side Force ft/sec^2	Max Rudder Deflection rad
A	Quartering	45^o	0.20	10 (approx)	0.150
B	Quartering	45^o	0.36	13 (approx)	0.167
A	Beam	90^o	0.17	6 (approx)	0.167
B	Beam	90^o	0.27	8 (approx)	0.167
A	Bow	135^o	0.33	10 (approx)	0.125
B	Bow	135^o	0.33	10 (approx)	0.167
C	Bow	135^o	0.38	10 (approx)	0.167

effectiveness. Thus, the assumption that strut rotation is confined to ± 1/6 rad but the flow is non-cavitating may result in roughly the same maximum rudder effectiveness as assuming strut rotation of something approaching ± 1/3 rad but allowing for flow cavitation. If the rudders consist of trailing edge flaps, the equivalent rudder effectiveness will be obtained by something near ± 2/3 rad of flap deflection when flow cavitation is taken into consideration. This is an unreasonably large flap deflection. Therefore, it is concluded that the rudder deflection limits used do, in fact, represent nearly maximum realizable effectiveness.

However, one effect noticeable with the rudder control was the variation of rudder effectiveness with changes in strut submergences, caused by the variation of the lengths of the rudders in the water. This was particularly noticeable in the beam sea. In a trough in the sea, the submergences of all struts were small, and consequently rudder effectiveness was reduced appreciably. In contrast, aileron effectiveness was independent of strut submergences.

Rudder stabilization was not investigated at a speed of 50 knots. It was felt that, with the rudder limits of ± 1/6 rad, manual control at 50 knots would very probably have proved to be impossible.

9.3.7 CONCLUSIONS REGARDING MANUAL CONTROL OF THE LATERAL MODES

The following conclusions are made:

(a) In an extreme emergency, it is reasonable to expect a human operator to be able to control the craft in calm water, or water in which the waves are small, with either the aileron or rudder stabilization systems. However, this operator must be well acquainted with the dynamic

characteristics of the craft; knowledge may be gained either by periodically flying the craft or by use of a simulator. Furthermore, the task of stabilizing the craft will be one to which the operator will have to give his undivided attention.

(b) It is unreasonable to expect a human operator to be able to control the craft laterally in a State 3 Sea.

With the control deflection limits used in the simulation, some runs were difficult to stabilize. There is little doubt that in these runs there was an unacceptable probability of control being lost. Also, the craft disturbances resulting from these runs were very large and may be unacceptable from the structural viewpoint.

Moreover, it is thought that, in an actual craft, the control effectiveness is likely to be less than assumed in the simulation, in which case the craft will be more difficult to control (if, indeed, control is possible) Due to the possible catastrophic consequences of losing control of the craft, it is concluded that manual control in a State 3 Sea is inadvisable.

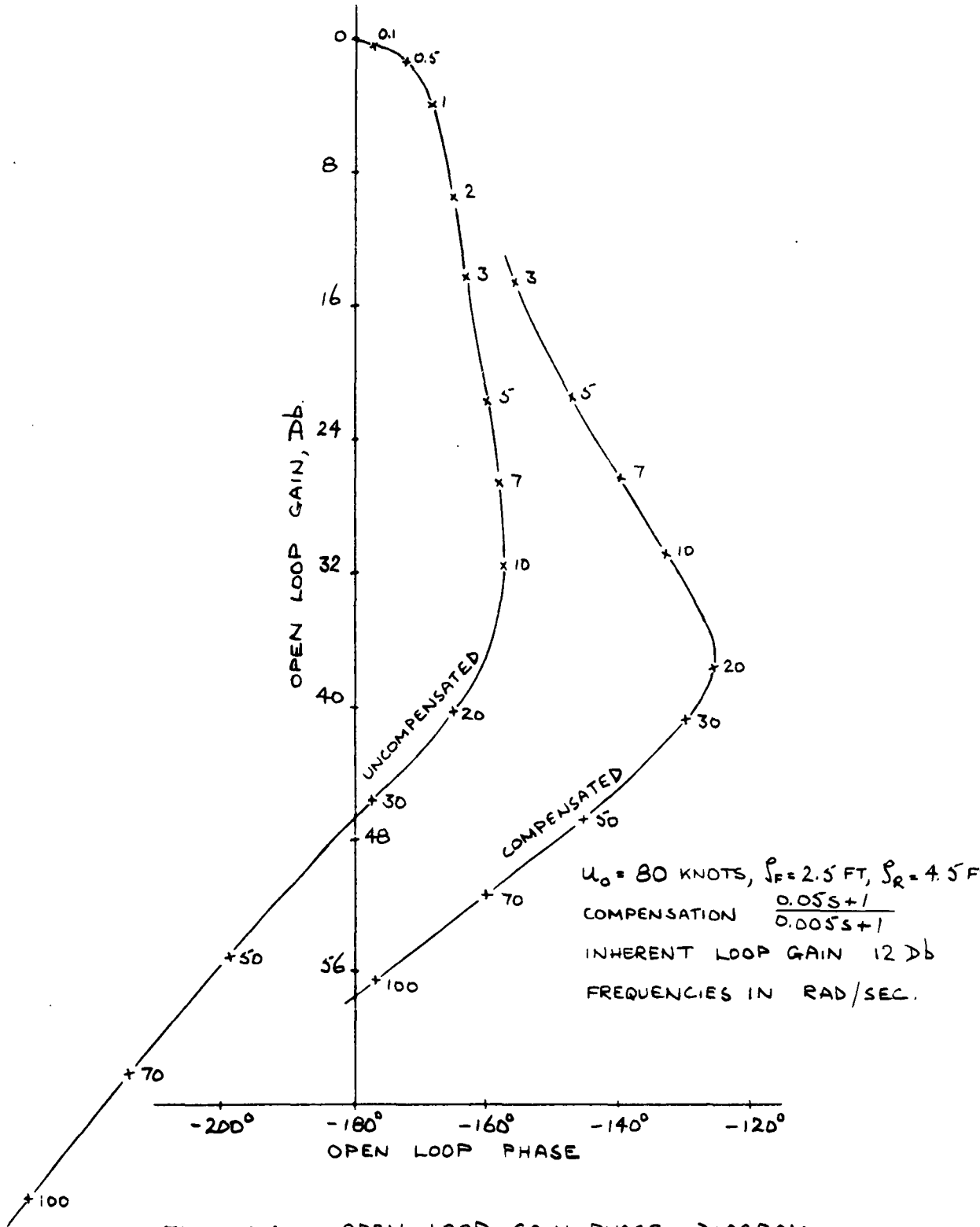

Figure 9-1 OPEN LOOP GAIN-PHASE DIAGRAM AILERON CONTROL, UNEQUAL INFLEXIBLE STRUTS.

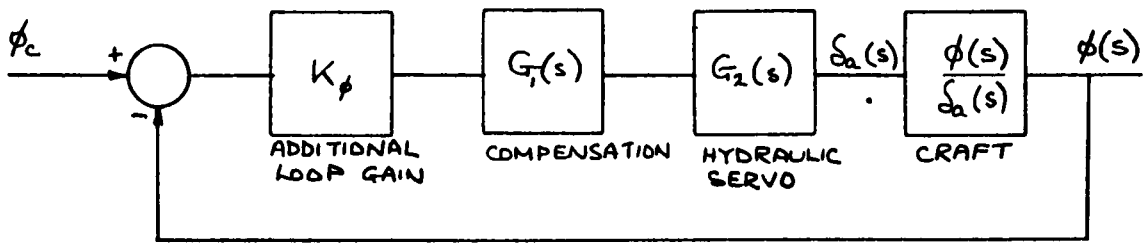

Figure 9-2 BLOCK DIAGRAM OF ROLL ANGLE - AILERON CONTROL SYSTEM.

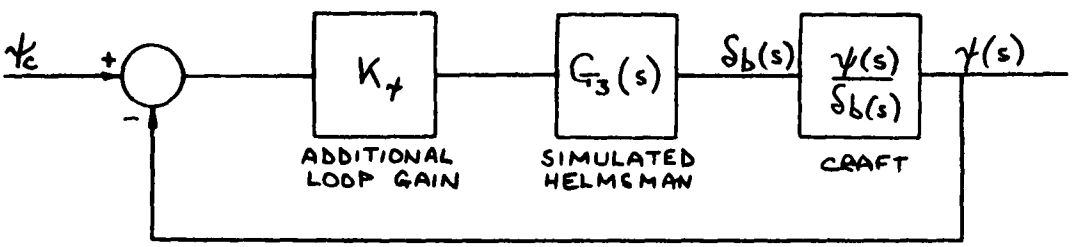

Figure 9-3. BLOCK DIAGRAM OF SIMULATED HELMSMAN'S LOOP

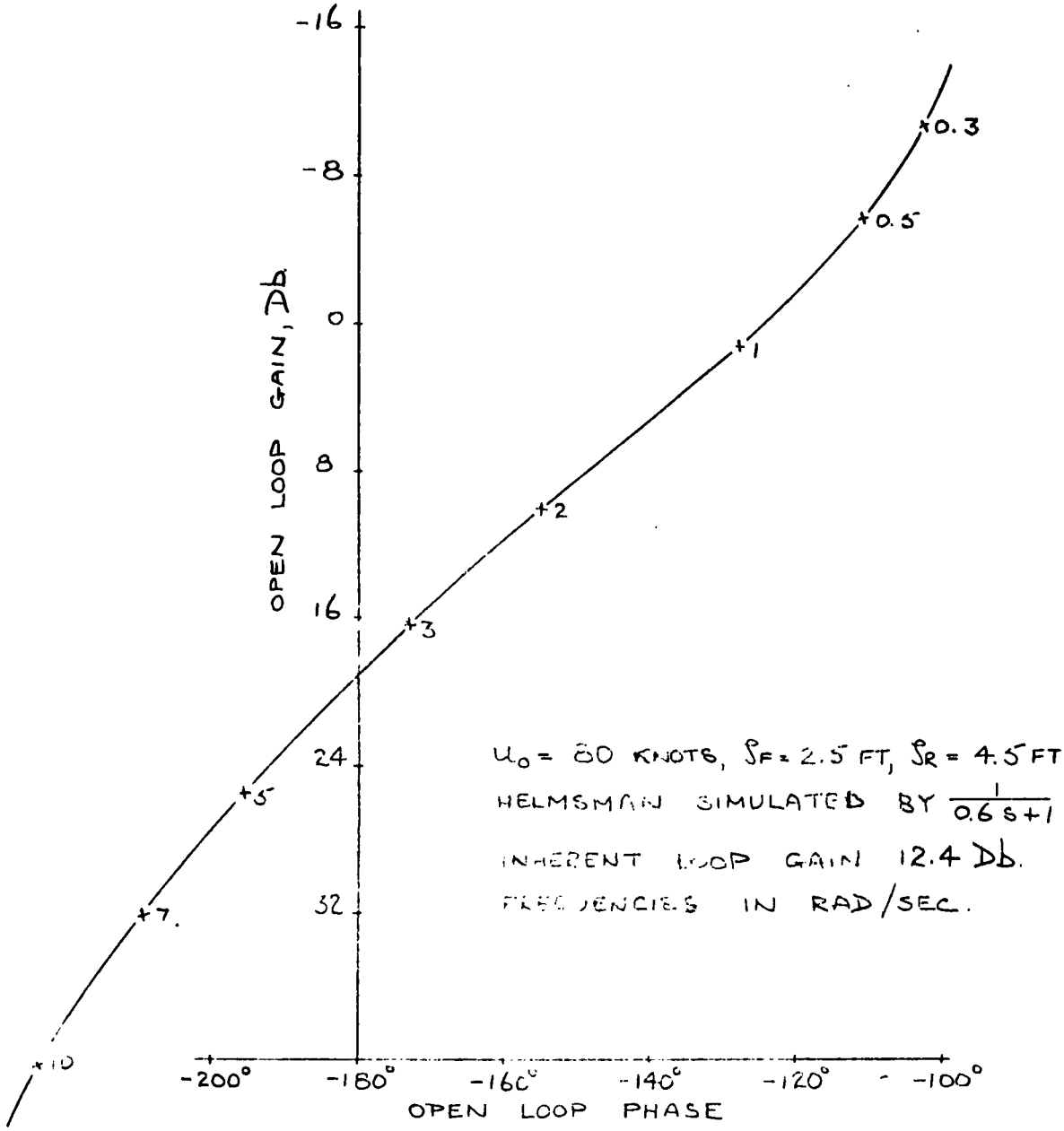

Figure 9-4

HEADING ANGLE CONTROL, OPEN LOOP GAIN PHASE DIAGRAM. UNEQUAL INFLEXIBLE STRUTS.

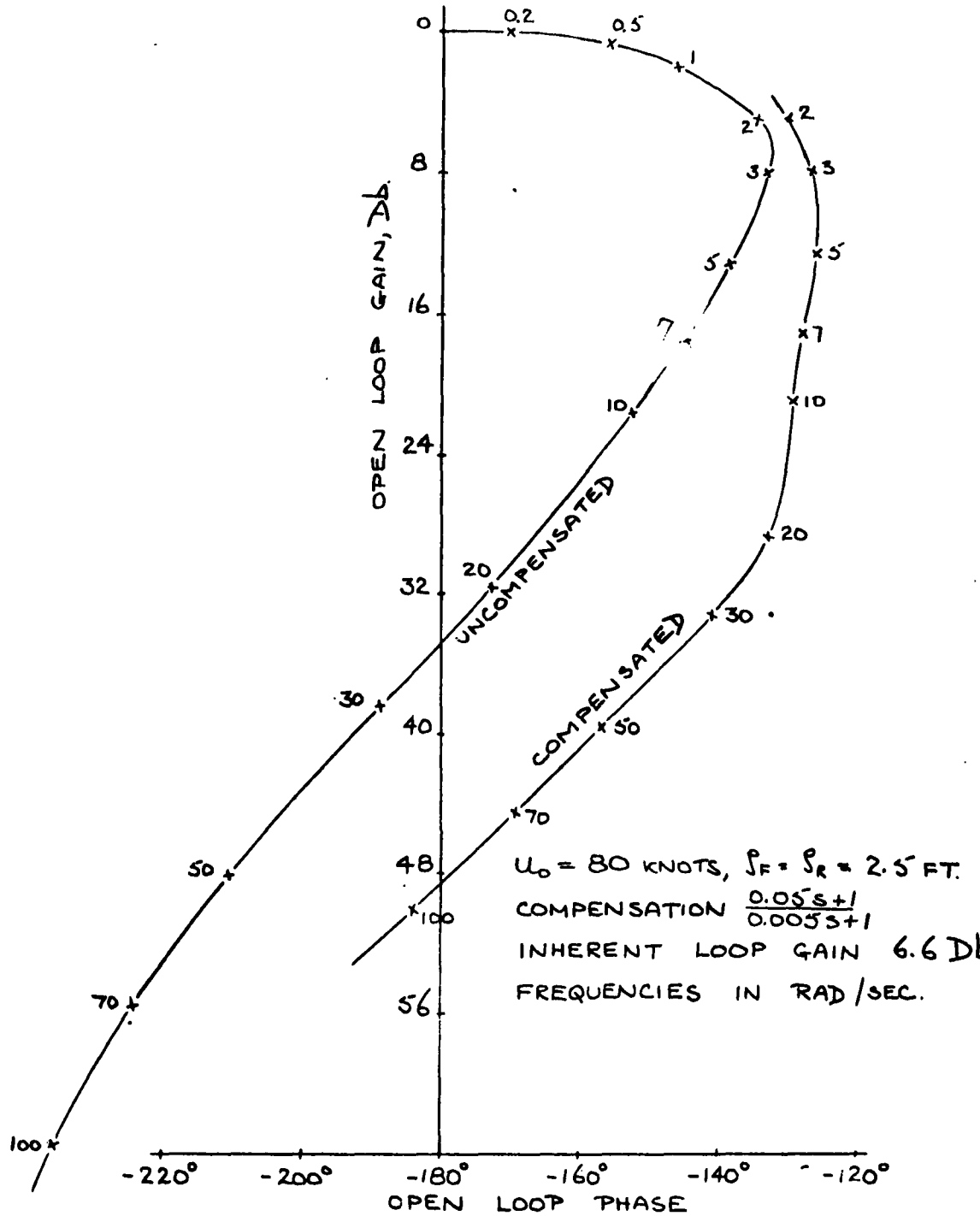

Figure 9-5. OPEN LOOP GAIN PHASE DIAGRAM
AILERON CONTROL, EQUAL INFLEXIBLE STRUTS

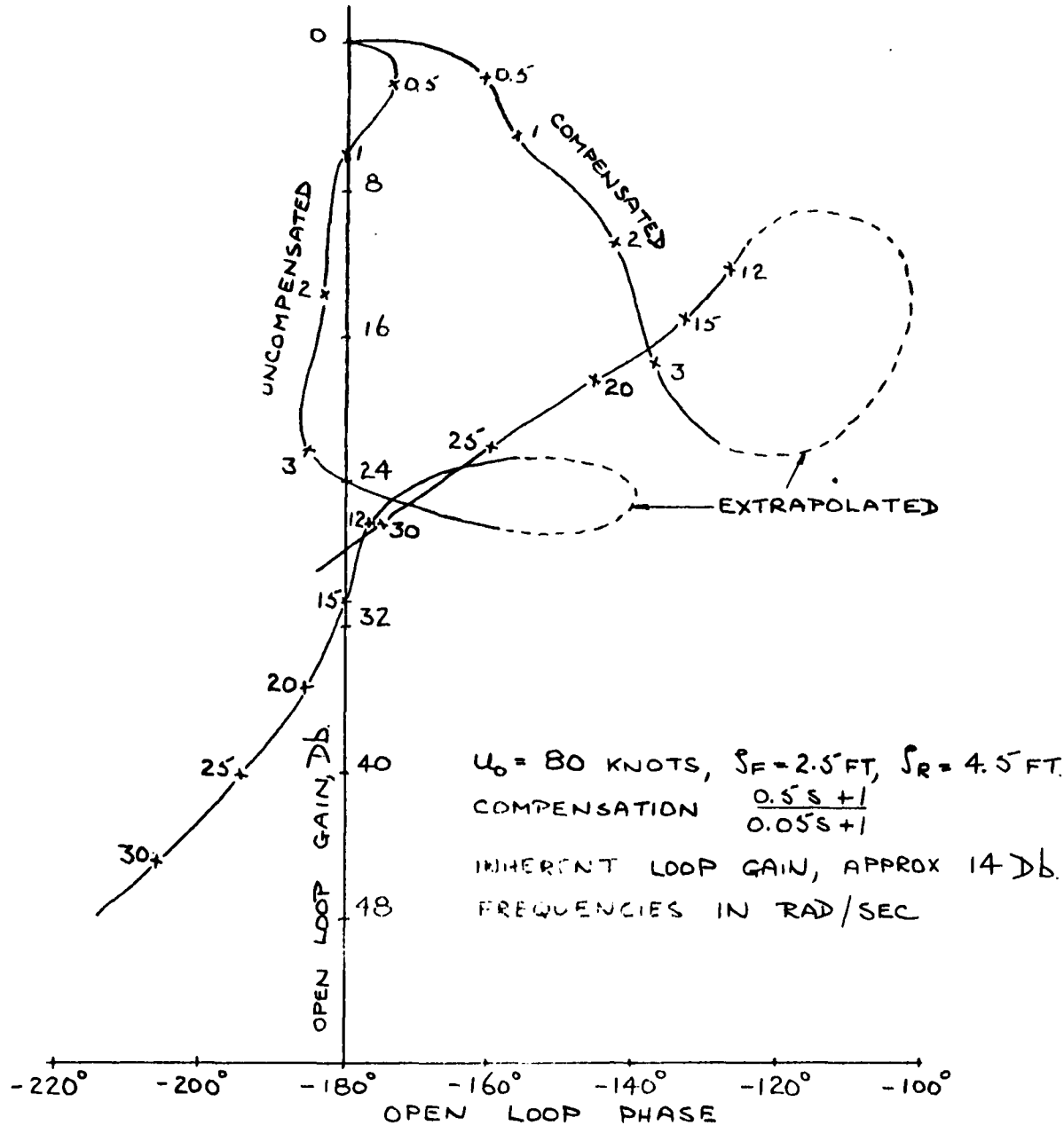

Figure 9-6.

APPROXIMATE OPEN LOOP GAIN PHASE DIAGRAM. AILERON CONTROL, UNEQUAL FLEXIBLE STRUTS.

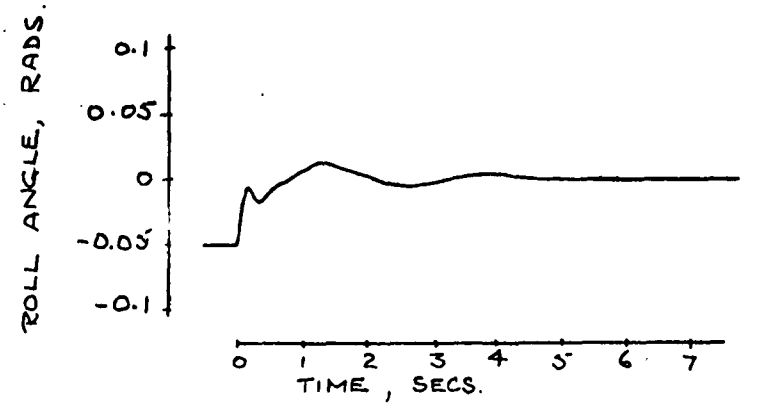

Figure 9-7.

TRANSIENT RESPONSE TO INITIAL ROLL DISTURBANCE. AILERON CONTROL UNEQUAL FLEXIBLE STRUTS.

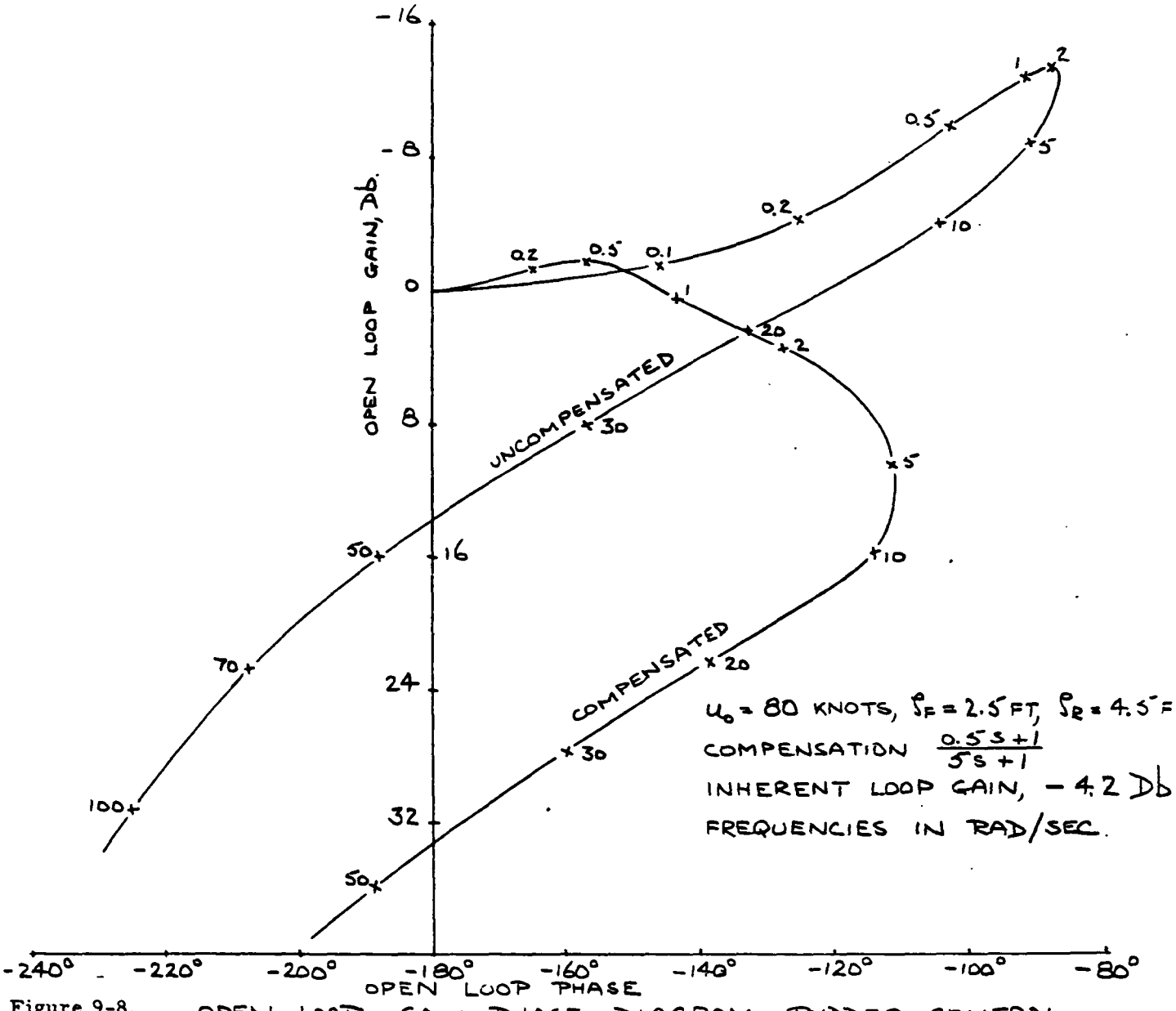

Figure 9-8. OPEN LOOP GAIN PHASE DIAGRAM. RUDDER CONTROL UNEQUAL INFLEXIBLE STRUTS.

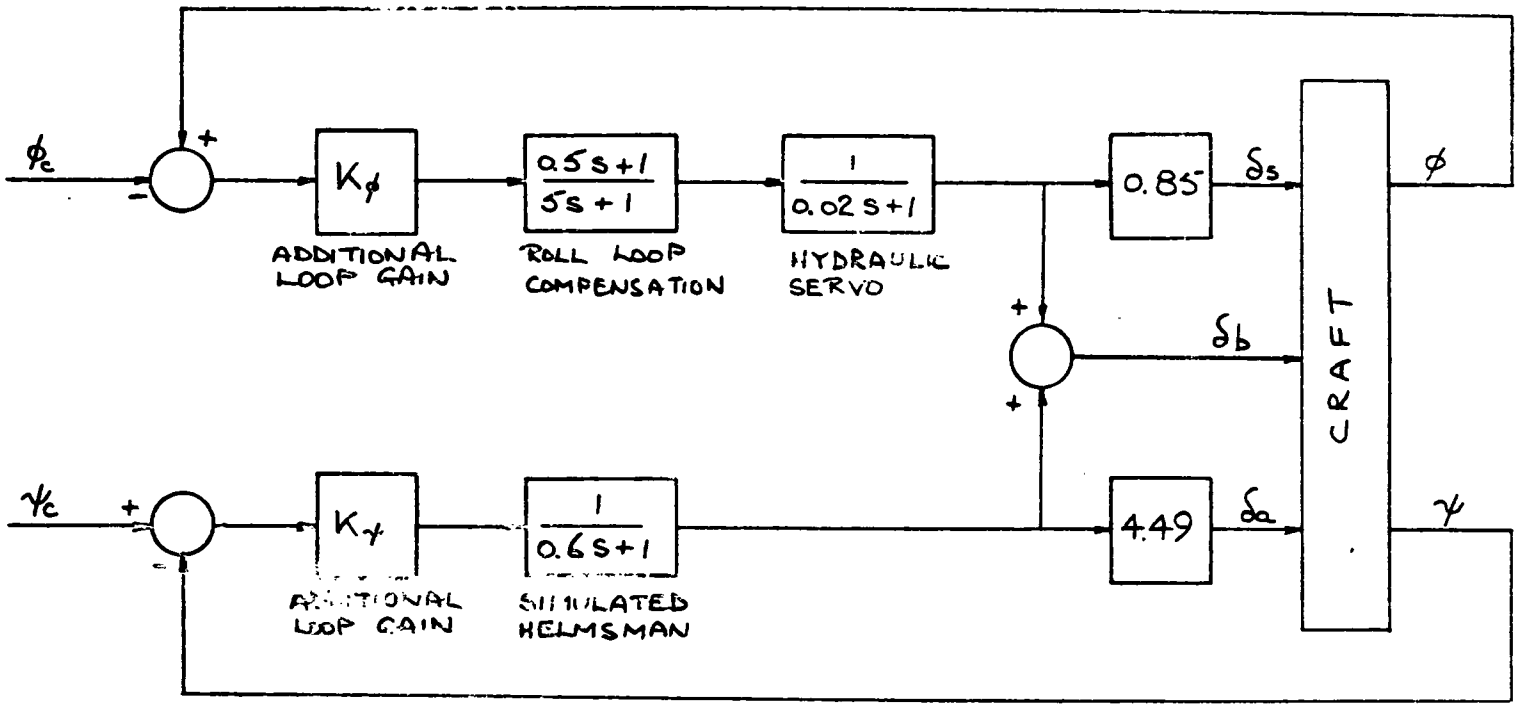

Figure 9-9. BLOCK DIAGRAM SHOWING ROLL AND HEADING CONTROL LOOPS. CRAFT STABILIZATION BY RUDDERS ALONE

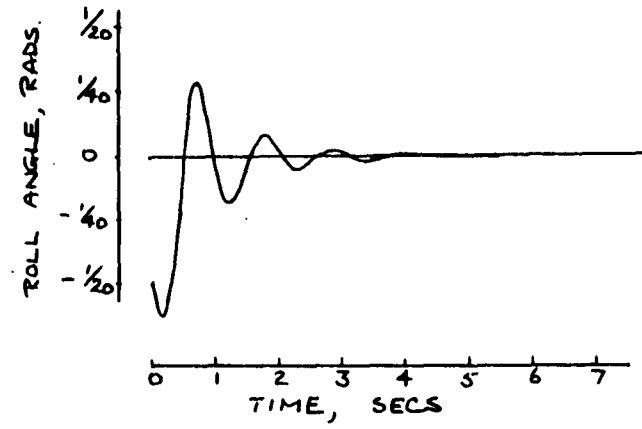

Figure 9-10. TRANSIENT RESPONSE. SIMULATED MANUAL CONTROL.

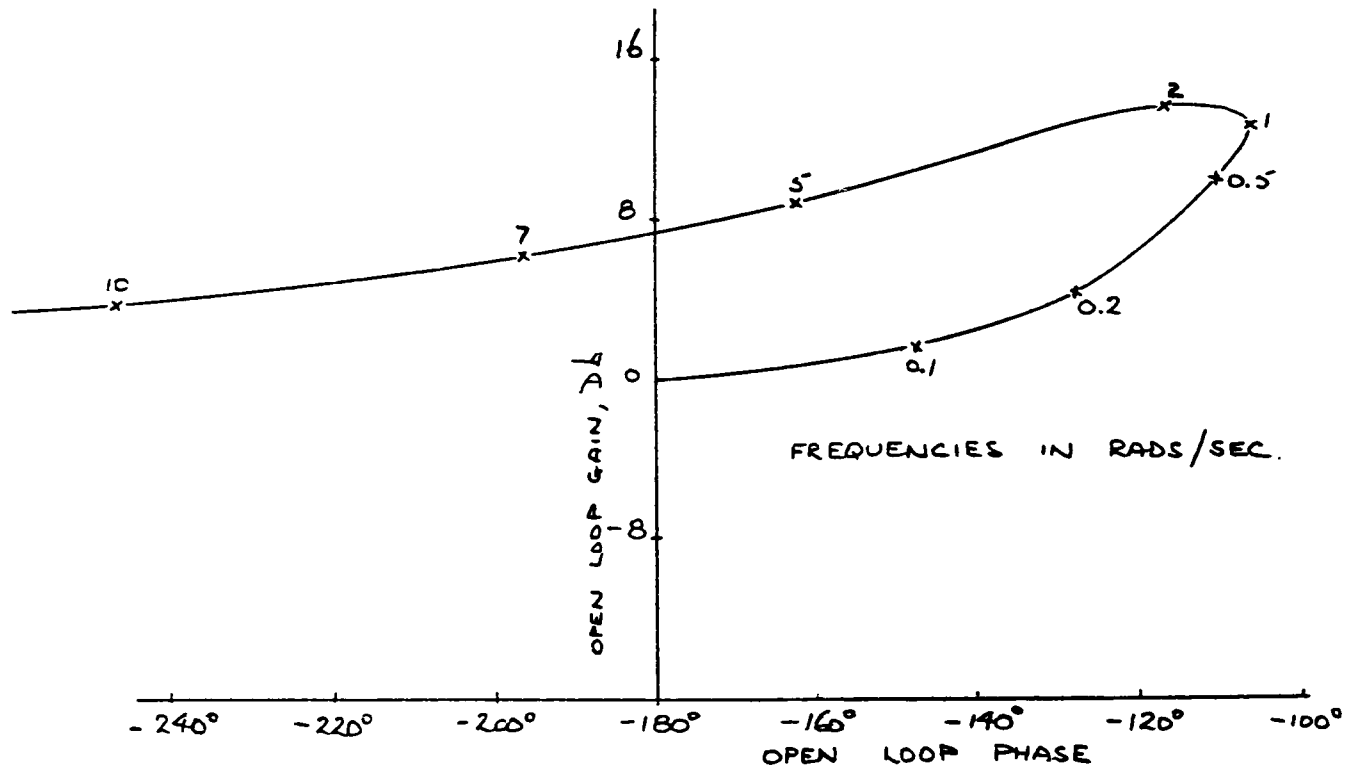

Figure 9-11. OPEN LOOP GAIN PHASE PLOT. ROLL ANGLE - RUDDER LOOP. 0.25 SECOND TRANSPORTATION LAG INCLUDED.

SECTION 10

LONGITUDINAL TWO-DIMENSIONAL SIMULATION OF THE SPRUNG FOIL CRAFT

10.1 INTRODUCTION

Section 6 explored a number of control configurations with a view toward permitting both automatic and manual stabilization of the sprung foil craft. None of the configurations investigated analytically in this section were found to show promise of satisfactory stability in either the automatic or manual modes. However, the root locus solutions developed in Section 6.6 were usefully employed in providing a check solution for the simulator setup. Initial attempts in the simulation to control the craft manually using either of the two configurations analyzed in Section 6.6 showed the job to be as difficult as implied by the analytical results with stabilization impossible over periods longer than 1/4 minute in calm water. Some additional manually controlled runs were made, however, using a pitch rate loop to the aft foil in both calm water and regular seas representing components of a State 3 Sea. In some cases where encounter frequencies are too high for the human to counter wave-induced disturbances, the sprung foils take over this task to provide an improved ride that would otherwise be impossible. Because of the length computations necessary for the analytic study of additional cases, especially where control system loops became more numerous, the analog computer was employed for further investigation and a stable automatic system was evolved employing the control loops defined in the following section.

10.2 CONTROL SYSTEM CONFIGURATION

These control loops may be characterized by the following equations:

$$\eta_F = \xi_F \left(k_{IF} + \frac{k_{2F}}{s}\right)\left(\frac{1}{s/\omega_{\eta_F} + 1}\right) \qquad (10\text{-}1)$$

and

$$\eta_R = \xi_R \left(k_{IR} + \frac{k_{2R}}{s}\right)\left(\frac{1}{s/\omega_{\eta_R} + 1}\right) \qquad (10\text{-}2)$$

where

η_F, η_R = fore and aft foil incidence control angle

ξ_F, ξ_R = fore and aft spring deflection perturbations

ω_{η_F}, ω_{η_R} = cutoff frequencies for fore and aft controls

The basic control system utilizes the following values for these loops

$$k_{IF} = k_{IR} = 0.15 \text{ ft}^{-1}$$

$$k_{2F} = k_{2R} = 0.025 \text{ ft}^{-1} - \text{sec}^{-1}$$

$$\omega_{\eta_F} = \omega_{\eta_R} = 15 \text{ rad/sec}$$

The bandwidth requirements on the hydraulic system controlling incidence are determined by the values of ω_{η_F} and ω_{η_R} and are obviously very modest.

The aft pitch angle loop is represented by the equation

$$R'_{CR} = \theta \left(k_{1\theta} + s\,k_{2\theta} + \frac{k_{3\theta}}{s}\right) \tag{10-3}$$

with values for the basic configuration of

$$k_{1\theta} = 10,000 \text{ lb/rad}$$

$$k_{2\theta} = 80,000 \text{ lb/sec}$$

$$k_{3\theta} = 800 \text{ lb} - \text{sec}^{-1}$$

The forward reaction control loop employs heave acceleration and a height sensor signal, with associated filters.

Thus,

$$R'_{CF} = -k_4 \left[\frac{\ddot{h}_{16}}{s + \omega_{x_1}} \left(k_1 + \frac{k_2}{s + \omega_{x_2}}\right) \left(\frac{s}{s + \omega_{h_x}}\right) + \frac{k_3 \left(h'_{HS} - h_{WHS}\right)}{1 + s/\omega_{HS}} \right] \tag{10-4}$$

where $\ddot{h}_{16}$ = heave acceleration signal derived at a point 16 feet forward of the C. G. and with the basic configuration having the following values

$$k_1 = 0.25 \text{ lb-sec/ft}$$

$$k_2 = 2.0 \text{ lb/ft}$$

$$k_3 = 0.80 \text{ lb/ft}$$

$$k_4 = 1000$$

$$\omega_{x_1} = \omega_{x_2} = 0.10 \text{ rad/sec}$$

$$\omega_{h_x} = \omega_{HS} = 1.0 \text{ rad/sec}$$

10.3 TRANSIENT RESPONSES IN A CALM SEA

Figures 10-1 and 10-2 illustrate the response of the craft using the basic control system configuration shown in the previous subsection. Transients were induced by beginning the problem with an initial height error of approximately 2 feet with the resulting response being quite similar for the 80 and 50 knot speeds. The relatively small transient overshoots exhibited by these records will minimize the possibility of broaching the foils or hull impact when sudden height changes are demanded by the operator.

10.4 PERFORMANCE IN REGULAR WAVES UNDER AUTOMATIC CONTROL

The response of the craft in regular waves is recorded in Tables 10-1 and 10-2 for 80 and 50 knots respectively. Nominal foil submergence was, as usual, 2.5 feet forward and 4.5 feet aft and the same control system constants as presented in Section 10.2 were used in these tests with the exception of the three automatic control runs noted in Table 10-1.

It is believed that the use of the basic configuration parameters for these three runs, rather than the somewhat different parameters noted at 80 knots, would not appreciably alter the trends apparent in Table 10-1.

Table 10-1. Performance in Regular Seas Under Automatic and Manual Control at 80 Knots

Type of Sea	H-ft	λ-ft	ψ_W-deg	ω_e-rad/sec	$\ddot{h}_{GV}$-ft/sec^2	$\ddot{\theta}$-rad/sec^2	θ-rad	ξ_F-ft	ξ_R-ft
Automatic Control									
Head	4.5	200	180	5.25	4.0	0.10	0.0035	0.28	0.10
Bow	4.5	200	120	3.13	3.0	0.042	0.0040	0.21	0.088
Beam	4.5	200	90	1.01	0.95	0.0016	0.0025	0.14	0.096
Quartering	4.5	200	60	-1.12*	1.05	0.008	0.0065	0.17	0.10
Following	4.5	200	0	-3.24	3.0	0.056	0.0050		
Beam	4.5	500	90	0.636	0.65	0.0030	0.0067	0.17	0.11
Head(1)	4.5	500	180	2.33	1.15	0.014	0.0023	0.17	0.07
Beam(1)	4	50	90	2.01	0.80	0.008	0.0013	0.17	0.11
Head(2)	4	50	180	19.0	0.70	0.12	0.001	0.42	0.24
Manual Control(1)									
Head	4.5	200	180	5.25	5.0	0.15	0.0075	0.25	0.20
Bow	4.5	200	120	3.13	3.8	0.15	0.0065	0.30	0.22
Beam	4.5	200	90	1.01	3.3	0.09	0.0070	0.30	0.18
Following	4.5	200	0	-3.24	4.2	0.12	0.0075	0.25	0.16
Head	4.5	50	180	19.0	1.20	0.10	0.0030	0.22	0.15

(1) $\omega_{h_x} = \omega_{HS} = 0.5$ rad/sec (2) $\omega_{h_x} = \omega_{HS} = 0.5$ rad/sec and $k_2 = 1.0$

* The negative sign implies only that the craft is approaching a wave crest from its rear face.

Table 10-2. Performance in Regular Seas Under Automatic and Manual Control at 50 Knots

Type of Sea	H-ft	λ-ft	ψ_W-deg	ω_e-rad/sec	h_{GV}-ft/sec^2	$\ddot{\theta}$-rad/sec^2	θ-rad	ξ_F-ft	ξ_R-ft
Automatic Control									
Head	4.5	200	180	3.66	3.25	0.07	0.0044	0.7	0.26
Bow	4.5	200	120	2.33	2.25	0.040	0.0050	0.6	0.24
Beam	4.5	200	90	1.01	1.0	0.005	0.0030	0.4	0.14
Quartering	4.5	200	75	0.319	0.30	0	0.0038	0.14	0.10
Manual Control(1)									
Head	4.5	200	180	3.66	3.0	0.14	0.0025	1.0	0.84
Quartering	4.5	200	75	0.319	2.25	0.10	0.01	0.8	0.36

(1) $\omega_{h_x} = \omega_{HS} = 0.5$ rad/sec

Experience with the minimization of heave accelerations for a typical large subcavitating craft with a conventional control system indicated that shorter wavelength waves produced heave accelerations with magnitudes of a similar order to those experienced with longer waves representative of the peak energies of the sea state in a head sea. Thus the fact that the craft's heave displacement response was increasingly attenuated at higher frequencies did not suffice to reduce accelerations because the square of the frequency contributes to the generated acceleration.

In contrast, a comparison of the head sea cases here with $\lambda = 200$ feet (corresponding to the peak energy region of a State 3 head sea) and $\lambda = 50$ feet shows much reduced heave accelerations for the latter case as a result of spring action at the higher frequencies.

Performance, as indicated by the transient responses of Figures 10-1 and 10-2 and by the performance in regular waves as noted in Tables 10-1 and 10-2, seems to indicate that no adjustment is necessary in autopilot parameters over the normal operating speed range.

10.5 SIMULATED PERFORMANCE UNDER MANUAL CONTROL

10.5.1 USE OF FORWARD FOIL INCIDENCE CONTROL

Initially it was deemed desirable to verify the difficulty of manual control implied by the analyses of Section 6.6. With Figures 6-2 and 6-3 indicating, at best, marginally unstable performance for a small range of gains and considering the typical additional delay associated with the human operator ($e^{-0.25\,s}$) it was anticipated that stability would not be possible under manual control. Such was the case under actual runs. Following these runs it was decided to investigate stability using a simple uncompensated signal from height sensor output to incidence control in the manner of the system described in Figure 6-2 but with different foil spring constants and using height at the height sensor rather than height at the forward foil. Thus with forward foil incidence control system represented by

$$\eta'_F = \underbrace{0.1\xi_F}_{\substack{\text{mechanical} \\ \text{incidence control loop}}} + k_{\eta_F}(h'_{\xi_F} - \xi_F)$$

and $k_{\eta_F} = 0.1$ (corresponding to a gain of 14.5 on the plot of Figure 6-2) but with $K_R = 5000$ lb/ft

$K_F = 1000$ lb/ft

the system was found to be marginally stable. Although this case represents the only stable configuration found in which simple foil incidence control, rather than reaction controls, could be used, such stability was not deemed sufficient to permit useful manual or automatic control. This was further verified by taking a transient response

using this simple automatic loop. The response is reproduced in Figure 10-3. Further, manually controlled runs were made in calm water under this condition in which heave excursions ranged from broaching foils to hull impact and a peak acceleration of 18 ft/sec^2 was recorded at one point not involving hull slapping. Both these and later runs under manual control made use of a control stick of the type described in Section 8, with the stick mounted horizontally to permit the tip freedom in the vertical direction. An oscilloscope display presented a horizontal bar whose heave motion is proportional to the required feedback signal. In an attempt to increase the damping of the transient of Figure 10-3, an additional loop involving the use of pitch rate inputs to automatic aft foil incidence control was used. It was found that the basic poorly damped frequency indicated in Figure 10-3 was virtually unaffected while a substantially higher frequency response appeared superimposed on the basic response.

10.5.2 MANUAL OPERATION OF THE CRAFT USING REACTION CONTROLS

Manual control of the craft using a simple forward reaction control loop in the manner analyzed in Section 6.6 was attempted and, as anticipated, was impossible.

Because craft stability and performance had been found to be adequate using reaction forces in the manner described in Section 10.2 for automatic control of the craft, a similar configuration was used to permit manual control of the craft in another series of simulator runs. Thus the control equations of Section 10.2 generally apply except that the right side of the equation describing R'_{CF} was displayed on an oscilloscope in the manner already indicated and the control stick was connected to introduce R'_{CF} inputs to the craft. The one exception

to this is the reduction of ω_{HS} and ω_{h_x} from 1.0 to 0.5 rad/sec in all manual controlled runs.

The display proposed in Section 8 for manual longitudinal control makes use of a long persistence phosphor on the face of a cathode ray tube so that the operator may observe the instantaneous wave height and may estimate the relative vertical position of mean water level. Since the craft's dynamic response contains a considerably higher rate of divergence than originally expected, it is not possible for the operator to allow the time for several waves to pass to make an estimate of craft-sea relative displacement, particularly for those headings resulting in fairly low encounter frequencies (beam, quartering seas). For this reason the acceleration signal, represented by the term h_{16} and its associated approximate integrating networks, is very useful in providing a feedback signal more nearly representative of the true hull heave displacement than the original height sensor display and, in fact, such a signal is essential in a Sea State 3 sea to maintain longitudinal control.

A comparison of the results of manually controlled runs with the automatic system responses in Table 10-1 for comparable cases indicates generally larger accelerations in the manual control case. This is particularly true for those sea types that involve low wave encounter frequencies (ω_e) and is partly a result of the fact that those runs made under human operator control are characterized by a random constituent superimposed on the basic wave frequency. At the lower encounter frequencies, the wave-induced disturbances are within the operator's "bandwidth" and it is his task to duplicate the automatic system's job, which he does imperfectly. For those cases of high encounter frequency ($\omega_e > 3$ rad/sec), the wave disturbances are above the human operator's bandwidth and, thus, the task appears to him to approach that of control in a calm sea.

Further, the quantities listed in Tables 10-1 and 10-2 under manual control are the peak values during the run (excluding the initial transient) and are therefore somewhat larger than the general maximum levels appearing cyclically at the wave encounter frequency.

10.6 CONCLUSIONS

The presence of sprung foils has reduced, significantly, heave accelerations, particularly at high encounter frequencies under both automatic and manual control. Under manual control, wave encounter frequencies above about 3 rad/sec are sufficiently rapid that the human operator cannot respond to counteract wave-induced disturbances and the sprung foil system is the only means by which these inputs are attenuated.

On the other hand, the presence of a sprung attachment between foils and hull definitely aggravates the stability problem which, principally as the result of strut-drag induced pitching moments, is particularly critical for the high-speed FRESH craft, even with rigid struts. Thus longitudinal manual stabilization using foil incidence control, while virtually impossible for this craft equipped with rigid struts, is even further beyond a human operator's capability when foil springs are introduced. A different method of control (reaction forces applied at fore and aft springs and sub-loops as an aid to stabilization) must be introduced to permit control by a human operator. The hydraulic systems used on foil incidence controls have, however, been relieved of the wide bandwidth that would normally be required in a conventional hydrofoil autopilot system; this is reflected by the low break frequency of 15 rad/sec for ω_{η_F} and ω_{η_R} (Section 10.2). Additionally, the height sensor bandwidth is also considerably reduced (ω_{HS} = 1.0 rad/sec) compared to typical requirements for a conventional autopilot.

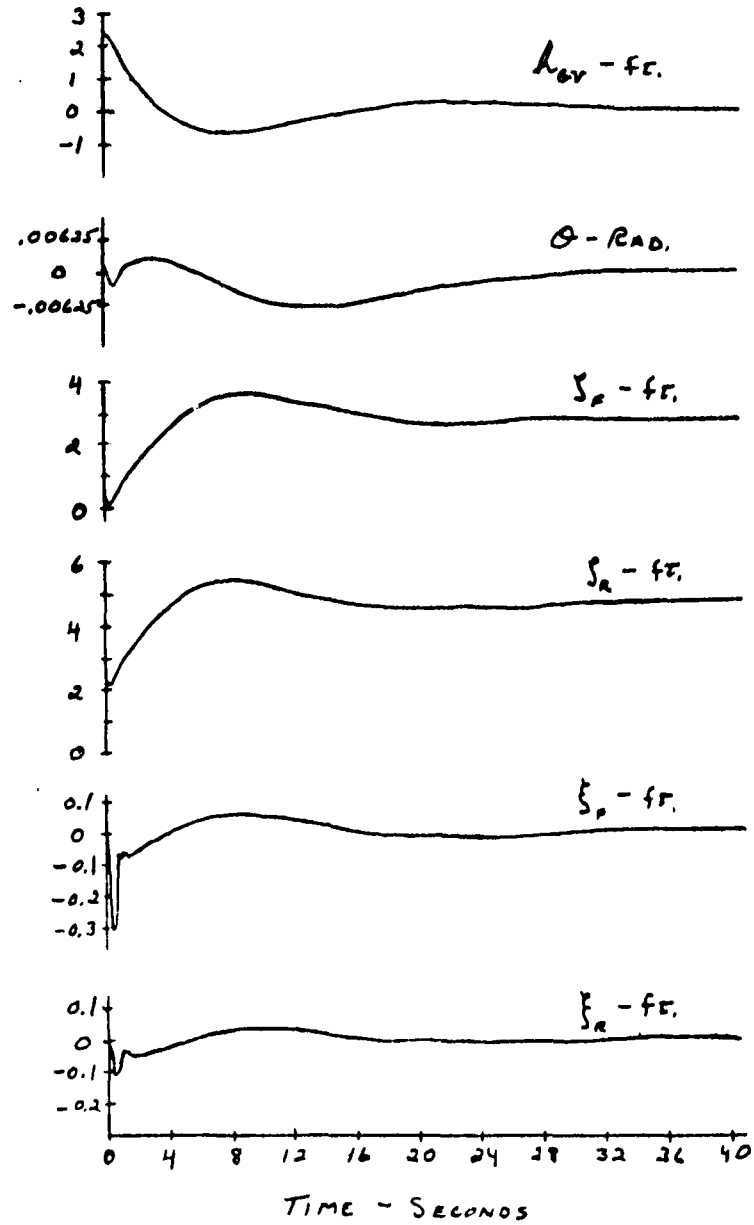

Figure 10-1. Typical Autopilot Controlled Transient Response at V_c = 80 Knots

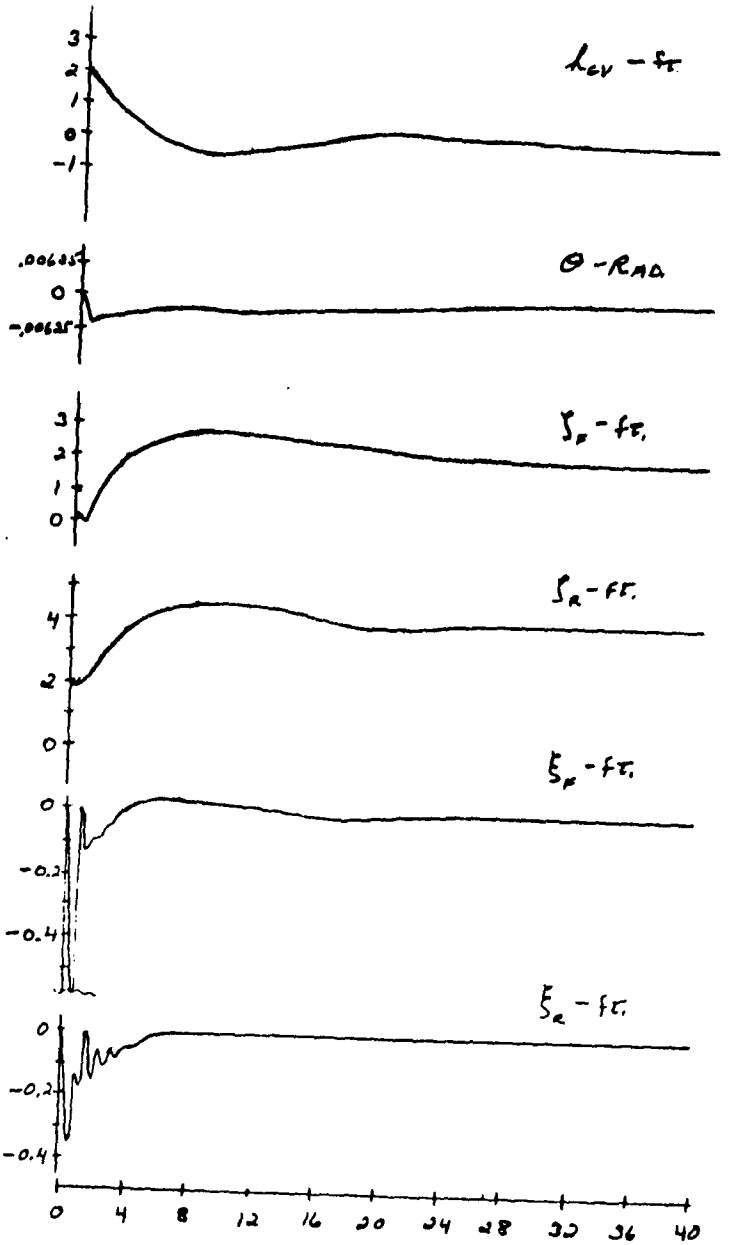

Figure 10-2. AUTOPILOT CONTROLLED TRANSIENT RESPONSE AT V_t = 50 KNOTS

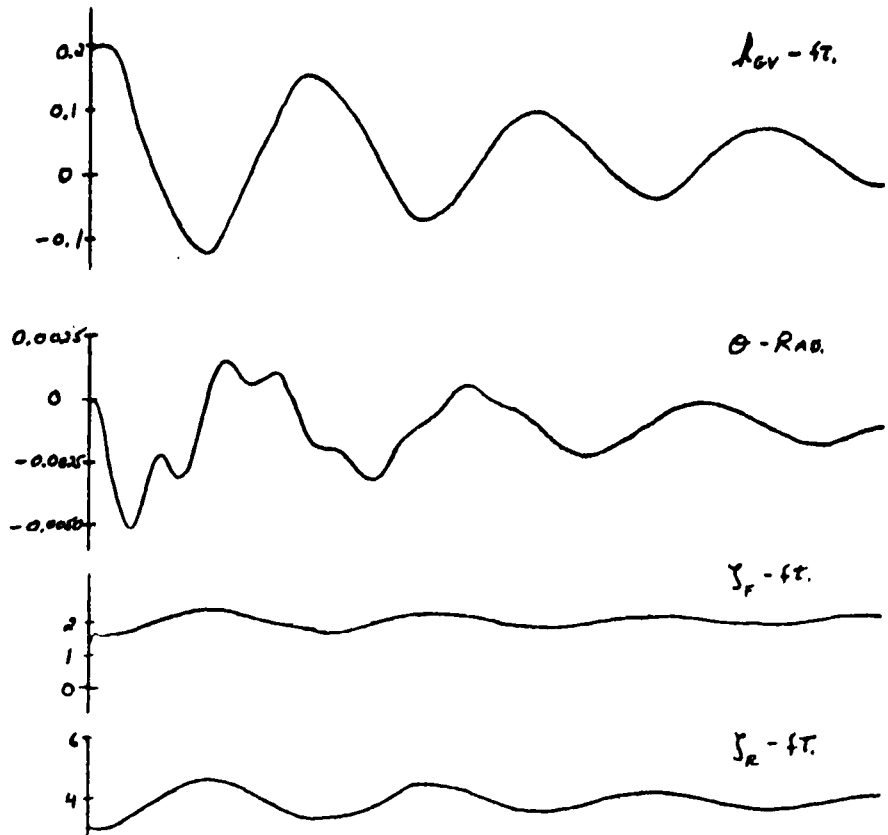

Figure 10-5. Response With Incidence Control of Forward Foil and $K_R = 5000$ #/Ft ($V_c = 80$ Knots)

SECTION 11

TECHNIQUES FOR THE LATERAL CONSTRAINT OF AFT FOILS AND THE PRODUCTION OF REACTION CONTROL FORCES

11.1 LATERAL FOIL CONSTRAINT

Because of the desirability of making use of an aileron-like hydrodynamic control for the lateral system, means of constraining adjacent (main) sprung foils to zero differential heave motion were considered. One of several possible techniques is diagrammed in Figure 11-1. The scheme presented is not necessarily a final design but does serve to demonstrate the feasibility of the idea of lateral foil constraint. The foils are in no way prevented from in-phase heave required to minimize heave accelerations in the longitudinal system.

An initial gas pressure of 1000 psi (P_G) and an oil pressure of 3000 psi (P_o) have been assumed as realistically attainable pressures for the scheme of Figure 11-1. Since the gas piston (area = A_G) must carry the total foil reaction loads of two foils, its area must be

$$A_G = \frac{2R}{P_G}$$

where

R = foil reaction

For a three-strut craft weighing 37,100 pounds, R = 12,400 pounds for evenly distributed weight.

Then

$$A_G = \frac{2(12,400)}{1000} = 24.8 \text{ in.}^2$$

and so piston diameter (d_G) becomes

$$d_G = \sqrt{\frac{4A_G}{\pi}} = 5.6 \text{ in.}$$

Now, for isentropic compression

$$P_G V_G^{\gamma} = \text{const} = C_1$$

$$2R = \frac{\pi}{4} d_G^2 \left(\frac{C_1}{V_G^{\gamma}}\right)$$

$$\frac{d(2R)}{dV_G} = \frac{\pi}{4} d_G^2 C_1 \left(\frac{-\gamma}{V^{\gamma+1}}\right)$$

and with

$$\frac{\pi}{4} d_G^2 dx = -dV_G$$

$$\frac{d(2R)}{dx} = \left(\frac{\pi d_G^2}{4}\right)^2 \frac{\gamma P_G}{V_G}$$

V_G = enclosed volume

γ = ratio of specific heat at constant pressure and volume

For a spring rate of 2000 lb ft (1000 lb/ft for a single foil displacement) and P_G = 1000 psi, d_G = 5.6 in., γ = 1.4

$$V_G = \left(\frac{\pi d_G^2}{4}\right)^2 \frac{\gamma P_G}{\frac{d(2R)}{dx}}$$

$$V_G = 5080 \text{ in.}^3 \text{ or } 2.94 \text{ ft}^3$$

where V_G includes volume above the piston in equilibrium position. With a differential piston area on the oil side of A_o and assuming P_o = 3000 psi (other side of piston vented to atmosphere)

$$A_o P_o = R = 12,400 \text{ lb}$$

$$A_o = \frac{12,400}{3000} = 4.13 \text{ in.}^2$$

Pressure drop along the interconnecting hydraulic line (Figure 11-1) must be minimized in pure heaving operation to prevent any serious differential foil loadings. The following estimate indicates the size of this line (d_r) required.

Taking an orbital motion input of $w_{(OM)}$ = 3 ft/sec as conservative ($\sqrt{\overline{w^2}_{OM}}$ = 1.26 from Figure 4-18), and a craft heave characteristic for c_η = 0 from Figure 4-15, and computing spring rate at about the peak encounter frequency for a State 3 head sea (ω_e = 6 rad/sec)

$$\dot{\xi} = \left| \frac{\xi}{w_{(OM)}} \right| w_{(OM)} \omega_e$$

$$= 0.18 (3) \omega_e = 0.54 \omega_e$$

$$\dot{\xi} = 0.54 (6) = 3.24 \text{ ft/sec}$$

and so, maximum oil flow rate (Q_{max}) is

$$Q_{max} = A_o \dot{\xi}_{max} = 4.13 (3.24) (12) = 161 \text{ in.}^3/\text{sec} \sim 42 \text{ GPM}$$

If a lift perturbation is permitted due to line pressure drop of only 1 percent of the nominal foil lift, then line pressure drop becomes

$$\Delta P_{\ell} = \frac{0.01(13000)}{4.13} = 31.5 \text{ lb/in.}^2$$

Now, using the relations of Reference 11-1, d_r may be computed as follows

$$\text{Friction factor } f = \frac{0.316}{(N_R)^{1/4}} \quad \text{for turbulent flow}$$

where

$$N_R = (\text{Reynold's number}) = \frac{4Q}{\pi d_r \gamma}$$

γ = kinematic viscosity

and

$$f = \frac{\pi^2 \Delta P_{\ell} d_r^5}{8 \rho L Q^2}$$

where L = line length; ρ = density.

Internal tube diameter may then be computed using

$\rho = 79 \times 10^{-6}$ lb-sec^2/in.^{4} at 100°F

$\gamma = 0.02$ in.^{2}/sec at 100°F

$L = 15$ ft

$Q = 161$ in.^{3}/sec

$\Delta P_{\ell} = 31.5$ lb/in.^{2}

The resulting tube diameter becomes

$$d_r = 0.86 \text{ in.}$$

which appears to be quite a reasonable size and one which might readily be made larger if other factors demand it.

11.2 DETAILS OF REACTION CONTROL TECHNIQUE

The spring mounting of foils, although it reduces hull accelerations due to high-frequency orbital motions, introduces a control problem. If conventional incidence control is applied to a foil, the spring must be compressed before a force can be transmitted to the hull. Unless the springs are very stiff, a serious lag (combined with unacceptably large foil displacements) will result. However, to effectively eliminate the hull accelerations resulting from orbital motions, low stiffness springs are required.

For example, if the foil system is represented by a mass connected to a stationary hull via a spring and a damping term (provided hydrodynamically), then

$$\frac{P(s)}{F(s)} = \frac{K}{s^2 + \frac{\beta}{m} s + \frac{K}{m}} \qquad (11\text{-}1)$$

where

- P is the force transmitted to the hull via the spring only
- F is the distrubing force applied to the foil
- m is the mass of the foil including virtual inertia
- K is the spring stiffness
- β is the hydrodynamic damping

$$\beta = \frac{\partial C_N}{\partial i} \frac{\rho}{2} uS$$

If K = 1000 lb/ft (a value found to give excellent attenuation of orbital motions), m = 20 slugs and β = 23.05 lb-sec/ft (80 knots), then the lower break frequency will occur at about 1.1 rad/sec. It is thus obvious that serious lags will occur at unacceptably low frequencies.

This difficulty may be circumvented by the use of a mechanical arrangement which permits hull forces to be developed at a rate limited only by the hydraulic system and is termed reaction control in the following discussion.

The reaction experienced by the hull, due to one foil-strut combination, depends not only on the instantaneous spring energy storage but also on the instantaneous mechanical advantage of the spring. If this mechanical advantage is available as a variable control quantity, a lag-less system (except for normal hydraulic dynamic effects) of applying control forces to the hull is available. The presence of this type of control leaves the isolation between the hull and foil, due to the spring, uneffected. Thus the isolating effect of the spring and satisfactory control characteristics have now been combined.

Since varying the reaction force between the hull and strut-foil combination displaces the latter, a self-centering loop relating foil incidence to spring deflection is also required to prevent excessive foil excursions. A mathematical description of this loop is presented in Equations 10-1 and 10-2 of Section 10. However, because substantial spring deflections would only occur at low frequency, it is not necessary for the self-centering loop to have a wide bandwidth.

Thus the feasibility of the reaction type control depends on practical mechanical implementation.

The principle of the system and its characteristics are illustrated in Figure 11-2. The arrangement shown is not considered practical, however, since, in addition to its doubtful mechanical features, a pneumatic spring's substantially non-linear properties are not acceptable with this linkage. It may reasonably be assumed that, as in aircraft, resilience associated with the elastic distortion of steel (leaf springs, torsion bars, coil springs, etc) is unacceptable from weight and space considerations. This leaves the pneumatic spring (or possibly the liquid spring) to be combined with a suitable mechanical linkage to give linear characteristics at the strut.

At frequencies of interest the compression of the gas in a pneumatic spring can be considered isentropic, and assuming that atmospheric pressure is negligibly small compared with the gas pressure, the force exerted by a pneumatic spring is

$$\frac{F}{F_o} = \left(\frac{1}{1+x}\right)^{\gamma} \qquad (11\text{-}2)$$

where

F_o is spring force at zero deflection

and

$$x = \frac{A_p}{V_o} \Delta\ell$$

where

γ is the ratio of specific heat

A_p is the piston area

V_o is the volume above the piston at zero deflection

$\Delta\ell$ is the extension of the spring from its datum position.

Equation 11-2 is plotted in Figure 11-3. It is obvious from this that to obtain even approximate linearity V_o would have to be very large.

The zero deflection stiffness is

$$\frac{dF}{d\ell} = -\gamma \frac{A_p}{V_o} F_o \qquad (11\text{-}3)$$

Now A_p depends on the mean working pressure.

Also since V_o affects both the zero deflection stiffness and the linearity, a value of V_o suitable for producing the spring stiffness desired does not result in a close approximation to a linear spring characteristic.

Further, a large V_o means a large volume of gas under high pressure, and, because of the pressure vessel required to contain it, therefore a severe weight-space penalty.

Thus, a mechanism is required which can utilize a highly non-linear spring and produce a linear reaction on the hull due to both vertical strut displacement and the application of reaction control.

Many mechanisms are possible to achieve this end, one of which is illustrated in Figure 11-4. Only the pneumatic spring, idler arm A, and reaction control jack are shown in other than line diagram form. The proportions of such a mechanism can be varied widely to suit individual requirements.

The linearizing cam on the upper surface of idler arm A is of such a form that the torque exerted by the spring roller about pivot B is a linear function of the idler arm angular movement ν; i.e.,

$$T = T_o - k\nu \qquad (11\text{-}4)$$

(Using the spring in the manner shown results in a cam surface of relatively little curvature.)

Then the reaction force P is directly proportional to the mechanical advantage represented by the factor x_1/x_j.

Thus

$$P = (T_o - k\nu) \frac{x_1}{x_o x_j} \qquad (11\text{-}5)$$

(neglecting small cosine effects).

Note that by making the jack control x_1 (locating the control jack between point D and the lower left hand pivot) and keeping x_j fixed, P can be made proportional to jack movement instead of inversely proportional to it as in Equation 11-5.

The force applied to the jack is proportional to the sine of the angle between the arm CD and the normal to the jack roller arc at the point of contact, times the compressive load in CD. The jack load is thus (for reasonable geometric proportions) a small fraction of P and is zero (apart from rolling friction) when ξ is zero.

For example, if the angle between CD and the normal is 10 degrees, P = 15,000 lb and $x_o/x_1 = 1.5$, then the force applied to the jack is 15,000 x 1.5 x 0.1736 ≈ 3900 lb.

Figure 11-4 represents only one possible mechanism and many other equally valid solutions are possible.

The above system gives a spring the stiffness of which is proportional to the mechanical advantage. In both the two-dimensional and three-dimensional simulations it was more convenient to maintain a constant

spring stiffness (K) independent of the controlled reaction (R_c). Since, under normal operation, R_c is fairly small compared with the foil lift, the variation between the model presented in this section and the mathematical model being simulated is not expected to significantly affect the results or alter the conclusions. Although it is possible to design spring systems in which the stiffness is independent of reaction this is probably undesirable in practice since it results in changes in the natural frequency of the foil-hull-suspension system with craft loading.

REFERENCES

11-1. Investigation of The Fundamental Characteristics of High Performance Hydraulic Systems, J.E. Campbell, June 1950, Published by USAF, Air Material Command, Wright-Patterson Air Force Base.

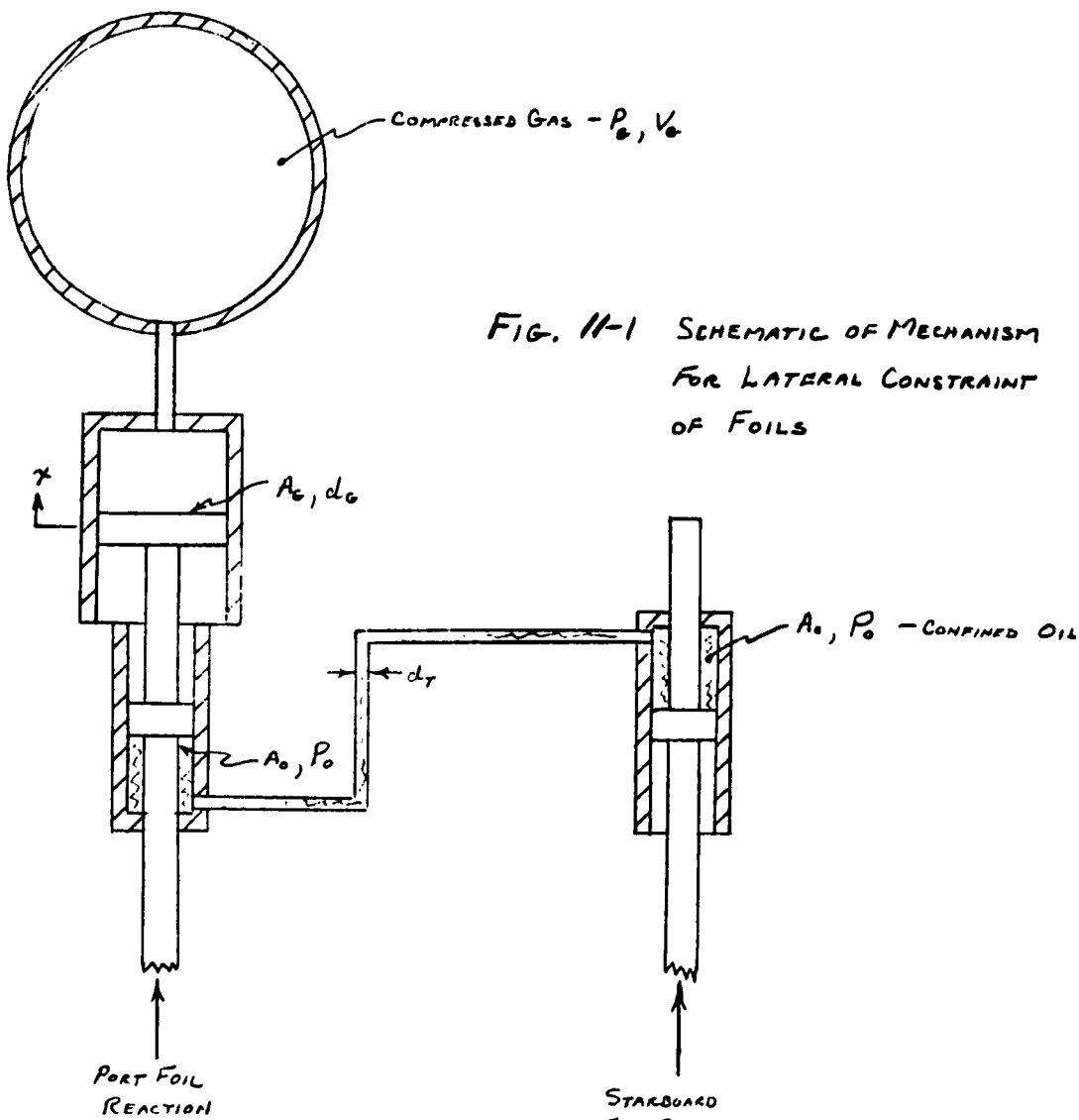

FIG. II-1 SCHEMATIC OF MECHANISM FOR LATERAL CONSTRAINT OF FOILS

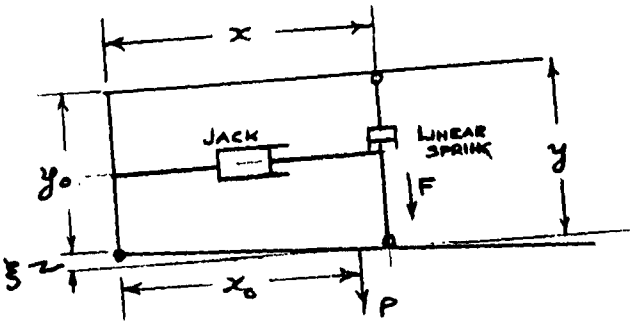

$$P = F\frac{x}{x_0} \qquad \text{WHERE} \quad F = F_0 - k(y - y_0)$$
$$= F_0 - k\frac{x}{x_0}\xi$$

REACTION CONTROL PRINCIPLE

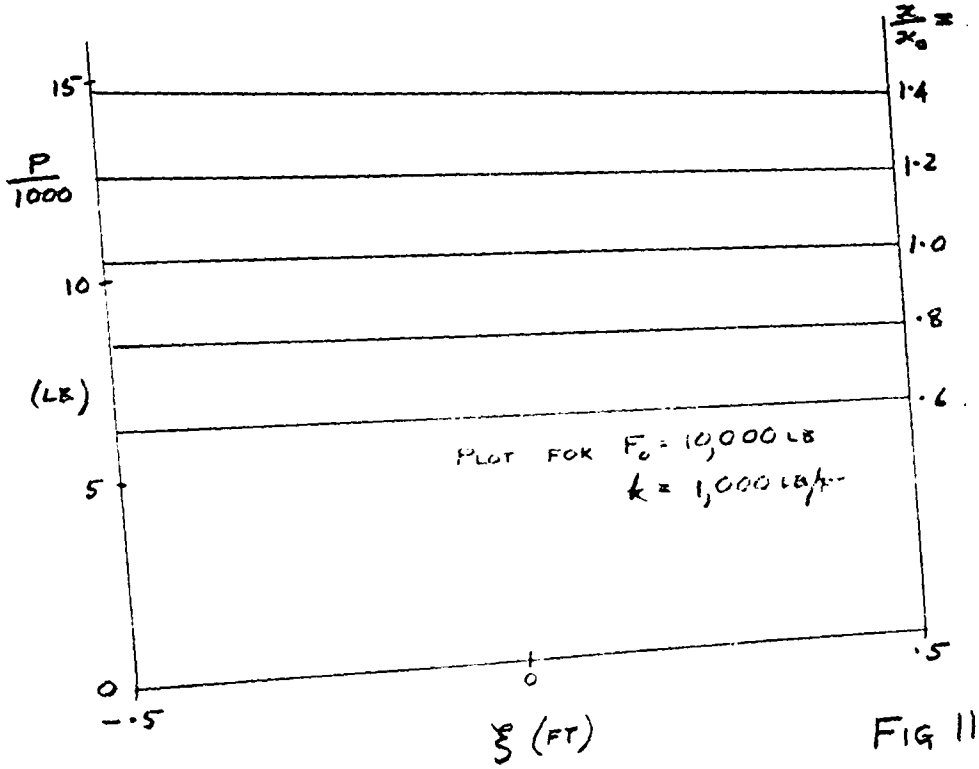

FIG 11-2

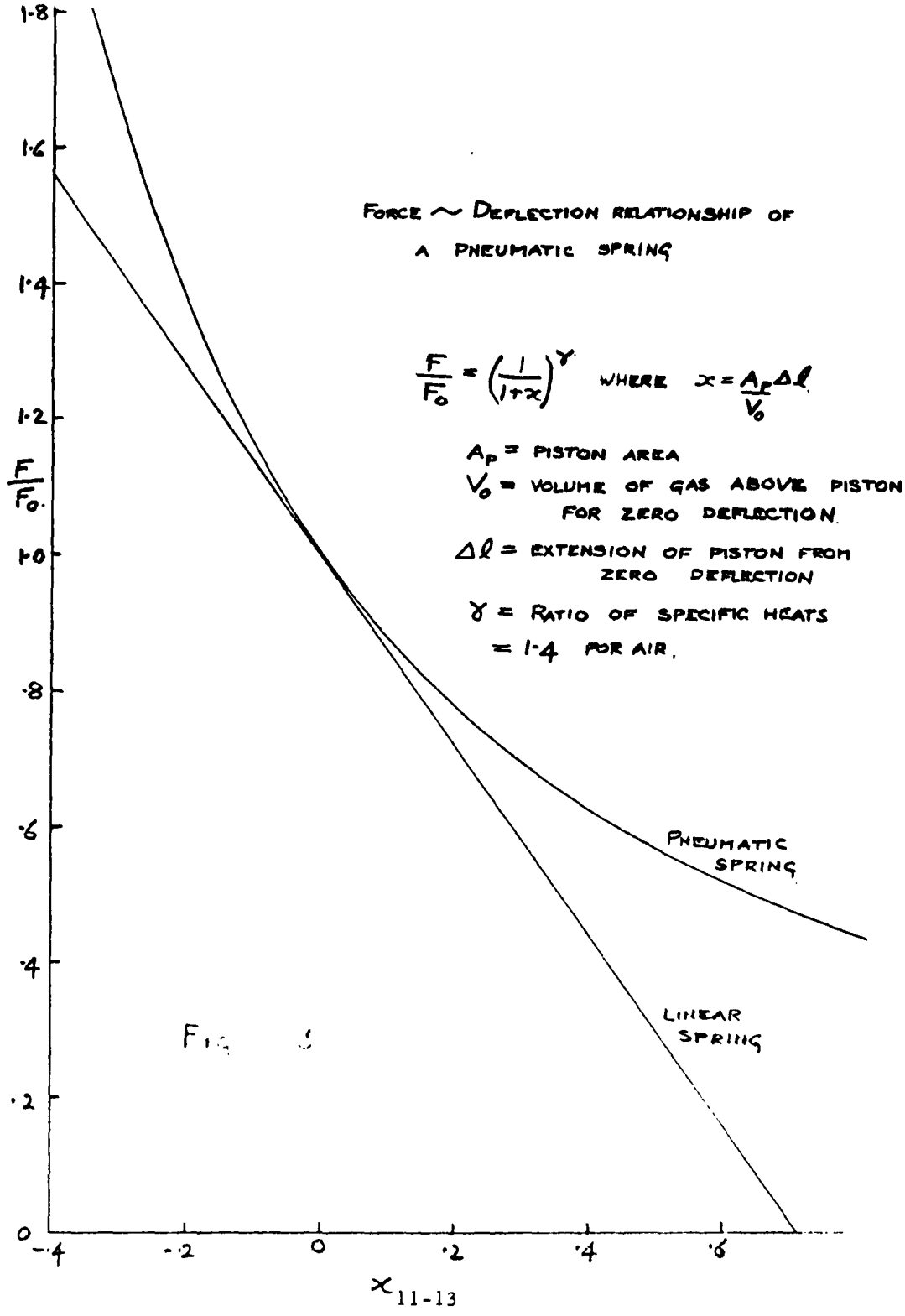
FORCE ~ DEFLECTION RELATIONSHIP OF A PNEUMATIC SPRING
$\frac{F}{F_0} = \left(\frac{1}{1+x}\right)^{\gamma}$ WHERE $x = \frac{A_p \Delta l}{V_0}$
A_p = PISTON AREA
V_0 = VOLUME OF GAS ABOVE PISTON FOR ZERO DEFLECTION.
Δl = EXTENSION OF PISTON FROM ZERO DEFLECTION
γ = RATIO OF SPECIFIC HEATS = 1·4 FOR AIR.
PNEUMATIC SPRING
LINEAR SPRING
$\frac{F}{F_0}$
1·8
1·6
1·4
1·2
1·0
·8
·6
·4
·2
0
-·4
-·2
0
·2
·4
·6
x

Fig.

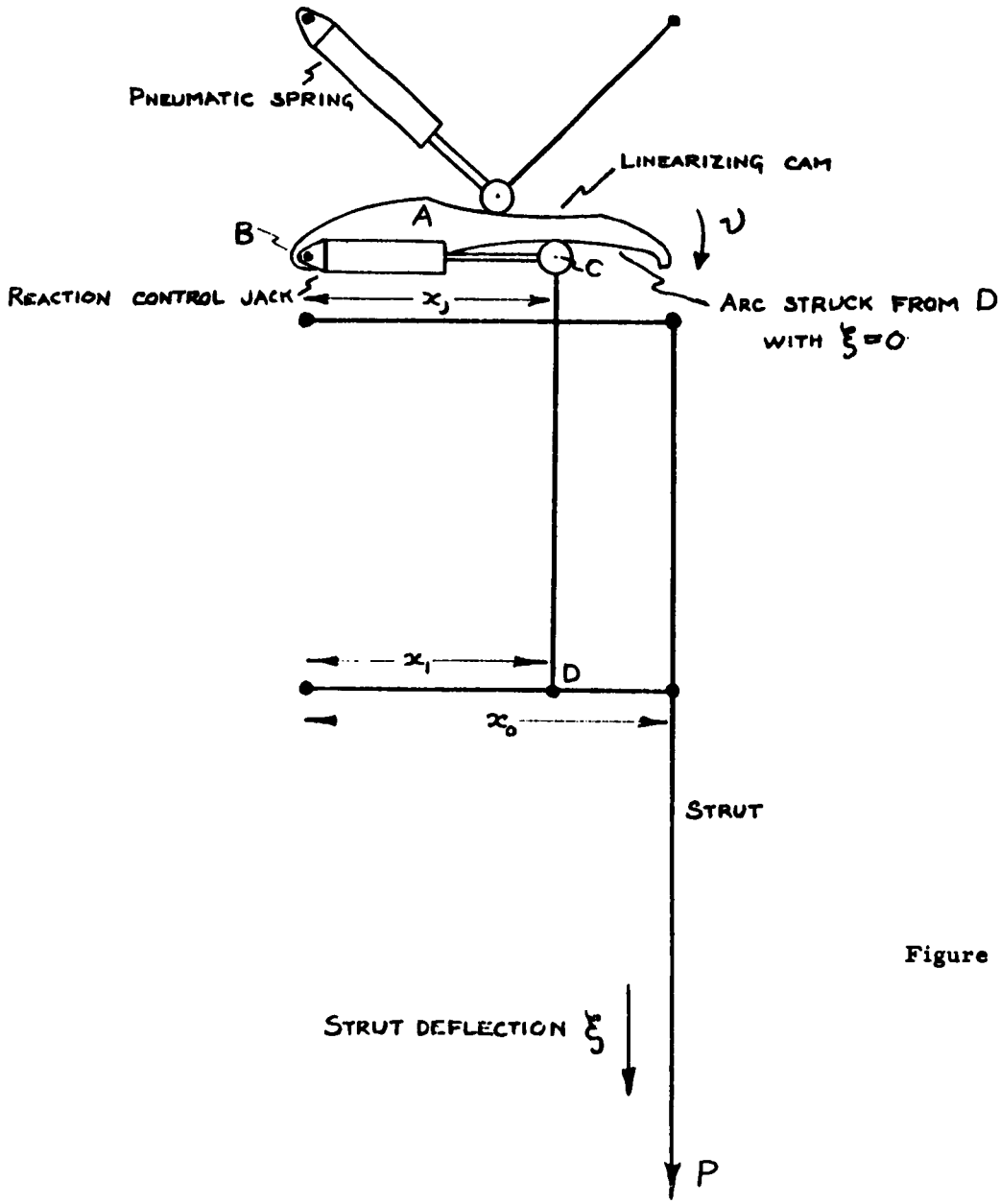
PNEUMATIC SPRING
LINEARIZING CAM
A
B
C
V
REACTION CONTROL JACK
x_j
ARC STRUCK FROM D
WITH $\xi = 0$
x_1
D
x_0
STRUT
STRUT DEFLECTION ξ
P

Figure 11-4.

SECTION 12

SIX-DEGREE-OF-FREEDOM SIMULATION OF THE SPRUNG FOIL CRAFT

12.1 INTRODUCTION

Following completion of the two-dimensional simulations of the separate lateral and longitudinal modes of the sprung-foil equipped FRESH craft, a three-dimensional (six-degree-of-freedom) simulation was undertaken to determine the extent of cross-coupling existing between longitudinal and lateral modes and the influence of the addition of a surge mode in normal operation of the craft. Representatives of the U.S. Navy, Bureau of Ships, were present for a demonstration of this simulation on 13 and 14 December 1962.

Strut and foil drag forces were computed in both the two-dimensional analysis and simulation and the three-dimensional simulation (even though craft speed perturbations were simulated only in the latter case) because the pitching moments produced by these forces, particularly strut forces, represent one of the major influences on the longitudinal dynamic behavior. Thus, in certain runs reported, the surge mode was constrained or locked out, implying that speed variations were held to zero while still permitting the normal development of drag forces on foils and struts.

Since manual as well as automatic runs were required, two operator control sticks (described in Section 8) were utilized simultaneously by two operators. (Operation was performed in exactly the same manner as described in Sections 9 and 10.)

Results are reported under three categories. First, the results of runs in calm water and irregular State 3 Seas, using fully automatic control and relative headings of ψ = 0 degree (following sea), and 45, 90, 135, and 180 degrees (head sea) are given. Second. runs in calm water and irregular State 3 Sea with the same range of headings under two-axis manual control are reported. Third special effects resulting from the inclusion of a surge mode are considered.

The generation of an irregular sea for use in the three-dimensional simulation was accomplished by using a white noise source with the output shaped to fit the Neumann spectrum for a State 3 Sea as seen by an observer aboard the craft for each relative heading. Vertical and horizontal orbital velocities were then computed from the resulting time history representing the sea surface and applied, after suitable delays, as inputs to the foils and struts. Details of the sea generation are covered in Appendix C and Reference 12-1.

Hydraulic lags have been assumed in both fore and aft foil incidence control with bandwidths taken at a moderate 20 rad/sec (ω_{η_F} and ω_{η_R}). While this value is a major influence on the lateral-aileron control loop, it is tolerable, and it is quite generous for purposes of incidence control in the spring self-centering loops of the longitudinal system.

No hydraulic lags have been assumed for the actuators (shown in Figure 11-4) to produce reaction forces, since the small size of the actuator required can be made to reflect a negligible inherent hydromechanical lag.

Because of the statistical nature of the input quantities in an irregular sea simulation, the output quantities should be measured with some kind of statistical yardstick. In most of the results reported, this yardstick has been the magnitude, including both polarities, which the signal is equal to or less than for 95 percent of the time during a run (occasionally the value for 100 percent of the time). In other words, an uppoer limit is recorded when the small scale of the recording made it difficult to obtain the 95 percent level.

12.2 DISCUSSION OF THE VARIOUS CONTROL SYSTEMS

Performances of three lateral control systems were investigated. These were:

(a) The aileron control system which used differential deflections of the two aft foils to control roll angle. This system required the aft foils to be laterally constrained.

(b) The reaction control system which used differential aft reaction forces to control roll angle. This system did not require the aft foils to be laterally constrained.

(c) The rudder control system which used rudders on the three struts to control roll angle. It was unnecessary to constrain the foils laterally for this system.

The longitudinal control system was used in the two-dimensional simulation reported in Section 10 with fore and aft reaction control techniques employed.

12.2.1 AILERON CONTROL SYSTEM

This system was basically the same as that used in the two-dimensional lateral simulation (see Section 9). However, two phenomena were neglected in the two-dimensional simulation which significantly affected the dynamics of the automatic roll control loop. They were:

(a) The dynamics of the system that produces lateral constraint of the sprung foils. (See Section 11.) In the two-dimensional simulation it was assumed that the constraint was perfect, i.e., that the hydraulic fluid used in the system was incompressible.

(b) Control foil incidence changes produced by rotating the foil-strut structures about hinge points that were appreciable distances from the foils. This rotation caused the speed of each foil relative to the water to change, and there was a consequent change in the forces acting on the foil due to this effect. Only the incidence-produced foil forces were considered in the two-dimensional lateral simulation; the incidence rate produced forces were neglected.

A linear analysis was performed to determine the effects of these phenomena on the stability of the roll control loop. (Strictly speaking, the lateral restraining system dynamics were present in the development of foil roll damping forces. However the response of the lateral restraining system was much faster than that of the craft so it was legitimate to neglect the lateral restraining system dynamics as far as damping was concerned.) A block diagram showing the dynamics relating rolling moment to differential foil incidence is shown in Figure 12-1. The lateral restraining system described in Section 11 was assumed, and the bulk modulus of the hydraulic fluid was taken as 220,000 lb/in^2.

It was found that the transfer function relating rolling moment to differential foil incidence was given by

$$\frac{K\delta_a(s)}{\eta\delta_a(s)} = \frac{\frac{1}{2}\rho u^2 S_R \left(\frac{\partial C_N}{\partial i}\right) b_S \left[1 + \frac{2 C_N \overline{\overline{RD}} S}{u\left(\frac{\partial C_N}{\partial i}\right)}\right]}{\left[\left(\frac{K_R + 2K_B m_R}{m_R + K_{IR}}\right)^{1/2} \frac{S}{}\right]^2 + \left(\frac{1}{2}\rho u S_R \frac{\partial C_N}{\partial i}\right) \cdot} \qquad (12\text{-}1)$$

$$\left(\frac{K_R + 2K_B m_R}{m_R + K_{IR}}\right)^{1/2} \left[\left(\frac{K_R + 2K_B m_R}{m_R + K_{IR}}\right)^{1/2} \frac{S}{}\right] + 1$$

which is equivalent to the following at 80 knots.

$$\frac{K_{\delta_a}(s)}{\eta_{\delta a}(s)} = \frac{1.731 \times 10^6 (1 + s/58.5)}{\left(\frac{s}{133}\right)^2 + 0.267 \frac{s}{133} + 1}$$

Using the same compensation and hydraulic servomechanism time constant, this addition to the roll control loop had the effect of increasing the bandwidth but reducing the permissible loop gain. Since the previous bandwidth was satisfactory and very little was to be gained by increasing it, the loop was modified to increase the permissible loop gain while retaining approximately the same bandwidth as before. The easiest way was to increase the time constant of the simple lag which was assumed to represent the hydraulic servo, from $\tau = 0.02$ sec to $\tau = 0.05$ sec.

Figure 12-2a is a block diagram of the aileron control system used in this simulation. The open loop gain-phase plot for this system is shown in Figure 12-3. To demonstrate the advantage of higher loop gain made possible by increasing the time constant of the hydraulic servo simple lag from 0.02 to 0.05 second, Figure 12-3 also shows the plot resulting from using the smaller value. Thus it was possible to retain approximately the same bandwidth as the system used in the two-dimensional simulation, while substantially relieving the dynamic requirements on the hydraulic servo.

The response of the system to a step input command is shown in Figure 12-4a and indicates the response is satisfactory. It should be noted that due to the compensation in the feedback loop, a step input command is equivalent to commanding a roll angle of a step multiplied by the factor $(1 - e^{-20t})$.

The simulated helmsman loop shown in Figure 9-3, Section 9, was used.

12.2.2 REACTION CONTROL SYSTEM

This control system is shown in Figure 12-2b. The system is the same as the aileron control system without the hydraulic lag and without the term relating aileron-induced rolling moment to aileron deflection. It was considered unnecessary to simulate the hydraulic servo used in this system (see Section 12.1). Apart from the lack of any simulated hydraulics, this system was similar to that used in the two-dimensional lateral simulation. However, it was not necessary to laterally constrain the aft foils, i.e., it was possible to apply control rolling moments without laterally constraining the foils. The reduction in roll damping resulting from this lack of lateral constraint of the aft foils was not significant at the reference foil

submersions, as demonstrated by the response of the system to an input step command, shown in Figure 12-4b. Again it is observed that an input step command is equivalent to commanding a roll angle of a step multiplied by the factor $(1 - e^{-20t})$.

The simulated helmsman loop shown in Figure 9-3 was used.

12.2.3 RUDDER CONTROL SYSTEM

Figure 12-5 illustrates the rudder control system. Also shown is the simulated helmsman heading control loop. This system is identical to the system used in the two-dimensional lateral simulation, (see Section 9), except that the lead term of the compensation has been included in the feedback path. This results in an input step command equivalent to a command yaw rate of a step multiplied by the factor $(1 - e^{-2t})$. This is demonstrated in Figure 12-6, which shows the response of the system to a step input.

In contrast to the two-dimensional rudder control simulation, the aft foils were not laterally constrained. However, as the response shown in Figure 12-6 was satisfactory, it was concluded that the loss in roll damping at reference foil submersions was not significant.

12.3 SIGNIFICANT EFFECTS PRODUCED BY THE SURGE MODE

Significant coupling exists between the longitudinal and surge modes. For example, the inclusion of the surge mode in the three-dimensional simulation has demonstrated certain effects which imply the necessity of automatic thrust control if extended operation at speeds between takeoff (about 50 knots) and 63 knots is required and under these conditions these cross-coupling effects can have an important influence on the stability of the longitudinal-surge mode system.

12.3.1 STATIC DRAG-SPEED CHARACTERISTICS

Because surge mode behavior is greatly influenced by the particular drag vs speed characteristics of the foil-strut combination, a drag vs speed curve has been constructed from measurements made during the three-dimensional simulation and is reproduced in Figure 12-7. This curve was obtained while holding the craft at the reference attitude (i.e., with CG height = 8.4 ft., pitch and roll angles at zero) by use of the automatic control system. The figure shows that drag decreases from take-off speed up to a speed of about 63 knots and then rises continuously to cruise speed. The exact shape of this curve is a strong function of the foil cross section and, as a result of the choice of a flat foil cross section to escape the sharp lift-slope changes that are more likely to occur within the operating regime at the point of transition from fully-wetted to fully cavitated flow with other cross sections, the drag characteristic exhibits a substantial trough.

12.3.2 THRUST-TRANSIENT RESPONSE

The negative drag speed slope implies that, for a given thrust setting, forward speed is a stable function of thrust only above 63 knots. The transient response of Figure 12-8 is a demonstration of the effect of cutting the thrust to zero with the craft under automatic control at cruise speed and returning the thrust to its original value when the speed drops to about 63 knots. In the absence of longitudinal effects (such as a change in strut submergence) the speed recovery characteristic may be expected to follow a path roughly as shown by the dashed line with the greatest slope corresponding to the 63-knot (107 ft/sec) speed where the difference between thrust and drag is maximum. However, as a result of longitudinal-surge cross coupling, the loss in

thrust and speed produces a longitudinal transient which results in a greater submersion of the aft foils and therefore increased drag at about the time the thrust is restored. Thus, speed recovery is much slower initially and appears as shown in the solid curve.

Surge mode stability was not possible below 107 ft/sec (63 knots) and it was necessary to introduce a simple automatic thrust control loop when attempting to hold speed below this level. Figure 12-9 presents the typical surge mode transient responses for three different surge-mode, longitudinal-mode control sets. (ΔT is, in this figure, used to denote a thrust increment.) Curve 'a' shows the surge response possible when using a simple error-proportional thrust control with the first set of aft system control gains and a 2-second lag representing engine-thrust lag. When a revised set of aft system gains was introduced, the same surge controller produced the response shown in 'b' which, as may be seen, is on the verge of instability. Alteration of the surge controller to double the low frequency gain once again produced an acceptable surge response as seen in curve 'c'.

12.3.3 INFLUENCE OF THE SURGE MODE ON THE LONGITUDINAL SYSTEM

A comparison of the longitudinal transient response to a step change in demanded forward height for the case with and without the surge mode influence is shown in Figure 12-10. This response was taken using aft system gains as recorded in Figure 12-9a.

Because there are several different ways in which to constrain the surge mode, it must be clearly understood what is meant in this case. This test was accomplished by permitting the normal strut drag induced pitching moments to act on the craft but preventing the drag changes from influencing craft speed. This is equivalent to

exerting an external force at the CG with perturbations equal and opposite to those resulting from drag. In this way, speed change effects are eliminated but the very important (to longitudinal behavior) pitching moment changes with depth of submersion are retained. The resulting curves of Figure 12-10 indicate no large effects resulting from the exclusion of the surge mode on transient behavior.

Thus, where the craft's drag characteristics provide inherent surge stability, responses of the longitudinal controlled craft are relatively unaffected by the presence of the surge mode. In the case of an inherently unstable surge mode, stabilization with a thrust control loop once again results in a controlled longitudinal transient that is only slightly affected by surge mode speed variations.

12.4 AUTOMATIC LATERAL CONTROL IN CALM WATER AND STATE 3 SEAS

Table 12-1 shows that the aileron control system as described in Section 9 was capable of maintaining stability under all the conditions that were simulated using a sufficiently high aileron rate limit. However, it was necessary to use aileron rate limits of ± 2 rad/sec and it was also necessary to reduce the loop gain in a head sea at 100 knots in order to avoid periods of high frequency oscillation. The system behaved well in the other seas at 100 knots with the design value of loop gain. It will be noted from an inspection of the transfer function relating aileron induced rolling moment to aileron deflection (see Equation 12-1) that the amount of phase lead introduced by the transfer function decreases as the speed increases. The time constant of the lead term is inversely proportional to u^3 (since C_n varies as $\frac{1}{u^2}$ for constant lift) while the damping of the quadratic term is proportional to u. This effect will contribute toward a reduction in gain margin at 100 knots. However, the reason for the

existence of the periods of high frequency oscillation in the head sea only is not clearly understood. All the analyses were conducted assuming constant craft dynamics, while, in fact, the craft dynamics continuously change as the strut submergences change. This variation of dynamics can be expected to be of significance when the frequency of the variation approaches that of the bandwidth of the loop. The frequency of strut submergence variation in a head sea, while still reasonably small relative to the bandwidth of the loop, is higher than in any other sea, so it is possible that this phenomenon is responsible for the periods of high frequency oscillation found in a head sea at 100 knots.

Table 12-1 also shows that the aileron control system and the reaction control configuration kept the roll angles in all seas to very small values, but the lateral accelerations were large in many cases. For example, in a bow sea at 80 knots, in two runs (runs 132 and 194 in Table 12-1) the lateral acceleration exceeded 10.9 ft/sec^2 5 percent of the time.

The rudder control system that was used was not capable of maintaining stability in all seas that were simulated. In all runs which ended in control being lost, the instability was due to a condition of very small front foil submergence persisting for a reasonable length of time. However, the rudder control system used was not proposed as an alternative to the aileron control system, but was a very simple system that demonstrated the reduction in lateral accelerations resulting from using rudders to control the craft. Table 12-1 shc vs, for example, that at 100 knots in a bow sea, using the rudder control system resulted in a lateral acceleration of 3.0 ft/sec^2 being exceeded 5 percent of the time. Using the aileron control system in the same sea and speed resulted in a lateral acceleration of 10.0 ft/sec^2 being

exceeded 5 percent of the time. A more sophisticated rudder control system could be designed to overcome the stability problems encountered with the simple system used, also reducing the lateral accelerations still further.

Alternatively, this problem may be eliminated by providing a short length of rudder below the forward foil but this solution is less desirable.

The results obtained with the reaction control system were very similar to those with the aileron control system. The aft foil lateral restraining system was not used, which had the effect of reducing roll damping that was otherwise provided by the aft foils but at the same time reducing the disturbing rolling moments caused by orbital motion induced differential lifts on the aft foils. The transient response tests showed that the reduction in roll damping was not significant, so it is concluded that the reduction in the disturbing rolling moment was likewise not significant.

12.5 AUTOMATIC LONGITUDINAL CONTROL IN CALM WATER AND STATE 3 SEAS

The response of the longitudinal system under automatic control in State 3 Seas of various headings is represented in Table 12-1 by recorded values of heave acceleration and surge acceleration. In general, the longitudinal control system parameters are those presented in Section 10.2 with exceptions as noted. Not all runs recorded have complete data since some are presented to show special effects connected with either longitudinal or lateral control problems.

Effects worthy of special mention are covered in the following paragraphs.

The sea state 3 spectra, transformed to wave encounter frequency for the various headings is discussed in Appendix C. It should be noted that the spectra generated for the 80-knot craft speed were used as an approximation for those tests recorded with craft speed of 100 knots. The true spectra for the higher speed would show a shift to a somewhat higher frequency.

12.5.1 TRANSIENT RESPONSE TO CG HEIGHT ERROR

The response to an initial height error of about 2 ft is reproduced in Figure 12-10. A comparison of transients with and without surge mode included shows a very similar response whether with or without surge mode influence.

12.5.2 TRANSIENT RESPONSE TO A SUDDENLY APPLIED PITCHING MOMENT

During the course of the simulation, it became apparent that the aft longitudinal system transient response could be substantially improved without incurring a significant increase in heave acceleration. The improvement achieved in response may be seen by referring to Figure 12-11 in which a pitch angle transient resulting from a sudden application of external pitching moment is shown. The three control gains indicated are inputs to the aft reaction control and the lower set produces an obviously better transient response than the original (upper) set. There then remains the demonstration of the effect that this change had on heave acceleration. One comparison that is possible is between two bow sea cases represented by runs 101 and 135 of Table 12-1. These are identical in the longitudinal system parameters except for the two gain sets indicated in Figure 12-11.

The results of this comparison may be anticipated by considering the source of inputs to the aft longitudinal system. The first is heave of the hull at the forward foil which produces pitch angle changes. These, in turn, result in aft heave reaction control forces and motions needed to hold these changes to a minimum. The second is wave-induced orbital velocities which act on the foils and, through the spring system, contribute accelerating forces on the hull. If, in a given sea, a significant contribution to aft hull acceleration (which is itself the major influence on CG acceleration) is from the pitch system generated aft reaction forces, then a substantial change in pitch gain parameters ($K_{1\theta}$, $K_{2\theta}$, $K_{3\theta}$) will result in a significant change in heave acceleration. This is demonstrated in a comparison of runs 101 and 135.

On the other hand, a comparison of two beam sea cases (runs 57 and 198) shows no change in CG acceleration since, for this sea condition, there are no significant pitching moment disturbances on the craft. (wave disturbances arrive at both fore and aft foils at about the same time.)

Because of the improved pitch transient response represented by the longitudinal control system parameters of Set 2, these values are used for all simulator runs following run 117.

12.5.3 TRADEOFF BETWEEN SPRING STIFFNESS AND HYDRAULIC SYSTEM RESPONSE

Notwithstanding the presence of springs to cushion the hull against wave-induced hydrodynamic foil forces, a foil incidence control loop is necessary to provide variation in foil lift with craft weight and to reduce foil lift variations at low frequencies to prevent excessive spring deflections. Clearly, then, a tradeoff exists between spring deflections and gain in the mechanical self-centering loops. (Higher

gain implies greater bandwidth and so greater hydraulic power requirements.) The nature of this tradeoff may be seen from a comparison of runs 101 and 103. In the latter runs, the centering loop gains have been reduced from $k_{1F} = k_{1R} = 0.15\ ft^{-1}$ to $0.02\ ft^{-1}$. This reduction in gain has brought with it an increased CG acceleration, as recorded, from $1.5\ ft/sec^2$ to $1.8\ ft/sec^2$ and has placed the burden of minimizing CG acceleration on the springs. Aft spring deflections for these two runs have gone from 0.12 ft to 0.60 ft, (each quantity derived from the usual 95% criterion.)

A comparison of relative hydraulic bandwidths may be made from Figure 12-12 in which the open loop gain-phase plot for the self-centering loop is shown with the closed loop frequency responses for $k_{1F,\ R} = 0.15$ and $0.02\ ft^{-1}$ shown on the same figure. Figure 12-13 defines the loop dynamics that are represented in the plots of Figure 12-12.

With the increase in spring deflections (about equal to 0.5 ft) resulting from the change of k_1 to $0.02\ ft^{-1}$ has also come a substantial phase lag between spring deflection and foil incidence within the sea spectrum (5 rad/sec) as implied by the drooping closed loop amplitude characteristics of Figure 12-12.

Although the bandwidth of this loop was markedly reduced by lowering the gain "k", there is no doubt that the same bandwidth with a much flatter amplitude and phase characteristic up to the cutoff point could be obtained by a different selection of the hydraulic lag, "ω_η". The gains $k_{1F,\ R}$ alone were used to control the centering loop bandwidths only because it was convenient during the simulation.

Acceleration of the CG is not proportionately increased with spring deflection because, as pointed out in the preceding sections, the

pitch angle controlled aft system is also an important contributor to CG acceleration and its control system parameters remained unchanged between runs 101 and 103.

12.6 COMPARISON OF SPRUNG FOIL WITH RIGID STRUT CASES

The discussion of the manual operation of the FRESH craft includes comments on the controllability of the craft with rigid aft struts with no aft foil incidence control and with a normally sprung forward foil. Since CG acceleration is largely controlled by acceleration at the aft foil location, it is interesting to compare some automatic controls runs with rigid aft struts and normal aft foil springs. This comparison may be made for a head and following sea at 80 knots and for a quartering sea at 50 knots (run pairs from Table 12-1 are Nos. 162 and 163(a), 151 and 139, and 176 and 179 respectively). Surge acceleration is not a function of whether foils are sprung since it depends primarily on the extent of alternate immersion of each strut as wave encounters occur (strictly speaking, spring extension causes alternating effective strut lengths affecting immersion drag but this effect is lost in the measurement uncertainty). Heave acceleration, however, is, for both head and following seas at 80 knots, strongly affected, being approximately doubled when rigid struts replace aft foil springs. For the quartering sea case, heave acceleration appears essentially the same for both co configurations, a result which seems surprising at first. The important parameter in this effect appears to be the vastly different sea spectra of the quartering sea (50 knots) case with peak energy at only 0.5 rad/sec compared with the head and following sea cases (80 knots) with peak energies at 4 rad/sec and 2.5 rad/sec respectively. (See Appendix C for complete spectra description.)

12.6.1 REVISED VALUES FOR ω_{h_x} AND ω_{HS}

Although earlier two-dimensional automatic control simulator runs used values of 1.0 rad/sec generally for these two variables, in order to maintain a common value for both automatic and manual control, and because lower heave accelerations are achieved, the same values as those used in the manual control runs (0.5 rad/sec) were used in most of the three-dimensional simulator runs. This latter effect may be compared in runs 57 and 71. It is true that the accuracy requirements of the accelerometer are affected by the choice of these cutoff frequencies. This aspect is considered in detail in Section 13.

12.7 MANUAL CONTROL IN CALM WATER AND STATE 3 SEAS

12.7.1 LATERAL DISPLAY AND CONTROL ELEMENTS

Manual control of the craft in the three-dimensional simulation was accomplished, laterally, by giving the operator direct control of the ailerons via the lateral control stick. No attempt was made to manually control the craft with rudders in a way analogous to that which was described for automatic control since the analysis of Section 7 indicated that manual control via the rudders is not likely to be as easy as with aileron control. The lateral display consisted, as in the two-dimensional simulation, of an artificial horizon rotating as a function of roll angle and roll rate. The particular relationship used was

$$\phi_{display} = 2\ (\phi + 0.75\dot{\phi}\ )$$

where

$\phi_{display}$ = angle that the bar display makes with a horizontal reference

12.7.2 LONGITUDINAL DISPLAY AND CONTROL ELEMENTS

A control stick, of the type recommended in Section 8 and identical to that used in the two-dimensional simulation of Section 10, was utilized for manual control of the forward controlled reaction force (R_c). Analyses of Section 6 indicated that neither automatic nor manual stabilization for the manual mode could be accomplished with a single loop feedback quantity. This was borne out by preliminary runs, in which forward reaction control was attempted with forward height and acceleration combined in the display but with no control loops around the aft reaction control. For most of the runs, then, the manual configuration resembled the automatic except that forward reaction was controlled directly and the height and acceleration signals formerly used for commanding forward reactions were now used to displace, vertically, a horizontal bar on a CRT.

The lead effect produced by the lift increment proportional to $\dot{\eta}$ (see Figure 12-13) that was of some significance in automatic longitudinal control is effective at a frequency too high to be of significance in assisting manual control. No operator felt that longitudinal control was essentially different for the three-dimensional simulation than for the comparable case for the previous two-dimensional simulation.

Some later runs were made in which manual control without an aft stabilization system was possible for a craft configuration using rigid aft struts. This case is considered in detail in this report.

12.7.3 TESTS FOR CROSS-COUPLING EFFECTS

Early runs were undertaken to demonstrate what, if any, cross-coupling effects might be present. As implied by experience with the automatic mode, calm water runs with both operators showed no such effect for normal deviations in either axis.

Indeed, even when a pulse disturbance of anything less than 10 to 15 degrees in roll angle was introduced intentionally by the lateral operator in a calm sea, there was no obvious effect on the behavior of the longitudinal system. Further, neither operator could detect a difference if the manual system of the other were replaced by the automatic system.

Results of calm sea runs are shown in Table 12-2 for manual control of both axes and, it is seen that, although there are no wave input disturbances, a certain minimum level of acceleration in all three axes is produced during the control by a human operator. In the absence of wave inputs, a surge acceleration is present as a result of changing drag produced by changing strut immersion (the low frequency characteristics of the surge acceleration records imply the cause is heave perturbations caused by longitudinal system control).

Cross-coupling effects between lateral and longitudinal systems were, however, much in evidence in many runs involving a State 3 Sea since large roll angles or very shallow foil-strut depths were generated on occasion. Just prior to a "splash" condition (the loss of manual control during a given run), each operator was usually aware of the presence of the other operator through the large disturbances on his system.

12.7.4 LONGITUDINAL CONTROL WITH RIGID AFT STRUTS

The time histories in Figure 12-14 have been included to demonstrate the effect of removing the aft pitch angle control loop during a manual longitudinal control run with sprung foils. In all cases of this type, the operator (who had as a display only forward height and heave acceleration) is quite unaware that the pitching motion and heave at the CG are increasing in a divergent way. His first indication of trouble is a fairly sudden displacement of the display off the scope

face but this does not occur until other parts of the problem have diverged well beyond the capability of the system to recover. Thus, it appears that the craft immediately begins this longitudinal divergence by pivoting about the forward (controlled) end and continues diverging (in an oscillatory manner) until splash.

Because of the desirability of simplifying the longitudinal configuration in manual control, some runs were made with rigid aft struts and without an aft control system.

The nature of the response of the longitudinal system when aft pitch angle control is removed suggests that the damping in pitch is insufficient. The aft sprung foils and the aft self-centering loop both act to prevent forces on the after hull during heave at that point. The presence of the pitch angle control loop provides the needed damping under the normal configuration. It was inferred that, in the absence of automatic control around both fore and aft foils, the greatest amount of pitch damping would be provided by the aft foils if they were rigidly attached to the hull. Runs in calm water under manual control have confirmed that stability is possible (see Table 12-2) under this arrangement and operator opinion for this condition indicates that, although heave damping is somewhat less than that obtained with a pitch control system, it is nevertheless sufficient to permit safe operation in calm water.

A comparison of operation with the normal manual control configuration and control with rigid aft struts is possible (see Table 12-2) for bow, quartering, and following seas and shows significantly greater CG accelerations in the 50-knot bow and 80-knot following seas where the maximum wave energy falls at a relatively high frequency (2.4 and 2.7 rad/sec respectively) and the same acceleration for the much lower encounter frequency (0.5 rad/sec) associated with the 50-knot quartering sea.

12.7.5 TEST RUNS USING TYPE OF HEIGHT DISPLAY DESCRIBED IN SECTION 8

In addition to the runs with rigid aft struts recorded in Table 12-2, some runs were made with rigid aft struts but with only forward height signal displayed (no acceleration signal or modifying filters) in both calm water and various sea-state relative headings. Performance in calm water was much like the equivalent run (174) recorded in Table 12-2 and operator opinion was also much the same (control difficulty is very similar to the comparable calm sea runs with an aft control system).

However, every attempt at control in a State 3 Sea using a height signal alone produced a splash shortly after the start of the run.

This latter result was anticipated and is a consequence of the rapid divergence rate of the longitudinal system. The simple height display (described in Section 8) for manual control of the longitudinal system was devised under the assumption that the longitudinal divergence rate would be much slower than typical wave encounter periods. It would have been possible, under such conditions, to use the envelope of displayed wave height to control the craft. However, with divergence rates comparable to wave encounter periods, wave envelope information is too slow for stable craft operation. Integrated hull heave acceleration (added to the height display) is then a necessary ingredient for longitudinal manual control in a State 3 Sea.

12.8 A COMPARISON OF MANUAL AND AUTOMATIC LATERAL CONTROL

It is interesting to compare roll angles and lateral accelerations for automatic aileron and manual control runs in similar seas and at similar speeds, for those cases in which manual control did not end in stability being lost. In each case, the automatically controlled roll

angles were smaller by a factor of the order of 100. However, apart from the following and head sea runs, the lateral accelerations were, generally speaking, quite similar. In fact, in bow seas at both 80 and 50 knots, manual control resulted in smaller lateral accelerations.

This behavior may be explained in a comparison of effective roll control for the two headings. Encounter frequencies in a beam sea are well within the bandwidth of the human operator to counter the induced rolling moments on the craft and maintain roll angles smaller than the open loop craft response at wave encounter frequencies would show (although certainly not as small as the automatic system achieved). On the other hand, bow sea encounter frequencies, while remaining well within automatic system capability to prevent rolling, are outside of a human operator's ability to control anything but the long-term average roll angle and so roll angle peaks assume values very like those of a craft uncontrolled at wave encounter frequencies. Such rolling action tends to reduce the wave-induced angles-of-incidence on the struts causing it and hence tends to reduce lateral strut-developed forces causing acceleration.

The acceleration experienced by a person on the craft, or measured by an accelerometer, would not be the total lateral acceleration, but would be the total acceleration minus the gravity component. This resultant acceleration is called the normalized side force. As the roll angles were very small when automatic control was used, the normalized side forces would be practically identical to the lateral accelerations. However, since large roll angles resulted when manual control was used, the normalized side forces could be appreciably different from the lateral accelerations. The difference between the two depends on the degree of correlation between the roll angle and lateral acceleration. A detailed investigation of the degree of correlation between the two quantities has not been undertaken, but an approximate analysis of one run indicated that the statistical properties

of the normalized side force were approximately the same as those of the lateral acceleration. Thus, it appears that, as far as normalized side force is concerned, nothing is gained by having a very tight roll loop. In fact, there are indications from the comparison of manual and automatic runs that reducing the loop gain and bandwidth of the roll control system may result in smaller normalized side forces in some seas.

12.9 CONCLUSIONS ON MANUAL CONTROL

The high-speed test craft equipped with sprung foils can be controlled manually in calm or nearly calm water by controlling the lateral system through a roll-angle roll-rate display and an aileron input and, in the longitudinal system, by simple height sensor feedback of forward height with control of forward reaction forces (an all-mechanical self-centering loop forward and locked (rigid) aft struts being required for such control).

For Sea State 3, longitudinal control is possible only when a forward accelerometer signal is added to the forward height display and it is then quite difficult. The task of longitudinal control can be made somewhat easier if the aft reaction control loop using pitch angle-rate feedback is included to provide pitch damping with the normal sprung aft foils. Heave accelerations in the latter case are much smaller, in general, than when rigid struts are employed.

However, manual control in State 3 Sea for either the lateral of longitudinal systems is not recommended since the difficulty of the task is such that there is an unacceptably high probability of control being lost during a run of a few minutes.

REFERENCES

12-1 Appendixes to the Engineering Summary Report on a Hydrofoil Autopilot System Design Study Program. Jan. 1962 RCA, NObs-84498

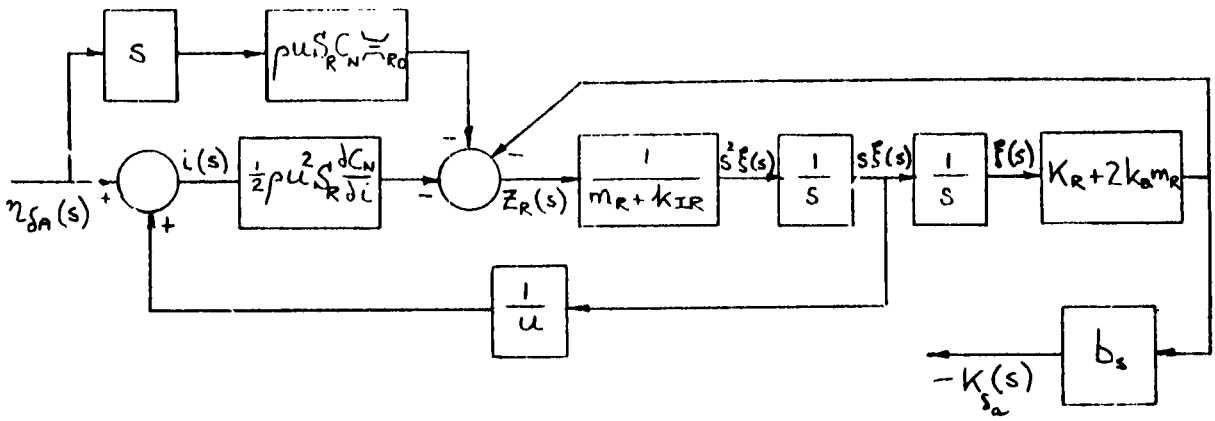

$\eta_{\delta A}$	DIFFERENTIAL FOIL ROTATION
K_{δ_a}	ROLLING MOMENT PRODUCED B AILERONS
s	LAPLACE OPERATOR
S_R	AREA OF ONE REAR FOIL (6.784 ft^2)
ρ	DENSITY OF WATER (2 slugs)
C_N	NORMAL FORCE COEFFICIENT (0.1)
u	VELOCITY OF CRAFT ALONG X-AXIS (80 knots)
i	INCIDENCE
Z_R	FORCE ON FOIL ALONG Z-AXIS
m_R	MASS OF FOIL AND STRUT (14.83 slugs)
k_{IR}	MASS OF ENTRAINED WATER (10.99 slugs)
ξ	SPRING DEFLECTION
K_R	SPRING STIFFNESS (1000 lb/ft)
$k_B m_R$	STIFFNESS OF LATERAL RESTRAINING SYSTEM (4.556×10^5 lb/ft)
$\bar{x}_{RO}$	REFERENCE DISTANCE FROM HINGE TO REAR FOIL (11.5 ft)
b_s	DISTANCE BETWEEN REAR STRUTS (14 ft)
$\frac{\partial C_N}{\partial i}$	NORMAL FORCE CURVE SLOPE ($1.0\ rad^{-1}$)

FIG 12-1 BLOCK DIAGRAM SHOWING RELATIONSHIP BETWEEN ROLLING MOMENT AND DIFFERENTIAL FOIL ROTATION

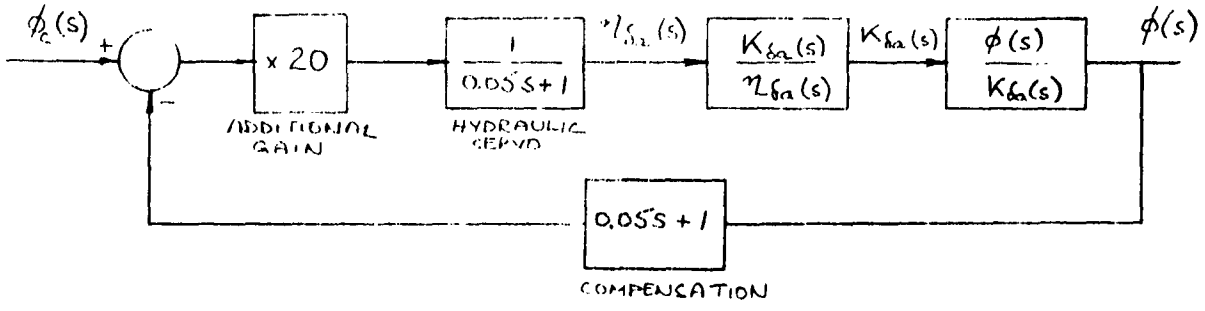

FIG 12-2(a) BLOCK DIAGRAM OF AILERON CONTROL SYSTEM

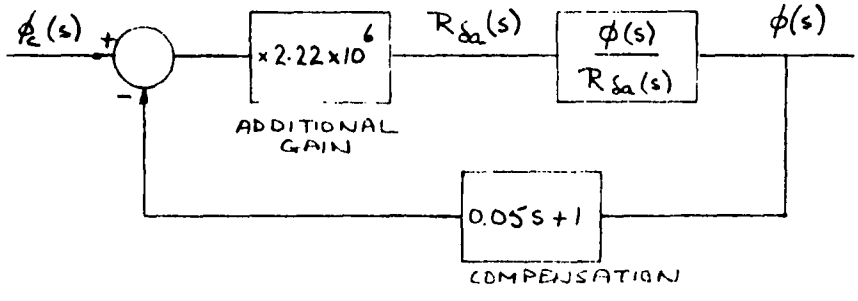

FIG. 12-2(b) BLOCK DIAGRAM OF REACTION CONTROL SYSTEM

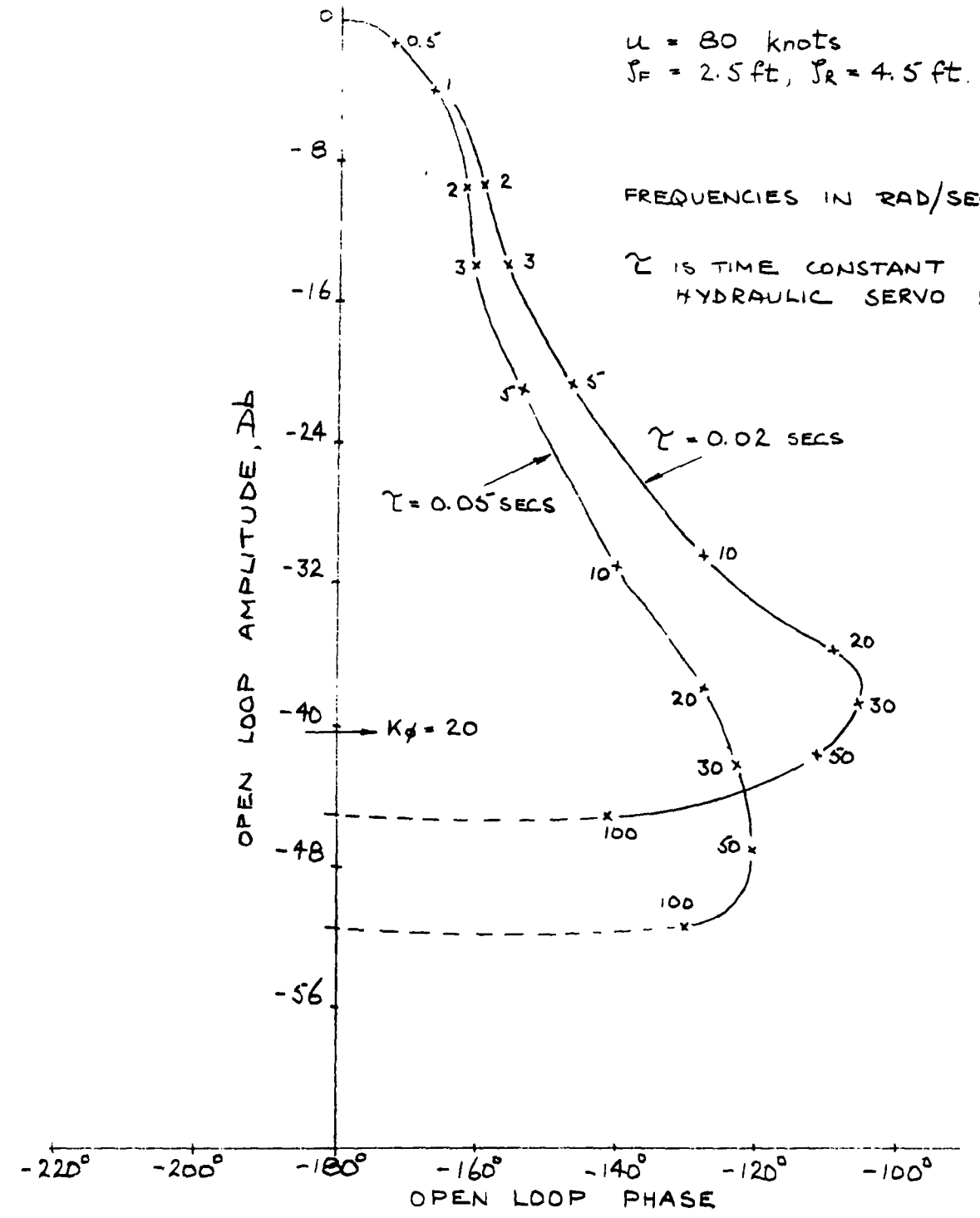

FIG 12-3 OPEN LOOP GAIN-PHASE PLOT FOR ROLL CONTROL LOOP

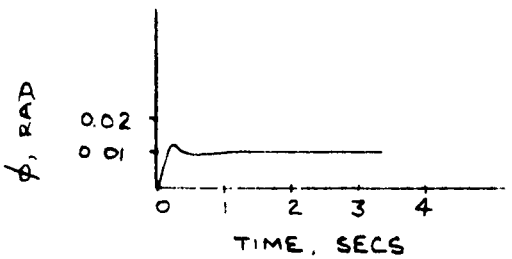

u = 80 KNOTS
ℓ_F = 2.5 ft., ℓ_R = 4.5 ft.

FIG 12-4(a) RESPONSE OF AILERON CONTROL SYSTEM TO A STEP COMMAND

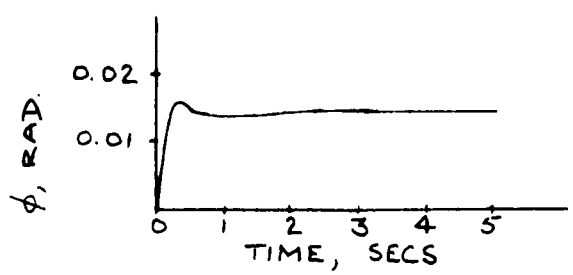

u = 80 KNOTS
ℓ_F = 2.5 ft., ℓ_R = 4.5 ft.

FIG 12-4(b) RESPONSE OF REACTION CONTROL SYSTEM TO A STEP COMMAND

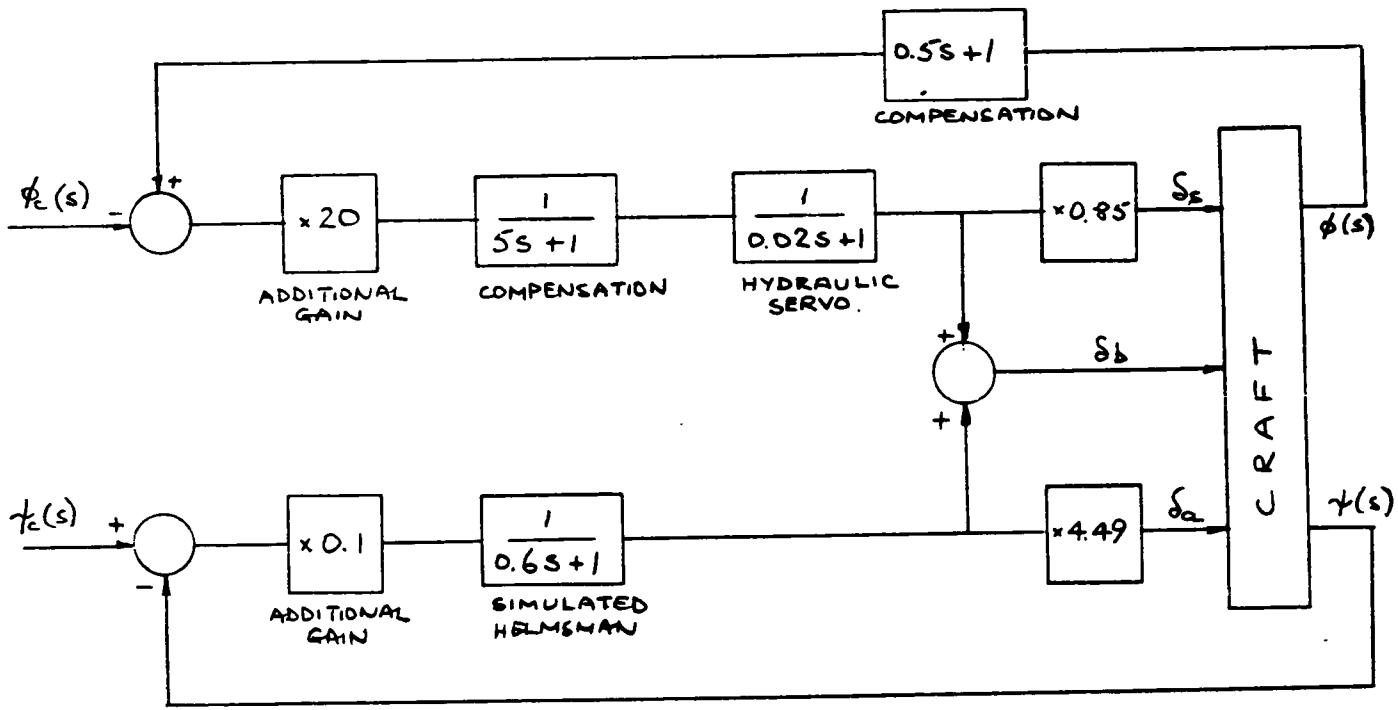

FIG. 12-5 BLOCK DIAGRAM OF RUDDER STABILIZING LOOP AND HEADING CONTROL LOOP.

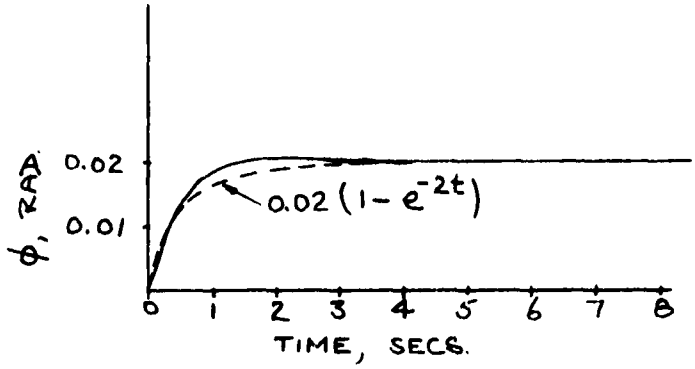

u = 80 KNOTS
ℓ_F = 2.5 ft., ℓ_R = 4.5 ft.

FIG. 12-6. RESPONSE OF RUDDER CONTROL SYSTEM TO A STEP COMMAND.

27 Nov 62

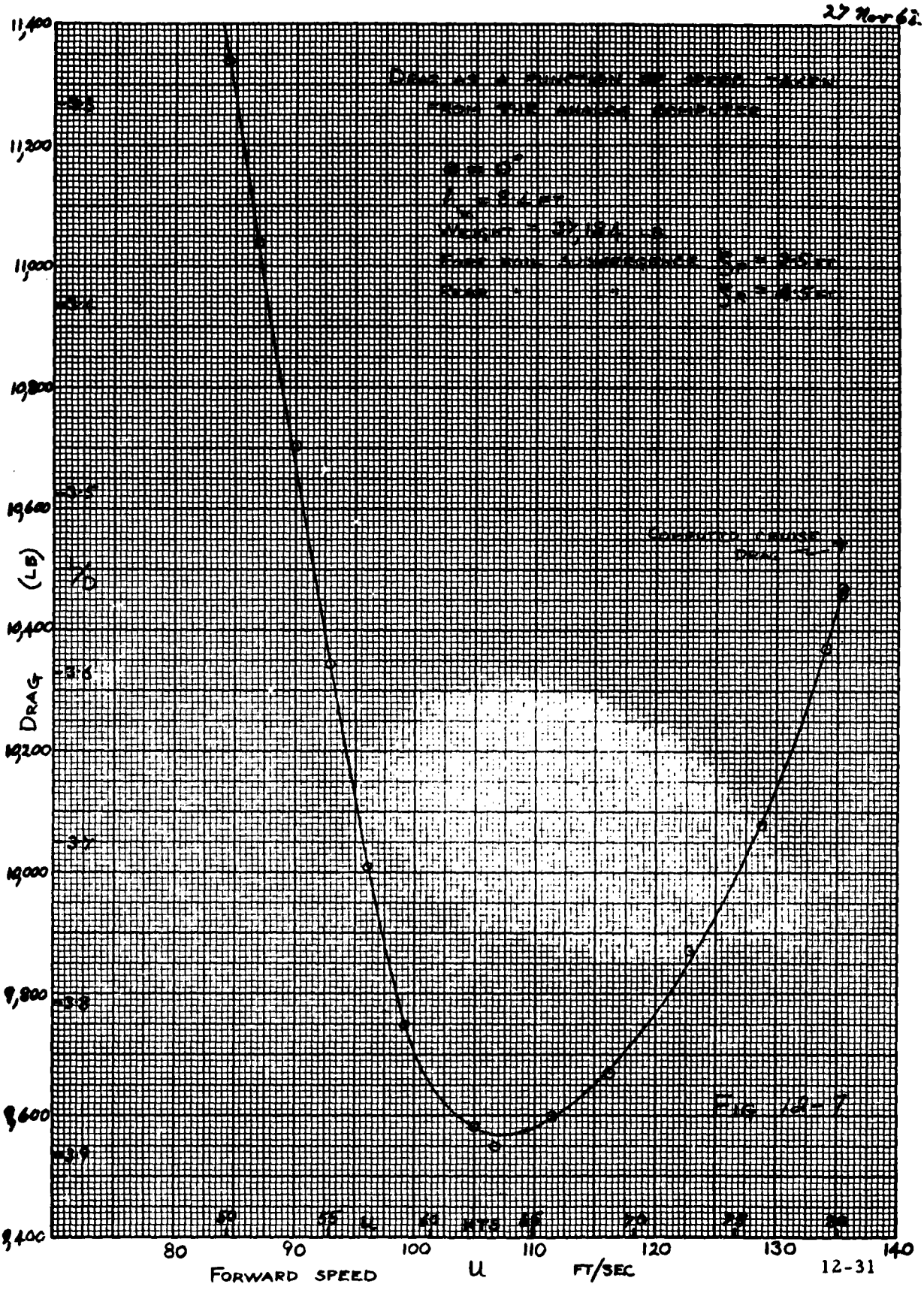
11,400
11,200
11,000
10,800
10,600
10,400
10,200
10,000
9,800
9,600
9,400
DRAG (LB)
80
90
100
110
120
130
140
FORWARD SPEED
U
FT/SEC
12-31

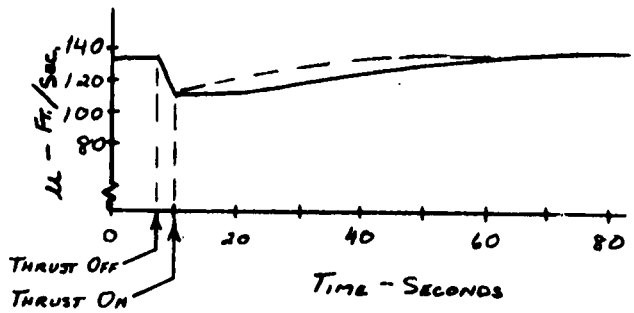

Fig 12-8 Demonstration of Natural Surge Stability Above 110 Ft./Sec.

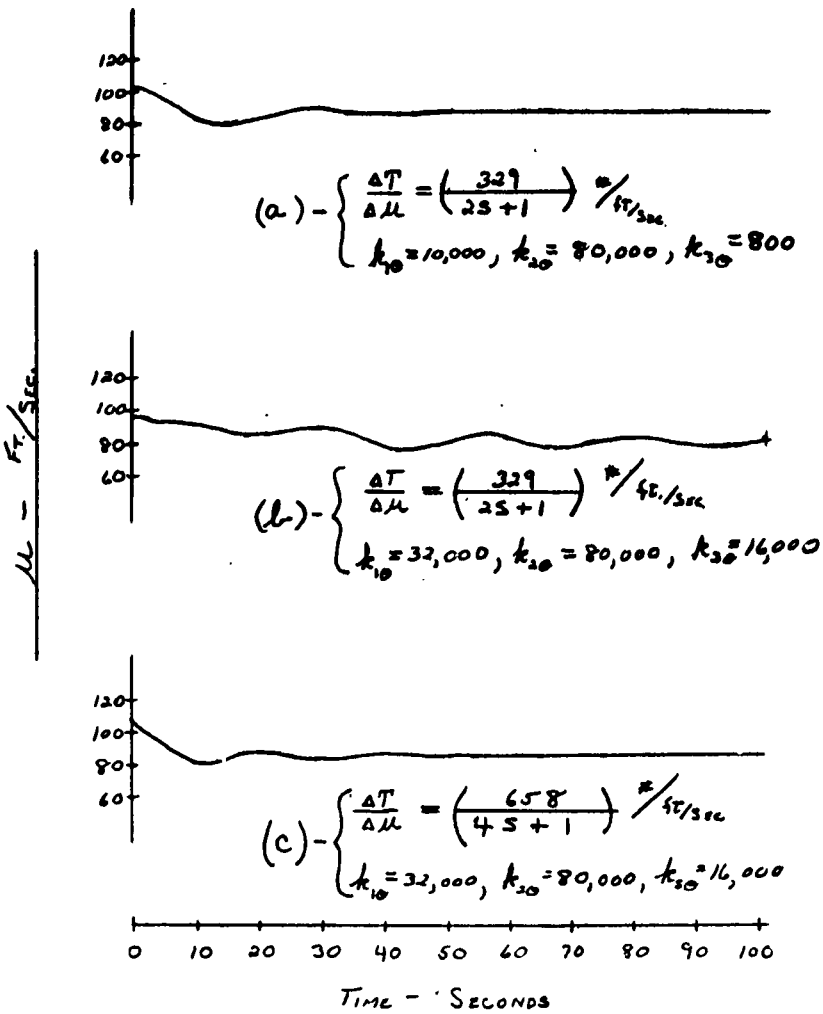

FIG 12-9 SURGE MODE
FOR THREE RUNS DEMONSTRATING
LONGITUDINAL - SURGE CROSS-COUPLING

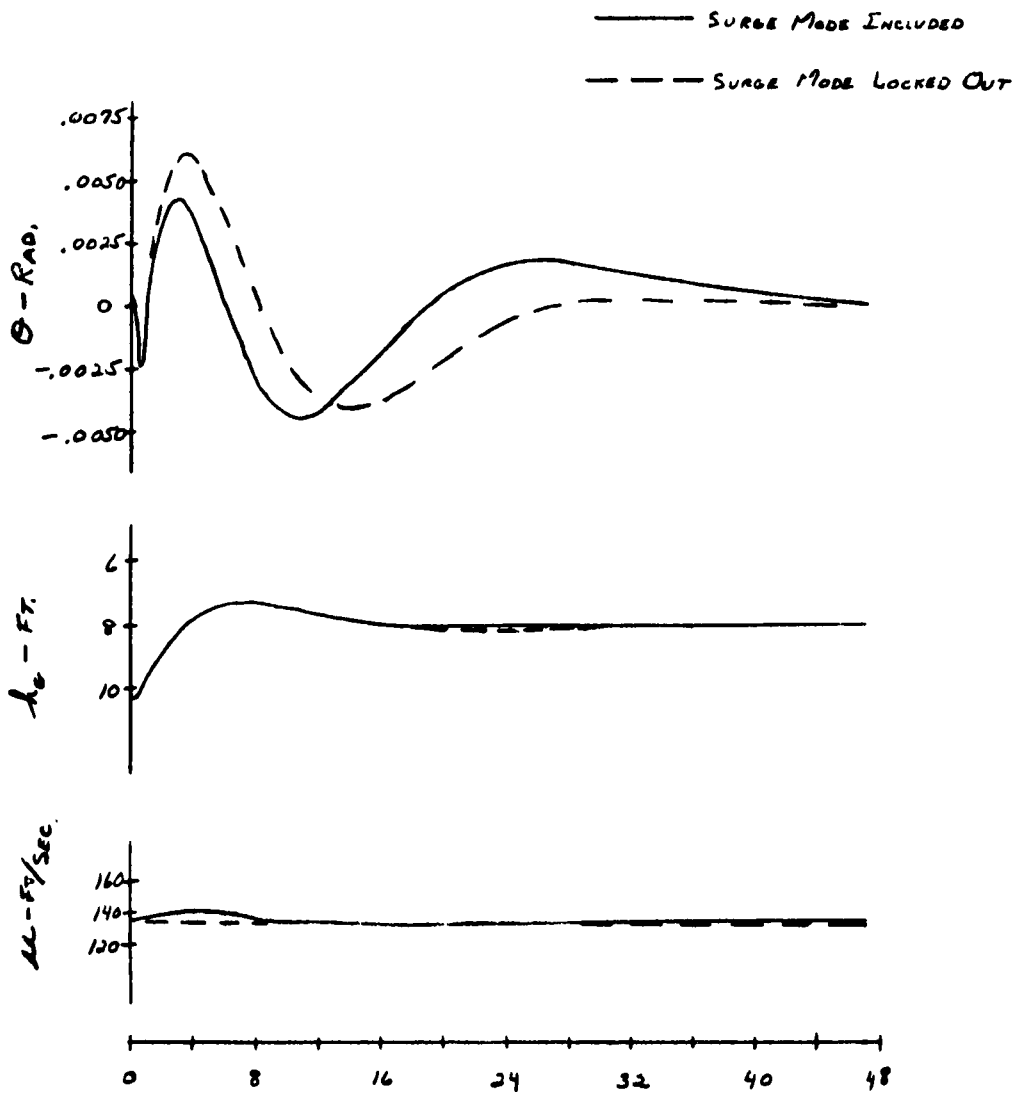

FIG 12-10 LONGITUDINAL TRANSIENTS WITH AND WITHOUT SURGE MODE (COMMANDED HEIGHT CHANGE)

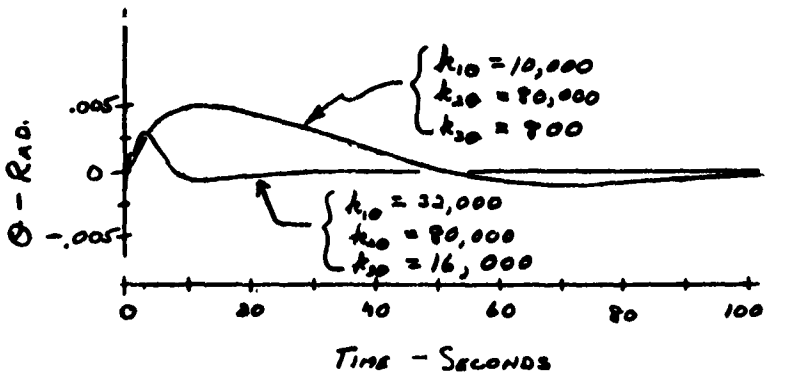

FIG 12-11 RESPONSES TO STEP PITCHING MOMENTS FOR TWO SETS OF AFT CONTROL SYSTEM GAINS

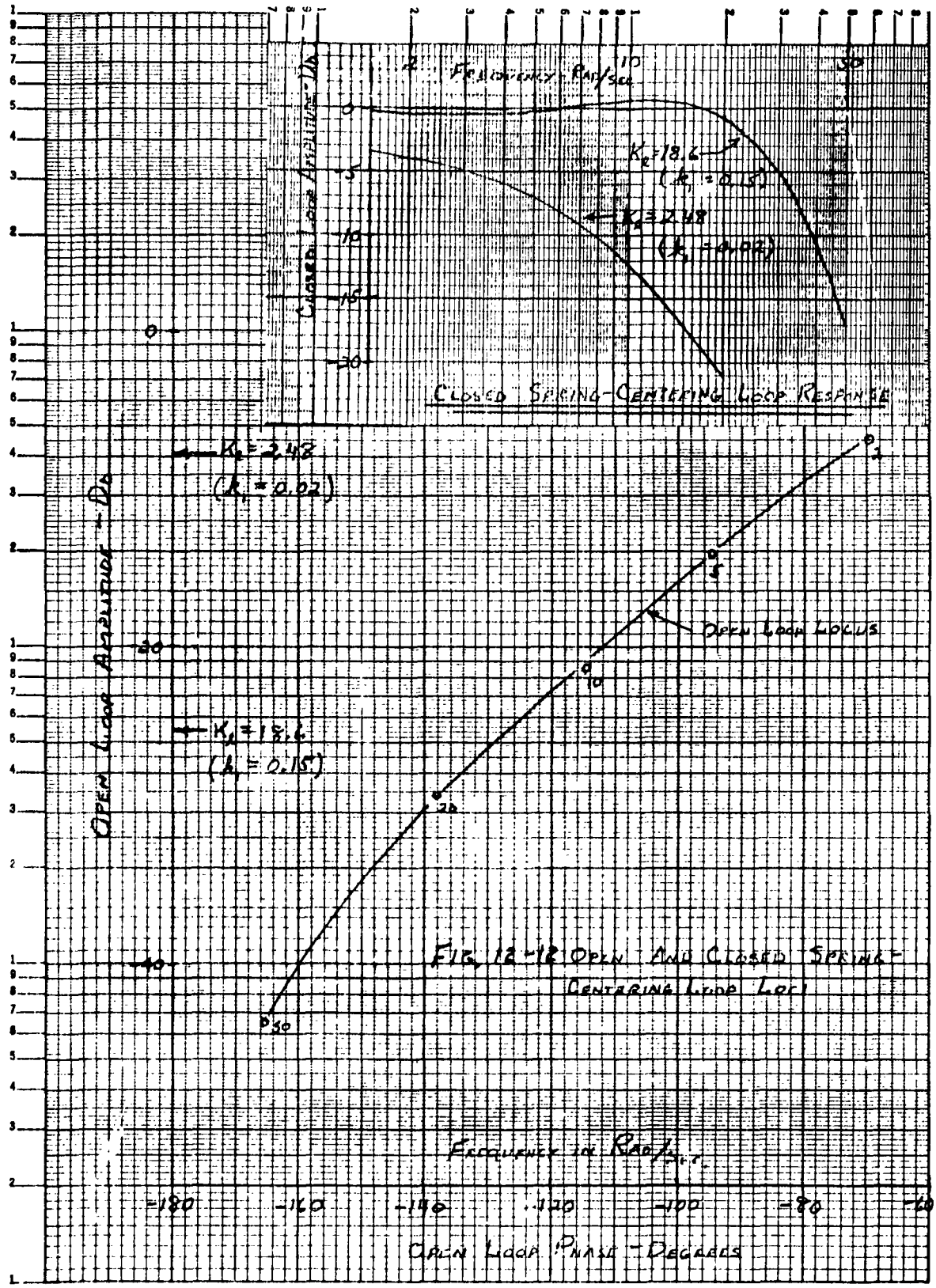

Fig. 12-18 Open And Closed Spring-Centering Loop Loci

FIG 12-13 DIAGRAM OF SPRING CENTERING CONTROL LOOP

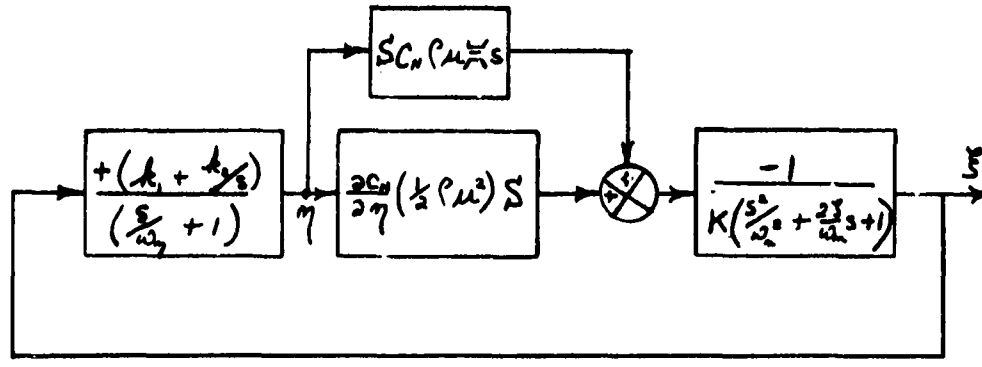

WHERE:—

$$\frac{1}{\left(\frac{s^2}{\omega_n^2} + \frac{2\zeta}{\omega_n} s + 1\right)} = \frac{1}{\left(\frac{s}{43.3} + 1\right)} \cdot \frac{1}{\left(\frac{s}{.993} + 1\right)}$$

FOR:

$K = 1000$ #/ft.
$S = 6.82$ ft²
$C_N \sim 0.1$
$\mu = 135$ ft/sec.
$(m_F + m_{a_{WF}}) = 23.4$ slugs

} SEE SECT. 6.3

$k_1 = 0.15$ OR 0.02
$k_2 \simeq 0$
$\omega_\eta = 20$ RAD/SEC.

$\frac{\partial C_N}{\partial \eta} \sim 1.0$

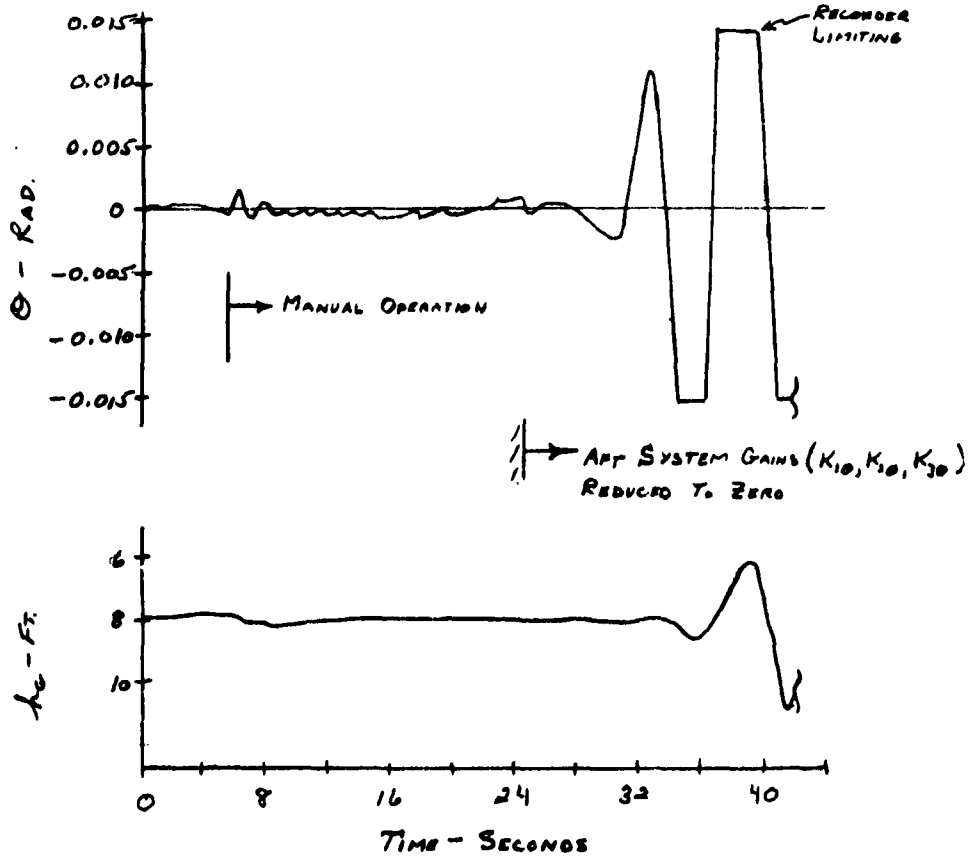

FIG 12-14 – DEMONSTRATION OF MANUAL UNCONTROLLABILITY WITH NO AFT CONTROL SYSTEM (SPRUNG FOILS)

Table 12-1. Automatic Control

Run No.	Sea	Speed	Type of Control System	Roll angle exceeded only 5% of time rad.	Lateral accel exceeded only 5% of time ft/sec^2	θ Parameter Set No. *	Heave Acceleration (Z/m_H) Exceeded only 5% of time- ft/sec^2	Surge Acceleration (X/m_T) Exceeded only 5% of time- ft/sec^2	Remarks Note: Values of ω_{hx} and ω_{HS} have been chosen at 0.5 rad/sec for all runs unless otherwise indicated.
139		80	Ail.	very small	very small	2	3.4	2.4	
144		100	Ail.	small	small	2	3.2	3.0	Signs of high frequency instability.
145		100	Rud.	small	small	2	-	-	Momentary instability when ζ_F small.
151		80	Ail.	very small	very small	2	6.6	2.4	Rigid struts.
110	Quar.	80	Ail.	<0.003	8.1	1	1.2	2.3	
111		80	Rud.	0.012	2.3	1	1.2	2.0	
179		50	Ail.	<0.003	3.3	2	0.90	2.0	
176		50	Ail.	-	-	2	0.85	surge mode constrained	Rigid aft struts
180		50	Rud.	Unstable	Unstable	2	-		
181		50	Rud.	Unstable	Unstable	2	0.90	until foil broach 1.5	h_{GO} = 6.9 ft, i.e., ζF_O = 4 ft, ζR_O = 6 ft
184		50	Rud.	Unstable	Unstable	2	0.80	until foil broach 1.7	
186		50	React.	<0.003	3.4	2	-	-	
187		50	React.	<0.003	3.0	2	-	-	k_{IR} = 0.05
57	Beam	80	Ail.	<0.002	3.1	1	1.2	2.8	$\omega_{hx} = \omega_{HS}$ = 1.0 rad/sec
71		80	Ail.	-	-	1	0.60	-	
85		80	Rud.	<0.012	2.2	1	0.60	2.1	
87		50	Ail.	<0.003	2.0	1	0.50	1.2	
89		50	Rud.	<0.012	1.1	1	0.50	1.2	
95		100	Ail.	<0.002	3.9	1	0.60	3.0	
97		100	Rud.	Unstable	Unstable	1	-	-	
98		100	Rud.	0.006	1.9	1	-	-	h_{GO} = 7 ft, i.e., ζ_{FO} = 3.9 ft, ζ_{RO} = 5.9 ft
198		80	React.	<0.003	3.9	2	1.3	3.5	
201		80	React.	<0.003	3.8	2	-	-	k_{IR} = 0.05
199	Beam	50	React.	<0.003	1.9	2	0.90	1.7	
202		50	React.	<0.003	3.0	2	-	-	k_{IR} = 0.05
200		100	React.	<0.003	4.3	2	-	-	
100	Bow	80	Ail.	Unstable	Unstable	1	-	-	$\lvert \dot{\eta} \text{ max} \rvert$ = 1 rad/sec
101		80	Ail.	<0.004	9.8	1	1.5	2.0	$\lvert \dot{\eta} \text{ max} \rvert$ = 2 rad/sec
135		80	Ail.	-	-	2	2.8	2.4	
102		80	Rud.	0.014	3.5	1	1.5	1.8	
103		80	Ail.	-	-	1	1.8	1.8	$k_{IF} = k_{IR}$ = 0.02
118		80	Ail.	<0.003	7.5	1	-	-	
119		80	Ail.	<0.003	7.2	1	-	-	$\omega_{hx} = \omega_{HS}$ = 1.0 rad/sec
132		80	Ail.	<0.005	10.9	2	-	-	
121		100	Ail.	small	10.0	1	2.6	2.7	
123		100	Rud.	0.009	3.0	1	-	-	
166		50	Rud.	0.019	2.6	2	3.2	1.2	
167		50	Ail.	0.006	7.8	2	2.8	1.7	
192		50	React.	<0.005	7.5	2	-	-	k_{IR} = 0.05
193		50	React.	<0.005	7.5	2	-	-	
194		80	React.	<0.005	10.9	2	2.2	2.1	k_{IR} = 0.05
195		80	React.	<0.005	9.4	2	2.3	2.9	
162	Head	80	Ail.	very small	very small	2	4.4	1.8	Rigid aft struts
163(a)		80	Ail.	very small	very small	2	2.2	1.8	
163(b)		100	Ail.	very small	very small	2	-	-	Kϕ halved - otherwise periodic high freq osc
164		100	Rud.	small	small	2	2.4	3.0	

* Set 1 = $K_{1\theta}$ = 10,000, $K_{2\theta}$ = 80,000, $K_{3\theta}$ = 36,000); Set 2 = ($K_{1\theta}$ = 32,000, $K_{2\theta}$ = 80,000, $K_{3\theta}$ = 16,000) - See Longitudinal Control Equations (Section 10).

Table 12-2. Manual Control

Sea	Speed Knots	Run No.	Roll Angle exceeded x% of time - rad	x	Lateral Accel Exceeded only x% of time (ft/sec^2)	Heave Acceleration Exceeded only x% of time - $(Z/_{mH})$ - ft/sec^2	Surge Acceleration Exceeded only x% of time - $(X/_{m_T})$ - ft/sec^2	Remarks - [The term "splash" indicates that during a manual run, control was lost by either or both operators]	
Calm	80	76	0.090	0	2.8	0.50	1.5		
		77	0.060	0	1.5	0.40	0.45	Operator opinion in these runs indicates that control is sufficiently easy to be judged acceptable for emergency craft operation	
	50	92	0.078	0	1.0	0.60 (5%)	0.75		
	50	174	-	0	-	0.80	-	- Rigid aft struts - no aft control	
Fol	80	146	0.060	5	1.5	4.8	2.5		
		147	0.075	5	2.4	-	-		
		152	0.058	5	1.5	6.8	2.3	Rigid aft struts - no aft control	
		153	0.125	5	2.2	-	-		
Quar	80	116	unstable			-	-		
		117	unstable	5		2.2 {until splash}	2.4		
	50	177	0.170	5	3.5	1.4	2.1	Rigid aft struts - no aft control	
	50	182	-	5	-	1.4	2.3		
Beam	80	78	0.110	5	3.8	1.6	3.0		
	50	93	unstable	0		2.8 {until splash at 45 sec.}	2.3		
		94	unstable	0		6.0 {until splash at 100 sec}	4.5		
	100	96	0.130	5	4.7	1.6	3.5		
Bow	80	120	0.180	5	6.9	-	-		
		133	unstable			-	-		
		134	0.250	5	4.4	4.0	2.1		
		106	unstable			-	-		
		107	unstable	5		2.4 {until splash at 30 sec}	3.0 (0%)		
		108	unstable			-	-		
	50	168	0.250	5	6.0	-	-		
		169	0.165	5	4.7	3.0	2.1		
		170	unstable	5		6.0 {until splash at 95 sec}	2.2	Rigid aft struts - no aft control	(This run was repeated with automatic control of the lateral system, without sustaining a splash, over 200 seconds)
Head	80	160 161			Both runs used height display alone (rigid aft struts) with manual longitudinal control, automatic lateral control. Stability was not possible in either run				

SECTION 13

FINALIZED CONTROL SYSTEM DESCRIPTION AND PERFORMANCE REQUIREMENTS OF CONTROL SYSTEM COMPONENTS

Finalized system descriptions for the automatic lateral and longitudinal control of the craft are presented in this section.

Although an automatic rudder controlled system was investigated during these studies and found to be superior to the automatic aileron controlled system in reducing lateral accelerations, the operators found it less easy to manually control since it is not sufficiently docile to yield an acceptable manual control system. Therefore, lateral control is represented here only for the aileron control configuration.

13.1 AILERON CONTROL SYSTEM

Figure 12-2 shows the general system diagram for this control system. The following parameters are recommended for control:

Hydraulic servo lag = 0.05 second

Additional loop gain (k_ϕ) = 20

Compensation = $(0.05\,s + 1)$ · · · · · to be generated by summing the output of rate and vertical gyros in the ratio of 1 to 20 respectively.

With these values, the control aileron deflection is related to roll angle as:

$$\eta_{\delta_a}(s) = 20 \left[-\phi(s) + \frac{\phi_c(s)}{0.05\,s + 1} \right] \qquad (13\text{-}1)$$

where

$\phi_c(s)$ = commanded roll angle

13.2 LONGITUDINAL CONTROL SYSTEM

13.2.1 MECHANICAL SPRING SELF-CENTERING LOOPS

The following equations represent the dynamic performance that can be produced by an all-mechanical (including hydraulics) spring centering loop (See Section 4.6.6).

$$\eta_F = \xi_F \left(k_{1F} + \frac{k_{2F}}{s} \right) \left(\frac{1}{s/\omega_{\eta_F} + 1} \right) , \qquad (13\text{-}2)$$

and

$$\eta_R = \xi_R \left(k_{1R} + \frac{k_{2R}}{s} \right) \left(\frac{1}{s/\omega_{\eta_R} + 1} \right) \qquad (13\text{-}3)$$

where

$k_{1F} = k_{1R} = 0.15$ ft^{-1}

$k_{2F} = k_{2R} = 0.025$ ft^{-1} - sec^{-1}

$\omega_{\eta_F} = \omega_{\eta_R} = 15$ rad/sec

13.2.2 REACTION CONTROLLED FORE AND AFT LOOPS

In addition to the mechanical spring centering loops, the following expressions define the fore and aft reaction control loops necessary for automatic longitudinal control. (See Section 11 and Figure 11-2.)

$$R_{CF} = -k_4 \left[\frac{k_3 (h_{HS} - h_{W_{HS}})}{1 + s/\omega_{HS}} + \frac{\ddot{h}_{16}}{s + \omega_{x_1}} \right. \left. (k_1 + \frac{k_2}{s + \omega_{x_2}}) \left(\frac{s}{s + \omega_{h_x}}\right) \right] \tag{13-4}$$

where

$k_1 = 0.25$ lb-sec/ft

$k_2 = 2.0$ lb/ft

$k_3 = 0.80$ lb/ft

$k_4 = 10,000$

$\omega_{x_1} = \omega_{x_2} = 0.1$ rad/sec

$\omega_{h_x} \quad \omega_{HS} = 0.50$ rad/sec

also

$$R_{CR} = \theta \left(k_{1\theta} + s\, k_{2\theta} + \frac{k_{3\theta}}{s}\right) \tag{13-5}$$

where

$$k_{1\theta} = 32,000 \text{ lb}$$

$$k_{2\theta} = 80,000 \text{ lb-sec}$$

$$k_{3\theta} = 16,000 \text{ lb-sec}^{-1}$$

13.3 DYNAMIC REQUIREMENTS OF HYDRAULIC INCIDENCE CONTROL

The values of ω_{η_F} and ω_{η_R} used previously in connection with the foil spring centering loops are indicative of the moderate bandwidth demands on the foil incidence control actuation system. Thus, this system may possess dynamic characteristics consistent with a 15 rad/sec simple lag break frequency (or better) over a similar bandwidth to yield the indicated results.

13.4 HEIGHT SENSOR STATIC AND DYNAMIC REQUIREMENTS

The longitudinal control equations show that the height sensor signal ($h_{HS} - h_{W_{HS}}$) is heavily filtered through a simple lag with a break frequency of 0.5 rad/sec. This implies that the system's dynamic requirements are met if the height sensor-filter calibration possesses such a characteristic. This represents an appreciable relaxation of height sensor requirements compared to those found necessary for typical fully submerged hydrofoil craft ($\omega_b \approx 10$ rad/sec).

Static accuracy requirements of ± 0.25 ft are considered reasonable and adequate for forward height control of the craft.

13.5 VERTICAL GYRO REQUIREMENTS

The 0.25-degree pitch and roll angle accuracy typical of vertical gyros widely available on the market is expected to prove sufficient for use in either the lateral or longitudinal systems. No significant dynamic requirements are pertinent for specification of a vertical gyro for use on hydrofoil craft.

The relatively short life of the typical vertical gyro (1000 hours) is, however, a source of inconvenience with hydrofoil craft operation but there are prospects of obtaining much longer life in special order units and, as may be seen in Section 14, at least two manufacturers offer units with 2000 hours mean-time-to-failure.

13.6 HEAVE ACCELEROMETER

Because of the presence of a high-pass filter in the heave accelerometer path (see Equation 13-4 and the term involving the quantity "ω_{h_x}"), steady-state errors in accelerometer output will not result in aft height error. However, there is a limiting value of the long term rate-of-change of accelerometer error that will produce a height error and this value may be computed from Equation 13-4 by setting the summed expressions within the brackets equal to each other, assigning the maximum height error that is tolerable, letting $\ddot{h}$ be $\dot{h}/s$ and solving for the value of $\dddot{h}_{16}$ as $s \rightarrow 0$ in the limit. With the parameter values as recorded below Equation 13-4, and an assumed height error (due to this cause alone) of 0.1 ft., this limiting accelerometer error rate becomes 0.0002 ft/sec^2 at frequencies below 0.1 rad/sec. Larger error rates are permissible at frequencies above 0.1 rad/sec.

Any of the commercial unconstrained mass accelerometers with total measurement ranges of 0 to 2 g's should be acceptable from the point of view of dynamic response characteristics.

SECTION 14

SURVEY OF AVAILABLE GYROS FOR RATE AND VERTICAL REFERENCE MEASUREMENTS

A survey of the present-day state of the art in the field of gyroscopic instruments has been conducted. In particular, the availability of both rate and vertical gyros of aircraft and marine types was compared. In addition, a comparison of, or tradeoff between, such factors as gyro size, weight, price, and lifetime expectancy (mean time before failure-MTBF) for marine and aircraft types and comparisons of various aircraft types was made.

Tables 14-1 and 14-2 give the figures for rate and vertical gyros presently or soon to be on the market. Wherever possible, estimated price and lifetime expectancy are shown, although price figures vary with the quantity ordered or with immediate market conditions.

Most of the rate gyros ranged in price from about $400 to $1400 highly accurate miniature rate gyros. Such gyros exhibited between 1000 and 5000 hours MTBF with an older larger unit (Type GG-79) manufactured by Minneapolis-Honeywell rated at operating times in excess of 5000 hours. Data on marine-type rate gyros was limited and only Muirhead could be found to permit a comparison with aircraft rate gyro manufacturers. Muirhead's product, D-894-A, has an MTBF of 44,000 hours. However, it is more bulky (1201 in.^{3}) and much heavier (50 pounds) than other types.

Vertical gyros were found to be more expensive than rate gyros, ranging from $1200 to $2000. Lear and Minneapolis-Honeywell types were advertised as MTBF of 2000 hours. M-H type GG-99 indicated

twice the vertical accuracy of other vertical gyros, but reliability was not checked. Lear is in a competitive position with M-H with its type 2153H. Muirhead (marine-type) is competitive in price but fails to match the aircraft types in accuracy, size, and weight.

From this study it is concluded that there is a better lifetime available for certain rate gyro models than for the vertical reference gyros. (Muirhead gyros normally are ineligible for hydrafoil craft operation because of their bulk and weight.) However, it appears that longer-lived vertical gyros are within present state of the art, but since they are not being offered off-the-shelf (above 2000 hours MTBF) the price of such units is high.

Table 14-1. Analysis of Rate Gyros

Company	Gyro Model	Range	Weight	Volume/ Dimensions	Price	Life time (hrs)	Remarks
Aircraft Types							
Daystrom	R50 special	15 to 720 deg/sec	1.1 lb	10 in.^{3}		1000	
Daystrom	R20 standard	6 to 1000 deg/sec	1.3 lb	11 in.^{3}		1000	
Fairchild	RG-101	±5 to ±4000 deg/sec	3 oz	1.1 in.^{3}	$800 $1000	1000	Accuracy 0.2 percent of full scale
Kearfott	T2008-1A-40	±40 deg/sec	1.6 lb	11.3 in.^{3}		1000	Accuracy 0.2 percent of full scale
Kearfott	T2009-1A-20	±20 deg/sec	1.7 lb	11.3 in.^{3}		1000	Accuracy 0.2 percent of full scale
Lear	Series 2157	±20 to ±1000 deg/sec	1.2 lb	9 in.^{3}	$700 ind pickoff	2000	Accuracy 0.2 percent of full scale
Minneapolis Honeywell	LN-100	±0.05 deg/sec	6 oz	2 in.^{3}		1000	
Minneapolis Honeywell	GG-79	±8 to ±175 deg/sec	2 lb	3.69 by 3.48 by 3.90	$450 (pot.) $1100 (ind)	Greater than 5000	Accuracy 1 percent of full scale
Minneapolis Honeywell	GG 13A-24	±450°/sec	2 lb	5-1/32 by 4-5/8 by 3-5/8	$350	Greater than 5000	
Nortronics	GRH 4	±10 to ±1000 deg/sec	4.50 oz	1.38 in.^{3}			
Sanders	RGA Series	±0.02 to ±400 deg/sec	3.50 oz	1.60 in.^{3}	$600	1000	
Whitaker	Type 517375	±10 deg/sec	7 oz	2.6 in.^{3}	$1375	1000	
Marine Types							
Muirhead	D-894-A	±0.025 to ±30 deg/sec	50 lb	12 by 10 by 11	$1580	44000	

Table 14-2. Analysis of Vertical Gyros

Aircraft Types

Company	Gyro Model	Range	Weight	Volume/ Dimensions	Price	Life time (hrs)	Remarks
Bendix	14132-1-A	±85 deg in pitch 360 deg in roll	4.3 lb	70 in.^{3}		1000	
Daystrom	Series VA-10	±85 deg in pitch 360 deg in roll	3.5 lb	32 in.^{3}		1000	
Daystrom	VG-11B-1	±85 deg in pitch 360 deg in roll	3.0 lb	36 in.^{3}		1000	
Kearfott	T2104-1B	±85 deg in pitch and roll	7.0 lb	5-1/8 in. dia 6-5/8 in. length	$2000		±1/6 deg. accuracy to vertical
Kearfott	T2105-1A	±85 deg in pitch 360 deg in roll	6.0 lb	5-1/2 in. dia 6 in. length	$2000	1000	
Kearfott	T4130-1A	±83 deg pitch 360 deg roll	3.5 lb	3-11/64 in dia 3.8 in length	$2000	1000	
Lear	2153H	±82 deg pitch 360 deg roll	5.5 lb	4-13/16 by 6-29/32 by 4-25/32		2000	±1/4 deg accuracy to vertical
Lear	Series 7000A	±85° pitch 360° roll	7.25 lb	4-7/8 by 4-27/32 by 4-25/32	$1250		
Lear	Series 1080	±85° pitch 360° roll	4.75 lb	90 in.^{3}	$1250		±1/4 deg accuracy to vertical
Minneapolis Honeywell	GG99	±85° pitch 360° roll		3.8 by 4-1/2	$2500 to 2100	2000	±1/8 deg accuracy to vertical

Marine Types

Muirhead	D-893-A	+45 deg in pitch +45 deg in roll	50 lb	13 by 9 by 9-1/2	$1580	44,000	±1/2 deg accuracy

APPENDIX A

DYNAMIC EQUATIONS FOR THE LATERAL ANALYSIS

The small perturbation linearized equations for the lateral dynamics are given below:

$$\begin{bmatrix} -ms + Y_{v'} & (Yr - mu_o)' & Y_p s + Y_\phi \\ N_{v'} & -I_Z s + N_{r'} & N_p s \\ K_{v'} & K_{r'} & -I_x s^2 + K_p s \end{bmatrix} \begin{bmatrix} v(s) \\ r(s) \\ \phi(s) \end{bmatrix}$$

$$= \begin{bmatrix} -Y_{\delta_b} \\ -N_{\delta_b} \\ -K_{\delta_b} \end{bmatrix} \delta_b(s) + \begin{bmatrix} -Y_{\delta_s} \\ -N_{\delta_s} \\ -K_{\delta_s} \end{bmatrix} \delta_s(s) + \begin{bmatrix} -Y_{\delta_a} \\ -N_{\delta_a} \\ -K_{\delta_a} \end{bmatrix} \delta_a(s)$$

APPENDIX B

PRELIMINARY LATERAL CRAFT CONFIGURATION

Using the equations in Appendix A, it can be shown that the lateral characteristic equation is given by

$$a_4 s^4 + a_3 s^3 + a_2 s^2 + a_1 s + a_0$$

where

$$a_4 = -m I_x I_z$$

$$a_3 = I_x (Y_v I_z + N_r m) + K_p m I_z$$

$$a_2 = -K_p (Y_v I_z + N_r m) + K_v I_z Y_p + K_r N_p m - I_x \left[Y_v N_r - N_v (Y_r - m u_o) \right]$$

$$a_1 = K_v \left[I_z Y_\phi - N_r Y_p + N_p (Y_r - m u_o) \right] + K_r \left[N_v Y_p - N_p Y_v \right] + K_p \left[Y_v N_r - N_v (Y_r - m u_o) \right]$$

$$a_0 = Y_\phi \left[N_v K_r - K_v N_r \right]$$

In general, for hydrofoil craft with fully submerged foils, this equation has one real positive root when the submergences of the fore and aft foils are at their trim depths. This is due to the coefficient a_0 in the above equation being positive while the remainder

of the coefficients are negative. The coefficient Y_ϕ is positive. In order to make a_0 negative, it is necessary for $(N_v K_r - K_v N_r)$ to be negative. Each coefficient in the first product is found by taking the difference of two quantities, and this difference is usually small. It is the second product which is usually the dominant one. The damping term N_r is always negative, so in order for $(N_v K_r - K_v N_r)$ to be negative, it is required that K_v be negative. However, for a craft that has foils with no dihedral or sweepback, K_v is always positive. Both dihedral and sweepback, but especially dihedral, tend to make K_v more negative. Dihedral is more effective the wider the foils are spaced. Thus it was assumed that the craft would have a pair of foils supported on struts spaced 14 feet apart. From drag considerations, a 3-strut configuration was assumed initially, the third strut supporting a foil with no dihedral or sweepback. (Since this foil is not split the effectiveness of dihedral would be very small.)

In the airplane configuration, dihedral tends to make K_v more negative as desired, but also tends to make N_v more negative. A positive value or N_v helps to make the coefficients a_1 and a_2 negative, and also makes the craft easier to control manually. (See Section 7.) It can also be shown that a moderately negative N_v results in the $\phi(s)/\delta_a(s)$ transfer function having a right-half plane zero. However, using the canard configuration, dihedral tends to make K_v more negative and N_v more positive, both of which are desirable. Thus, for the initial investigation, a canard configuration was taken.

Further assumptions were also made about the craft. A front strut length of 4.5 ft was used. Assuming a normally distributed sea surface displacement, it was found that the waves in Sea State 3 will be higher than 4.5 ft for 4.5 percent of the time. The rear struts were taken to be 1 ft longer than the front strut. The CG of the craft was taken to be 8 ft above the front foil and 9 ft above the rear foil. A foil fore and aft spacing of 25 ft was used, with the quarter chord points of the mean geometric chord of the rear foils being 7.25 ft aft of the CG, and that of the front foil being 17.75 ft ahead of the CG, (this CG position relative to the fore and aft foils is typical for a canard configuration.) The foils were taken to be operating at a C_L of 0.1 at 80 knots. This implied a C_L of 0.4 at take-off speed of 40 knots, which appeared to be reasonable. As far as lateral stability is concerned, the larger the foils, the slower will be the uncontrolled divergence.

Thus, with no dihedral or sweepback, the area of the front foil was 5.91 ft^2, and the area of each rear foil was 7.23 ft^2. An aspect ratio of 3 was assumed for each foil which resulted in a front foil chord of 1.40 ft and rear foil chords of 1.55 ft. A value of 1.0 was used for foil lift curve slope. This is approximately the same value as that of a flat plate of aspect ratio 3 operating at a depth of one chord at zero cavitation number, and at C_L of 0.1, (Ref. B-1). Strut chords of 1.5 ft were taken, i.e., the strut chords were assumed approximately the same as the foil chords, and a value of 0.75 was used for the strut lift curve slopes at normal submergences. Normal submergences of the front and rear foils were taken as 2 and 3 ft respectively. No data on supercavitating struts were available, so the value of lift curve slope of 0.75 which approximately corresponds to that of a flat plate of aspect ratio 1 operating as a foil at a depth of one chord and zero cavitation number, was used, (Ref. B-1).

The mass of the craft was taken as 37,100 pounds. The moments of inertia I_{xx} and I_{zz} were calculated by assuming that the craft consisted of two homogeneous parallel cylinders with centers 19 ft apart, each cylinder being 4 ft in diameter and 45 ft long. The moments of inertia were found to be 9.53×10^4 slug ft^2 and 2.882×10^5 slug ft^2 respectively.

Reference

B-1. NASA Technical Report R-93.

APPENDIX C

GENERATION OF AN IRREGULAR STATE 3 SEA

In the course of this study it was necessary to generate, in an analog fashion, the disturbance applied to the struts and foils of the craft arising from wave encounters in a State 3 Sea. Two methods for such generation are being utilized currently, the first involving the summation of a number of sine waves as an approximation to the Neumann spectra; the second utilizing a shaped noise source to generate the required statistical properties of the sea. It is the latter method which has been used in this simulation. The details of this method may be found in Reference C-1. It is necessary for such sea generation to supply three important characteristics for each sea (where it is understood that a "sea" is described by a set of three numbers giving sea state, sea relative heading and craft speed). The first required characteristic is a filter which, when subjected to white noise, produces the necessary wave encounter spectrum. The second is a phase delay that produces the delay associated with craft speed and wave propagation speed acting over the strut separations. (Because of the difference in propagation speed with wave length, this phase delay is not, in general, precisely proportional to wave encounter frequency.) Additionally, it is necessary ideally to provide a 90-degree phase shift to all frequencies to generate vertical wave orbital motions from horizontal orbital motions. In the operation of this process, some magnitude distortion over the spectrum of vertical orbital motion velocities is inevitable and the network is chosen to keep this effect to a minimum.

The following figures present the results of computation and simulator data for:

(1) The Neumann spectra for a State 3 Irregular Sea, transformed, in general, to reflect relative heading and craft speed. (The beam sea case is the only sea state in which such transformation yields the same spectra as that seen by a stationary observer.)

(2) Phase delay function to account for disturbance phase relationships between the forward, port-rear and starboard-rear foils.

(3) The "best fit" 90-degree phase shift network that is used to compute vertical orbital motions form horizontal orbital motions.

The phase-delay functions are computed for various strut location pairs, (forward, port-rear; port, starboard-rear etc.). The pairs chosen depend on the sequence in which a wave encounters each strut and thus are dependent on the relative heading and craft speed. Also relative wave headings have been chosen only through an angle of 180 degrees since response of the craft to wave encounters from the opposite side may be expected to be symmetrical.

Figure C-2 presents two different forms of the 90-degree phase shift network used because, in general, the bandwidth over which phase shift is required is larger for some cases than for others thus requiring a somewhat different compromise of phase-magnitude errors. The actual networks used are noted on the figures which present the phase delay functions.

The wave spectra shown have measured data points superimposed on the desired (computed) curves. The area under the curve through these data points is not, in general, equal to that under the computed curve, ("E" = 2.58 ft^2 for a State 3 Sea) but, before each such sea was run, a measurement of the spectrum power was made and adjustment was accomplished to ensure the proper sea state.

Additionally, a calculation was made to establish the mean square magnitude of the orbital motion velocities and previously generated surface wave spectra were thereafter adjusted to yield a value of $\left[\overline{V(\omega)}\right]^2 = 1.6\ ft^2/sec^2$ at an average depth of 2.5 ft.

Some abbreviations used in Figure C-1 to C-19 are:

$\left[A(\omega)\right]^2$ - Spectral density in ft^2 - sec

ω_e, ω_o - wave encounter frequency and network characteristic frequency

V_W - wind speed generating waves

E - total energy of the sea spectrum

K - H - abbreviation for a Krohnhite Filter

cps - cycles/sec

H_i (ω_{Hi}), Lo (ω_{Lo}) - break frequency settings used on the Krohnhite Filter

Reference

C-1. Appendixes to the Engineering Summary Report on a Hydrofoil Autopilot System Design Study Program. Appendix D. NObs - 84498. RCA. January, 1962.

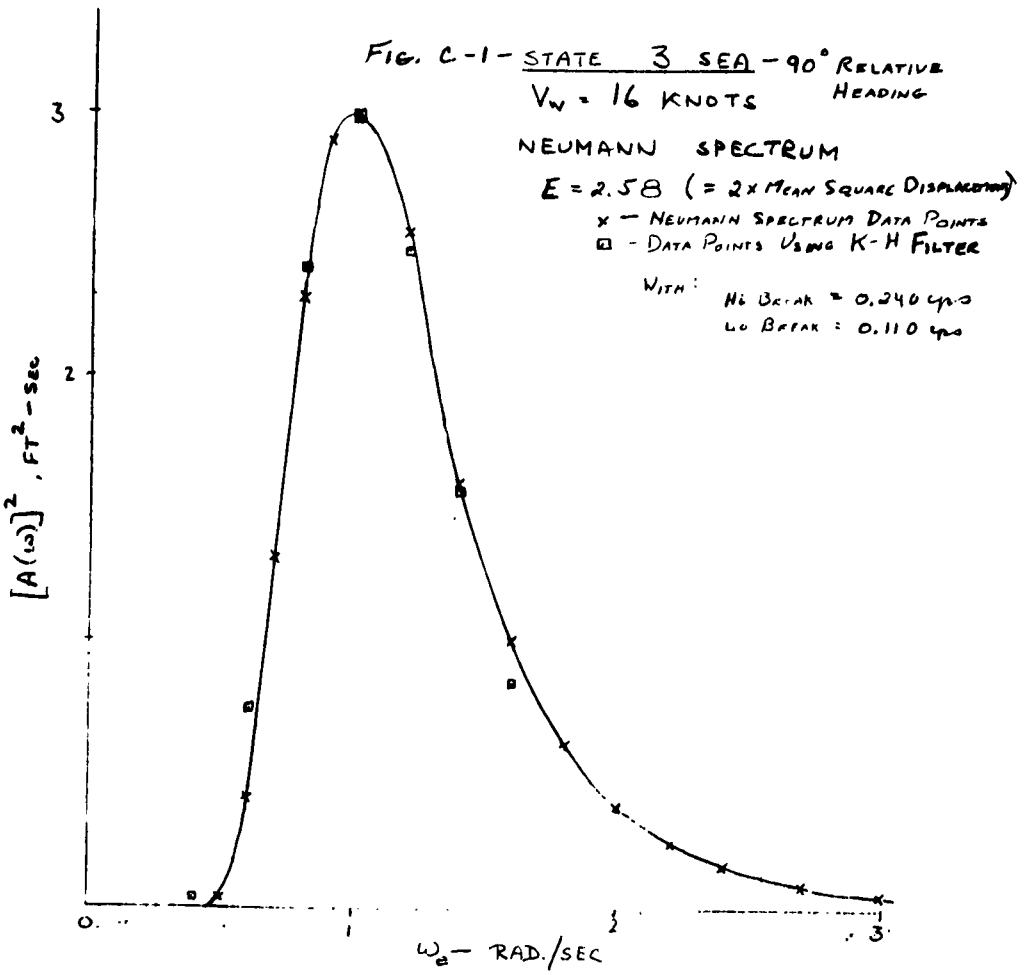
FIG. C-1 - STATE 3 SEA - 90° RELATIVE HEADING
V_W = 16 KNOTS
NEUMANN SPECTRUM
E = 2.58 (= 2 x MEAN SQUARE DISPLACEMENT)
x - NEUMANN SPECTRUM DATA POINTS
□ - DATA POINTS USING K-H FILTER
WITH:
HI BREAK = 0.240 cps
LO BREAK = 0.110 cps
$[A(\omega)]^2$, FT^2-SEC
3
2
0
1
2
3
ω_e - RAD./SEC

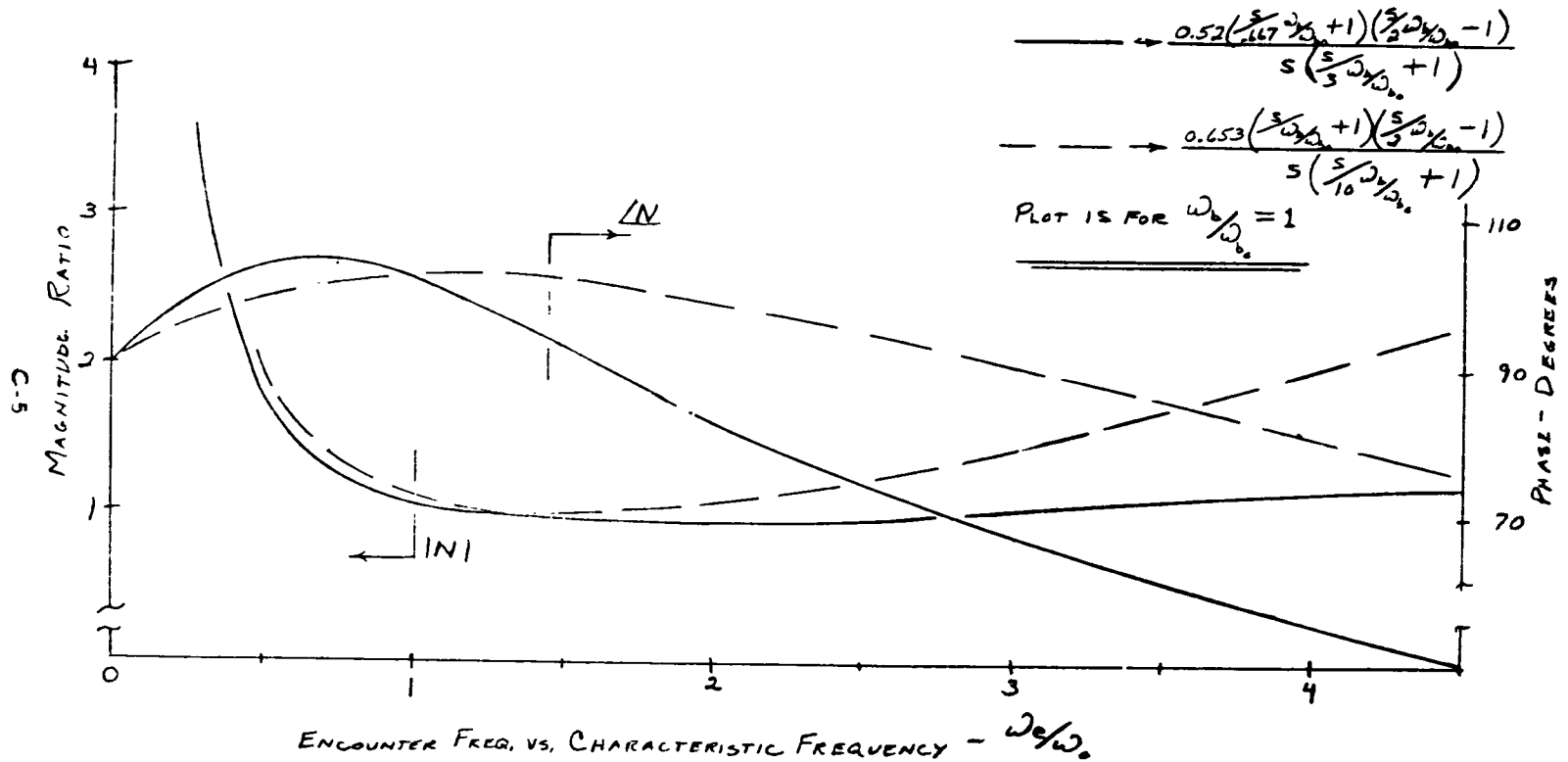

C-5

FIG. C-2 - 90° PHASE SHIFT NETWORK CHARACTERISTICS

FIG. C-3 - FRONT FOIL TO PORT REAR FOIL AND PORT REAR FOIL TO STARBOARD & FRONT FOIL PHASE SHIFTS VS ω_e (SEA FREQUENCY) FOR 90° INCIDENCE ANGLE IN A STATE 3 SEA

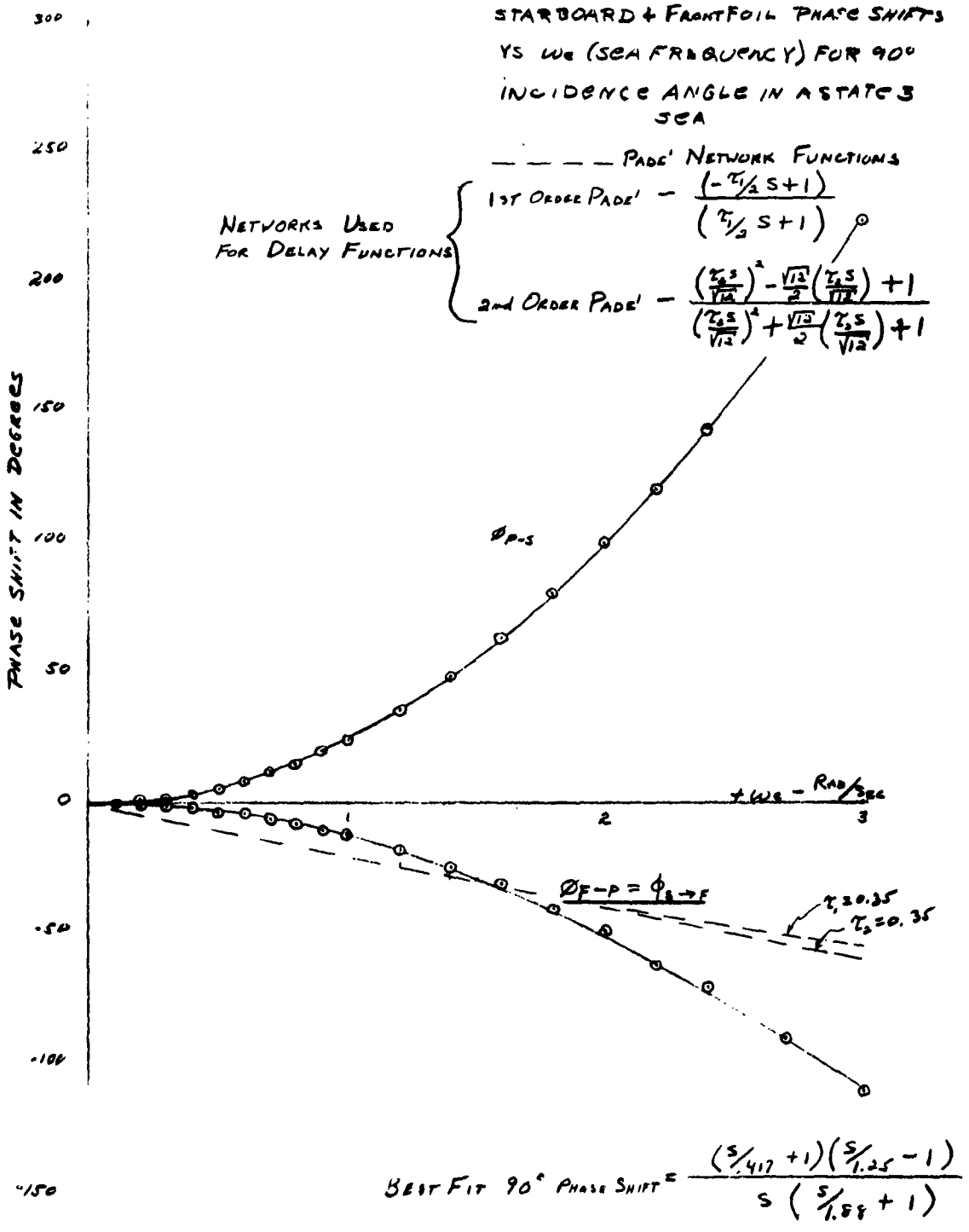

NETWORKS USED FOR DELAY FUNCTIONS

- 1ST ORDER PADE' - $\dfrac{\left(-\frac{\tau_1}{2}s+1\right)}{\left(\frac{\tau_1}{2}s+1\right)}$
- 2nd ORDER PADE' - $\dfrac{\left(\frac{\tau_2 s}{\sqrt{12}}\right)^2 - \frac{\sqrt{12}}{2}\left(\frac{\tau_2 s}{\sqrt{12}}\right)+1}{\left(\frac{\tau_2 s}{\sqrt{12}}\right)^2 + \frac{\sqrt{12}}{2}\left(\frac{\tau_2 s}{\sqrt{12}}\right)+1}$

BEST FIT 90° PHASE SHIFT = $\dfrac{\left(\frac{s}{.417}+1\right)\left(\frac{s}{1.25}-1\right)}{s\left(\frac{s}{1.88}+1\right)}$

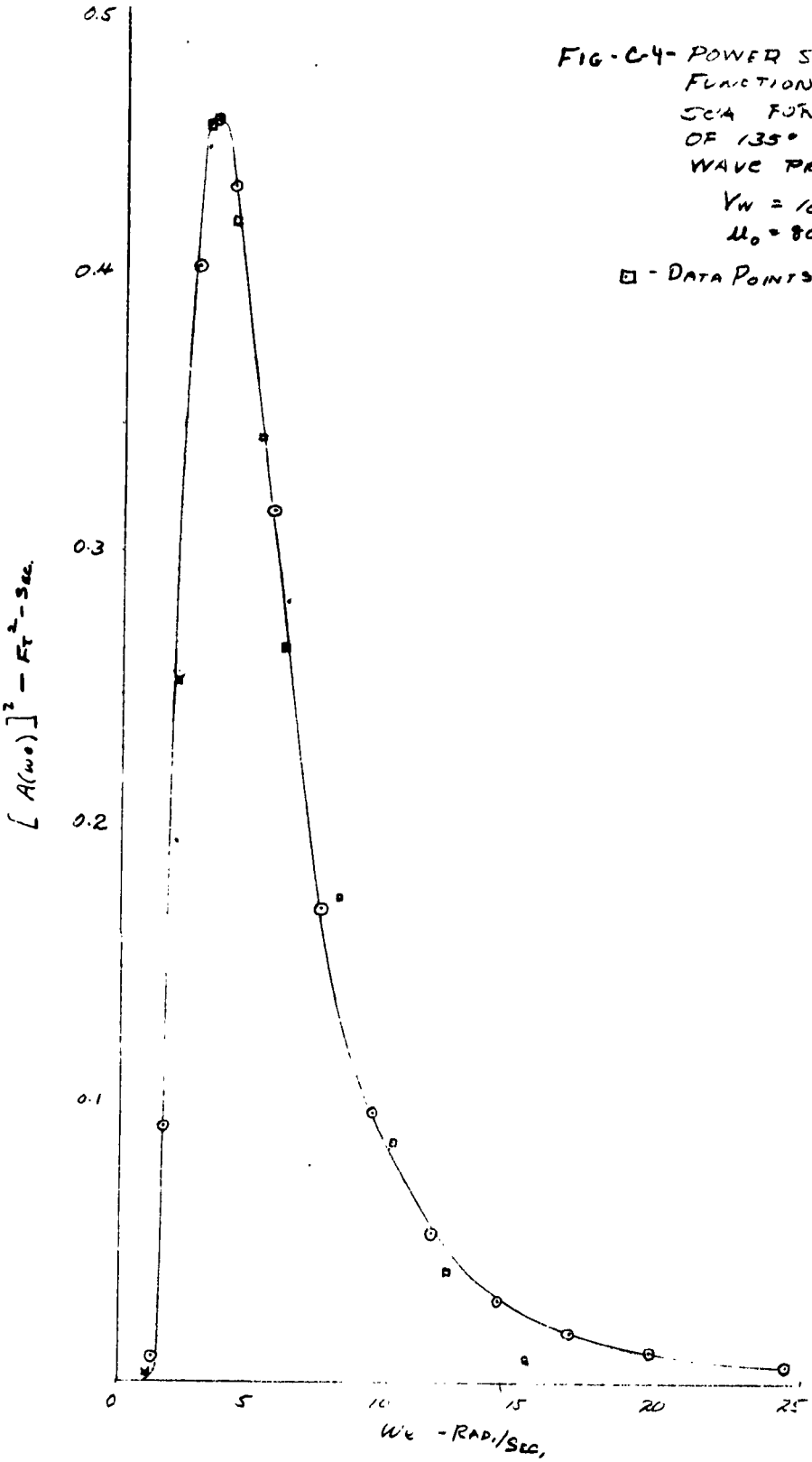

FIG-C-4- POWER SPECTRAL DENSITY FUNCTION OF A STATE 3 SEA FOR A SHIP HEADING OF 135° RELATIVE TO THE WAVE PROPOGATION DIRECTION

V_W = 16 KNOTS

V_0 = 30 KNOTS

□ - DATA POINTS FOR K-H:

ω_{Lo} = 0.33 cps

ω_{Hi} = 2.10 cps

ω_b = 5.6 Rad/Sec.

↑ SIMPLE LAG

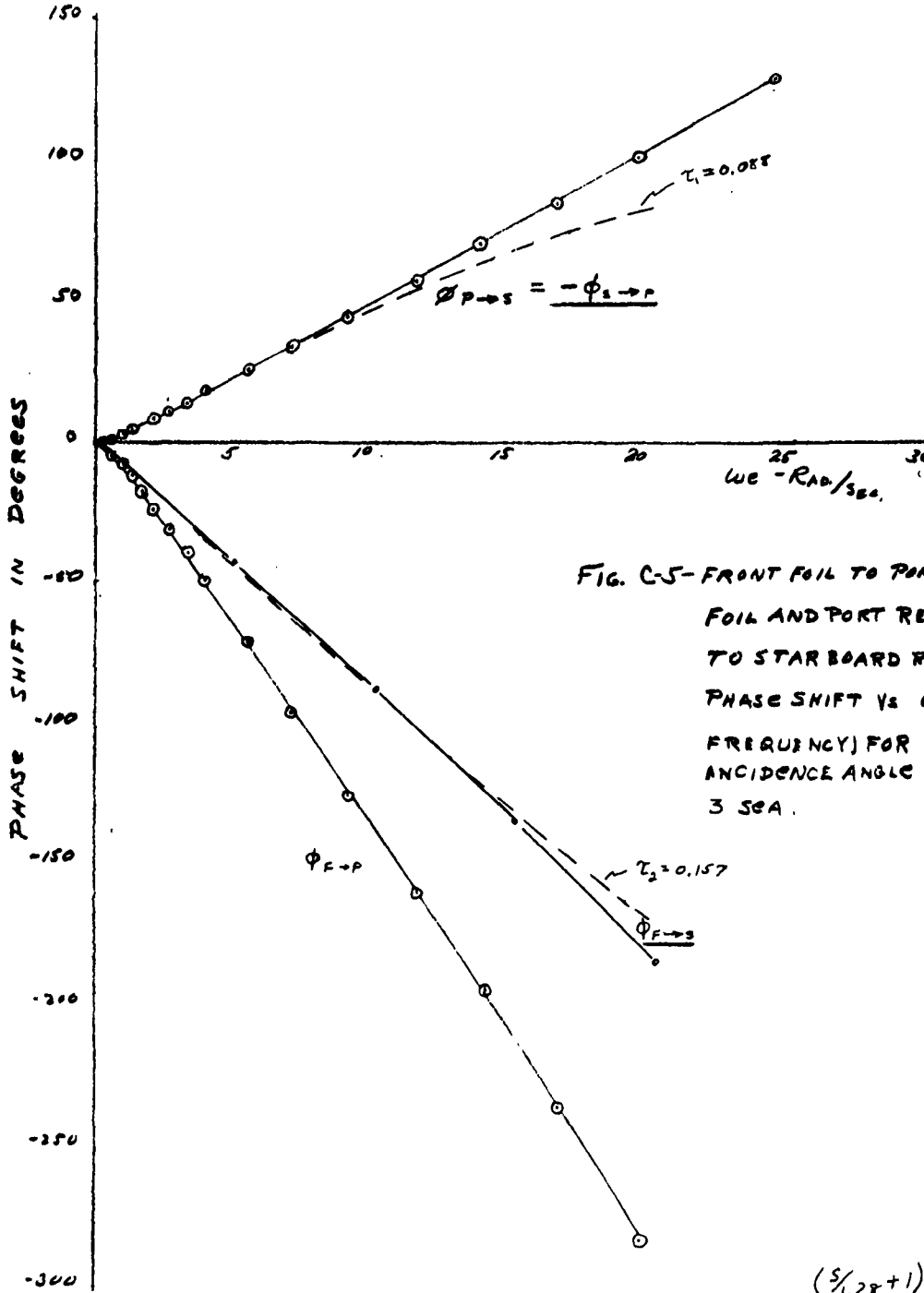

FIG. C-5- FRONT FOIL TO PORT REAR FOIL AND PORT REAR FOIL TO STARBOARD REAR FOIL PHASE SHIFT Vs We (SEA FREQUENCY) FOR 135° INCIDENCE ANGLE IN A STATE 3 SEA.

BEST FIT 90° PHASE SHIFT $= \dfrac{(S/1.78+1)(S/5.33-1)}{S(S/\tau+1)}$

$(\omega\varepsilon/\omega = 2.17)$

FIG. C-6 – POWER SPECTRAL DENSITY FUNCTION OF A STATE 3 SEA FOR A SHIP HEADING OF 180° RELATIVE TO THE WAVE PROPOGATION DIRECTION

V_W = 16 KNOTS

V_0 = 80 KNOTS

Δ – DATA POINTS FOR K-H $\omega_{L_0} = 0.47$

$\omega_{H_1} = 3.2$

$\omega_b = 5.5$ Rad/sec

↳ Straight Log Line

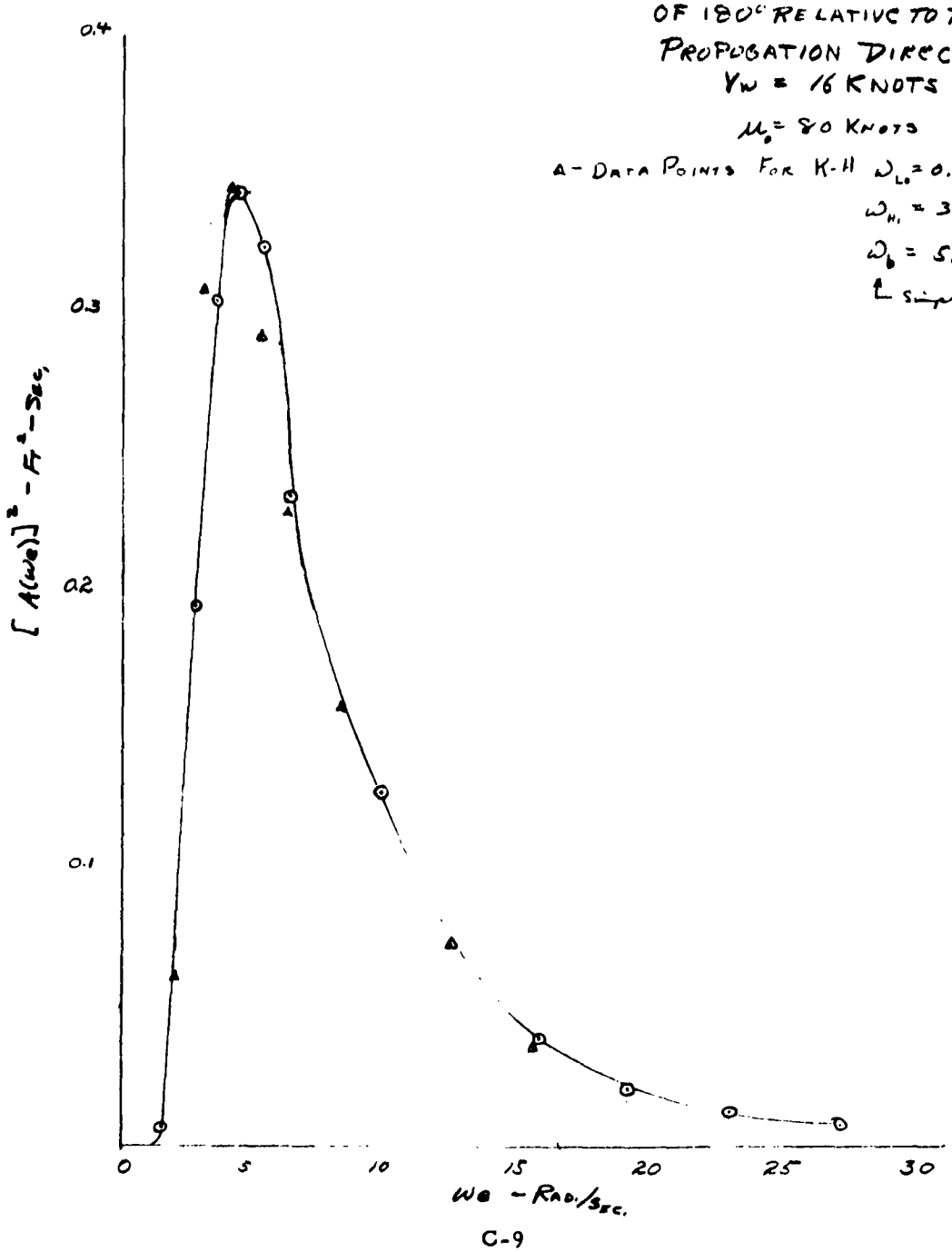

FIG. C-7 - FRONT FOIL TO PORT REAR FOIL AND PORT REAR FOIL TO STARBOARD REAR FOIL PHASE SHIFT VS ω_e (SEA FREQUENCY) FOR 180° INCIDENCE ANGLE IN A STATE 3 SEA

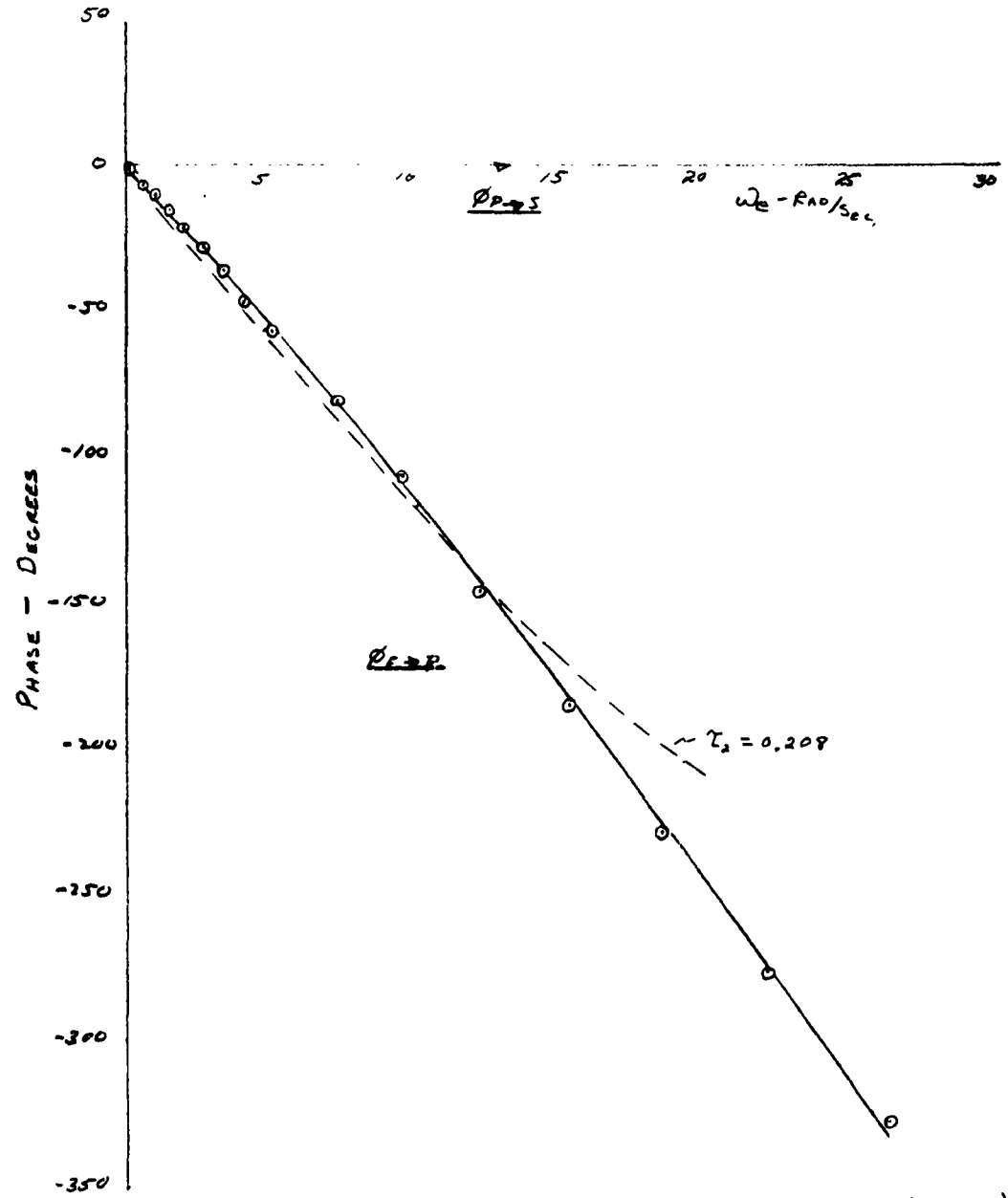

BEST FIT 90° PHASE SHIFT $= \dfrac{(S/2.32+1)(S/6.67-1)}{S(S/10+1)}$

$(\omega_e/_0 = 3.33)$

FIG. -C-8

POWER SPECTRAL DENSITY FUNCTION OF A STATE 3 SEA FOR A SHIP HEADING OF 45° RELATIVE TO THE WAVE PROPOGATION DIRECTION

$V_W = 16$ KNOTS

$\mu_0 = 90$ KNOTS

▣ - Data Point, For K-H;

$\omega_{Lo} = 0.11$ rps $\omega_{Hi} = 1.2$ rps

$\omega_b = 3.7$ Rad/sec

↑ SIMPLE LAG

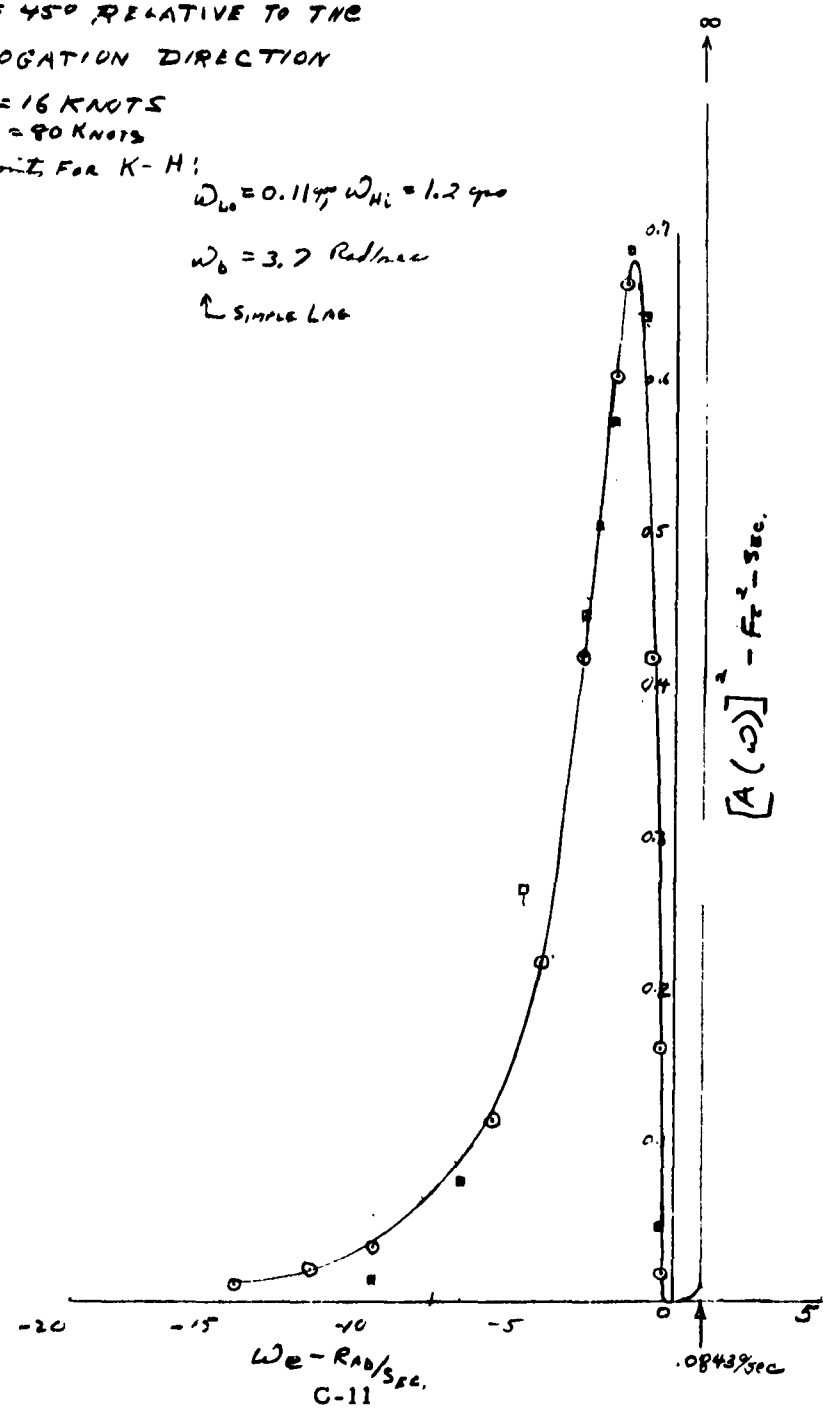

FIG C-9 - FRONT FOIL TO PORT REAR FOIL AND PORT REAR FOIL TO STARBOARD REAR FOIL PHASE SHIFT VS ω_e (SEA FREQUENCY) FOR 45° INCIDENCE ANGLE IN STATE 3 SEA.

$$\text{BEST FIT } 90^\circ \text{ PHASE SHIFT} = \frac{\left(\frac{S}{0.89}+1\right)\left(\frac{S}{2.67}-1\right)}{S\left(\frac{S}{4}+1\right)}$$

$$\left(\omega_e/_S = 1.33\right)$$

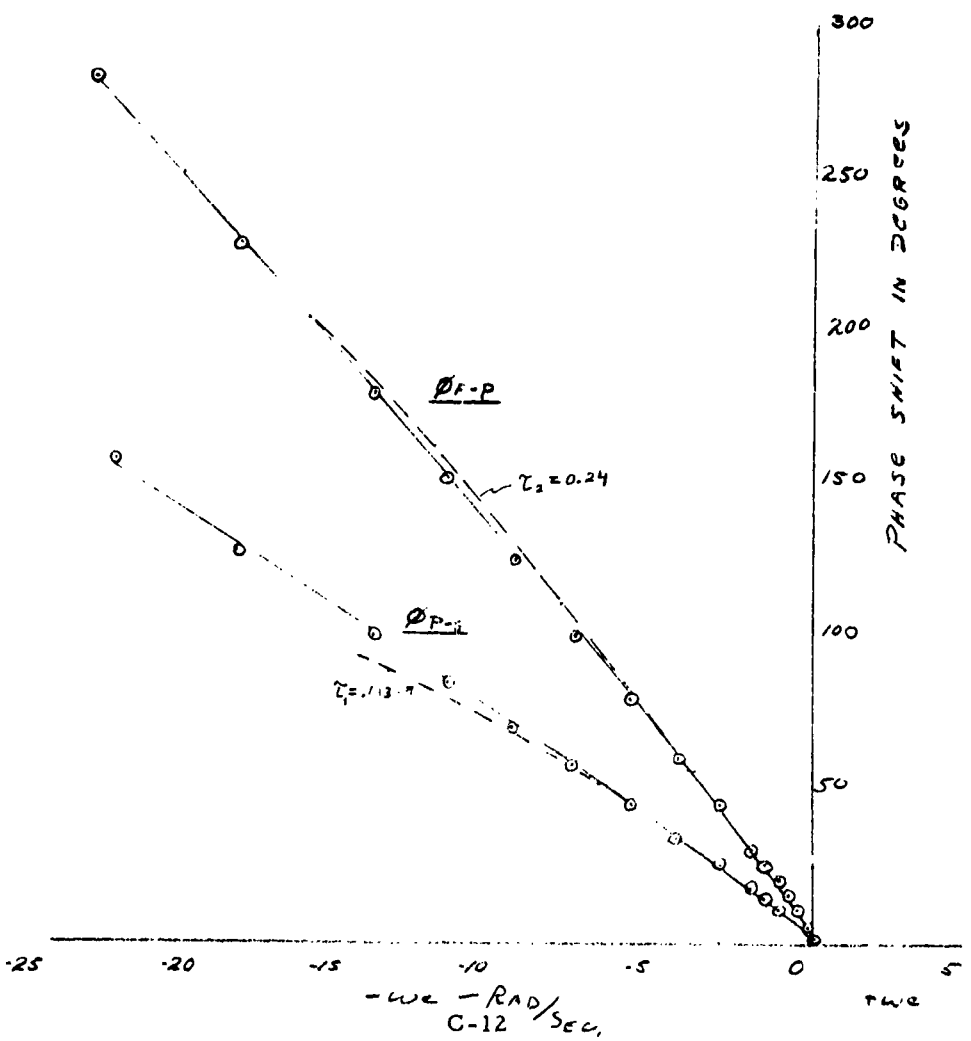

POWER SPECTRAL DENSITY FUNCTION OF A STATE 3 SEA FOR A SHIP HEADING OF 0° RELATIVE TO THE WAVE PROPOGATION DIRECTION

V_W = 16 KNOTS

μ_0 = 30 KNOTS

Δ- DATA POINTS FOR K-H; ω_{Lo} = 0.23 cps

ω_{Hi} = 2.0 cps

ω_b = 4.5 Rad/sec.

↑ SIMPLE LAG

FIG. C-10

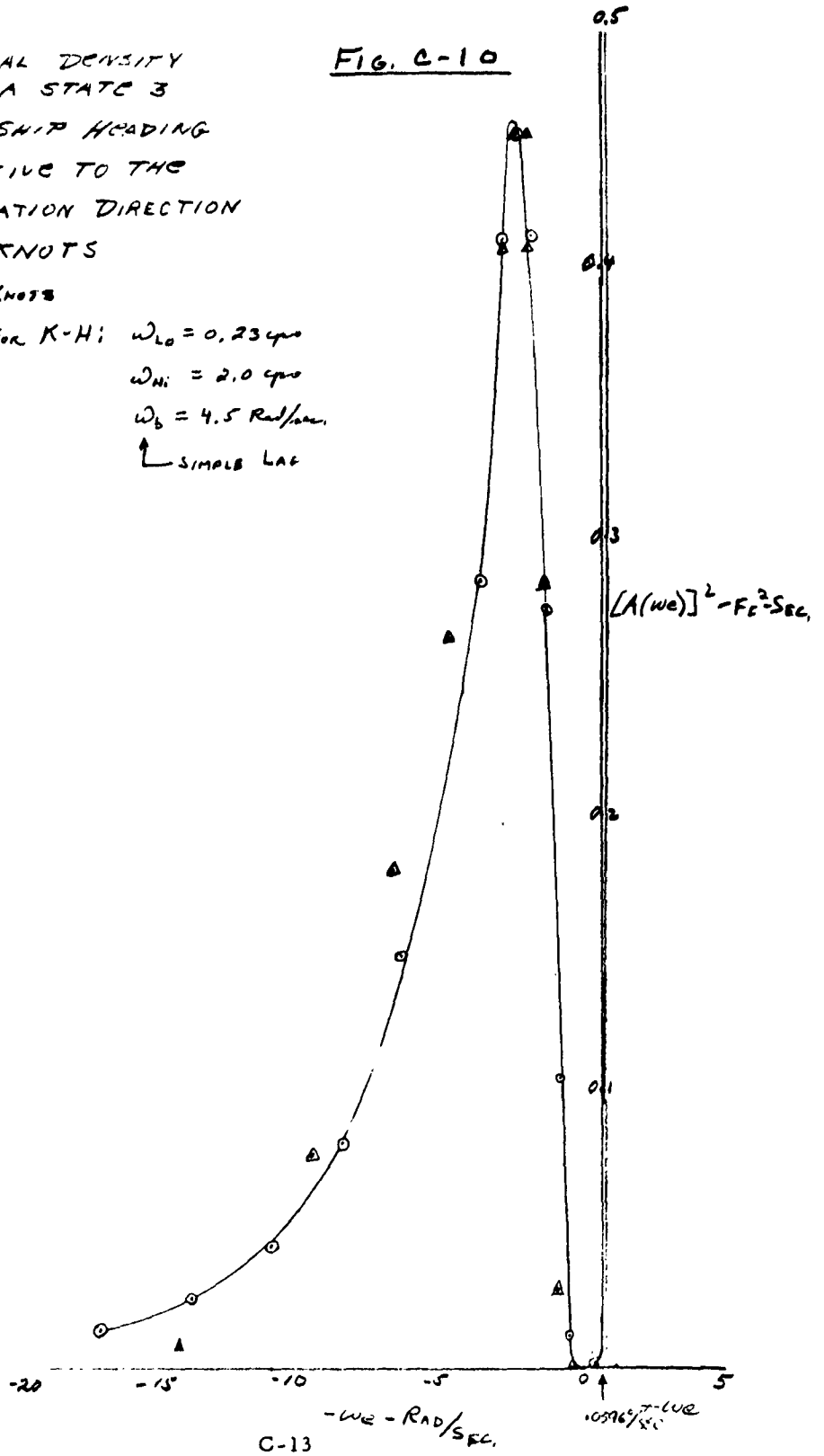

FIG. C-11 - FRONT FOIL TO PORT REAR FOIL AND PORT REAR FOIL TO STARBOARD REAR FOIL PHASE SHIFT VS ω_e (SEA FREQUENCY) FOR 0° INCIDENCE ANGLE IN A STATE 3 SEA

$$\text{BEST FIT } 90^\circ \text{ PHASE SHIFT} = \frac{(s/1.33+1)(s/4-1)}{s(s/6+1)}$$

$$(\omega_e/\omega = 2)$$

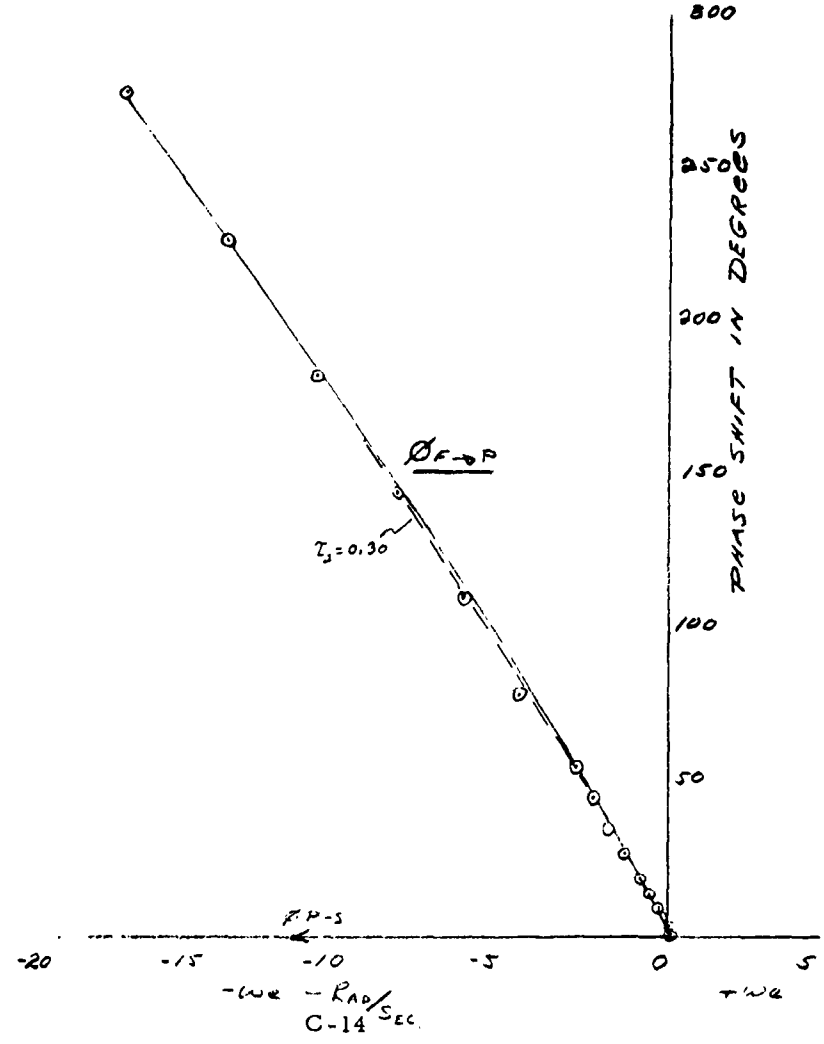

FIG. - C-12

$u = 50$ knots

$\psi_w = 0°$

$\omega_{LO} = 0.1$ c/s
$\omega_{HI} = 1$ c/s
$\omega_b = 3$ RAD/SEC

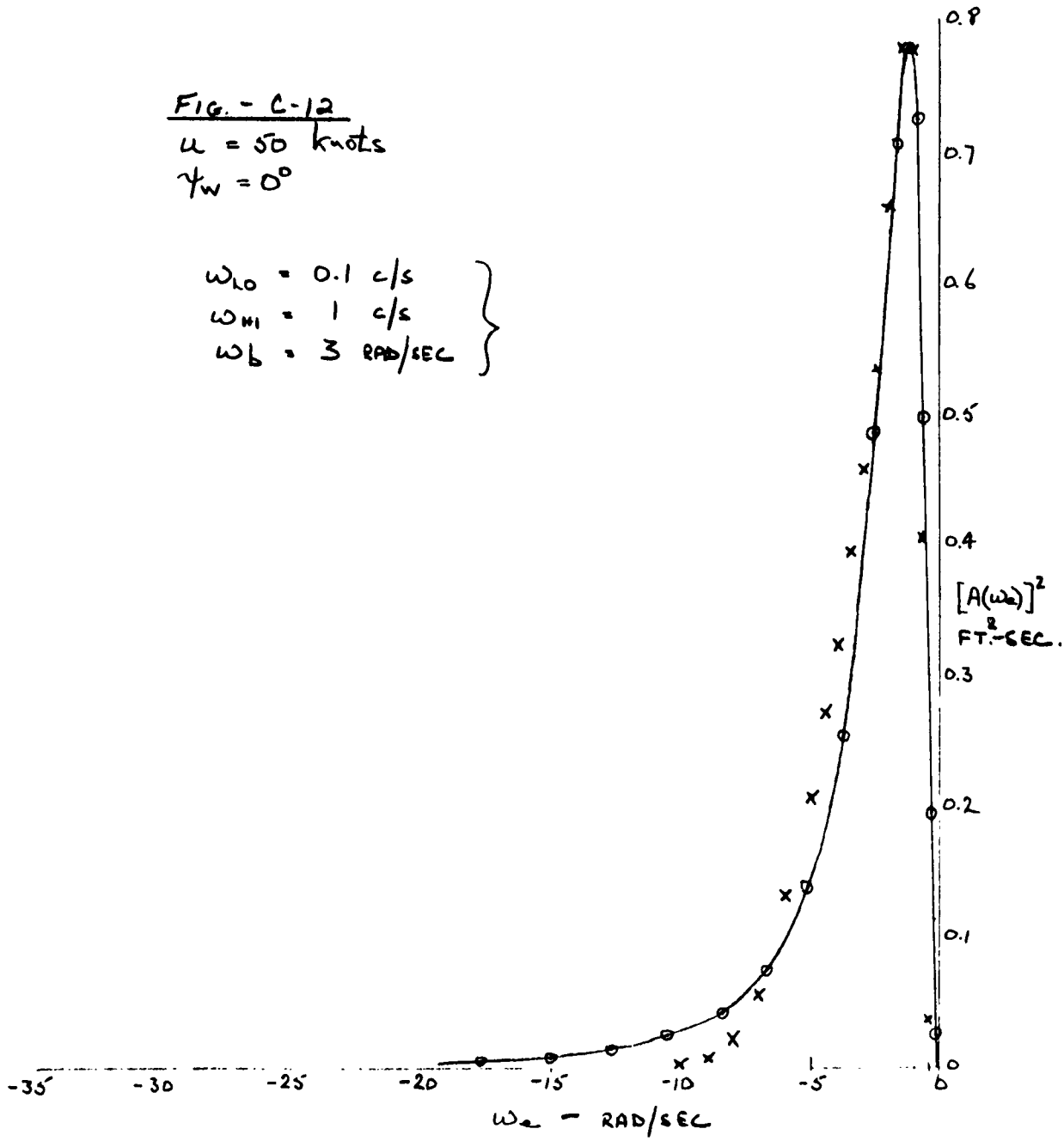

FIG C-13-50 knots — $\psi = 0°$

BEST FIT 90° PHASE SHIFT $\dfrac{0.51\left(\frac{s}{.667}+1\right)\left(\frac{s}{2}-1\right)}{s\left(\frac{s}{3}+1\right)}$

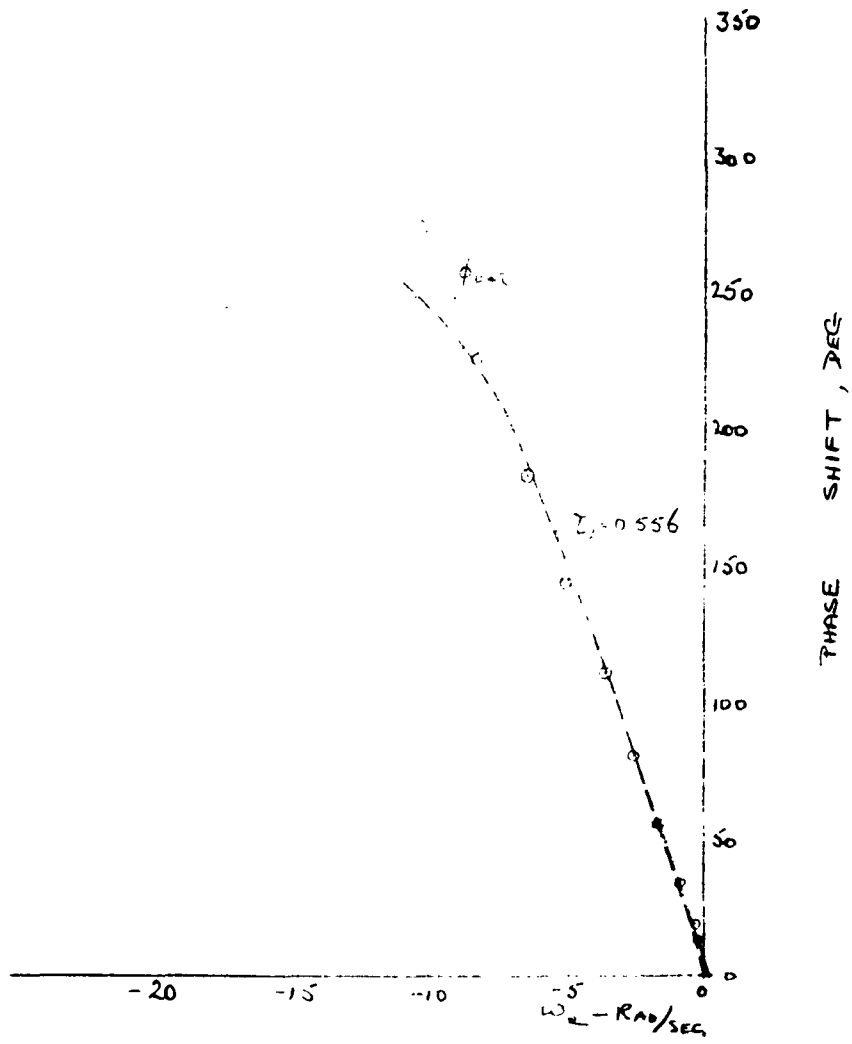

FIG. C-14

U_o = 50 knots.

ψ_w = 45°

ω_{LO} = NOT USED
ω_{HI} = 0.5 c/s
ω_b = 1.2 RAD/SEC

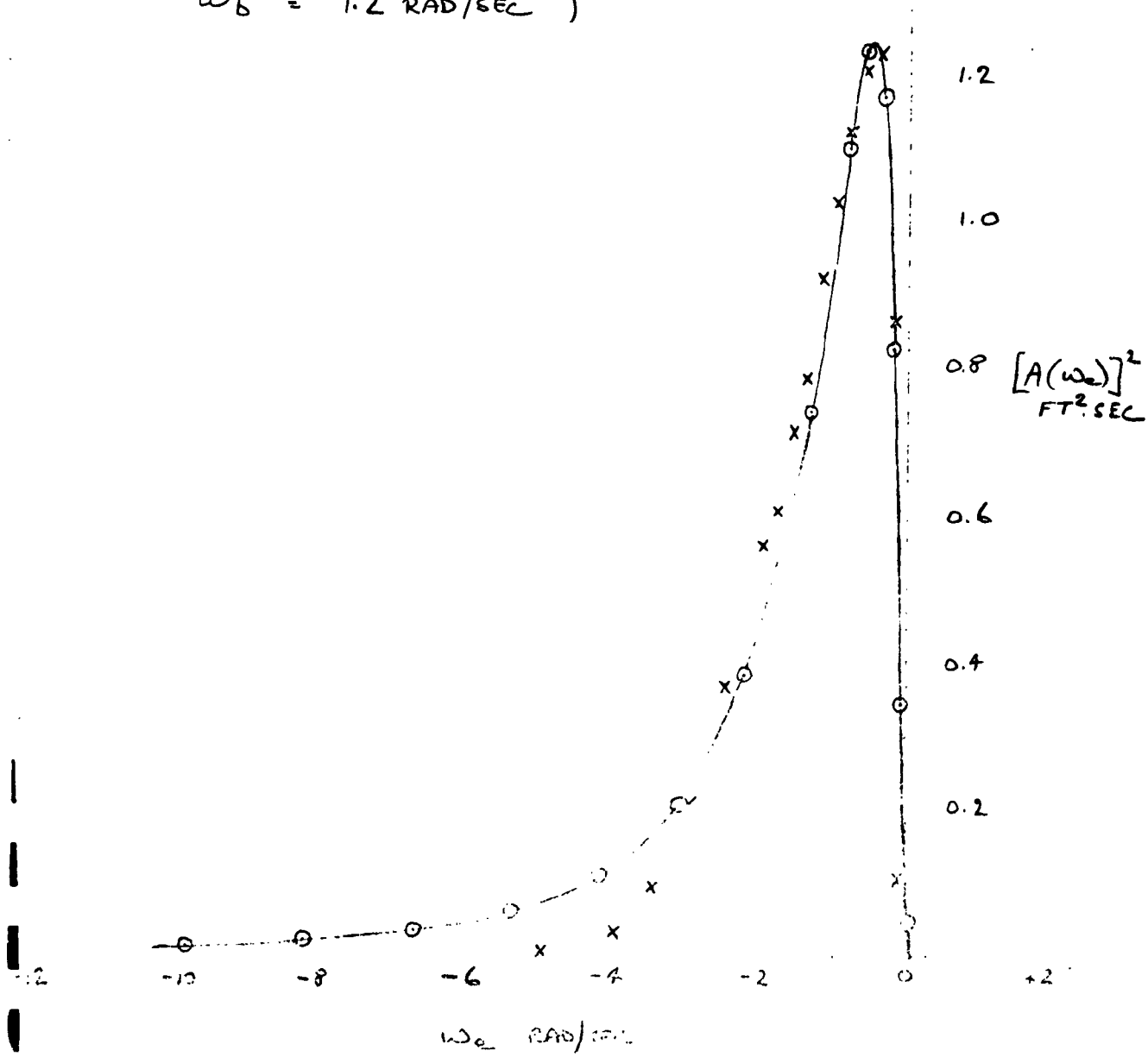

Fig. C-10 10 knots $\psi = 45°$

BEST FIT TO PHASE SHIFT $\cdot 260 \frac{\left(\frac{s}{.333}+1\right)\left(\frac{s}{1}+1\right)}{s\left(\frac{s}{1.5}+1\right)}$

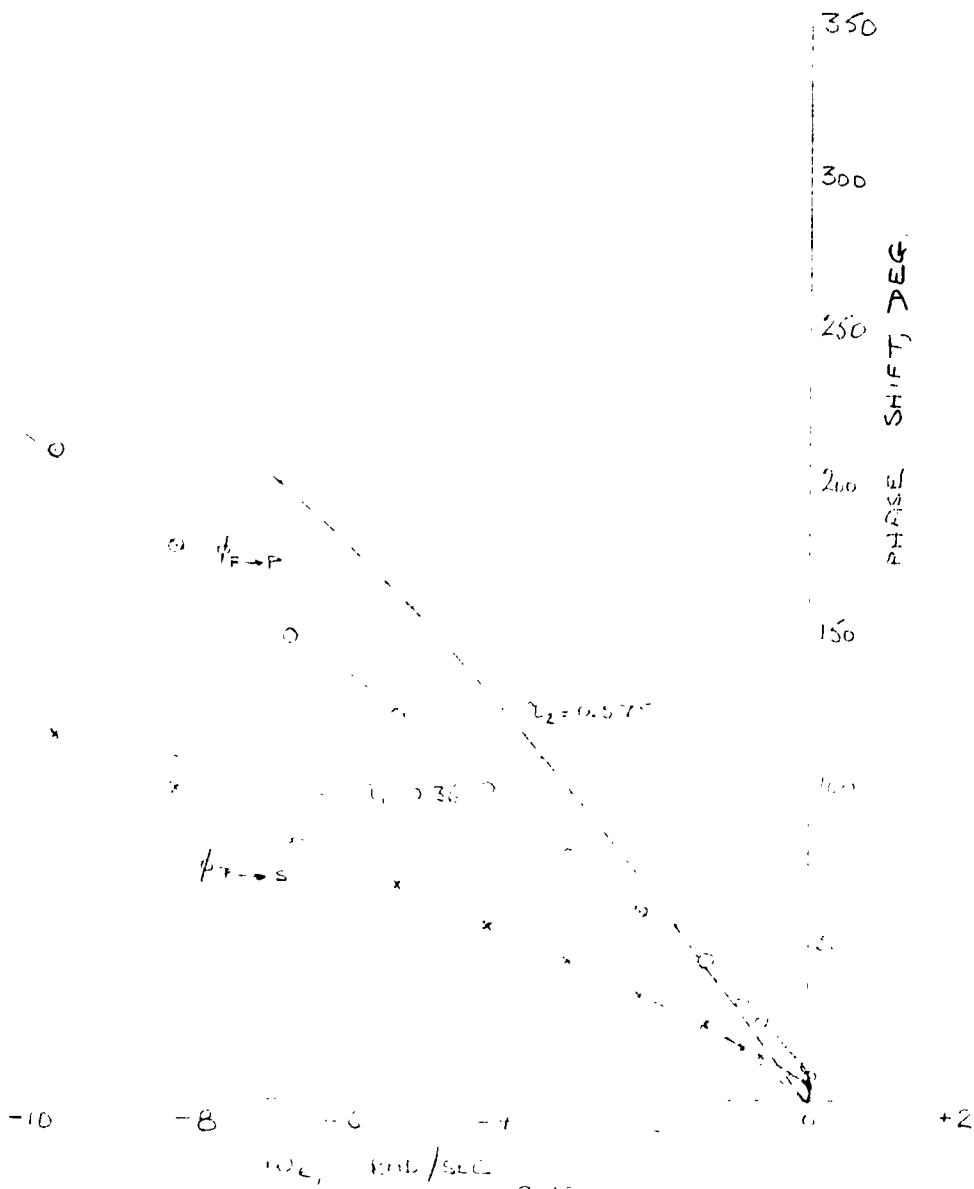

FIG. C-16 – U_o = 50 knots.

ψ = 135°

ω_{n_o} = 1.57 Rad/sec. → .25 g's

ω_{n_c} = 6.9 Rad/sec → 1.1 g's

ω_b = 9.0 rad/sec

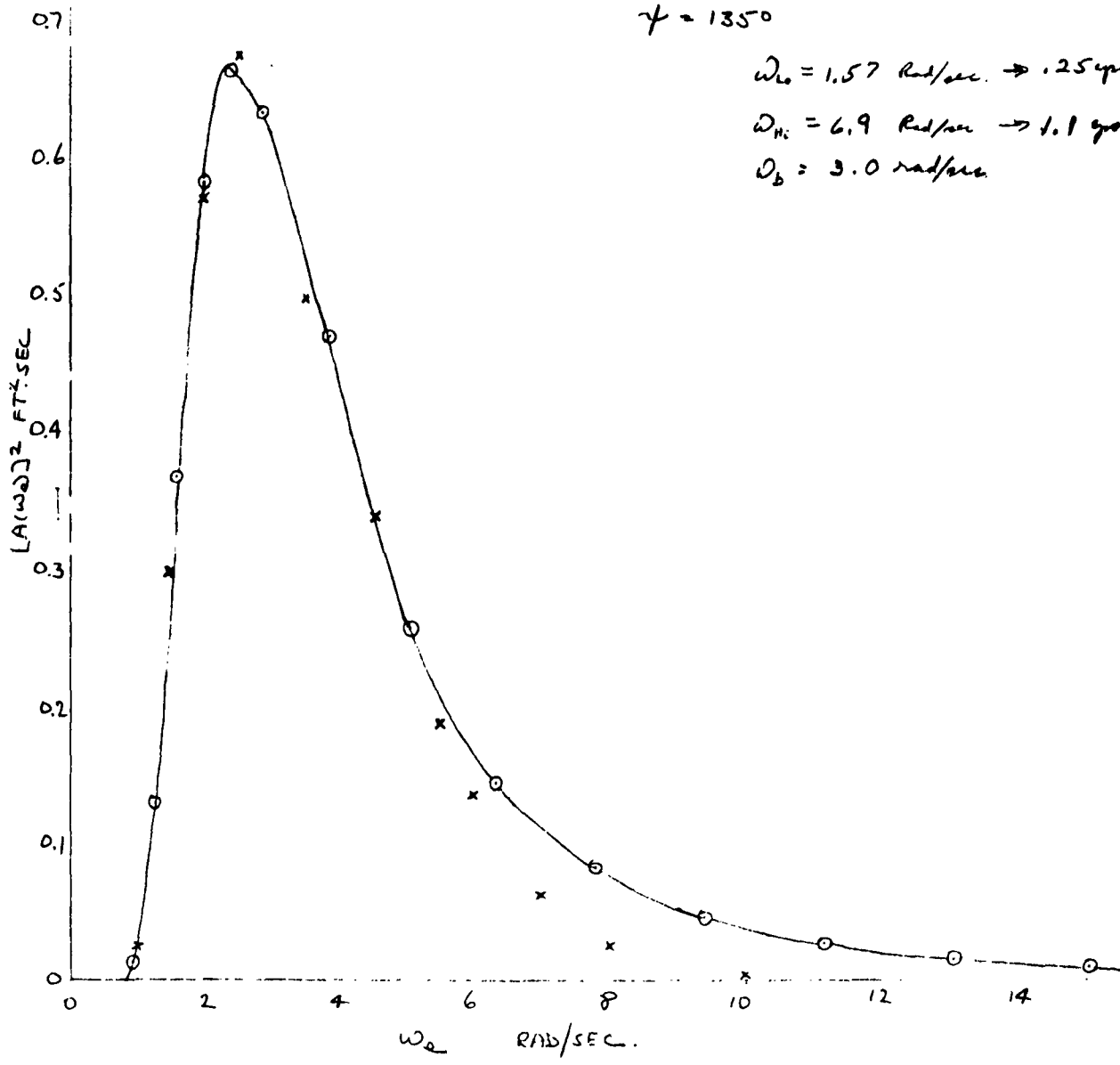

FIG. C-17

BEST FIT 90° PHASE SHIFT $\dfrac{1.02\left(\frac{s}{1.33}+1\right)\left(\frac{s}{4}-1\right)}{s\left(s/6+1\right)}$

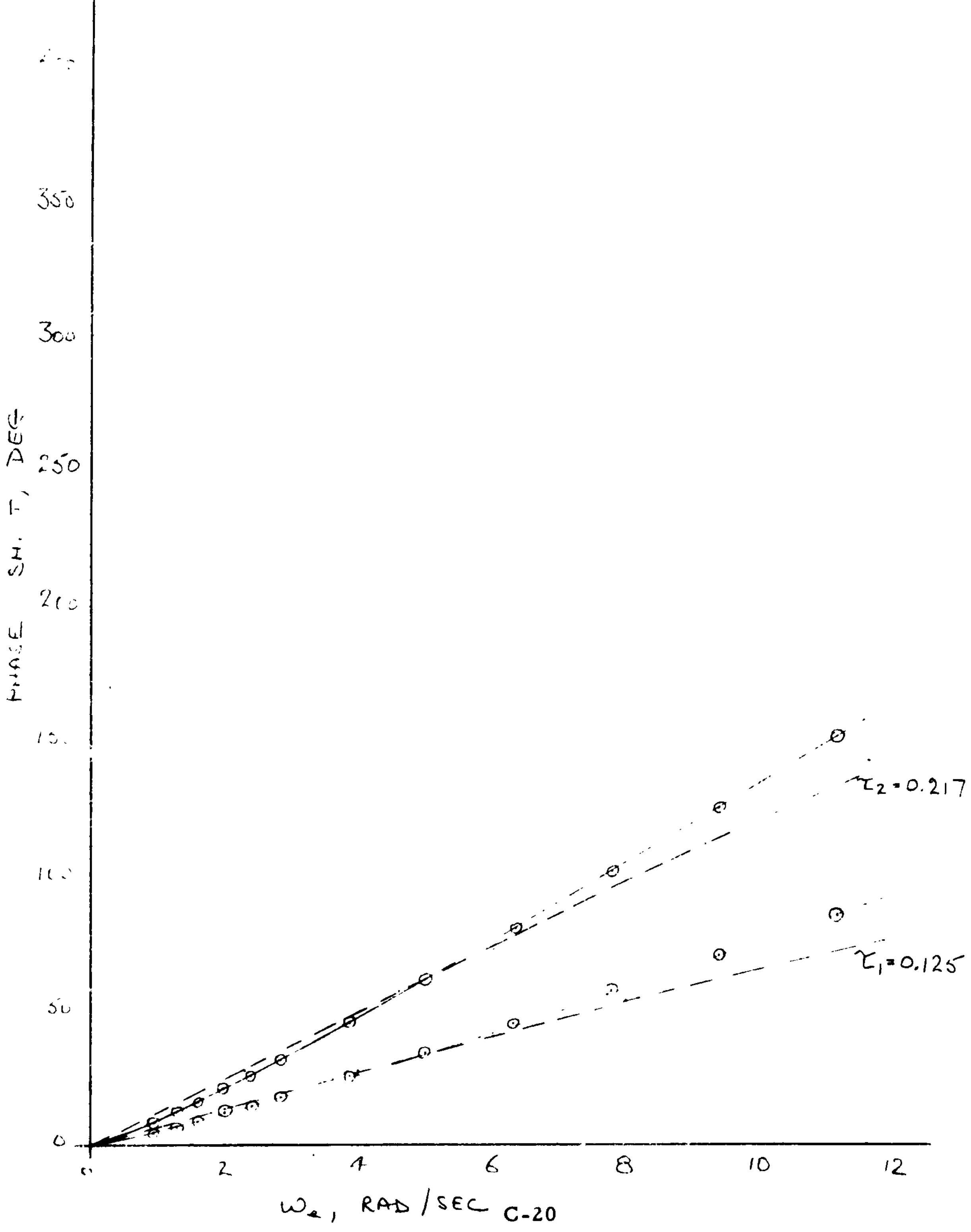

FIG. C-18 - U_o = 50 knots
$\psi_w = 180°$

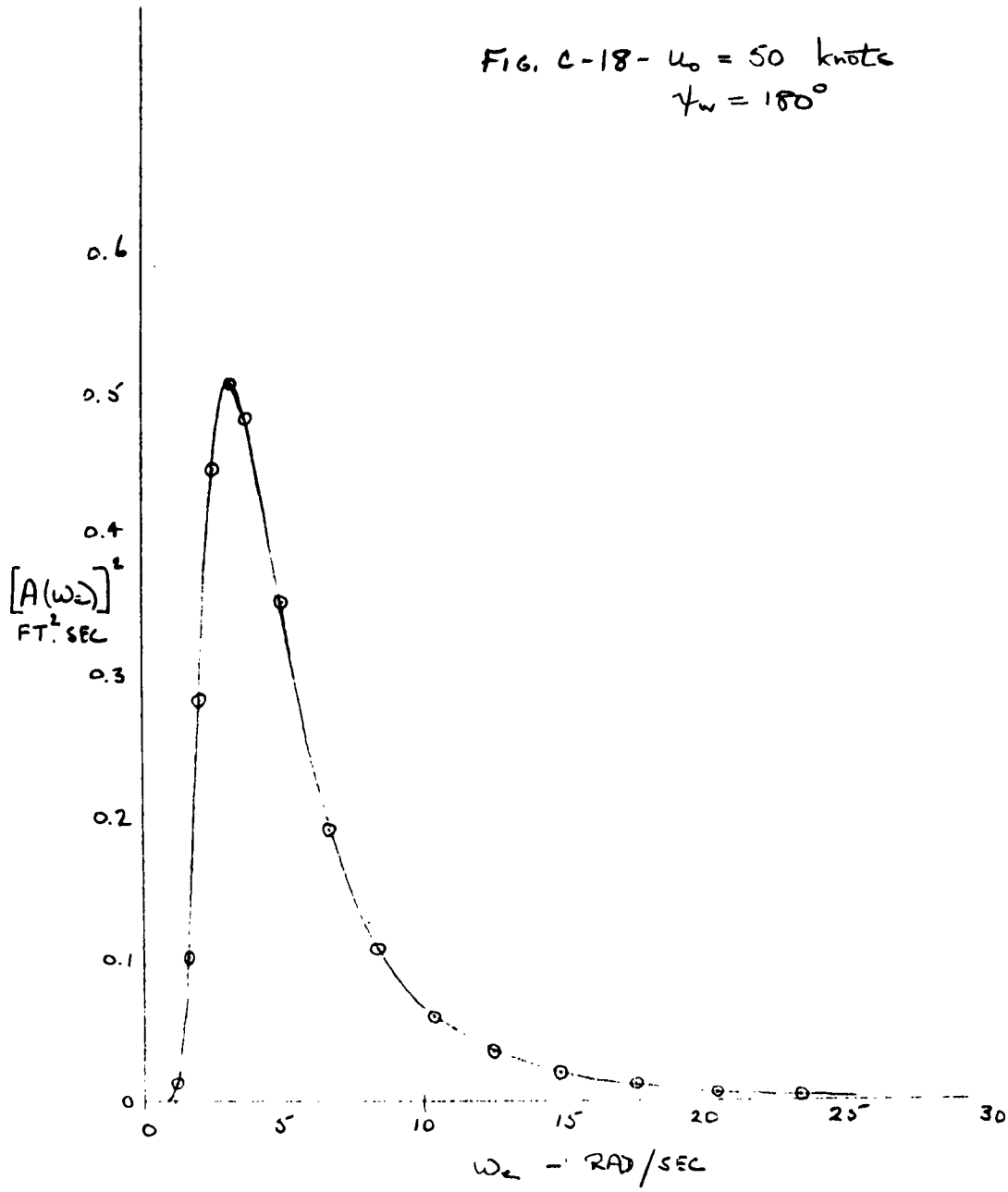

FIG. C-19 350 knots $\gamma = 18.5^\circ$

BEST FIT 90° PHASE SHIFT $\frac{1.553\left(\frac{s}{2}+1\right)\left(\frac{s}{6}-1\right)}{s\left(\frac{s}{9}+1\right)}$

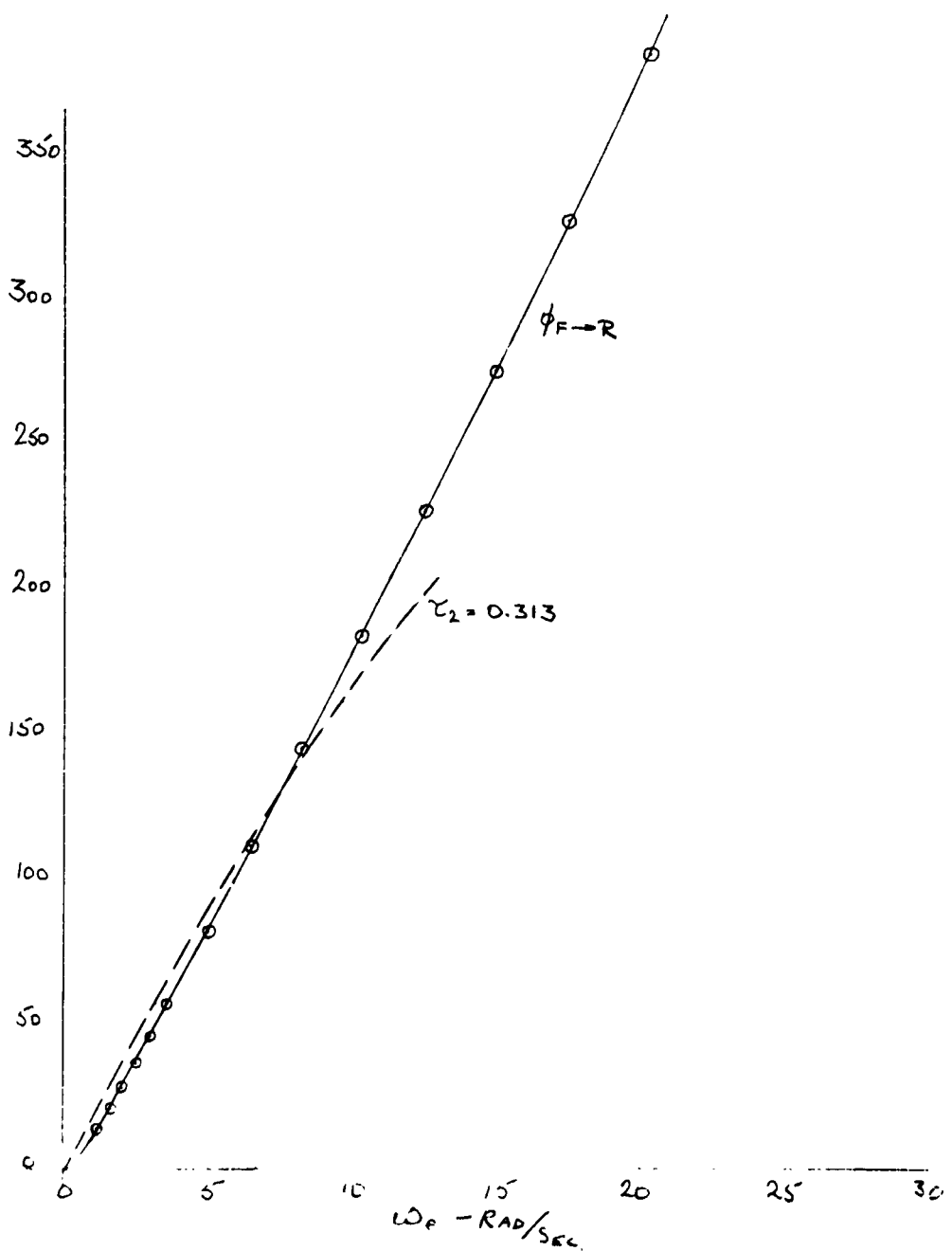

APPENDIX D

EQUATIONS FOR THE TWO-DIMENSIONAL LATERAL SIMULATION

The forces acting on the struts and foils were found using the same methods used to find the stability derivatives. (See Section 5.2) The function shown in Figure 5-2 was used to give the variation of $(S\ \partial C_L/\partial i)$ with depth for all three struts. At a given strut depth, $\partial\ C_L/\partial i$ was taken to be constant. This is a reasonable assumption provided the strut incidences are small so that both sides of each strut remain wetted. A value of 1.0 was used for the lift curve slope of each foil. (See Appendix B.) Provided one surface of a foil is cavitated, this is reasonably accurate. There is a small incidence range (approximately 3 degrees for the foil suggested in Section 3) in which both surfaces of a foil will be wetted, and in this range the lift curve slope will be approximately equal to 2. Because of the relatively narrow incidence range involved, it was believed that the omission of this phenomenon from the simulation would not affect the results appreciably. The effect of depth of the foils from the free surface is small and was ignored, except that broaching was simulated by assuming that the lift force on a foil was zero when it had broached. In some runs, a very approximate simulation of laterally flexible struts was made. (See Section 9.)

The way in which a regular sea was simulated is described in Ref. D-1, Appendix E, from which the simplifying sinusoidal approximation was utilized in the following equations.

Additions to the Glossary

K_{FS}, K_{SS}, K_{PS} - lateral spring stiffness of forward, aft starboard, and aft port struts

y_{FS}, y_{SS}, y_{PS} - lateral deflections of mid-depth of submergence points of forward, aft starboard and aft port struts

v_{FS}, v_{SS}, v_{PS} - lateral velocities, relative to the hull, of the mid-depth of submergence points of forward, rear starboard, and rear port struts.

Subscripts

FS - forward strut
SS - starboard rear strut
PS - port rear strut
SR - mid-span point of rear starboard foil
PR - mid-span point of rear port foil.

Lateral Simulation Equations

These equations were written assuming a canard configuration.

1. $$i_{FS} = \frac{1}{u_o}\left[pd_{FS} - v - \dot{y}_{FS} - r\ell_F - (u_{om})_{FS} \sin\psi_w \right] + \delta_b$$

2. $$i_{SS} = \frac{1}{u_o}\left[pd_{SS} - v - \dot{y}_{SS} + r\ell_R - (u_{om})_{SS} \sin\psi_w \right] + \delta_S$$

3. $$i_{PS} = \frac{1}{u_o}\left[pd_{PS} - v - \dot{y}_{PS} + r\ell_R - (u_{om})_{PS} \sin\psi_w \right] + \delta_S$$

4. $Y_{FS} = \frac{1}{2} \rho u_o^2 i_{FS} \left(\frac{\partial C_L}{\partial i} S \right)_{FS}$

5. $Y_{SS} = \frac{1}{2} \rho u_o^2 i_{SS} \left(\frac{\partial C_L}{\partial i} S \right)_{SS}$

6. $Y_{PS} = \frac{1}{2} \rho u_o^2 i_{PS} \left(\frac{\partial C_L}{\partial i} S \right)_{PS}$

7. $y_{FS} = \frac{Y_{FS}}{K_{FS}}$

8. $y_{SS} = \frac{Y_{SS}}{K_{SS}}$

9. $y_{PS} = \frac{Y_{PS}}{K_{PS}}$

10. $v_{SR} = v + v_{SS} - pd_R - r\ell_R + (u_{om})_{SR} \sin \psi_w$

11. $v_{PR} = v + v_{PS} - pd_R - r\ell_R + (u_{om})_{PR} \sin \psi_w$

12. $w_{SR} = p \frac{b_S}{2} - (w_{om})_{SR}$

13. $w_{PR} = - p \frac{b_S}{2} - (w_{om})_{PR}$

14. $u_{SR} = - r \frac{b_S}{2} - (u_{om})_{SR} \cos \psi_w$

15. $u_{PR} = + r \frac{b_S}{2} - (u_{om})_{PR} \cos \psi_w$

16. $u'_{SR} = \left[a_1\right]_{SR} u_{SR} + \left[a_2\right]_{SR} v_{SR} + \left[a_3\right]_{SR} w_{SR}$

17. $u'_{PR} = \left[a_1\right]_{PR} u_{PR} + \left[a_2\right]_{PR} v_{PR} + \left[a_3\right]_{PR} w_{PR}$

18. $w'_{SR} = \left[c_2\right]_{SR} v_{SR} + \left[c_3\right]_{SR} w_{SR}$

19. $w'_{PR} = \left[c_2\right]_{PR} v_{PR} + \left[c_3\right]_{PR} w_{PR}$

20. $i_{SR} = i_o + \dfrac{w'_{SR}}{\left[a_1\right]_{SR} u_o}$

21. $i_{PR} = i_o + \dfrac{w'_{PR}}{\left[a_1\right]_{PR} u_o}$

22. $(C_L)_{SR} = f(i_{SR})$

23. $(C_L)_{PR} = f(i_{PR})$

24. $-Z'_{SR} = \frac{1}{2}\rho\left(\left[a_1\right]_{SR} u_o\right)^2 S (C_L)_{SR} + \rho\left[a_1\right]_{SR} u_o S C_{L_o} u'_{SR}$ $\zeta_{SR} \geq 0$, $\zeta_{SR} \leq 0$

25. $-Z'_{PR} = \frac{1}{2}\rho\left(\left[a_1\right]_{PR} u_o\right)^2 S (C_L)_{PR} + \rho\left[a_1\right]_{PR} u_o S C_{L_o} u_{PR}$ $\zeta_{PR} \geq 0$, $\zeta_{PR} \leq 0$

26. $Y_{SR} = \left[c_2\right]_{SR} Z'_{SR}$

27. $Y_{PR} = \left[c_2\right]_{PR} Z'_{PR}$

28. $K_{SR} = - Y_{SR} d_R + \left[c_3\right]_{SR} Z'_{SR} \frac{b_S}{2}$

29. $K_{PR} = - Y_{PR} d_R - \left[c_3\right]_{PR} Z'_{PR} \frac{b_S}{2}$

30. $\left[a_1\right]_{SR} = \left[a_1\right]_{PR} = + \cos\Lambda \cos\beta + \sin\Lambda \sin\Gamma \sin\beta$

31. $\left[a_2\right]_{SR} = - \left[a_2\right]_{PR} = + \sin\Lambda \cos\beta - \cos\Lambda \sin\Gamma \sin\beta$

32. $\left[a_3\right]_{SR} = - \left[a_3\right]_{PR} = - \cos\Gamma \sin\beta$

33. $\left[c_2\right]_{SR} = - \left[c_2\right]_{PR} = + \sin\Lambda \sin\beta + \cos\Lambda \sin\Gamma \cos\beta$

34. $\left[c_3\right]_{SR} = \left[c_3\right]_{PR} = + \cos\Gamma \cos\beta$

35. $\beta = \tan^{-1} \left\{\tan\Lambda \sin\Gamma\right\}$

36. $Y = Y_{FS} + Y_{SS} + Y_{PS} + Y_{SR} + Y_{PR}$

37. $N = Y_{FS} \ell_F - (Y_{SS} + Y_{PS} + Y_{SR} + Y_{PR}) \ell_R$

38. $K = - Y_{FS} d_{FS} - Y_{SS} d_{SS} - Y_{PS} d_{PS} + K_{SR} + K_{PR}$

39. $v = \frac{1}{s} \left(\frac{Y}{m} - ru_o\right)$

40. $p = \frac{1}{s} \left(\frac{K}{I_x}\right)$

41. $\phi = p/s$

42. $r = \frac{1}{s} \left(\frac{N}{I_z}\right)$

43. $\psi = r/s$

44. $x'_F = \frac{1}{s} \left\{1/\lambda \ (C - u_o \cos \psi_w)\right\}$

45. $x'_{PR} = x'_{PS} = x'_F + \ell/\lambda \cos \psi_w - \frac{b_S}{2\lambda} \sin \psi_w$

46. $x'_{SR} = x'_{SS} = x'_F + \ell/\lambda \cos \psi_w + \frac{b_S}{2\lambda} \sin \psi_w$

47. $\zeta_F = \frac{H}{2} \cos (2\pi x'_F) + (z'\lambda)_F$

48. $\zeta_{PR} = \zeta_{PS} = \frac{H}{2} \cos (2\pi x'_{PR}) + (z'\lambda)_R - \frac{b_S}{2} \phi$

49. $\zeta_{SR} = \zeta_{SS} = \frac{H}{2} \cos (2\pi x'_{SR}) + (z'\lambda)_R + \frac{b_S}{2} \phi$

50. $d_{FS} = d_F - \frac{1}{2} \zeta_F$

51. $d_{PS} = d_R - \frac{1}{2} \zeta_{PR}$

52. $d_{SS} = d_R - \frac{1}{2} \zeta_{SR}$

53. $z'_{FS} = \frac{1}{\lambda} \left[(z'\lambda)_F - \frac{1}{2} \zeta_F\right]$

54. $(u_{om})_{FS} = \frac{CH}{\lambda} \cos (2\pi x'_F) \pi e^{-2\pi z'_{FS}}$

---

* Note that these primed variables are defined in Reference D-1.

55. $z'_{PS} = \frac{1}{\lambda} \left[(z'\lambda)_{PR} - \frac{1}{2} \zeta_{PR} \right]$

56. $(u_{om})_{PS} = \frac{CH}{\lambda} \cos (2\pi x'_{PR}) \pi e^{-2\pi z'_{PS}}$

57. $z'_{PR} = \frac{1}{\lambda} \left[(z'\lambda)_{R} - \frac{b_S}{2} \phi \right]$

58. $(u_{om})_{PR} = \frac{CH}{\lambda} \cos (2\pi x'_{PR}) \pi e^{-2\pi z'_{PR}}$

59. $(w_{om})_{PR} = \frac{CH}{\lambda} \sin (2\pi x'_{PR}) \pi e^{-2\pi z'_{PR}}$

60. $z'_{SS} = \frac{1}{\lambda} \left[(z'\lambda)_{SR} - \frac{1}{2} \zeta_{SR} \right]$

61. $(u_{om})_{SS} = \frac{CH}{\lambda} \cos (2\pi x'_{SR}) \pi e^{-2\pi z'_{SS}}$

62. $z'_{SR} = \frac{1}{\lambda} \left[(z'\lambda)_{R} + \frac{b_S}{2} \phi \right]$

63. $(u_{om})_{SR} = \frac{CH}{\lambda} \cos (2\pi x'_{SR}) \pi e^{-2\pi z'_{SR}}$

64. $(w_{om})_{SR} = \frac{CH}{\lambda} \sin (2\pi x'_{SR}) \pi e^{-2\pi z'_{SR}}$

65. $\left(\frac{\partial C_L}{\partial_i} S \right)_{FS} = f(\zeta_F)$

66. $\left(\frac{\partial C_L}{\partial_i} S \right)_{SS} = f(\zeta_{SR})$

67. $\left(\frac{\partial C_L}{\partial_i} S \right)_{PS} = f(\zeta_{PR})$

Reference

D-1 Appendixes To The Engineering Summary Report on a Hydrofoil System Design Study Program. NObs - 84498, January, 1962. RCA.

APPENDIX E

EQUATIONS FOR THE TWO-DIMENSIONAL LONGITUDINAL SIMULATION

The following equations have been implemented on the analog computer for studies of the longitudinal control of the high-speed test craft. They are, in general, partially linearized and are analogous to the equations presented in Section 6.
However, they are derived in a vertical-horizontal coordinate system which accounts for the new variable (h_{GV}) representing vertical heave of the C.G., and are somewhat simplified by the condition that $\theta_o = 0$. Products of variables, in general have been neglected.

E.1 VERTICAL ACCELERATION

$$m_H \ddot{h}_{GV} \approx n_F \left\{ R_F' \cos \eta_{F_o} - (\eta_F' + \theta) R_{F_o} \sin \eta_{F_o} \right\}$$
$$+ n_R \left\{ R_R' \cos \eta_{R_o} - (\eta_R' + \theta) R_{R_o} \sin \eta_{R_0} \right\} + T_o \theta \qquad \text{E-1}$$

where static equilibrium required that:

$$n_F R_{F_o} \cos \eta_{F_o} + n_R R_{R_o} \cos \eta_{R_o} - m_H g = 0 \qquad \text{E-2}$$

$$R_F = R_{F_o} + R_F' \qquad R_R = R_{R_o} + R_R'$$

$$\eta_F = \eta_{F_o} + \eta_F' \qquad \eta_R = \eta_{R_o} + \eta_R'$$

$T = T_o + T'$ since $\theta_o = 0$; $\theta = \theta'$ for all following equations

also $\xi_{F_o} = \xi_{R_o} = 0$ so that $\xi_F = \xi'_F$;

$\xi_R = \xi'_R$

(θ is assumed small at all times and therefore is treated as a perturbation quantity. Thus $R'_F\theta$, $R'_F\eta'_F$, $R'_R\theta$, $R'_R\eta'_R + T'\theta$ are neglected.)

E.2 PITCHING ACCELERATION

Again, products of perturbation quantities have been neglected.

$$I_y\ddot{\theta} \approx n_F \left[R'_F \left\{ \ell_{HF} \cos \eta_{F_o} - d_{HF} \sin \eta_{F_o} \right\} - \eta'_F R_{F_o} \times \left\{ \ell_{HF} \sin \eta_{F_o} + d_{HF} \cos \eta_{F_o} \right\} \right]$$

$$+ n_R \left[-R'_R \left\{ \ell_{HR} \cos \eta_{R_o} + d_{HR} \sin \eta_{R_o} \right\} + \eta'_R R_{R_o} \times \left\{ \ell_{HR} \sin \eta_{R_o} - d_{HR} \cos \eta_{R_o} \right\} \right]$$

$$+ n_F M'_{\bar{F}} + n_R M'_{\bar{R}} - T' d_T \qquad \text{E-3}$$

and static equilibrium results in: -

$$n_F R_{F_o}\left\{\ell_{HF}\cos\eta_{F_o} - d_{HF}\sin\eta_{F_o}\right\} - n_R R_{R_o}$$

$$\chi\left\{\ell_{HR}\cos\eta_{R_o} + d_{HR}\sin\eta_{R_o}\right\} + n_F M_{\overline{F}_o} + n_R M_{\overline{R}_o} - T_o d_T = 0$$

E.2.1 PITCHING MOMENT PERTURBATION DUE TO STRUTS

The pitching moment equations may be written as:

$$M'_{\overline{F}} = -\left(D'_{\overline{F}} A_{\overline{F}_o} + D_{\overline{F}_o} A'_{\overline{F}} + D'_{\overline{F}} A'_{\overline{F}}\right) \qquad \text{E-4}$$

where $A_{\overline{F}}$ is the effective lever arm of the strut drag.

The third non-linear term is included since it is likely to be of equal magnitude to the linear terms.

Similarly,

$$M'_{\overline{R}} = -\left(D'_{\overline{R}} A_{\overline{R}_o} + D_{\overline{R}_o} A'_{\overline{R}} + D'_{\overline{R}} A'_{\overline{R}}\right) \qquad \text{E-5}$$

and

$$A'_{\overline{F}} \approx -\eta'_F \curlywedge_{F_o} \sin\eta_{F_o} - \theta\left(\ell_{HF} + \curlywedge_{F_o} \sin\eta_{F_o}\right)$$

$$+ \xi_F \cos\eta_{F_o} - \zeta'_{F/2} \qquad \text{E-6}$$

and, for static equilibrium: -

$$A_{\overline{F}_o} = d_{HF} + \overline{\overline{F}}_{F_o} \cos \eta_{F_o} - \frac{\zeta_{F_o}}{2} \qquad \text{E-7}$$

$$D_{\overline{F}_o} = \beta_1 \zeta_{F_o}$$

$$= \beta_1 \left(d_{HF} + \overline{\overline{F}}_{F_o} \cos \eta_{F_o} - h_{G_o} \right) \qquad \text{E-8}$$

where $\beta_1 = C_{D\overline{F}} \frac{\rho}{2} C_{\overline{F}} u^2$

Similarly: -

$$A'_R = - \eta'_R \overline{\overline{R}}_{R_o} \sin \eta_{R_o} + \theta \left(\ell_{HR} - \overline{\overline{R}}_{R_o} \sin \eta_{R_o} \right)$$

$$+ \xi_R \cos \eta_{R_o} - \zeta'_R/2 \qquad \text{E-8}$$

E.2.2 STRUT DRAG INCREMENTS

$$D'_{\overline{F}} = \beta_1 \zeta'_F \qquad \text{E-9}$$

$$D'_R = \beta_2 \zeta'_R \qquad \text{E-10}$$

E.2.3 FOIL SUBMERGENCE

(From Equation 2-7, Progress Report No. 3)

$$\zeta_F' \approx -\eta_F' \, \Xi_{F_o} \sin \eta_{F_o} - \theta \left(\ell_{HF} + \Xi_{F_o} \sin \eta_{F_o} \right)$$

$$+ \xi_F \cos \eta_{F_o} - h_{GV}' + h_{WF} \qquad \text{E-11}$$

with

$$\zeta_{F_o} - d_{HF} - \Xi_{F_o} \cos \eta_{F_o} + h_{GV_o} = 0 \text{ for equilibrium}$$

and

$$\zeta_R' \approx -\eta_R' \, \Xi_{R_o} \sin \eta_{R_o} + \theta \left(\ell_{HR} - \Xi_{R_o} \sin \eta_{R_o} \right)$$

$$+ \xi_R \cos \eta_{R_o} - h_{GV}' + h_{WR} \qquad \text{E-12}$$

also with

$$\zeta_{R_o} - d_{HR} - \Xi_{R_o} \cos \eta_{R_o} + h_{GV_o} = 0 \text{ for equilibrium.}$$

E.3 FOIL REACTION.

$$R'_F = R'_{CF} - K_F \xi_F \qquad \text{E-13}$$

$$R'_R = R'_{CR} - K_R \xi_R \qquad \text{E-14}$$

E.3.1 FOIL ACCELERATION

$$a_F \approx \ddot{\theta} \left\{ d_{HF} \sin \eta_{F_O} - \ell_{HF} \cos \eta_{F_O} \right\} + \ddot{\xi}_F - \ddot{h}'_{GV} \cos \eta_{F_O} \qquad \text{E-15}$$

and, by analogy:

$$a_R \approx \ddot{\theta} \left\{ d_{HR} \sin \eta_{R_O} + \ell_{HR} \cos \eta_{R_O} \right\} + \ddot{\xi}_R - \ddot{h}'_{GV} \cos \eta_{R_O} \qquad \text{E-16}$$

E.3.2 FOIL KINEMATICS

$$m_F a_F = R'_F - F'_F \qquad \text{E-17}$$

where static equilibrium requires:

$$R_{F_O} - F_{F_O} + m_F g \cos (\eta_{F_O} + \theta_O) = 0$$

similarly:

$$m_R a_R = R'_R - F'_R \qquad \text{E-18}$$

$$\text{and } R_{R_O} - F_{R_O} + m_R g \cos (\eta_{R_O}) = 0$$

E.4 FOIL HYDRODYNAMIC NORMAL FORCES

$$F'_F = \left(\frac{C'_{L_{CF}}}{\cos(\theta_o + \eta_{F_o})} + C_{N_{I_F}} \right) \frac{\rho}{2} S_F u^2 \qquad \text{E-19}$$

$$F'_R = \left(\frac{C'_{L_{CR}}}{\cos(\theta_o + \eta_{R_o})} + C_{N_{I_R}} \right) \frac{\rho}{2} S_R u^2 \qquad \text{E-20}$$

E.4.1 NORMAL FORCE COEFFICIENT INCREMENT DUE TO CIRCULATION

$$\frac{C'_{L_{CF}}}{\cos(\theta_o + \eta_{F_o})} \simeq (e_F + b_F i_F) \; f(\zeta_F) - C_{NC_{F_O}} \qquad \text{E-21}$$

$$\frac{C'_{L_{CR}}}{\cos(\theta_o + \eta_{R_o})} \simeq (e_R + b_R i_R) \; f(\zeta_R) - C_{NE_{R_O}} \qquad \text{E-22}$$

where $f(\zeta_F)$, $f(\zeta_R)$ are shown in Figure E-1.

where:

$$C_{NC_{F_O}} = (e_F + b_F \, i_{F_O}) \, f(\zeta_{F_O})$$

and

$$C_{NC_{R_O}} = (e_R + b_R i_{R_O}) \, f(\zeta_{R_O})$$

E.4.2 INSTANTANEOUS FOIL INCIDENCES

$$i_F + \eta_{F_O} + \eta'_F + \theta + \frac{1}{u}\left[\dot{\xi}_F \cos \eta_{F_O} - \dot{h}'_{GV} - \dot{\theta}\left\{\ell_{HF} + \overline{FO} \sin \eta_{FO}\right\}\right.$$

$$\left. - w_{OMF} - \dot{\eta}'_F \overline{FO} \sin \eta_{FO}\right] \qquad \text{E-23}$$

$$i_R + \eta_{R_O} + \eta'_R + \theta + \frac{1}{u}\left[\dot{\xi}_R \cos \eta_{R_O} - \dot{h}'_{GV} + \dot{\theta}\left\{\ell_{HR} - \overline{RO} \sin \eta_{RO}\right\}\right.$$

$$\left. - w_{OMR} - \dot{\eta}'_R \overline{RO} \sin \eta_{RO}\right] \qquad \text{E-24}$$

E.4.3 INERTIAL NORMAL FORCE COEFFICIENT

$$C_{N_{I_F}} = 1.063 \frac{C_F^2}{u} (a_F - \dot{w}_{OMF} \qquad \text{E-25}$$

$$C_{N_{I_R}} = 1.063 \frac{C_R^2}{u} (a_R - \dot{w}_{OMR}) \qquad \text{E-26}$$

E.5 STATIC EQUILIBRIUM OF DRAG AND THRUST FORCES

$$n_F R_{F_O} \sin \eta_{F_O} + n_R R_{R_O} \sin \eta_{R_O} + n_F D_{\overline{F}_O} + n_R D_{\overline{R}_O} + D_{A_O} - T_O = 0$$

where D_{A_O} = air drag E-27

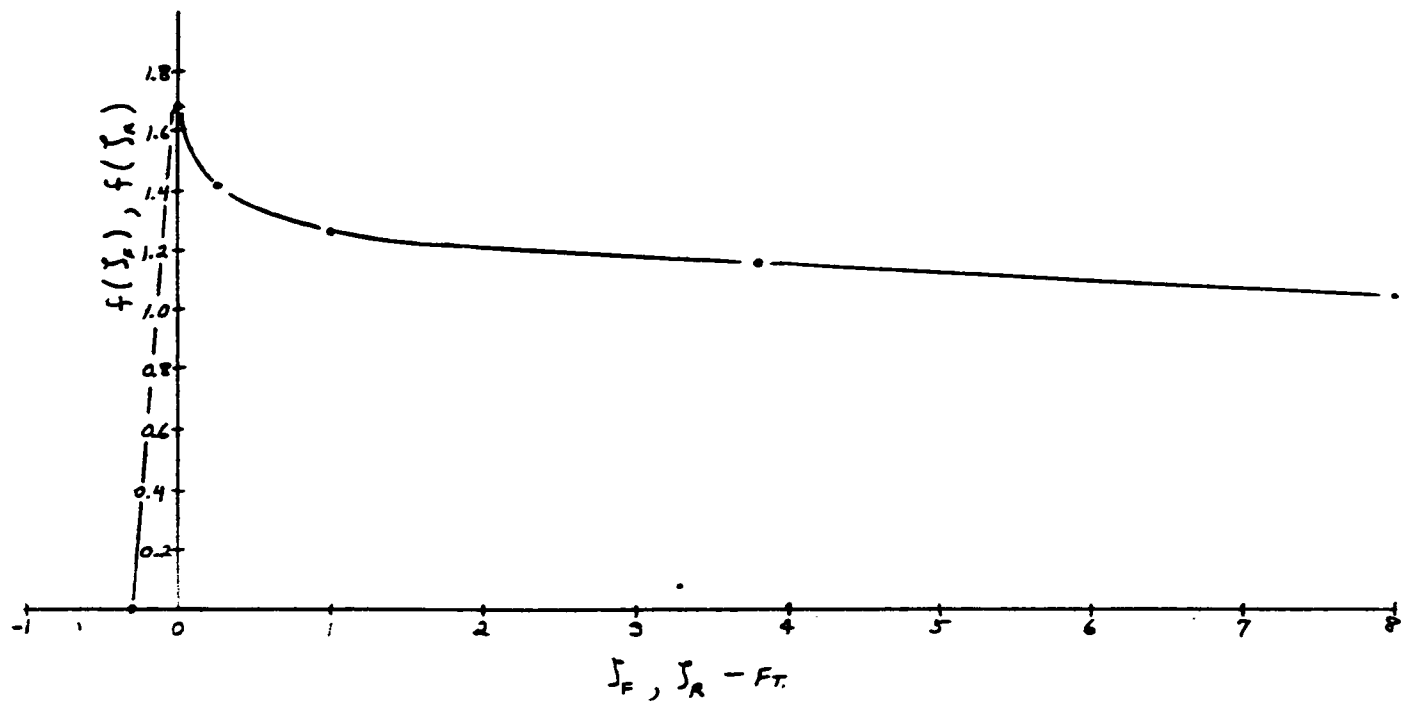

Fig. E-1. LIFT SUBMERGENCE FUNCTION VS. DEPTH OF SUBERGENCE

APPENDIX F

EQUATIONS FOR THE THREE-DIMENSIONAL (6 DEGREES-OF-FREEDOM) SIMULATION

The following equations have been implemented on the analog computer to represent the craft dynamics in 6 degrees of freedom.

A conventional body centered coordinate system has been chosen with the origin at the craft C.G., the x-axis positive forward, y-axis positive toward the starboard side, and the z-axis positive downward. Although most of the symbols used have been defined in the final report. definitions will be included here for completeness.

HULL DYNAMICS

$$\dot{u} = \frac{X}{m_T} - q\,w + r\,v \qquad \text{F-1}$$

$$\dot{v} = \frac{Y}{m_T} - r\,u + p\,w \qquad \text{F-2}$$

$$\dot{w} = \frac{Z}{m_H} - p\,v + q\,u \qquad \text{F-3}$$

$$\dot{p} = \frac{K}{I_x} - \left(\frac{I_z - I_y}{I_x}\right) q\,r \qquad \text{F-4}$$

$$\dot{q} = \frac{M}{I_y} + \frac{\left(I_z - I_x\right)}{I_y} r\,p \qquad \text{F-5}$$

$$\dot{r} = \frac{N}{I_z} - \frac{\left(I_y - I_x\right)}{I_z} p\,q \qquad \text{F-6}$$

$$\dot{\theta} \approx q - r\,\phi \qquad \text{F-7}$$

$$\dot{\phi} \approx p + r\,\theta \qquad \text{F-8}$$

$$\dot{\psi} \approx q\,\phi + r \qquad \text{F-9}$$

$$\dot{z} \approx w - u\,\theta = -\dot{h}_G \qquad \text{F-10}$$

X, Y, Z are forces along x, y, z axes.

u, v, w are linear velocities along x, y, z axes.

K, M, N are moments about x, y, z axes.

p, q, r are angular velocities about x, y, z axes.

ψ, θ, ϕ are heading, pitch and roll angles.

m_T is total mass of craft

m_H is mass of hull

I_x, I_y, I_z are moments of inertia about x, y, z axes

CRAFT GEOMETRY

$$\ell_F \approx \ell_{HF} + \overline{\overline{\wedge}}\, F_o\ \eta_F \qquad \text{F-11}$$

$$d_F \approx d_{HF} + \overline{\overline{\wedge}}\, F_o + \xi_F \qquad \text{F-12}$$

$$\ell_{SR} \approx \ell_{HR} - \overline{\overline{\wedge}}\, R_o\ \eta_{SR} \qquad \text{F-13}$$

$$d_{SR} \approx d_{HR} + \overline{\overline{HR}} \; R_o + \xi_{SR} \qquad \text{F-14}$$

$$\ell_{PR} \approx \ell_{HR} - \overline{\overline{HR}} \; R_o \; \eta_{PR} \qquad \text{F-15}$$

$$d_{PR} \approx d_{HR} + \overline{\overline{HR}} \; R_o + \xi_{PR} \qquad \text{F-16}$$

Subscript F refers to fore foil
Subscript R refers to aft foils
Subscript SR refers to starboard aft foil
Subscript PR refers to port aft foil
Subscript HF refers to forward hinge point
Subscript HR refers to aft hinge point
Subscript o refers to reference conditions.

ℓ is distance in x direction from C. G.
d is distance in z direction from C. G.
η is foil rotation
ξ is spring deflection
$\overline{\overline{HR}}$ is nominal distance along strut from hinge point to foil.

FOIL DYNAMICS

$$\ddot{\xi}_F = a_{\overline{GF}} - \frac{X}{m_T}\eta_F - \frac{Z}{m_H} + \overline{\overline{GF}}_o \left\{(\dot{\eta}_F + q)^2 + p^2\right\}$$

$$-\ell_{HF}(pr - \dot{q}) + d_{HF}\,p^2 \qquad \text{F-17}$$

$$\ddot{\xi}_{SR} = a_{\overline{GSR}} - \frac{X}{m_T}\,\eta_{SR} - \frac{Z}{m_H} + \overline{\overline{\wedge}}_{GRo}\left\{(\dot{\eta}_{SR} + q)^2 + p^2\right\}$$

$$+ \ell_{HR}(pr - \dot{q}) + d_{HR}\,p^2 - \frac{bs}{2}(q\,r + \dot{p}) \qquad \text{F-18}$$

$$\ddot{\xi}_{PR} = a_{\overline{GRP}} - \frac{X}{m_T}\,\eta_{PR} - \frac{Z}{m_H} + \overline{\overline{\wedge}}_{GRo}\left\{(\dot{\eta}_{PR} + q)^2 + p^2\right\}$$

$$+ \ell_{HR}(pr - \dot{q}) + d_{HR}\,p^2 + \frac{bs}{2}(qr + \dot{p}) \qquad \text{F-19}$$

$$a_{\overline{GF}} = \frac{1}{m_F}\left\{m_F g - K_F \xi_F + R_{CF} - F_F\right\} \qquad \text{F-20}$$

$$a_{\overline{GSR}} = \frac{1}{m_R}\left\{m_R g - K_R\,\xi_{SR} + R_{CSR} - F_{SR}\right\} \qquad \text{F-21}$$

$$a_{\overline{GPR}} = \frac{1}{m_R}\left\{m_R g - K_R\,\xi_{PR} + R_{CPR} - F_{PR}\right\} \qquad \text{F-22}$$

These equations are written for laterally unconstrained aft foils. With laterally constrained aft foils, the following primed quantities are used in place of the unprimed quantities.

$$a'_{GSR} = a_{\overline{GSR}} + \frac{F_B}{m_R} \qquad \text{F-23}$$

$$a'_{\overline{GPR}} = a_{\overline{GPR}} - \frac{F_B}{m_R} \qquad \text{F-24}$$

$$\frac{F_B}{m_R} = \frac{1}{2m_R}\left(R_{CPR} - R_{CSR} + F_{SR} - F_{PR}\right)$$

$$+ \frac{1}{2}\left[\overline{\overline{\wedge}}_{GRo}\left\{(\dot{\eta}_{PR} + q)^2 - (\dot{\eta}_{SR} + q)^2\right\} + b_s\,(q\,r + \dot{p})\right] \qquad \text{F-25}$$

$\overset{\smile}{\frown}_G$ is nominal distance along strut from hinge point to C. G sprung foil strut mass

m_F is mass of forward sprung foil and strut

m_R is mass of each aft sprung foil and strut

b_s is distance in y direction between aft struts

g is acceleration due to gravity

K_F is forward spring stiffness

K_R is aft spring stiffness

R_C is control reaction force

F is total normal force on foil

F_B is aft foil laterally constraining force

FOIL VELOCITIES

$$u_F \approx u + (d_{HF} + \overset{\smile}{\frown} F_o)\, q + \overset{\smile}{\frown} F_o\, \dot{\eta}_F - (u_{om})_F \cos\psi_w \qquad \text{F-26}$$

$$u_{se} \approx u + (d_{HR} + \overset{\smile}{\frown}_{Ro})\, q + \overset{\smile}{\frown}_{Ro}\, \dot{\eta}_{SR} - \frac{bs}{2} r - (u_{om})_{SR} \cos\psi_w \qquad \text{F-27}$$

$$u_{PR} \approx u + (d_{HR} + \overset{\smile}{\frown}_{Ro})\, q + \overset{\smile}{\frown}_{Ro}\, \dot{\eta}_{PR} + \frac{bs}{2} r - (u_{om})_{PR} \cos\psi_w \qquad \text{F-28}$$

(u_{om}) is horizontal component of water particle velocity.

FOIL FORCES

$$i_F \approx \eta_F + \frac{\left\{w + \dot{\xi}_F - q\,\ell_F - (w_{om})_F\right\}}{u_F} \qquad \text{F-29}$$

$$i_{SR} \approx \eta_{SR} + \frac{\left(w + \dot{\xi}_{SR} + q\ell_{SR} + p\frac{bs}{2} - (w_{om})_{SR}\right)}{u_{SR}} \qquad \text{F-30}$$

$$i_{PR} \approx \eta_{PR} + \frac{\left(w + \dot{\xi}_{PR} + q\ell_{PR} - p\frac{bs}{2} - (w_{om})_{PR}\right)}{u_{PR}} \qquad \text{F-31}$$

$$C_{NF} = f_1(i_F)\, f_2(\zeta_F) \qquad \text{F-32}$$

$$C_{NSR} = f_1(i_{SR})\, f_2(\zeta_{SR}) \qquad \text{F-33}$$

$$C_{NPR} = f_1(i_{PR})\, f_2(\zeta_{PR}) \qquad \text{F-34}$$

$$F_{CF} = C_{NF}\ \frac{1}{2}\ \rho\, S_F\, u_F^2 \qquad \text{F-35}$$

$$F_{CSR} = C_{NSR}\ \frac{1}{2}\ \rho\, S_R\, u_{SR}^2 \qquad \text{F-36}$$

$$F_{CPR} = C_{NPR}\ \frac{1}{2}\ \rho\, S_R\, u_{PR}^2 \qquad \text{F-37}$$

$$w_F = w + \dot{\xi}_F - q\ell_F \qquad \text{F-38}$$

$$w_{SR} = w + \dot{\xi}_{SR} + q\ell_{SR} + \frac{1}{2}\ p\ bs \qquad \text{F-39}$$

$$w_{PR} = w + \dot{\xi}_{PR} + q\ell_{PR} - \frac{1}{2}\ p\ bs \qquad \text{F-40}$$

$$F_{IF} = k_{IF} \left[\dot{w}_F - (\dot{w}_{om})_F \right] \qquad \text{F-41}$$

$$F_{ISR} = k_{IR} \left[\dot{w}_{SR} - (\dot{w}_{om})_{SR} \right] \qquad \text{F-42}$$

$$F_{IPR} = k_{IR} \left[\dot{w}_{PR} - (\dot{w}_{om})_{PR} \right] \qquad \text{F-43}$$

$$k_{IF} = 1.3677 \ \frac{\pi}{8} \rho \, S_F \, c_F \qquad \text{F-44}$$

$$k_{IR} = 1.3677 \ \frac{\pi}{8} \rho \, S_R \, c_R \qquad \text{F-45}$$

$$F_F = F_{CF} + F_{IF} \qquad \text{F-46}$$

$$F_{SR} = F_{CSR} + F_{ISR} \qquad \text{F-47}$$

$$F_{PR} = F_{CPR} + F_{IPR} \qquad \text{F-48}$$

i is incidence

C_N is normal lift coefficient

F_C is normal foil incidence produced force

F_I is normal foil inertia force

(w_{cm}) is vertical component of water particle velocity.

FOIL FORCES AND MOMENTS ON HULL

Let $$P_F = K_F \xi_F - R_{CF} \qquad \text{F-49}$$

$$P_{SR} = K_R \xi_{SR} - R_{CSR} (-F_B) \qquad \text{F-50}$$

$$P_{PR} = K_R \xi_{PR} - R_{CPR} (+F_B) \qquad \text{F-51}$$

Note: The F_B terms are included when the aft foils are laterally constrained.

Then $$X_{foils} \approx P_F \eta_F + P_{SR} \eta_{SR} + P_{PR} \eta_{PR} \qquad \text{F-52}$$

$$Z_{foils} \approx P_F + P_{SR} + P_{PR} \qquad \text{F-53}$$

$$K_{foils} \approx \frac{bs}{2} (P_{SR} - P_{PR}) \qquad \text{F-54}$$

$$M_{foils} \approx P_F (d_{HF} \eta_F - \ell_{HF}) + P_{SR} (d_{HR} \eta_{SR} + \ell_{HR}) + P_{PR} (d_{HR} \eta_{PR} + \ell_{HR}) \qquad \text{F-55}$$

$$N_{foils} \approx (P_{PR} \eta_{PR} - P_{SR} \eta_{SR}) \frac{bs}{2} \qquad \text{F-56}$$

STRUT FORCES AND MOMENTS ON HULL

$$i_{FS} = \frac{1}{u_F} \left[p\, d_{FS} - v - r\ell_F - (u_{om})_{FS} \sin \psi_w \right] + \delta_b \qquad \text{F-57}$$

$$i_{SS} = \frac{1}{u_{SR}} \left[p\, d_{SS} - v + r\ell_{SR} - (u_{om})_{SS} \sin \psi_w \right] + \delta_s \qquad \text{F-58}$$

$$i_{PS} = \frac{1}{u_{PR}} \left[p d_{PS} - v + r\ell_{PR} - (u_{om})_{PS} \sin \psi_w \right] + \delta_s \qquad \text{F-59}$$

$$Y_{FS} = \frac{1}{2} \rho u_F^2 \, i_{FS} \left(S \frac{\partial C_L}{\partial i} \right)_{FS} \qquad \text{F-60}$$

$$Y_{SS} = \frac{1}{2} \rho u_{SR}^2 \, i_{SS} \left(S \frac{\partial C_L}{\partial i} \right)_{SS} \qquad \text{F-61}$$

$$Y_{PS} = \frac{1}{2} \rho u_{PR}^2 \, i_{PS} \left(S \frac{\partial C_i}{\partial i} \right)_{PS} \qquad \text{F-62}$$

$$\zeta_F = (h_w)_F - \ell_F \theta - h_G + d_F \qquad \text{F-63}$$

$$\zeta_{SR} = (h_w)_{SR} + \ell_{SR} \theta - h_G + d_{SR} + \frac{1}{2} bs \phi \qquad \text{F-64}$$

$$\zeta_{PR} = (h_w)_{PR} + \ell_{PR} \theta - h_G + d_{PR} - \frac{1}{2} bs \phi \qquad \text{F-65}$$

$$d_{FS} = d_F - \frac{1}{2} \zeta_F \qquad \text{F-66}$$

$$d_{PS} = d_{PR} - \frac{1}{2}\zeta_{PR} \qquad \text{F-67}$$

$$d_{SS} = d_{SR} - \frac{1}{2}\zeta_{SR} \qquad \text{F-68}$$

$$\left(S \frac{\partial C_L}{\partial i}\right)_{FS} = f_1(\zeta_F) \qquad \text{F-69}$$

$$\left(S \frac{\partial C_L}{\partial i}\right)_{SS} = f_1(\zeta_{SR}) \qquad \text{F-70}$$

$$\left(S \frac{\partial C_L}{\partial i}\right)_{PS} = f_1(\zeta_{PR}) \qquad \text{F-71}$$

$$Y_{struts} = Y_{FS} + Y_{SS} + Y_{PS} \qquad \text{F-72}$$

$$K_{struts} = -Y_{FS}d_{FS} - Y_{SS}d_{SS} - Y_{PS}d_{PS} \qquad \text{F-73}$$

$$N_{struts} = Y_{FS}\ell_F - Y_{SS}\ell_{SR} - Y_{PS}\ell_{PR} \qquad \text{F-74}$$

$$X_{FS} = -\frac{1}{2}\rho u_F^2 \, c_{\overline{F}} \zeta_F C_D \qquad \text{F-75}$$

$$X_{SS} = -\frac{1}{2}\rho u_{SR}^2 \, c_{\overline{R}} \zeta_{SR} C_D \qquad \text{F-76}$$

$$X_{PS} = -\frac{1}{2}\rho u_{PR}^2 \, c_{\overline{R}} \zeta_{PR} C_D \qquad \text{F-77}$$

$$X_{struts} = X_{FS} + X_{SS} + X_{PS} \qquad \text{F-78}$$

$$M_{struts} = X_{FS}d_{FS} + X_{SS}d_{SS} + X_{PS}d_{PS} \qquad \text{F-79}$$

Subscript FS refers to forward strut.
Subscript SS refers to starboard aft strut.
Subscript PS refers to port aft strut

AERODYNAMIC FORCES

$$D_A \approx K_D (u^2 - 2 uu_A \cos\psi_w + u_A^2 \cos^2\psi_w) \qquad \text{F-80}$$

$$K_D = 0.111 \qquad \text{F-81}$$

u_A is wind velocity

ψ_w is angle between the velocity vectors of the wave front and the craft.

D_A is aerodynamic drag.

TOTAL FORCES AND MOMENTS ON HULL

$$X = X_{foils} + X_{struts} + T - D_A - m_T g\ \theta \qquad \text{F-82}$$

$$Y = Y_{struts} + m_T g\ \phi \qquad \text{F-83}$$

$$Z = Z_{foils} + m_H g \qquad \text{F-84}$$

$$K = K_{foils} + K_{struts} \qquad \text{F-85}$$

$$M = M_{foils} + M_{struts} - T\, d_T \qquad \text{F-86}$$

$$N = N_{foils} + N_{struts} \qquad \text{F-87}$$

T is thrust

d_T is distance in z direction from thrust line to C. G.

APPENDIX G

CALCULATION OF LATERAL STRUT COMPLIANCE

The strut stiffness was calculated on the basis of simple bending, i. e., torsional compliance was neglected. (This assumption was made for expediency, although it is recognized that torsional compliance can play an important part in the bending modes of unsymmetrical sections.)

Stiffness was calculated for an 11. 5-ft long strut pinned at the top and constrained on a knife edge 3 ft from the top. This strut length corresponds to the longer aft struts used in the lateral canard configuration study.

The strut was assumed to have a uniform external shape defined by

$$y = \frac{t}{2}\sqrt{\frac{x}{C}} \qquad \text{(G-1)}$$

Where

t is the strut trailing edge thickness of 2.86 inches
x is the distance from the LE
C is the chord of 26 inches
y is the strut semi-thickness at station x (symmetrically disposed around the centerline

The section was assumed to be the approximately uniform shell formed by maintaining a uniform thickness δ (measured perpendicular to the chord) from the parabolic contour defined in Equation G-1; the trailing edge of the section being closed by a flat plate of the same thickness δ.

This gives a section with a second moment of area.

$$I = \delta C \left(\frac{t^2}{4} - \frac{2}{3}\delta t + \frac{2}{3}\delta^2 - \frac{4}{15}\frac{\delta^4}{t^2}\right) + \frac{\delta}{12}(t - 2\delta)^3 \quad \text{(G-2)}$$

With $\delta = 0.2$ inch, the section second moment of area $I = 9.287$ in.^{4}.

The wall thickness δ is assumed to be 0.1 inch at its point of attachment to the foil; the corresponding second moment of area is 4.995 in.^{4}. (The wall thickness assumed at the lower end of the strut is of less significance in respect to bending deflections than that at the top of the strut.)

The strut is assumed to be $\delta = 0.2$ inch between the supports and tapered between the lower pin and the foil so that the second moment of area varied linearly.

Thus, the second moment of area

$$I = 9.287 \text{ in.}^4 \qquad 0 < z < 36''$$

$$= 11.024 - 0.04832\, z \text{ in.}^4 \qquad 36'' \leq z \leq 126'' \quad \text{(G-3)}$$

where z is measured along the span.

For bending deflection it is necessary to doubly integrate the equation

$$\frac{d^2y}{dz^2} = \frac{M}{EI} \quad \text{(G-4)}$$

where y is the lateral deflection at station z along the span and E is the elastic modulus.

Assuming a lateral force Y applied at 126 inches, the bending moment

$$M = 2.5\,z\ Y \text{ lb in.} \qquad 0 \leq z \leq 36''$$
$$= (126 - z)\ Y \text{ lb in.} \qquad 36'' \leq z \leq 126'' \qquad \text{(G-5)}$$

Substitution of the first Equation G-5 into Equation G-4 integrating twice and satisfying the condition that y = 0 at z = 0 and z = 36 inches gives

$$y = \left(\frac{2.5}{6} z^2 - 540\right) \frac{zY}{EI} \qquad \text{for } 0 \leq z \leq 36''$$

so that

$$\frac{dy}{dz} = 1030 \frac{Y}{EI} \qquad \text{at } z = 36''$$
$$= 116.29 \frac{Y}{E} \qquad \text{for } I = 9.287 \text{ in.}^4 \qquad \text{(G-6)}$$

Substituting the second Equation G-3 and Equation G-5 into Equation G-4 and integrating with Equation G-6 and, y = 0 at z = 36" as boundary conditions, gives

$$y = \frac{Y}{E} \left\{10.367z^2 - 7496.6z + 1,169,200 + (2126.7z - 486,100) \times \ell n\,(11.026 - 0.06823z)\right\}$$

At z = 126 inches (the assumed point of application of Y)

$$y = 40,441 \frac{Y}{E}$$

Thus the effective strut stiffness

$$\frac{Y}{y} = \frac{E}{40,441} = 742 \text{ lb/in. (assuming } E = 30 \times 10^6 \text{ lb/in.}^2)$$